



**HAL**  
open science

# Characterizing transport modalities of glutathione towards the mammalian endoplasmic reticulum, and chemical screenings for the discovery of novel compounds modulating its metabolism

Aurélie Rachet

► **To cite this version:**

Aurélie Rachet. Characterizing transport modalities of glutathione towards the mammalian endoplasmic reticulum, and chemical screenings for the discovery of novel compounds modulating its metabolism. Molecular biology. Université Paris-Saclay, 2023. English. NNT : 2023UPASL108 . tel-04500938

**HAL Id: tel-04500938**

**<https://theses.hal.science/tel-04500938>**

Submitted on 12 Mar 2024

**HAL** is a multi-disciplinary open access archive for the deposit and dissemination of scientific research documents, whether they are published or not. The documents may come from teaching and research institutions in France or abroad, or from public or private research centers.

L'archive ouverte pluridisciplinaire **HAL**, est destinée au dépôt et à la diffusion de documents scientifiques de niveau recherche, publiés ou non, émanant des établissements d'enseignement et de recherche français ou étrangers, des laboratoires publics ou privés.

Characterizing transport modalities of glutathione  
towards the mammalian endoplasmic reticulum, and  
chemical screenings for the discovery of novel  
compounds modulating its metabolism

*Caractérisation des modes de transport du glutathion vers le Réticulum  
Endoplasmique mammifère, et criblage chimique à la découverte de nouvelles  
molécules modulant son métabolisme*

**Thèse de doctorat de l'université Paris-Saclay**

École doctorale n° 577, Structure et Dynamique des Systèmes Vivants (SDSV)  
Spécialité de doctorat : Biologie moléculaire et cellulaire  
Graduate School : Sciences de la vie et santé  
Référent : Faculté des sciences d'Orsay

Thèse préparée dans l'unité de recherche **I2BC (Université Paris-Saclay, CEA, CNRS)**, sous la  
direction de **Agnès DELAUNAY-MOISAN**, directrice de recherche CEA

**Thèse soutenue à Paris-Saclay, le 24 Novembre 2023, par**

**Aurélié RACHET**

**Composition du Jury**

Membres du jury avec voix délibérative

<b>Sophie DUPRE-CROCHET</b> Professeure des universités, Université Paris-Saclay	Présidente
<b>Geneviève DUPONT</b> Directrice de recherche, Université libre de Bruxelles	Rapporteuse & Examinatrice
<b>Jean-François COLLET</b> Professeur des universités, Université Catholique de Louvain	Rapporteur & Examineur
<b>Meng-Er HUANG</b> Directeur de recherche, Université Paris-Saclay	Examineur
<b>Anna BABOUR</b> Directrice de recherche, HDR, Université Paris-Cité	Examinatrice

**Titre :** Caractérisation des modes de transport du glutathion vers le Réticulum Endoplasmique mammifère, et criblage chimique à la découverte de nouvelles molécules modulant ce métabolisme.

**Mots clés :** Glutathion, Réticulum endoplasmique, Redox, Transport, Criblage chimique

**Résumé :** Le réticulum endoplasmique est le lieu de synthèse et de maturation des protéines destinées à être secrétées ou adressées à la membrane plasmique. Il est aussi le lieu de stockage du calcium cellulaire et coordonne la synthèse et le trafic lipidique. De part ces fonctions, il joue un rôle central dans de nombreux processus de signalisation. La maturation des protéines dans le RE implique très fréquemment la formation de ponts disulfures. De fait le RE est doté d'une machinerie enzymatique permettant d'oxyder les protéines en cours de repliement, ce qui le distingue de la plupart des autres compartiments cellulaires. La présence dans le RE de glutathion, en concentrations millimolaires, pose question quant au rôle joué par ce tripeptide réducteur dans un compartiment oxydant. L'objectif de ma thèse a été d'appréhender quel(s) rôle(s) pouvait avoir le glutathion dans le RE mammifère, en m'attachant plus particulièrement à comprendre les mécanismes responsables de et/ou stimulant son entrée dans le RE.

Pour cela, nous avons mis au point un système de sondes nous donnant accès aux niveaux intraluminaux de GSH. Ce système nous a permis de proposer un modèle décrivant l'import du GSH vers le RE qui fonctionnerait selon deux modes ; Le premier implique un transport passif imposé par le gradient de concentration établi entre le cytosol et le RE. La hausse des niveaux cytosoliques de GSH entraîne une réduction modérée du RE. Cette réduction reste limitée et n'est pas suffisante pour induire une UPR efficace, suggérant l'existence de mécanismes de contrôle. Les modalités de ce transport ont montré une dépendance au métabolisme de la cystéine, bien qu'une réduction directe de notre système de sondes par la cystéine semble écartée.

Le second mode de transport du GSH est induit par une déplétion des stocks calciques du RE, et survient sans modification des niveaux de GSH intracellulaires, ce qui suggère un transport actif. Ce mode de transport semble indépendant du métabolisme de la cystéine

Dans un second temps, nous avons mis à profit ces connaissances pour mettre en place un crible chimique haut débit en vue d'identifier des molécules capables de moduler l'import provoqué par le second mode de transport décrit ci-dessus. Plusieurs types de molécules ont été identifiées, parmi lesquelles de possibles inhibiteurs ou stimulateurs du transport du GSH vers le RE. Des expériences de caractérisations des concentrations luminales de GSH mais aussi de calcium ont permis d'initier l'étude mécanistique de l'action des composés identifiés lors du crible.

Nos résultats ont permis de développer des systèmes de détection et de caractérisation des flux du glutathion au sein du réticulum endoplasmique. S'il semble clair que son transport s'effectue selon différentes modalités, certaines semblent nécessiter des caractérisations plus approfondies. Notamment, la maîtrise du métabolisme de la cystéine et l'équilibre du pH au sein du RE semblent être deux voies qui permettront de compléter nos modèles de transport. Le crible chimique mis en place a révélé un grand nombre de molécules jouant sur le potentiel du GSH au sein du RE. Identifier une molécule dont le mécanisme module le transport du GSH permettra à terme de gérer plus finement le transport du GSH, et ainsi d'apprécier sa fonction localement.

**Title :** Characterizing transport modalities of glutathione towards the mammalian endoplasmic reticulum, and chemical screenings for the discovery of novel compounds modulating this metabolism

**Keywords :** Glutathione, Endoplasmic reticulum, Redox, Transport, Chemical screening

**Abstract :** The endoplasmic reticulum is the site of synthesis and maturation of proteins destined to be secreted or sent to the plasma membrane. It is also the storage site for cellular calcium and coordinates lipid synthesis and trafficking. As a result of these functions, it plays a central role in many signaling processes. Protein maturation in the ER frequently involves the formation of disulfide bridges. In fact, the ER has an enzymatic machinery dedicated to the oxidation of proteins during folding, which distinguishes it from most other cellular compartments. The presence of millimolar concentrations of glutathione in the ER raises questions about the role played by this reducing tripeptide in such an oxidizing compartment. The aim of my thesis was to understand the role(s) of glutathione in the mammalian ER, with a particular emphasis on the mechanisms responsible for and/or stimulating its entry into the ER.

To achieve this, we developed a probe system giving us access to intraluminal GSH levels. This system has allowed us to propose a model describing the import of GSH into the ER, which would operate in two modes. The first involves passive transport imposed by the concentration gradient established between the cytosol and the ER. The increase in cytosolic GSH levels leads to a moderate reduction in the ER. This reduction remains limited and is not sufficient to induce effective UPR, suggesting the existence of control mechanisms. The modalities of this transport showed a dependence on cysteine metabolism, although a direct reduction of our

probe system by cysteine seems to be ruled out. The second mode of GSH transport is induced by depletion of ER calcium stores, and occurs without any change in intracellular GSH levels, suggesting active transport. This mode of transport appears to be independent of cysteine metabolism.

We then used this knowledge to set up a high-throughput chemical screening in order to identify molecules capable of modulating the import caused by the second mode of transport described above. Several types of molecules were identified, including possible inhibitors or stimulators of GSH transport to the ER. Experiments to characterize luminal concentrations of GSH and calcium were used to initiate a mechanistic study of the action of the compounds identified during the screen.

Our research has led us to develop systems for detecting and characterizing glutathione flows within the endoplasmic reticulum. While it seems clear that glutathione is transported in a variety of ways, some would appear to require more detailed characterization. In particular, control of cysteine metabolism and pH balance within the ER appear to be two avenues that will enable our transport models to be completed. The chemical screen set up revealed a large number of molecules that influence the potential of GSH within the ER. Identifying a molecule whose mechanism modulates GSH transport will eventually enable us to manage GSH transport more finely, and thus assess its function locally.

# REMERCIEMENTS

J'aimerais en tout premier lieu adresser mes remerciements aux membres de mon jury de thèse, Sophie Dupré-Crochet, Geneviève Dupont, Jean-François Collet, Meng-Er Huang, et Anna Babour. Merci d'avoir pris le temps d'évaluer mon travail de thèse, ainsi que pour vos précieux retours et discussions durant ma soutenance. J'aimerais ajouter une mention particulière à Anna Babour, qui a aussi accepté de suivre mon travail de thèse pendant 4 ans en participant aux comités de suivi annuels, merci pour les encouragements, conseils et aiguillages réguliers qui auront été cruciaux pour ma thèse et pour moi. De même, j'aimerais étendre ces remerciements aux autres membres de mes comités de suivi successifs, Benjamin Ezraty, Jean-Christophe Cintrat et Sébastien Gaumer pour leur attention et conseils avisés.

Naturellement, je remercie Agnès Delaunay-Moisan, premièrement, pour m'avoir fait confiance en m'offrant ce projet. Merci, pour ta passion contagieuse de la science, et nos discussions, parfois à rallonge, souvent tardives, qui me manquent déjà. Merci pour ta bienveillance, ton souci de l'autre, et ta confiance en moi, qui ont créé le parfait équilibre entre encadrement et autonomie, faisant de moi le bébé chercheur que je suis.

Je ne serais évidemment même pas un embryon de chercheur sans Gwenaëlle Le Pavec. Merci, pour m'avoir prise sous ton aile et appris tout ce que je sais faire aujourd'hui dans un labo, de la simple solution de glutathion à l'imbrication de 3 manips de 63 échantillons en un temps record de 3 heures et 42 minutes. Au-delà de la pratique, merci pour ta présence quotidienne à mes côtés, je pense qu'il n'y a pas eu un jour sans que je rie au labo, et c'est en grande partie grâce à toi, merci donc pour ton soutien (littéral dès le premier jour, n'est-ce pas !). Ces 4 années auraient paru plus longues sans toi !

Pareillement, j'aimerais remercier tous les membres du laboratoire et au-delà, sans qui l'environnement n'aurait pas été ce qu'il a été. Merci à Jean-Yves, Carl, Jean-Christophe et Benoît, pour nos échanges, scientifiques ou existentiels, et les bons moments « entre ». J'ai une pensée particulière pour Régis, « la Gwen mais dans le labo d'en face ». Je suis désolée de ne pas avoir repoussé ma soutenance, tu as raison, étais-je vraiment à quelques mois près ? On dira que c'est ma vengeance pour avoir tenté de me vendre un gramme de MES pour 50€ !

Je voudrais également remercier quelques membres du Service de Chimie Bioorganique et de Marquage qui m'ont permis de garder un pied dans des labo de chimie. Merci alors à Jean-Christophe Cintrat et Egor Chirkin, pour l'intro à la synthèse peptidique et le feu vert pour un nombre indéterminé d'essais plus ou moins catastrophiques. Merci à David, Amélie et Sabrina, d'avoir pris le temps d'essayer d'y comprendre quelque chose avec moi. Enfin, merci à Frédéric Taran et Maxime Ribéraud ! Pour finir, merci évidemment à Sophia, pour m'avoir ouvert les portes de cette forteresse, mais aussi pour avoir lyophilisé mes produits et parfois même aidée avec la RMN. Tschüss !

Je pense évidemment aux co-thésards, post-docs, stagiaires, et autres personnes, rencontrées pendant ma thèse : Marouane et Sylvain, la paire indissociable, qui m'ont immédiatement accueillie et intégrée, Valentin avec qui j'ai partagé l'angoisse du bébé thésard. A Julien, pour avoir été le Robin de mon Batman pendant plusieurs mois (encore désolée pour cette histoire de couvercle en polystyrène, j'espère que tu t'en remets), à Emilie pour les escapades en amazonie (aka son bureau), Beata, Léo (Ich lerne Deutsch, wann werden wir klettern gehen ?). Merci à Rémi, Hubert, à Christophe, Assmaa, à Reem, Manon, Batoul, Adèle, à Clément, Clément et sans oublier, à Clément, Justine, Mélissa et Sirine, ... J'ai une pensée particulière pour Kris (even though you missed my defense which i would not dare to shame you for, publicly and forever, in my acknowledgements, ça va mon super pote ?) et Clément, copains de café, bière ou escalade, force et courage, c'est bientôt fini !!

Merci aux copains qui m'ont suivie de loin, merci à Tiphaine/Thiophène, camarade d'infortune à bien des aspects, pour ta présence inconditionnelle depuis le master, et jusqu'ici, on l'a fait !! Merci à Sacha, Clément, à tous les chevaliers du dancefloor de la soundboard, qui ont rendu la dernière ligne droite plus douce. Merci particulièrement à Nath, pour avoir refait surface à un moment qui, j'en ai conscience, a été particulièrement crucial. Merci à Aymeline, pour ta curiosité sincère, ta présence, ton amitié, et plus encore, depuis plus d'année que je n'ose compter. A Davina, pour le soutien et les madeleines de Proust, même si je suis qu'une fayotte. Evidemment, merci à Sophia, qui je l'espère a hurlé à la fin du paragraphe pré-précédent. Merci, pour m'avoir tenu la tête hors de l'eau à tant d'occasions et pour avoir plongé avec moi, parfois. Merci pour ton amitié, dont je mesure la valeur, et surtout, merci d'être aussi drôle (wink wink). Merci également à Yanneau, pour ta recette de la poutine qui me remplit de nostalgie, les escapades lyonnaises, les escapes games et autres apérals qui ont souvent renouvelé mon capital santé mentale.

J'aimerais remercier ma maman, pour avoir cru en moi depuis toujours en sans conditions, pour sa fierté qui m'a portée si loin, et pour avoir été ma brillante et première source d'inspiration. Merci également à mes frères et sœurs, Morgane, Poluuuuune, Mathieu, Clem, Estelle et à Mamie.

Enfin, j'aimerais remercier Caroline, pour son indulgence lorsque je l'ai oubliée à la fin de ma soutenance. Merci pour ton soutien et ta présence, qui ont souvent calmé mes tempêtes, et parfois juste pour avoir accepté de les traverser avec moi à l'insu de ton plein gré :D. Plus encore, merci, Caroline, pour des choses qui rempliraient bien plus que ce manuscrit.

A Liliane et Robert Joyaux

Pour l'absolu depuis toujours,  
et récemment, de bien trop loin

# TABLE OF CONTENTS

<b>FIGURES AND TABLES</b> .....	<b>VI</b>
<b>ABBREVIATIONS</b> .....	<b>X</b>
<b>INTRODUCTION</b> .....	<b>- 1 -</b>
CHAPTER 1: GLUTATHIONE .....	- 1 -
I.    GENERAL INFORMATION .....	- 1 -
A. <i>Discovery and structural description of glutathione</i> .....	- 1 -
B. <i>The different forms of glutathione in cells</i> .....	- 2 -
C. <i>Glutathione can be found in a vast majority of organisms at the subcellular level</i> .....	- 4 -
D. <i>Glutathione synthesis and metabolism within cells</i> .....	- 5 -
II.   GLUTATHIONE FUNCTIONS .....	- 9 -
A. <i>Glutathione serves as an antioxidant either alone or as a protein cofactor</i> .....	- 9 -
B. <i>Role in iron metabolism</i> .....	- 15 -
C. <i>Role as a thioredoxin back-up system</i> .....	- 16 -
III.  GLUTATHIONE TRANSPORT SYSTEMS .....	- 17 -
<i>Nuclear import of glutathione?</i> .....	- 18 -
<i>Mitochondrial transport</i> .....	- 18 -
<i>Vacuolar transport</i> .....	- 19 -
<i>Plasma membrane transport</i> .....	- 20 -
<i>Endomembrane system transport</i> .....	- 21 -
IV.  GLUTATHIONE VISUALIZATION AND STUDY TOOLS .....	- 23 -
A. <i>Cell and tissue biochemical analysis</i> .....	- 23 -
B. <i>Redox probes: rxYFPs and roGFPs</i> .....	- 24 -
C. <i>Clickable GSH</i> .....	- 29 -
CHAPTER 2: THE ENDOPLASMIC RETICULUM.....	- 33 -
I.    INTRODUCTION TO THE ENDOPLASMIC RETICULUM .....	- 33 -
II.   REDOX REACTIONS IN THE ER .....	- 34 -
A. <i>Oxidative Protein Folding in the ER: the Ero1-PDI relay</i> .....	- 34 -
B. <i>Additional and alternative pathways</i> .....	- 39 -
III.  THE UNFOLDED PROTEIN RESPONSE .....	- 45 -
A. <i>IRE-1</i> .....	- 45 -
B. <i>PERK</i> .....	- 46 -
C. <i>ATF6</i> .....	- 47 -
IV.  GLUTATHIONE IN THE ER .....	- 49 -
A. <i>History of the suspected function of GSH in the redox state of the ER</i> .....	- 49 -
B. <i>Transport of glutathione into the ER</i> .....	- 53 -
<b>AIMS OF THE PROJECT</b> .....	<b>- 57 -</b>
<b>RESULTS</b> .....	<b>- 59 -</b>
CHAPTER 1: PUBLICATION: GLUTATHIONE UPTAKE INTO THE ENDOPLASMIC RETICULUM:	
MECHANISTIC INSIGHTS AND ER REDOX IMPACT .....	- 59 -
INTRODUCTION .....	- 59 -
RESULTS.....	- 63 -
DISCUSSION.....	- 83 -
<b>SUPPLEMENTARY FIGURES</b> .....	<b>- 92 -</b>
CHAPTER 2: PRELIMINARY RESULTS .....	- 103 -

I.	DISCRIMINATING THE EFFECT OF CYSTEINE FROM THAT OF GLUTATHIONE .....	- 103 -
A.	<i>Presence of extracellular cystine is necessary for ER probe reduction .....</i>	- 103 -
B.	<i>Cysteine can cause ER probe reduction without GSH in whole cells .....</i>	- 105 -
C.	<i>Cysteine reduction is not matched in semi-permeabilized cells.....</i>	- 107 -
D.	<i>Cysteine does not markedly reduce the probes at the concentrations where reduction occurred .....</i>	- 110 -
E.	<i>Thapsigargin-induced reduction of the ER is independent of cysteine availability.....</i>	- 112 -
	<i>Discussion.....</i>	- 113 -
II.	CHEMICAL SCREENING .....	- 117 -
A.	<i>Setting up the high throughput screening.....</i>	- 117 -
B.	<i>Results of the primary screens .....</i>	- 132 -
C.	<i>Secondary screen – functional characterization.....</i>	- 140 -
	<i>Discussion.....</i>	- 151 -
	<b>CONCLUSION AND PERSPECTIVES.....</b>	<b>- 155 -</b>
	<b>MATERIALS AND METHODS .....</b>	<b>- 159 -</b>
	<b>BIBLIOGRAPHY.....</b>	<b>- 169 -</b>
	<b>RÉSUMÉ SUBSTANTIEL EN FRANCAIS.....</b>	<b>- 170 -</b>

## FIGURES AND TABLES

FIGURE 1 – STRUCTURE OF GLUTATHIONE .....	- 1 -
FIGURE 2 – GLUTATHIONE HALF REDUCTION REACTION AND EQUILIBRIUM WITH GLUTATHIONE DISULPHIDE (LEFT) GLUTATHIONE PREDOMINANT FORM AT PH 7.4 (RIGHT) .....	- 3 -
FIGURE 3 – GLUTATHIONE SPECIES ENCOUNTERED IN CELLS .....	- 4 -
FIGURE 4 – ABUNDANT, REDUCED, AND LOW MOLECULAR WEIGHT THIOLS IDENTIFIED AMONG SPECIES .	- 5 -
FIGURE 5 – GLUTATHIONE ENZYMATIC SYNTHESIS PROCESS IN MAMMALS.....	- 6 -
FIGURE 6 – <i>THE <math>\Gamma</math>-GLUTAMYL CYCLE</i> .....	- 7 -
FIGURE 7 – THE REVISED <i>GLUTATHIONE CYCLE</i> .....	- 7 -
FIGURE 8 – GLUTATHIONE REDUCTASE (GLR) CYCLE .....	- 9 -
FIGURE 9 – GLUTATHIONE RECYCLES REDUCED GPX IN THE PROCESS OF PEROXIDE REDUCTION .....	- 11 -
FIGURE 10 – PROTEIN-GLUTATHIONE SPECIES .....	- 11 -
FIGURE 11 – MONOTHIOLE MECHANISM OF GRX CATALYSIS FOR GLUTATHIONYLATED SUBSTRATES. ....	- 12 -
FIGURE 12 – DITHIOLE MECHANISM OF GRX CATALYSIS FOR OXIDIZED SUBSTRATES .....	- 13 -
FIGURE 13 – GST TRANSFERS A GLUTATHIONE MOLECULE ONTO ELECTROPHILE BY NUCLEOPHILIC SUBSTITUTION .....	- 14 -
FIGURE 14 – THE THIOREDOXIN PATHWAY MAINTAINS CYSTEINES REDUCED IN AN NADPH-DEPENDENT WAY.....	- 16 -
FIGURE 15 – GLUTATHIONE TRANSPORTERS DESCRIBED AND VALIDATED IN YEAST AND MAMMALIAN CELLS. .....	- 17 -
FIGURE 16 – DTNB ASSAY APPLIED TO GSH QUANTIFICATION.....	- 23 -
FIGURE 17 – REDOX SENSITIVE GFP EQUILIBRATES WITH GSH (TOP) AND THE RATIO OF OXIDIZED AND REDUCED FORMS CAN BE GENERATED FROM FLUORESCENCE SPECTRA (BOTTOM) .....	- 25 -
FIGURE 18 – GLUTATHIONE REDOX POTENTIAL IN CELLS .....	- 28 -
FIGURE 19 – COPPER-CATALYSED ALKYNE-AZIDE CYCLOADDITION.....	- 30 -
FIGURE 20 – PRINCIPLE OF <i>IN SITU</i> CLICK CHEMISTRY FOR GLUTATHIONYLATION DETECTION. ....	- 30 -
FIGURE 21 – PDI CATALYZED REACTIONS. ....	- 35 -
FIGURE 22 - ERO1-PDI CATALYZED DISULFIDE BOND FORMATION .....	- 37 -
FIGURE 23 - SCHEMATIC REPRESENTATION OF MAMMALIAN ERO1A DISULFIDES. BOLD ARROWS REPRESENT ELECTRON TRANSFERS, GREEN BONDS ARE PRESENT IN THE ACTIVE FORM, RED BONDS IN THE INACTIVE FORM. THE SPECIFIC CASE OF REGULATORY CYSTEINES 208 AND 241 IS NOT REPRESENTED. .....	- 39 -
FIGURE 24 - PRX4 MECHANISM OF ACTION .....	- 40 -

FIGURE 25 – UPR TRANSDUCERS. ....	- 47 -
FIGURE 26 – PROPOSED MODEL FOR ER IMPORT OF GSH. ....	- 56 -
FIGURE 27 – GLUTATHIONE TREATMENT DOES NOT CAUSE VARIATIONS OF THE RATIO OF ER-LOCALIZED, PH-SENSITIVE PHLUORIN2. ....	- 85 -
FIGURE 28 – INHIBITION OF PROTEIN SYNTHESIS CAUSES A MORE OXIDIZING $E_{GSH}$ ....	- 86 -
FIGURE 29 – EXTRACELLULAR CYSTINE IS NECESSARY FOR ER PROBE REDUCTION BY GSH.....	- 104 -
FIGURE 30 – GLUTATHIONE EXOGENOUS TREATMENT, BUT NOT GCL OVEREXPRESSION, INCREASES INTRACELLULAR CYSTEINE LEVELS.....	- 105 -
FIGURE 31 – CYSTEINE CAUSES ER PROBE REDUCTION INDEPENDENTLY OF GSH.....	- 106 -
FIGURE 32 – CYSTEINE REDUCTION OF THE PROBE IN NON-PERMEABILIZED CELLS IS NOT MIRRORED UPON SEMI-PERMEABILIZATION .....	- 108 -
FIGURE 33 – CYSTEINE ADDITION DOES NOT CAUSE A GSH-EQUIVALENT REDUCTION IN SEMI- PERMEABILIZED CELLS .....	- 109 -
FIGURE 34 – THIOL EQUIVALENTS OF CYSTEINE AND GSH DO NOT REDUCE PURIFIED GRX1-ROGFPIE TO THE SAME EXTENT .....	- 110 -
FIGURE 35 – CYSTEINE DOES NOT REDUCE ER LOCALIZED GRX1-1CYS TO THE SAME EXTENT AS GSH IN THE CONCENTRATIONS THAT DO IN WHOLE CELLS .....	- 111 -
FIGURE 36 – THAPSIGARGIN-ELICITED REDUCTION IS INDEPENDENT OF THE AVAILABILITY OF CYSTEINE- -	112
FIGURE 37 – IE SF1 MUTANT PROBE IS RESPONSIVE TO REDOX TREATMENT.....	- 118 -
FIGURE 38 – THE TRANSIENTLY EXPRESSED SF GRX1-ROGFPIE HAS A FLUORESCENCE INTENSITY INCREASED BY MORE THAN TWO TIMES .....	- 119 -
FIGURE 39 – IE SF A206V PROBE IS UNRESPONSIVE TO REDOX TREATMENT.....	- 120 -
FIGURE 40 – COMMERCIAL IE SF PROBE SHOWS NO REDOX RESPONSIVITY .....	- 121 -
FIGURE 41 – IE SF A206V F145Y PROBE IS RESPONSIVE TO REDOX TREATMENT BUT LOSES RATIO METRIC ABILITY.....	- 122 -
FIGURE 42 – COMPARISON OF $E_{GSH}$ VARIATIONS ACCORDING TO GSH INTRACELLULAR LEVELS BETWEEN GRX1-ROGFPIE AND SF GRX1-ROGFPIE .....	- 123 -
FIGURE 43 – SPECTRAL SCAN OF STABLY EXPRESSED SF GRX1-ROGFPIE .....	- 124 -
FIGURE 44 – RECAP OF THE OPTICAL PROPERTIES OF THE 4 TESTED SF MUTANTS .....	- 126 -
FIGURE 45 – REDUCTION KINETICS UPON MANUAL TG TREATMENT .....	- 128 -
FIGURE 46 - REDUCTION KINETICS UPON AUTOMATED TG TREATMENT.....	- 128 -
FIGURE 47 – INFLUENCE ON $E_{GSH}$ IN IE SF CELLS OF A DOSE RESPONSE TREATMENT OF THAPSIGARGIN....	- 129 -

FIGURE 48 – SCREENING TIMELINE .....	- 130 -
FIGURE 49 – DECISION DIAGRAM FOR SORTING CHEMICALS BY EFFECT. ....	- 131 -
FIGURE 50 – COMMON HITS IN BOTH SCREENING ROUNDS .....	- 132 -
FIGURE 51 – RECAP OF THE DIFFERENT KINDS OF HITS .....	- 133 -
FIGURE 52 – SSMD OF ER STRESS HITS .....	- 134 -
FIGURE 53 – SSMD OF PRESTWICK HITS .....	- 134 -
FIGURE 54 – MOST OF ER STRESS OXIDIZING MOLECULES HAVE A TG INHIBITORY EFFECT .....	- 135 -
FIGURE 55 – MOST OF PRESTWICK OXIDIZING MOLECULES HAVE A TG INHIBITORY EFFECT .....	- 136 -
FIGURE 56 – MOST OF ER STRESS REDUCING MOLECULES HAVE A TG POTENTIATING EFFECT .....	- 137 -
FIGURE 57 – MOST OF PRESTWICK REDUCING MOLECULES HAVE A TG POTENTIATING EFFECT .....	- 138 -
FIGURE 58 – RECAP OF ALL SCREENS HIT FILTERING .....	- 139 -
FIGURE 59 – POLYPHYLLIN I SUPPRESSES TG-ELICITED ER REDUCTION IN A DOSE-DEPENDENT WAY. -	141 -
FIGURE 60 – TIME DEPENDENCY OF POLYPHYLLIN I TREATMENT .....	- 143 -
FIGURE 61 – IMPACT OF PLP I TREATMENT ON TG-DRIVEN ER GSH ENTRY .....	- 145 -
FIGURE 62 – PLP I TREATMENT INCREASES ER CALCIUM CONTENT AND DECREASES ER REPLETION KINETICS .....	- 148 -
FIGURE 63 – PLP I TREATMENT INCREASES ER CALCIUM CONTENT AND DECREASES ER REPLETION KINETICS .....	- 149 -

---

TABLE 1 – COMPARTMENT SPECIFICITY OF E <sub>GSH</sub> , IN YEAST AND MAMMALIAN CELLS .....	- 27 -
--	--------

---

PUBLICATION FIGURE 1 – GSH REDUCTION POTENTIAL IN THE ENDOPLASMIC RETICULUM VARIES ACCORDING TO GSH INTRACELLULAR LEVELS. ....	- 64 -
PUBLICATION FIGURE 2 – QUANTITATION OF GSH ER TRANSPORT USING GRX1-1CYS PROBE AND SEMI- PERMEABILIZED CELLS. ....	- 71 -
PUBLICATION FIGURE 3 – GSH-TRIGGERED ER REDUCTION IS NOT SIGNIFICANTLY IMPACTED BY SEC61 INHIBITION. ....	- 73 -
PUBLICATION FIGURE 4 – GSH-INDUCED ER REDUCTION DOES NOT TRIGGER UPR .....	- 75 -

PUBLICATION FIGURE 5 – MODULATION OF ERDJ5 AND ERO1 REDOX STATE AND OXIDATIVE FOLDING UPON  
GSH-INDUCED ER REDUCTION ..... - 78 -

PUBLICATION FIGURE 6 – CYTOSOLIC GSH GRADIENT AND THAPSIGARGIN ACT INDEPENDENTLY TO  
TRIGGER ER REDUCTION AND GSH ER TRANSPORT. .... - 81 -

## ABBREVIATIONS

### A

**ATF:** Activating transcription factor

**ATP:** Adenosine triphosphate

**$\alpha$ 1-AT:** alpha1-antitrypsin

### B

**BiP:** Binding Immunoglobulin Protein

**BSO:** Buthionine sulfoximine

### C

**Cys2:** Oxidized form of cystine

**CysH:** Reduced form of cystine

**CHOP:** CAAT/enhancer-binding protein (C/EBP) homologous protein

### D

**DMEM:** Dulbecco's modified eagle medium

**DNA:** Desoxyribonucleic acid

**DTNB:** 5,5'-dithio-bis(2-nitrobenzoic acid)

**DTT:** Dithiothreitol

**DUG:** Defective in utilization of glutathione

### E

**eIF2 $\alpha$ :** eukaryotic translation Initiation Factor 2 $\alpha$

**ER:** Endoplasmic reticulum

**ERAD:** ER associated degradation

**ERO1:** ER oxydoreductin-1

### G

**$\gamma$ -GCT:**  $\gamma$ -glutamyl cyclotransferase

**GCL:**  $\gamma$ -glutamylcysteine ligase

**GCLC:** GCL catalytic subunit

**GCLM:** GCL modifier subunit

**GFP:** Green fluorescent protein

**GGT:**  $\gamma$ -glutamyl transpeptidase

**GLR:** Glutathione reductase

**GPX:** Glutathione peroxidase

**GRX:** Glutaredoxin

**GS:** Glutathione synthetase

**GSH:** Glutathione (reduced)

**GSSG:** Glutathione disulfide (oxidized)

**GST:** Glutathione S-transferase

### H

**HPLC:** High-performance liquid chromatography

**HTS:** High throughput screening

### I

**iE cell:** Cell line stably expressing ER-localized Grx1-roGFPiE

**iE SF cell:** Cell line stably expressing ER-localized SF Grx1-roGFPiE

**IMM:** Inner mitochondrial membrane

**IMS:** Intermembrane space

**IpoF:** Ipomoeassin F

**IRE-1:** Inositol-requiring enzyme 1

**ISC:** Iron sulfur cluster

### K

**kDa:** Kilodalton

### L

**LDL:** Low density lipoprotein

### M

**MRP1:** Multidrug resistance protein 1

## N

**NHK:** Null Hong Kong mutation

**NP:** Non-permeabilized

## O

**OAT:** Organic anion transporter

**OMM:** Outer mitochondrial membrane

**OPT:** Oligopeptide transporter

**OxD:** Percentage of probe oxidation

## P

**PDI:** Protein Disulfide Isomerase

**PERK:** Protein kinase RNA-like ER Kinase

**PLP I:** Polyphyllin I

**PM:** Plasma membrane

**Prx:** Peroxiredoxin

## R

**RIDD:** Regulated IRE-1 dependent decay

**RNA:** Ribonucleic acid

**roGFP:** redox sensitive GFP

**ROS:** Reactive oxygen species

**RyR:** Ryanodine receptor

## S

**SD:** Standard deviation

**SF:** Superfolder

**SP:** Semi-permeabilized

**SSMD:** Strictly standardized mean difference

## T

**Tg:** Thapsigargin

**TRR:** Thioredoxin reductase

**Trx:** Thioredoxin

## U

**UPR:** Unfolded protein response

## X

**XBP1:** X-box Binding Protein 1

## Y

**YFP:** Yellow fluorescent protein

## A. DISCOVERY AND STRUCTURAL DESCRIPTION OF GLUTATHIONE

Joseph de Rey-Pailhade described philothion, a “sulfur-loving” compound, more than 130 years ago (de Rey-Pailhade, 1888). He discovered in yeast extracts, and later in other animal tissues such as liver and muscle, a substance with a labile hydrogen, that was able to reduce sulfur to hydrogen sulphide.

Frederick Gowland Hopkins later took on Rey-Pailhade’s findings, and described an ‘autoxidisable constituent of the cell’. He characterized a compound bearing an oxidizable sulfhydryl function and two amino acids: glutamate and cysteine, and therefore gave the molecule the name Glutathione as a contraction of the names of both its constituents (Hopkins, 1921).

A few years after, George Hunter and Blythe Alfred Eagles questioned the structure of the molecule in their article (Hunter and Eagles, 1927). They realized that the nitrogen count they obtained for their glutathione preparation did not correspond to the theoretical one that glutamylcysteine would yield. A couple of years later, Hopkins admitted that his initial findings were erroneous and corrected the description of glutathione, stating that the molecule was in fact composed of glutamate, cysteine and a third amino acid: glycine.

Finally, in 1929, Norman W. Pirie and Kathleen Godwin Pinhey performed titrations of glutathione in water and formaldehyde as well as pK determinations. Their combined data led them to propose the structure of glutathione we know now, in which a standard amide bond links glycine and cysteine, whereas cysteine and glutamate are coupled *via* an atypical *gamma* peptide linkage, involving the side-chain carboxyl group of the glutamate amino acid (Pirie and Pinhey 1929, **Figure 1**).

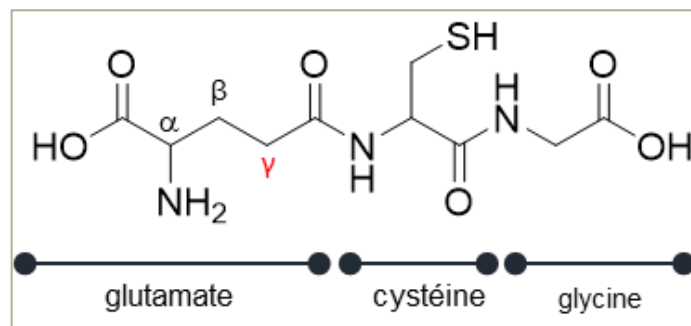


**Figure 1 – Structure of glutathione** as first described by Pirie and Pinhey

---

## B. THE DIFFERENT FORMS OF GLUTATHIONE IN CELLS

Glutathione, GSH or  $\gamma$ -L-glutamyl-L-cysteinylglycine bears a central cysteine, which is the labile proton function that initially led to its discovery. This function allows for the release of proton and electron, making GSH a reductant. The subsequent formation of a covalent link between the two deprotonated sulfur atoms of two GSH molecules forms glutathione disulphide (GSSG). This half reduction reaction has a standard potential of -240mV (Rost and S. Rapoport, 1964).

In an oxidation-reduction reaction, the oxidizing and reducing species are, in the absence of external factor, determined by the standard potential: the lowest being the reductant, and the highest, the oxidant. This value of -240mV at pH 7 makes glutathione the reductant in numerous biological reactions. This property can be verified by the necessity for glutathione-deficient cell lines to be supplemented with other reductants such as dithiothreitol (DTT),  $\beta$ -mercaptoethanol or cysteine (Chris M Grant, MacIver, and Dawes, 1996; Cuozzo and Kaiser, 1999). While these observations were conducted in yeasts, the necessity for a thiol-reducing system is also mirrored in mammals lacking glutathione, that either need cystine import and reduction (Mandal et al., 2010). or N-acetylcysteine supplementation (Z.-Z. Shi et al., 2000) to restore viability.

The standard reduction potential can be injected into the Nernst equation to calculate the half reduction potential of glutathione.

$$E = E^{\circ} - \frac{RT}{zF} \ln \frac{a_{red}}{a_{ox}}$$

$$\Leftrightarrow E_{GSH} = E'^{\circ}_{GSH} - \frac{RT}{2F} \ln \frac{[GSH]^2}{[GSSG]}$$

Where:

E is the reduction potential at the condition of interest

$E^{\circ}$  is the standard reduction potential

$E'^{\circ}$  is the formal standard reduction potential

R is the universal gas constant

T is the temperature (in kelvins)

z is the number of electrons transferred

F is the Faraday constant

$\alpha$  is the chemical activities of the reduced and oxidized forms

The formula can be simplified by turning the activities into concentrations by using the formal standard reduction potential, which takes the activities into account under specified conditions such as pH. This calculation then gives access to the ratio of GSH<sup>2</sup>/GSSG as well as a comparison point to whether the glutathione couple is more reducing or oxidizing.

However, thermodynamics might not be as relevant in biological setups. The reduction potential quantifies the tendency for the considered species to be reduced in closed, controlled and equilibrated media. Living organisms are everything but these, with reactions often relying on enzymes that can put the system under kinetic control. Therefore, the values should not be interpreted as decisive values, but rather as informative (Flohé, 2013).

On top of this redox equilibrium, glutathione molecules can be found in different protonation states, due to the two carboxylic acids, amine and thiol functions within its structure. The predicted pKa of each function suggests that the most abundant form of glutathione at physiological pH is negatively charged, with the glutamic acid moiety in its zwitterionic form, the thiol in the neutral protonated form, and the glycine carboxylic acid deprotonated (

**Figure 2).** This form then suggests that GSH cannot diffuse across membranes, which entails transport systems across lipid layers (Matsui et al., 2020).

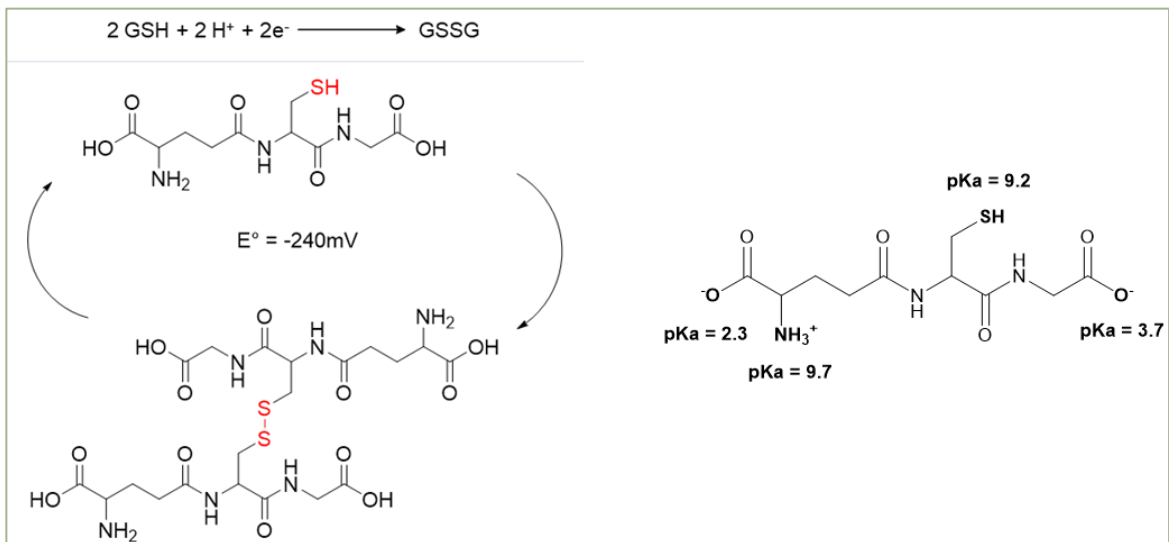


**Figure 2 – Glutathione half reduction reaction and equilibrium with glutathione disulphide (left) Glutathione predominant form at pH 7.4 (right) , adapted from (Matsui et al., 2020)**

We saw that free glutathione could be found in its reduced form, or as a disulfide. But glutathione species include more than those two forms, and other oxidized glutathione structures have been described (**Figure 3**). Indeed, glutathione can be found as a conjugate with either toxic electrophiles or heavy metals. A single glutathione molecule can also be linked to protein cysteine residues. Glutathione has also been observed, although more scarcely, as a polysulfide, a persulfide or as an S-nitrosated derivative (Oestreicher and Morgan, 2019).

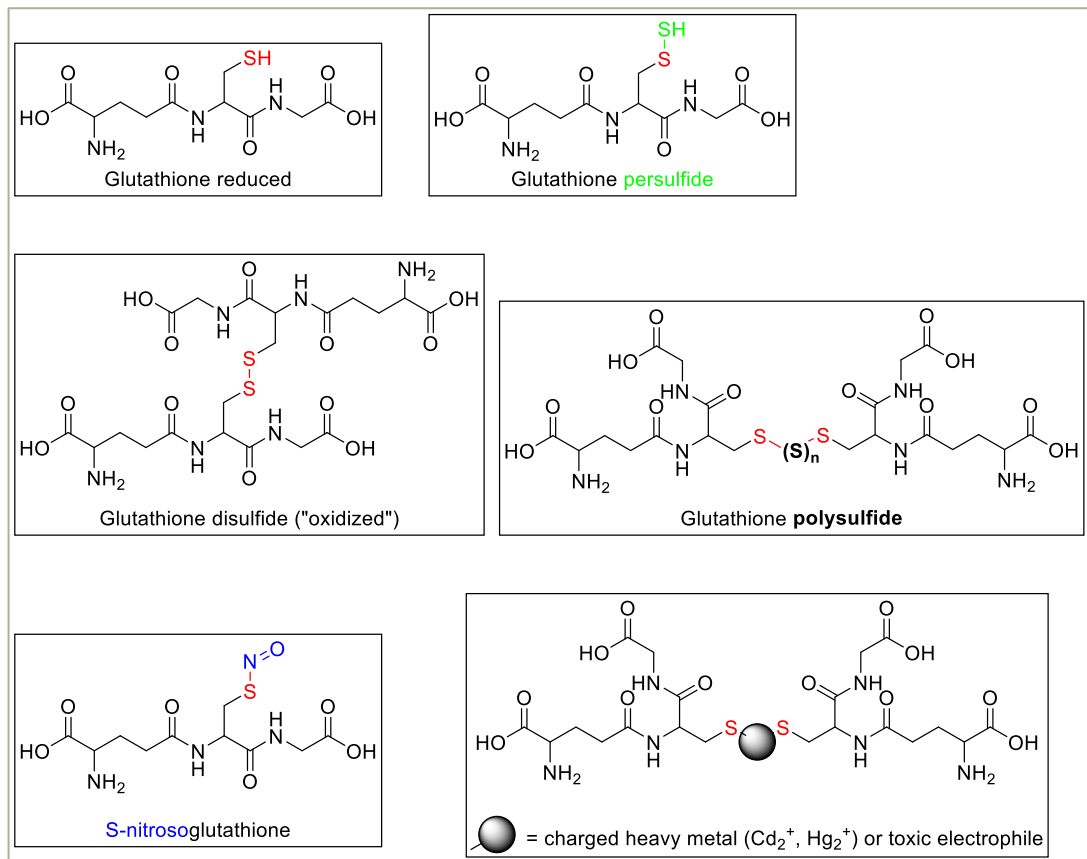


**Figure 3 – Glutathione species encountered in cells**, adapted from (Oestreicher and Morgan, 2019)

### C. GLUTATHIONE CAN BE FOUND IN A VAST MAJORITY OF ORGANISMS AT THE SUBCELLULAR LEVEL

Glutathione has been observed in many prokaryotes, as well as in a wide range of eukaryotic species, such as yeast, drosophilae, nematodes, plants, mice and humans (Oestreicher and Morgan, 2019). The few species devoid of glutathione also display an alternative low molecular thiol (**Figure 4**). Hence, mycothiol and bacillithiol are sugar-based thiols that can be found in actinobacteria, that perform the same functions with a somewhat comparable system (Ezeriņa and Messens, 2022). In parasitic protozoa, trypanothione replaces glutathione and its functions (Fairlamb et al., 1985). Likewise, in plants, slightly modified glutathione molecules are described. The usual glycine can be replaced with alanine, serine or even another glutamate amino acid, and in some cases, the modified GSH coexists with the standard glutathione form (Noctor et al., 2011). This was observed for example in legumes that display both glutathione and homoglutathione systems, each of the molecules having a dedicated synthetase with a higher specificity for glycine and  $\beta$ -alanine respectively (Moran et al., 2000). The same was observed in plants of the *Poaceae* family from which  $\gamma$ -glutamylcysteinylserine was extracted alongside glutathione (Klapheck et al., 1992).

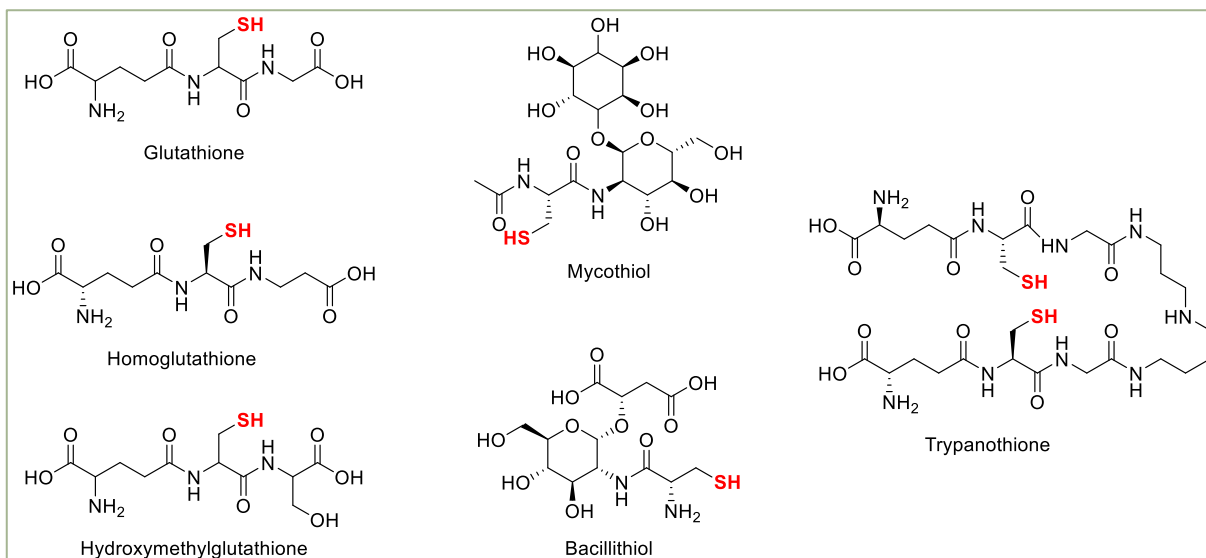


**Figure 4 – Abundant, reduced, and low molecular weight thiols identified among species**

In the cytosol, glutathione is frequently detected in the millimolar range, mostly in its reduced state. Quantification of glutathione relies on techniques that are able to sense free glutathione both in the reduced GSH or oxidized GSSG forms, so they might miss out on some forms or conjugated species of glutathione. Moreover, up until recently, glutathione quantifications were made on cell lysates, meaning only total cellular glutathione was actually assessed. Even though subcellular estimations are often lacking, it is believed that glutathione is present in many, if not all organelles.

This metabolite is essential in many species. For instance, the deletion of a fragment of the gene encoding the rate-limiting enzyme for glutathione synthesis leads to embryonic lethality in mice (Winkler et al., 2011) and *Arabidopsis* plants (Cairns et al., 2006). Similarly, yeasts lacking this synthesis enzyme show a growth impairment that can only be rescued by exogenous glutathione supplementation. Notably, while glutathione is detected in the millimolar range, submillimolar quantities of GSH are enough to restore viability of the depleted strains (Chris M Grant, Maclver, and Dawes, 1996; Kumar et al., 2011). The essential role of GSH was therefore suggested to be linked to its implication in the mitochondrial steps of iron-sulfur clusters biogenesis (see **Role in iron metabolism**) rather than its redox buffering properties. (Sipos et al., 2002; Kumar et al., 2011; Y. Wang et al., 2021)

#### D. GLUTATHIONE SYNTHESIS AND METABOLISM WITHIN CELLS

##### GLUTATHIONE SYNTHESIS

In 1951, Robert Johnston and Konrad Bloch described glutathione synthesis for the first time. They observed that the conversion of marked glycine into glutathione is possible in liver extract, and that ATP is a necessary component of the reaction (Johnston and Bloch, 1951). One year later, John E. Snoke and Bloch observed that the reaction was actually divided into two ATP-dependent steps, of which  $\gamma$ -glutamylcysteine is the middle point (Snok and Bloch, 1952). Their research led subsequently to the extraction and description of the enzyme system responsible for such transformation:  $\gamma$ -glutamylcysteine ligase (GCL) that would link glutamate and cysteine (Mandel

and Bloch, 1955), and glutathione synthetase (GS) that produces GSH from  $\gamma$ -glutamylcysteine and glycine (Snoke *et al.*, 1953, **Figure 5**).

In mammals, GCL is a heterodimer of two units: a heavy catalytic subunit GCLC (73 kDa) and a light modifier subunit GCLM (31kDa). While GCLC is the catalytically active subunit, GCLM is inactive, but enhances both the affinity of GCLC for glutamate and the inhibition of the enzyme by the terminal product, GSH. GCLC also shows drastically reduced GSH synthesis when *Gclm* is knocked out in mice (Lu, 2013). In yeast, the GCL equivalent Gsh1 is a single protein with two domains (Ohtake and Yabuuchi, 1991).

Overexpression of Gsh1 in yeast, leads to GSH accumulation (Grant *et al.*, 1997), however, overexpression of GS does not. Besides, the intermediate  $\gamma$ -glutamylcysteine is present in extremely low concentration in the cell when GS levels are untouched (Lu, 2013). These findings indicate that the rate-limiting step of glutathione synthesis is the first one, catalysed by GCL. Two factors regulate GCL activity: GSH, acting as an inhibitor for the enzyme (Richman and Meister, 1975), and cysteine availability (Meister and Anderson, 1983).

Localisation-wise, glutathione synthesis takes place for the vast majority of organisms in the cytosol solely. One exception stands in the plant kingdom, where GCL is located in the plastids, while GS is located both in the plastids and in the cytosol (A. Wachter *et al.*, 2005; Maughan *et al.*, 2010).

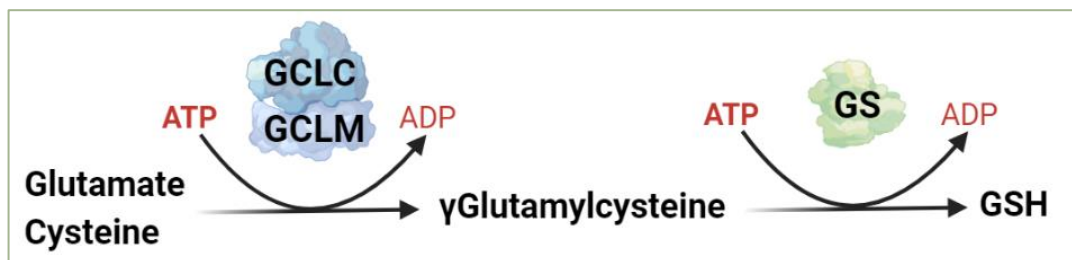


**Figure 5 – Glutathione enzymatic synthesis process in mammals**

## GLUTATHIONE DEGRADATION

The atypical  $\gamma$ -link in the structure of GSH renders the tripeptide immune to aminopeptidase degradation. Extracytosolic degradation of GSH rather occurs *via* a specific enzyme,  $\gamma$ -glutamyl transpeptidase (GGT) that localizes to the plasma membrane of mammalian cells and bacteria, or to the vacuolar membrane of plants (Nakano *et al.*, 2006) and yeasts (Jaspers, 1984; Mehdi, Thierie, and Penninckx, 2001). Although the fate of vacuolar GSH is unclear in yeast because it was shown that GSSG transported into the vacuole remains intact for at least 60 minutes (Morgan *et al.*, 2013)

Alton Meister initially proposed this degradation step as a link in a process he coined the  *$\gamma$ -glutamyl cycle*, a pathway integrating glutathione synthesis, export and degradation within and outside the cell for the purpose of exchange and storage of amino acids (Orlowski and Meister, 1970, **Figure 6**).

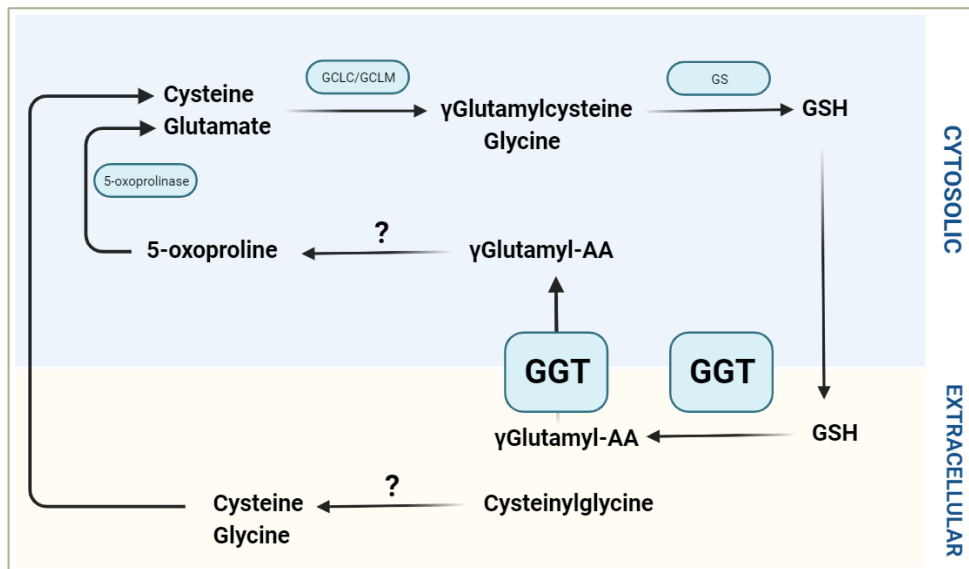


**Figure 6 – The  $\gamma$ -glutamyl cycle**, proposed by Alton Meister, adapted from Bachhawat and Yadav, 2018

This cycle underwent a few arrangements and corrections since its first proposition in 1970. As proposed in 2018 in a revised form of the *Glutathione cycle* (Figure 7), glutathione is synthesized in the cytosol by the GCL holoenzyme and GS as described above. After, GSH is transported and broken down outside of the cytosol by GGT into cysteinylglycine and glutamate. Dipeptidases break down cysteinylglycine into cysteine and glycine that can then be transported back alongside glutamate into the cytosol for GSH synthesis (Anand Kumar Bachhawat and Yadav, 2018).

This reviewed cycle integrates a novel cytosolic degradation pathway for glutathione by the recently described ChaC enzymes (Kumar 2012). ChaC enzymes belong to a family of  $\gamma$ -glutamyl cyclotransferases ( $\gamma$ -GCT). Those enzymes can convert GSH to 5-oxoproline and cysteinylglycine, and the resulting 5-oxoproline can in turn be recycled into glutamate by 5-oxoprolinases, rendering the three amino acids constitutive of GSH.

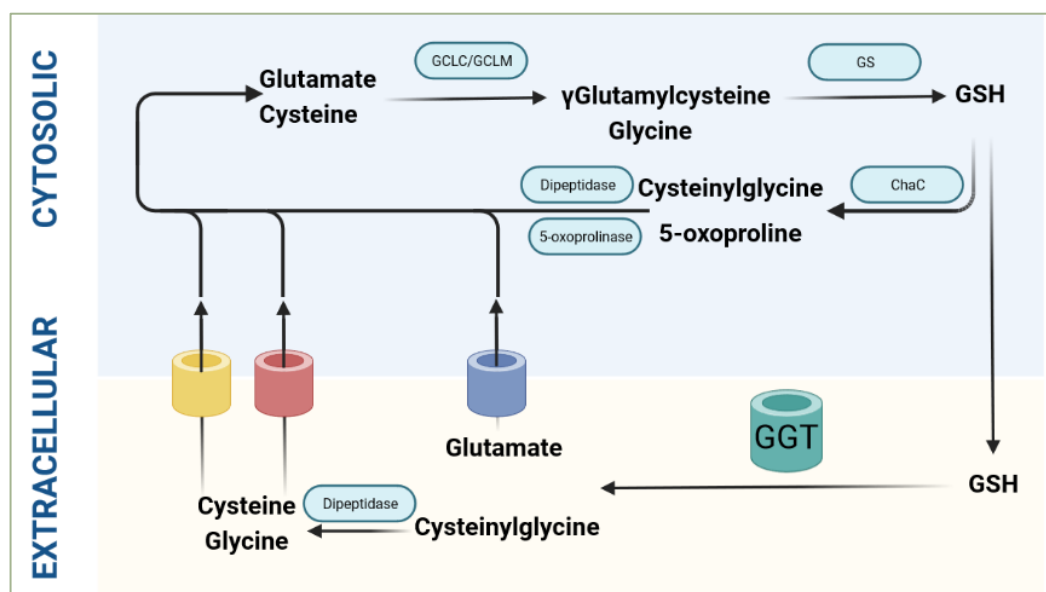


**Figure 7 – The revised *Glutathione Cycle***, proposed by and adapted from Bachhawat and Yadav, 2018

Although it can be compared to its mammalian counterpart, the yeast glutathione cycle includes an additional intracytosolic degradation route coined the DUG (**D**efective in **U**tilization of **G**lutathione) pathway. Bachhawat *et al.* initially proposed a glutathione degradation pathway independent of GGT in yeast, after observing that *Saccharomyces cerevisiae* strains could use glutathione as their sole sulfur source even in the absence of the GGT protein (Kumar, Sharma, and Bachhawat, 2003). They later described a set of three genes involved in the GGT-independent degradation, DUG1, DUG2, and DUG3. DUG1 encodes the cys-gly dipeptidase that breaks down the degradation product of Dug2p and Dug3p that form the heterodimeric enzyme responsible for glutathione cleavage (Ganguli, Kumar, and Bachhawat, 2007). While the DUG pathway has been observed in yeast and fungi, it is absent in plants, bacteria and animals.

Another difference in yeast is the presence of the high affinity glutathione transporter HGT1 (described in a following chapter) that allows the specific uptake of glutathione species directly from the extracellular milieu to the cytosol. However, this transporter is absent in higher eukaryotes.

## II GLUTATHIONE FUNCTIONS

### A. GLUTATHIONE SERVES AS AN ANTIOXYDANT EITHER ALONE OR AS A PROTEIN COFACTOR

#### GLUTATHIONE REDUCTASE

As described above, glutathione can be found in a large variety of organisms and organelles. As one of the most abundant non-protein thiols, one of the main adjectives used to qualify glutathione is *antioxidant*, or reductant. Therefore, glutathione is oxidized in cellular processes and needs to be recycled back into its reduced state. This is guaranteed by glutathione reductase (GLR), a flavoenzyme highly conserved across evolution. The enzyme can be found in the cytosol, but also in the mitochondrial matrix as well as in chloroplasts (Outten and Culotta, 2004; Mbemba et al., 1985; Creissen et al., 1995). GLR utilizes the reducing power of NADPH in a two-step ping-pong mechanism. In the first part, the disulphide bridge between the catalytic cysteines is reduced thanks to a charge transfer from NADPH to FAD. The cysteine right next to the FAD group engages in a charge transfer, while the second, more distant cysteine is free to perform a nucleophilic attack on oxidized GSSG, freeing one GSH molecule (Figure 8).

The second GSH molecule is liberated when the charge transfer cysteine attacks the second, glutathionylated one, generating an intramolecular disulphide on GLR (Deponte, 2013).

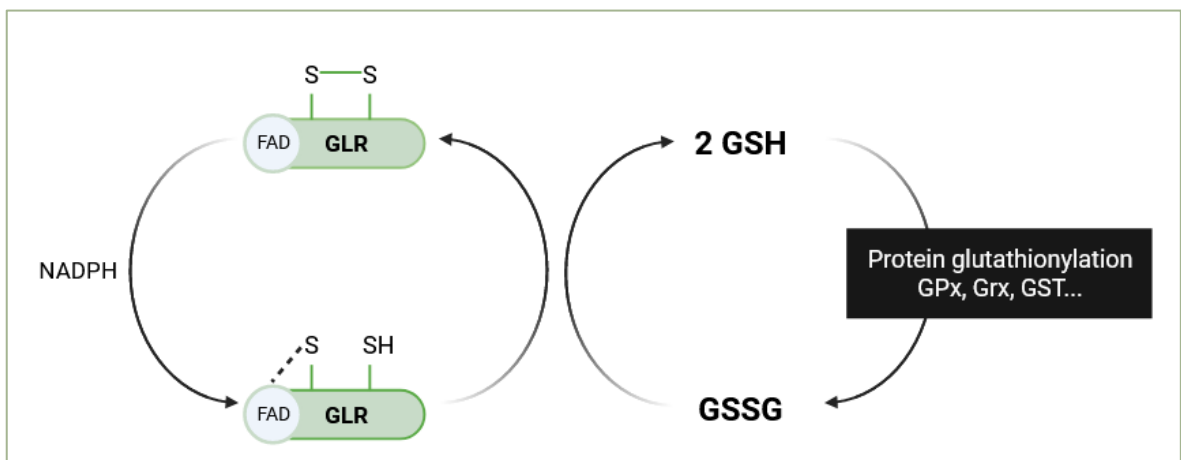


**Figure 8 – Glutathione Reductase (GLR) cycle** Glutathione disulfide is reduced in the cytosol, the mitochondrial matrix, or chloroplasts, by glutathione reductase at the expense of NADPH. Dotted lines indicate a charge transfer bond

---

## GLUTATHIONE PEROXIDASES

Reactive Oxygen Species (ROS) are naturally occurring, oxygen-containing byproducts of aerobic metabolism. The reduction of molecular  $O_2$  leads to the formation of the superoxide anion  $O_2^{\cdot-}$  which in turn leads to the formation of most other ROS such as  $OH^{\cdot}$  or  $H_2O_2$ . One of the key features of ROS is their high reactivity and ability to cross react with membranes, proteins or even DNA, making them hazardous when produced in unmanageable amounts (Imlay, 2008). However, ROS also fulfil crucial roles from signalling (Hancock, Desikan, and Neill, 2001) to being a part of enzymatic mechanisms such as ribonucleotide reduction (Lundin et al., 2010).

Glutathione being an antioxidant means that it can prevent the accumulation of ROS by scavenging some of them, both non-enzymatically (Galano and Alvarez-Idaboy, 2011) as well as with the assistance of enzymes like glutathione peroxidases (GPXs). These enzymes are thiol-based oxidoreductases that rely on the affinity of their active site thiols for peroxides to reduce hydrogen peroxide and other lipid peroxides to their corresponding alcohols. GPXs then necessitate GSH molecules to be recycled back to their active form. This reduction process then yields GSSG molecules that need to be recycled by glutathione reductase at the expense of NADPH. (Deponte, 2013)

In mammals, 8 GPXs have been identified and detected in the cytosol, both the mitochondrial IMS and matrix as well as the nucleus (Buday and Conrad, 2021). Interestingly, GPX7 and GPX8 were shown to be resident of the endoplasmic reticulum. Although they are called glutathione peroxidases, Ruddock *et al.* showed that they have a weak activity in that regard. Instead, they exhibit a PDI-dependant peroxidase activity. This activity could be relevant to oxidative protein folding, as discussed in a subsequent chapter (Nguyen et al., 2011).

GPXs either display selenocysteine or cysteine as a catalytic residue. In a ping pong mechanism again, the catalytic (seleno)cysteine attacks the peroxide, freeing its corresponding alcohol. While this mechanism is conserved for any thiol-based peroxidases, its resolution is what distinguishes GPXs from glutathione-independent peroxidases. In GPXs, the catalytic residue remaining is a selenic or sulfenic acid that can be reduced back to the corresponding (seleno)cysteine thanks to the sequential attack of two GSH molecules that yields one  $H_2O$  molecule as well as GSSG (Deponte 2013, **Figure 9**). The resolution of the acid rather proceeds by formation of a disulfide that can be undone by distinct reductant depending on their subtype and organism (Wood et al., 2003).

Yeasts do display 3 GPX-like enzymes with similar subcellular localizations, as well as peroxiredoxins but both are actually relying on thioredoxin rather than GSH as a reducing power (Toledano et al., 2007).

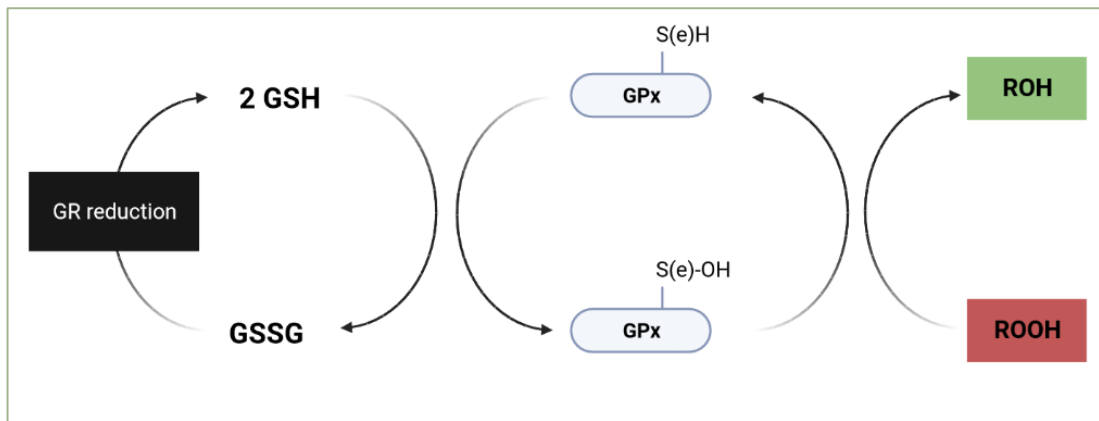


**Figure 9 – Glutathione recycles reduced GPx in the process of peroxide reduction**

## GLUTAREDOXINS

Free –SH groups in proteins are sensitive to oxidation. On one hand this supports the necessary formation of disulphide bridges that allows the proper functioning of proteins, but on the other hand, these functions can be oxidized up to an irreversible point by reactive oxygen or nitrogen species. These modifications can in turn affect the protein function, stability, or localization (Ulrich and Jakob, 2019). Glutathione molecules can form mixed disulphide bridges with the free cysteines of these proteins, in a process called S-glutathionylation. This modification, glutathionylation, can be the result of various reactions of a glutathione moiety, either with free cysteine, or modified cysteines such as thiyl radicals, sulfenic acids or nitrosothiols that were formed following radical damage (Figure 10). The reversible modification of free thiols by glutathione is suggested to have a role in protecting protein and GSH pools from such an oxidative challenge that could irreversibly damage the protein, and possibly hinder its functions (Dalle-Donne et al., 2009).

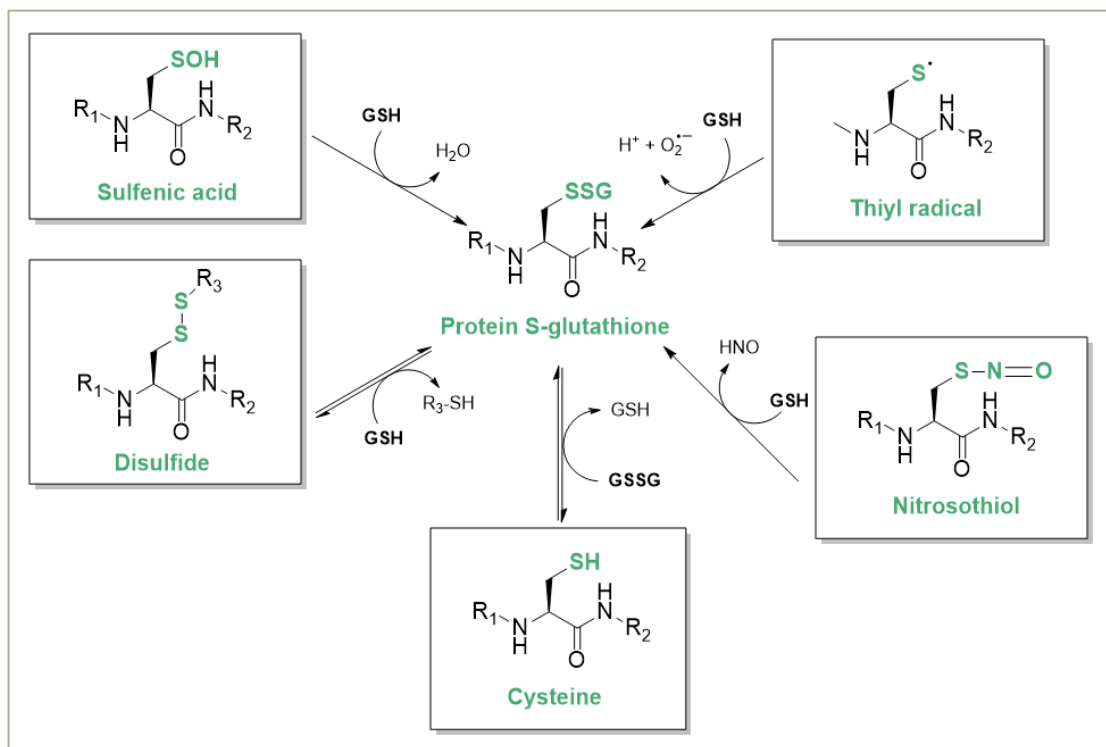


**Figure 10 – Protein-glutathione species** Multiple thiol species can be modified by glutathione to yield glutathionylation products. Adapted from (Alcock, Perkins, and Chalker, 2018)

These glutathionylated thiols in proteins can be reversed to their reduced state thanks to the action of Glutaredoxins (GRXs). GRXs were initially named after studies in *E. coli* lacking a thioredoxin system. Arne Holmgren identified an alternative ribonucleotide reductase (RNR) hydrogen donor that was depending on GSH, although in this case, the protein was involved in the reduction of a disulfide bridge in RNR, which is another ability of GRXs (Holmgren, 1976). GRXs are members of the thioredoxin superfamily, and as such, possess a characteristic thioredoxin fold, an architecture made of 100 or less amino acids arranged in central  $\beta$ -strands flanked by  $\alpha$ -helices, as well as an active site with a CXXC/S motif (Martin, 1995). While structurally related to thioredoxins, GRXs differ from these by their specificity towards glutathione, supported by the presence of a GSH binding site (Deponete, 2013).

Yeasts display 8 GRXs that can be distinguished by their active site structure. GRXs 1/2/8 are dithiol glutaredoxins (CXXC active site), and GRXs 3/4/5/6/7 are monothiol glutaredoxins (CXXS active site). Humans display dithiol Grx1 in the cytosol mostly, and Grx2 in the mitochondria. Grx3 and Grx5 are very conserved and found in human as well, in the cytosol and the mitochondria respectively (Ogata et al., 2021).

GRXs also use glutathione as a cofactor and produce GSSG in the process, just like GPXs. Their mechanism can be divided in two categories, each depending on their active sites.

- In the monothiol mechanism (Figure 11), a nucleophilic attack from the GRX thiolate transfers the mixed disulfide from the protein to the attacking cysteine. While the reduced protein is freed, the GRX is regenerated by the attack of a GSH molecule, and yields one GSSG molecule, and the reduced GRX (Deponete, 2013). Monothiol mechanism refers to the involvement of one cysteine of the GRX protein, but it has to be noted that dithiol GRXs can perform deglutathionylation reactions.

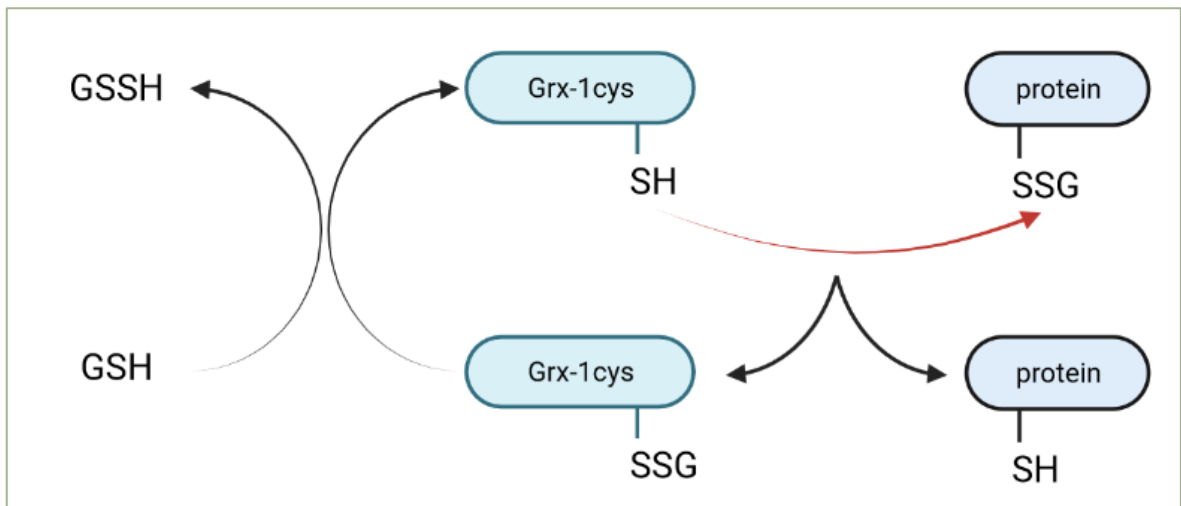


**Figure 11 – Monothiol mechanism of Grx catalysis for glutathionylated substrates.** Note that dithiol GRX can perform the same reaction.

- In the dithiol mechanism (**Figure 12**), a disulfide exchange occurs between the initially oxidized substrate, and the reduced GRX: the thiolate from the CXXC active site attacks one cysteine of the disulfide bond in the protein and thus forms an intermolecular bond. This bond is resolved by the attack of the second cysteine of the GRX active site, yielding the reduced substrate and oxidized GRX. Two GSH molecules then reduce the disulfide bond of the GRX, regenerating a reduced GRX as well as one GSSG molecule (Deponce, 2013). The ability of monothiol GRXs to achieve this dithiol mechanism is less clear. While the *E. coli* version of Grx1 needs two cysteine residues to perform the reduction of a disulfide model (Bushweller et al., 1992), human dithiol Grx with a mutation of its resolving cysteine to serine was still able to carry out the reduction of Ribonucleotide Reductase (Avval and Holmgren, 2009)

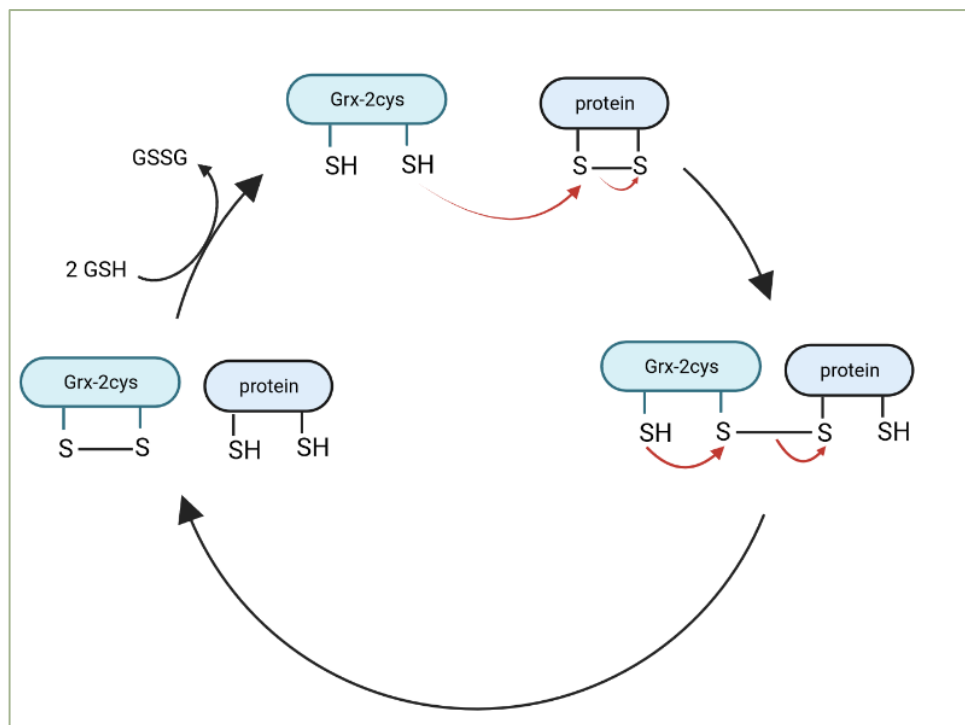


**Figure 12 – Dithiol mechanism of Grx catalysis for oxidized substrates**

## GLUTATHIONE S-TRANSFERASES

Glutathione also intervenes in the protection of cells *via* its role in detoxification of xenobiotics and other broad electrophiles. Glutathione S-transferases (GSTs) are enzymes that catalyse the binding of a GSH molecule to the electrophilic center of drugs, pesticides and xenobiotics and as such, make up for 10% of the soluble protein mass in liver extracts. The conjugate can then be transported out of the cell for further elimination. (Board and Menon, 2013)

Enzymes of the GST family can be found in the cytosol, the mitochondria, and in microsomes, although these enzymes are structurally different from the 2 formers, and are described as membrane-associated proteins involved in eicosanoid and glutathione metabolism (MAPEG) (Hayes, Flanagan, and Jowsey, 2005).

Mechanisms seem highly dependent on the geometry of the substrate, but relies on the principle of nucleophilic substitution (Deponte, 2013).

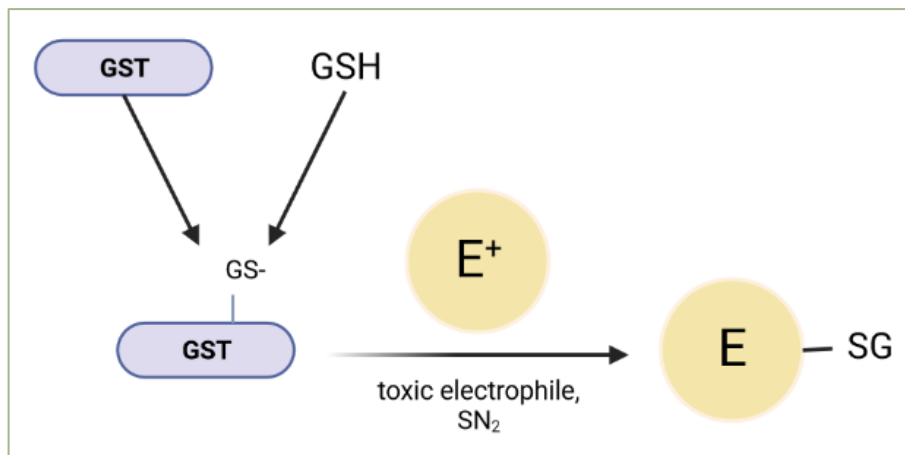


**Figure 13 – GST transfers a glutathione molecule onto electrophile by nucleophilic substitution**

---

## B. ROLE IN IRON METABOLISM

A link between glutathione and iron metabolism has been suggested for the first time in 1997. Kispal *et al* tried to elucidate the role of the ABC transporter ATM1 in yeasts and designed mutants carrying a disruption of the *ATM1* gene. They observed that these cells accumulated 30 times more free iron in their mitochondria. On top of that, mitochondria of  $\Delta atm1$  yeasts also had increased glutathione levels as well as a shift towards a more oxidized GSH:GSSG ratio (Kispal *et al.*, 1997).

Iron accumulation in the mitochondria is one of the key features of defective Iron-Sulfur (Fe/S) Clusters (ISC) biogenesis (Lill and Kispal, 2000), which is why Sipos *et al.* investigated the correlation between glutathione levels and ISC biogenesis (Sipos *et al.*, 2002). While mitochondrial Fe/S proteins were intact upon GSH depletion (achieved by deletion of *GSH1*, the gene encoding the rate-limiting enzyme for GSH synthesis), cytosolic Fe/S proteins showed drastically decreased Fe incorporation and activities in  $\Delta gsh1$  strains. While DTT restores cells viability, the addition of the reductant was no help in rescuing the activities of the proteins, suggesting the specific need for GSH rather than a protection against oxidative damage.

Additional studies have since then taken a look at the relationship between glutathione and iron metabolism. For instance, Rutherford and colleagues showed that glutathione depletion induced elements of the iron regulon, a set of genes involved in iron sensing and transport, regulated by the transcriptional activators Aft1 and Aft2 (Rutherford *et al.* 2005). Overall, glutathione depletion shares similarities in phenotype with the depletion of proteins involved in the export of ISC, indicating a potential involvement in that aspect (Lill, 2009).

Finally, a genome-wide study of the consequences of both GSH depletion as well as GSH overload in *S. cerevisiae* was published in 2011 (Kumar *et al.*, 2011). GSH depletion was achieved by growing  $\Delta gsh1$  yeast strains in the absence of exogenous GSH. Conversely, GSH overload was provoked by using strains overexpressing HGT1, the high affinity GSH transporter, and treating them with  $\mu\text{M}$  of exogenous GSH. Saturation of HGT1 led to a 10-time increase of GSH intracellular levels, and a 5-time increase was used to conduct transcriptomic analysis.

The interpretation of the mRNA profiles of both experimental conditions highlighted in each case a strong iron starvation-like signature which included an upregulation of the Aft1/Aft2 regulon. Toxic levels of GSH did cause a redox response with the induction of the Unfolded Protein Response (UPR), a stress response to ER proteins reduction. This effect was not mirrored in GSH-depleted cells, in which the alteration of iron metabolism was the pre-eminent effect, leading to cell death. In these conditions, while DTT could not fully rescue the wild-type phenotype, the addition of exogenous iron could. These data led Kumar and coworkers to suggest that the necessity of glutathione for viability was rather linked to an activity in iron metabolism rather than the conventional reductase activity of the tripeptide.

### C. ROLE AS A THIOREDOXIN BACK-UP SYSTEM

The aforementioned study from Kumar *et al.* examined the already questioned role of glutathione in thiol redox control which seemed minimal, compared to the implications of GSH availability in iron metabolism. They renewed the observation that GSH depletion did not cause major redox imbalance in the yeast *S. cerevisiae* (Le Moan et al., 2006). To further assess the function of GSH in regards to redox control, they evaluated how GSH intervenes in strains lacking thioredoxin reductase (TRR).

Acting in parallel to the GSR/GSH/Grx pathway, the thioredoxin pathway shuttles electrons from NADPH to thioredoxin reductase, to thioredoxin, to target proteins and their thiol groups in order to maintain them in a reduced state (Figure 14).

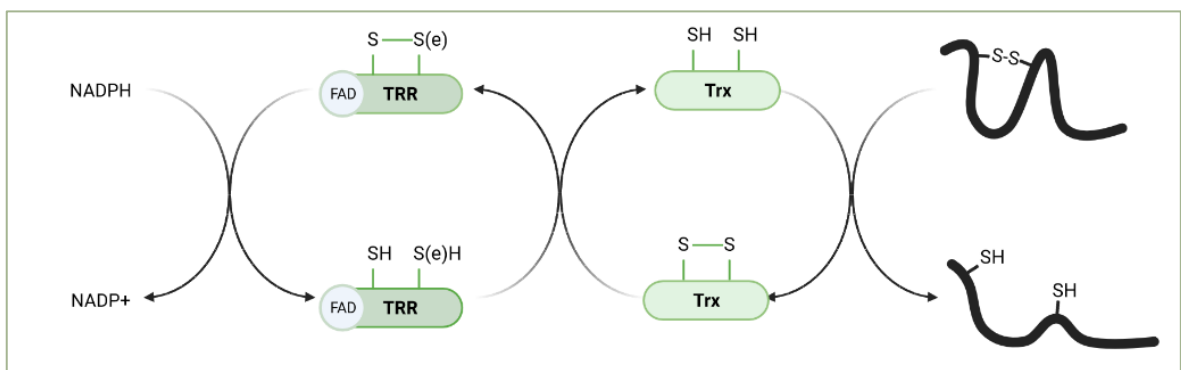


**Figure 14 – The thioredoxin pathway maintains cysteines reduced in an NADPH-dependent way.** (TRR = thioredoxin reductase, Trx = thioredoxin)

There seems to be a redundancy between the thioredoxin and glutaredoxin systems since one becomes essential when the other is inactivated in either yeast (Draculic, Dawes, and Grant, 2000) or mammalian cells (Mandal et al., 2010), but then again, the lack of viability of  $\Delta gsh1$  strains suggests a role for GSH that would be independent of the Trx system.

Kumar *et al.* observed that a strain lacking TRR holds 1.5 to 3 times more total GSH. However, even with this higher GSH content, the strain still required the addition of 200  $\mu\text{M}$  GSH to recover wild-type growth. While  $\Delta gsh1$  strains needed the addition of 0.5  $\mu\text{M}$  exogenous GSH to recover wild-type growth, double mutants  $\Delta gsh1\Delta trr$  needed 400 times more (200  $\mu\text{M}$ ) added GSH to recover the same growth rate.

Strikingly, high levels of glutathione were required to compensate for a thioredoxin system impairment, but the thioredoxin system alone in the absence of GSH maintained a stable redox state. The contrast between the very low demand for GSH in viability and the very high quantities needed to back-up a thioredoxin defect suggests that the essential properties of GSH might in fact not be related to its role in thiol redox control, where it would only serve as a mediocre backup for the thioredoxin system. Alternatively, they suggest that the requirement of glutathione for viability, rather lies in its role in iron metabolism, as depicted by the strong iron starvation-like response to GSH depletion, leading to cell death, and the reversibility of this signature with the addition of trace amounts of GSH.

### III GLUTATHIONS TRANSPORT SYSTEMS

As mentioned above, glutathione is almost always synthesized in the cytosol. However, initial studies have identified glutathione species in almost every compartment of the cell, based on the use of cell fractionation, compartment specific derivatization of GSH with monochlorobimane molecules associated with high-performance liquid chromatography (HPLC), or even electron microscopy coupled with GSH and GSSG specific antibodies (Smith et al., 1996). Those methods allowed the detection of glutathione in microsomes and mitochondria (O W Griffith and Meister, 1985; Hwang, Sinsky, and Lodish, 1992), the cytosol or the nucleus (Bellomo et al., 1992).

These techniques sparked controversies because of technical challenges related to the nature of GSH. Indeed, small molecules such as GSH are known to diffuse, even more so if membranes are somewhat damaged. The sensitivity of GSH to oxidation also makes it hard to appreciate its redox properties in the context of sample extraction. Sample preparation also impedes the evaluation of time-sensitive processes by fixing time. Nonetheless, the observation in subcellular compartments still entails transport systems from the cytosol where GSH is made, to the organelles where it was observed.

The rise of redox sensors and their targeting has confirmed the subcellular presence of GSH, but only a few transporters have been clearly identified, mostly in yeast models. Data on GSH transporters in mammals still remain scarce.

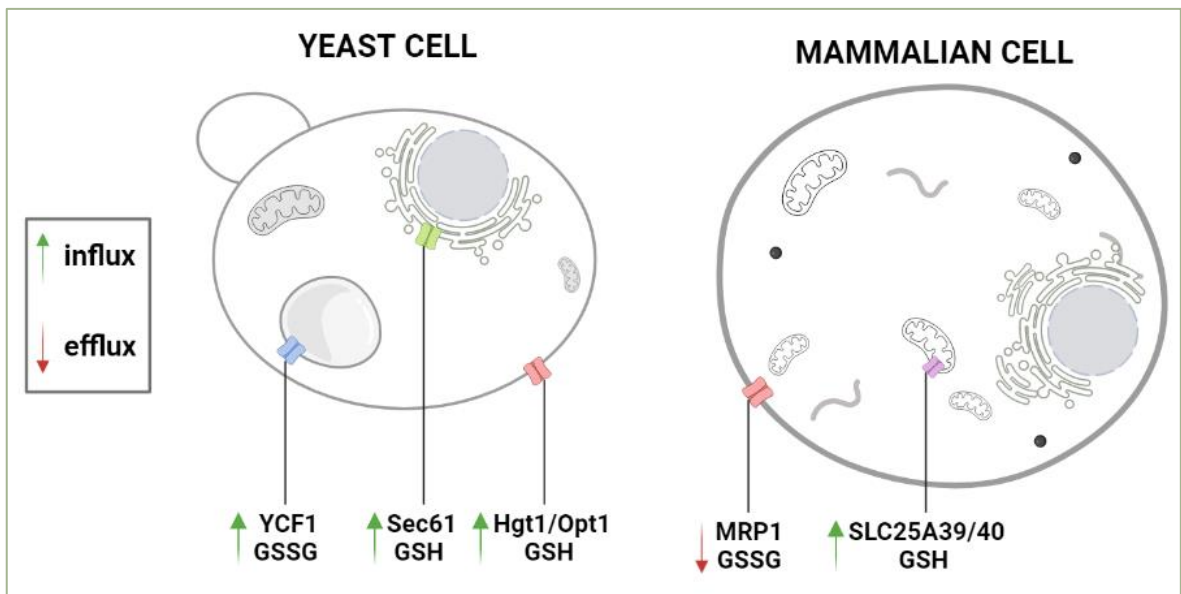


**Figure 15 – Glutathione transporters described and validated in Yeast and Mammalian cells.**

Adapted from Oestreicher and Morgan, 2019

---

## NUCLEAR IMPORT OF GLUTATHIONE?

The nuclear envelope is covered with pores that allow small molecules to get in or out by passive diffusion. It can be admitted that GSH diffuses freely into the nucleus and mirrors cytosolic GSH pools. Yet, some studies suggest that specific accumulation of GSH would take place in the nucleus and play an important part in the cell cycle and proliferation (Vivancos et al., 2010; Diaz-Vivancos et al., 2015; Markovic et al., 2007). Voehringer *et al.* also suggest that glutathione nuclear localization might be a function of Bcl-2 expression (Voehringer et al., 1998). However, as highlighted in an extensive review (Oestreicher and Morgan, 2019), those observations were essentially made using 5-chloromethylfluorescein diacetate (CMFDA) as a specific glutathione tracer which was proven unsuitable (Sebastià et al., 2003). Huang *et al.* did observe nuclear pools of glutathione in yeast with the use of more appropriate targeted rxYFP probe (technique detailed in **Glutathione visualization and study tools**). Interestingly, while wild-type *S. cerevisiae* cells displayed comparable redox properties of cytosolic and nuclear rxYFPs, mutants of the thioredoxin pathway showed significant differences in the oxidation state of the cytosolic and nuclear rxYFPs, which argues in favor of distinct nuclear and cytosolic pools of GSH (Dardalhon et al., 2012).

---

## MITOCHONDRIAL TRANSPORT

---

### IMPORT

Glutathione is present in both sub-compartments of the mitochondria: the intermembrane space (IMS) separating the inner mitochondrial membrane (IMM) and the outer mitochondrial membrane (OMM), and the mitochondrial matrix.

In 2012, Kojer *et al.* observed that the IMS of yeast cells had an  $E_{\text{GSH}}$  value of -301 mV, which is roughly equal to that of the cytosol (-306 mV). They also showed that the GSH content in this compartment equilibrates with the cytosolic GSH content. Then, they established that this equilibration depended on the presence of por1, the predominant isoform of porins on the OMM, suggesting that GSH pools equilibrate between the cytosol and the IMS *via* porins, although a direct transport of GSH was not demonstrated (Kojer et al., 2012).

Regarding the mitochondrial matrix, two members of the SLC25 mitochondrial carriers family were initially proposed: dicarboxylate carrier and 2-oxoglutarate carrier (Z. Chen and Lash, 1998). However, the expression of these transporters in *Lactococcus lactis*, a bacterial system for expression and characterization of mitochondrial membrane proteins (Monné et al., 2005), failed to confirm their involvement in GSH transport (Booty et al., 2015).

Instead, SLC25A39 and its paralogue SLC25A40 were recently identified *via* proteomic studies as the most upregulated mitochondrial transporter upon GSH depletion conditions (GCLC inhibition by BSO treatment or deletion). This result was replicated in multiple human cell lines, namely HeLa cells, K562 cells (myelogenous leukemia bone marrow cells) and 293T cells (Wang *et al.*, 2021).

The authors showed that knockout of *SLC2A39* caused a significant 5 to 10-fold decrease in mitochondrial GSH content, as well as a 6-fold decrease in isotope-labelled GSH uptake, without any modifications of whole cell GSH content. These effects were recapitulated by the mutation of

candidate substrate-binding residues in the protein. These results suggest that a functional SLC25A39 protein is required for mitochondrial GSH import.

Single knockout of *SLC25A39* did not affect proliferation, but the *SLC25A39* and *SLC25A40* double knockout cells could not proliferate in standard culture conditions. Extracellular GSH addition could not rescue this lethal phenotype, but the design of a GSH synthesis system targeted to the mitochondria restored the viability of the double knockout cells, confirming that the essential role of the protein set was due to its involvement in GSH import.

Investigating the physiological impact of mitochondrial GSH depletion led Wang and colleagues to observe that *Slc25a39* knocked-out mouse embryos were not viable past day 13 and showed a severe anemic phenotype. The proteomic analysis of double knockout cells revealed that the most downregulated proteins were iron-sulfur cluster proteins, and that aconitase, an Fe/S protein, had reduced activity. The authors therefore argued, just like Kumar *et al.* (Kumar *et al.*, 2011), that mitochondrial GSH fulfills a crucial role in ISC biogenesis.

---

## EXPORT

In 2014, Lill *et al.* published crystal structures of Atm1, one of which showed glutathione bound to the protein within a cavity made of conserved, charged and polar amino acids (Srinivasan, Pierik, and Lill, 2014). The yeast and plant Atm proteins were both expressed in *Lactococcus lactis* for functional assays and proved to be able to export GSSG outwards but not GSH, in an ATP-dependent manner (Schaedler *et al.*, 2014).

Although these results could hint towards an export system for glutathione, the physiological relevance of these *in vitro* assays remains to be elucidated. Moreover, the yeast protein Atm1p was shown to be involved in the export of Fe-S cluster intermediates from the matrix to the cytosol (Kispal *et al.*, 1999), and glutathione is known to be required in the Atm1-mediated export of ISC as well (Lill, Srinivasan, and Mühlenhoff, 2014), so this *in vitro* assay could just mirror the involvement of GSH in such a process.

---

## VACUOLAR TRANSPORT

In yeast, the ABC-C transporter Yeast Cadmium Protein (YCF1) was identified in 1996 as a cadmium-induced stress resistance protein. Li *et al.* demonstrated that the vacuolar membrane transporter shuttled cadmium-(glutathione)<sub>2</sub> conjugates into the vacuole (Li *et al.*, 1996). Several studies after showed the importance of the transport of glutathione conjugates with either toxic electrophiles or heavy metals such as mercury (Gueldry *et al.*, 2003), lead (Sousa *et al.*, 2015), selenite (Lazard *et al.*, 2011) and arsenite (Ghosh *et al.*, 1999).

Regarding free glutathione, YCF1 transports reduced GSH with a  $K_m$  of ~15mM (Rebbeor *et al.*, 1998) while a higher affinity for GSSG is supported by a  $K_m$  value around 290μM (Lazard *et al.*, 2011). This value supports the argument that GSSG whole-cell level are for the most part determined by vacuolar GSSG levels, which was observed by Morgan *et al.* They also observed that this transport is actually in competition with GSSG reduction by GLR for disposing of cytosolic GSSG and maintenance of the highly reducing GSH pool.

These observations highlighted the necessity of understanding GSH distribution at the subcellular level. Indeed, previous estimations of GSSG concentrations in the cytosol were extrapolated from whole cell measurements, but their experiments involving the deletion of YCF1 demonstrated a highly reduced GSH pool in the cytosol, with a concentration of GSSG potentially up to 1000 times lower than previously estimated (Morgan et al., 2013)

The YCF1 homologs in *Arabidopsis thaliana* ABC-C1 and C2 were expressed in yeasts and proved working in both GSSG and glutathione conjugates import in vitro (Y.-P. Lu, Li, and Rea, 1997; Y. P. Lu et al., 1998). The protein involvement in heavy metals was also replicated (Park et al., 2012; Song et al., 2010).

---

## PLASMA MEMBRANE TRANSPORT

---

### IMPORT

Hgt1/Opt1 is the first high affinity/specificity GSH transporter. It was identified in *Saccharomyces cerevisiae* and displays a Km for reduced GSH around 54µM, but proved to be able to transport GSSG and GSH conjugates as well. Hgt1 uses the inward proton gradient as a driving force to transport both H<sup>+</sup> and glutathione into the cell (Osawa, Stacey, and Gassmann, 2006). Knockout experiments revealed that suppression of Hgt1 abolished uptake of radiolabeled GSH. The deletion of both *HGT1* and *GSH1* (the yeast GCL homologue) is synthetic lethal (Bourbouloux et al., 2000). This result shows that Hgt1 is the main GSH importer in yeast since *GSH1* deleted strains are viable if GSH is supplemented in their media (Chris M Grant, MacIver, and Dawes, 1996).

While protein members of the oligopeptide transporter (OPT) family can be found in prokaryotes, plants and fungi, they do not seem to have homologues in higher eukaryotes and mammals, and to this day, there is no evidence for a high affinity importer of GSH in mammalian cells. Some tissues showed sodium-dependent or independent glutathione transport and led to the identification of organic anion transporters OAT1 and OAT3 as well as dicarboxylate carrier NaC3 in the renal basolateral membrane (Anand K. Bachhawat et al., 2013). These findings were questioned by Hagos *et al.* who suggested that OATs actually transport glutamate derivatives rather than glutathione (Hagos, Burckhardt, and Burckhardt, 2013). It is important to remember that glutathione can also be synthesized after the uptake of its constitutive amino acids as was described in the glutathione cycle previously.

---

### EXPORT

Regarding the export of GSH, the yeast proteins Gex1 and its paralogue Gex2 were reported as potential glutathione/proton antiporters (Dhaoui *et al.* 2011). They localize both to the vacuolar and plasma membranes, and their overexpression induced acidification of the cytoplasm along with a rise in glutathione extracellular levels. Interestingly, Gex expression is induced in conditions of sulfur depletion. Direct measurements of the transport of GSH are still lacking however.

Mammalian cells express members of the ABC-C family proteins: multidrug resistance-associated proteins (MRP). These ATP-dependent proteins seem to be able to excrete glutathione from the cytosol. MRP1 is the closest homologue to YCF1, the vacuolar GSSG importer in yeasts. MRP1 was shown to transport labelled [<sup>3</sup>H]-GSSG from the cytosol to the extracellular milieu with a Km of 93µM

in MRP-transfected HeLa cells (Leier et al., 1996). This observation was replicated in a haploid genetic screen of human HAP1 cells. Cao *et al.* identified MRP1 as a “negative regulator of GSH abundance” and showed that knockout of this transporter promoted ferroptosis resistance in their model by retaining GSH inside cells (J. Y. Cao et al., 2019).

Other ABC family members have been shown to mediate glutathione transport, such as CFTR (ABCC7), ABCG2 in both yeasts (Gxa1, Kiriya *et al.* 2012) and human epithelial cells (Brecht *et al.* 2010), however, the latter results could not be replicated in HEK293 and MCF7 cells (Gauthier *et al.* 2013) and the observations in yeasts were made using extracellular dosage, which would require a more sensitive experiment to confirm them.

---

## ENDOMEMBRANE SYSTEM TRANSPORT

The transport of glutathione in the endomembrane system was first tackled in the endoplasmic reticulum. As the ER was also our focus in this study, a whole section of chapter 2 will be dedicated to the findings of the studies that proposed a combination of multiple quantification techniques to assess glutathione concentration and transport in the ER (see **Transport of glutathione into the ER**)

Little is known about GSH transport into the Golgi, lysosomes or peroxisomes, although transport into the latter could be supported by transient translocation pores. An Opt1/Hgt1 homologue in yeasts, Opt2, was shown to localize at the peroxisome membrane and its deletion disrupted glutathione homeostasis, however, a direct involvement in transport of GSH was not demonstrated (Elbaz-Alon et al., 2014).

Literature is especially scarce regarding the rest of the endomembrane system, but it could be assumed that transport of glutathione could happen partially by vesicular transport between each organelle since they pinch off each other (Deponter, 2017; Oestreicher and Morgan, 2019).



## IV GLUTATHIONE VISUALIZATION AND STUDY TOOLS

The observations conducted above were made possible with the use of different techniques allowing access to GSH. The redox nature of the tripeptide makes it hard to study and extract it without oxidation artifacts, and its small size and molecular weight, along with the specificity of its interactions with proteins as a cofactor makes it impossible to tag and track with proportionally bulky groups. GSH is also ubiquitous and required for normal cell function, making the task even harder. For that reason, specific techniques have been developed to study GSH, and the next chapter will focus on three specific techniques that we used in our study: quantifications of glutathione levels with a specific recycling assay, assessment of  $E_{\text{GSH}}$  with genetically encoded sensors, and marking of glutathione with the use of click chemistry.

### A. CELL AND TISSUE BIOCHEMICAL ANALYSIS

The oldest and most extensively used method for specific glutathione quantification is a recycling assay involving a cycle between glutathione, GLR, and 5,5'-dithio-bis(2-nitrobenzoic acid) (DTNB), also known as Ellman's reagent (Queval and Noctor, 2007; Rahman, Kode, and Biswas, 2006; Owen W. Griffith, 1980).

DTNB is an aromatic disulphide, and was initially developed for the stoichiometric detection of sulfhydryl functions in tissue sample (Ellman, 1959). The cross reaction of DTNB with -SH functions yields one protein-TNB adduct as well as one  $\text{TNB}^{2-}$  molecule. The latter is a coloured molecule whose production can be quantified by measuring the absorbance at 412nm.

In the case of glutathione quantification, glutathione reductase and NADPH are added to the mixture, and the rate of change in absorbance at 412nm is linearly proportional to the quantities of total glutathione in the cell, with  $[\text{GSx}]_{\text{total}} = [\text{GSH}] + 2 \times [\text{GSSG}]$  (Figure 16). The multiplication term for GSSG stems from the reduction of GSSG into 2 GSH molecules.

This assay allows for the quantification of total glutathione and can be derived for the quantification of GSSG only, by blocking free GSH beforehand with 2-vinylpyridine, meaning that GSH and GSSG levels can be separately quantified with this technique.

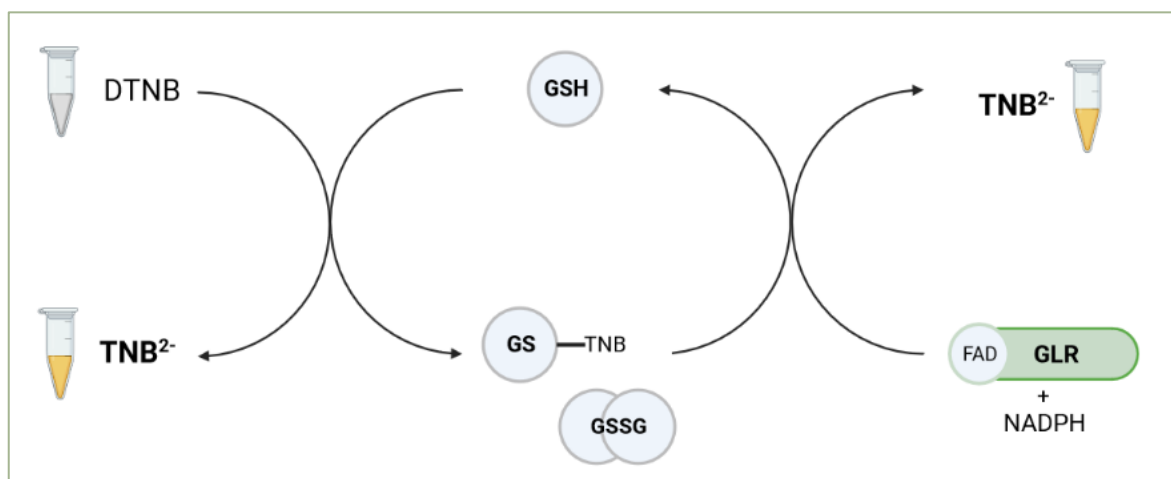


**Figure 16 – DTNB assay applied to GSH quantification.** In the presence of GLR, the generation rate of colored  $\text{TNB}^{2-}$  is proportional to reduced and oxidized GSH in the sample

While this method allows for the precise detection and quantification of both the oxidized and the reduced forms of glutathione, this technique lacks in temporal resolution in a sense that sample preparation fixes the study at specific timepoints, and short or rapid effects in glutathione pools can be missed. Another major drawback of this technique is the lack of spatial resolution that is implied by the sample preparation technique. Since the assay is conducted on cell lysates, only the content of GSH in cells as a whole is assessed, precluding access to information in terms of GSH compartmentation. This information is all the more problematic now that studies acknowledge distinct GSH:GSSG balance in separate subcellular compartments. (Oestreicher and Morgan, 2019)

---

## B. REDOX PROBES: RXYFPS AND ROGFPS

---

### DESIGN

More recently, genetically encoded sensors were developed to sense glutathione on a subcellular scale when addressed to a specific compartment of the cell. These sensors were optimized to equilibrate with the glutathione redox couple and thus provide access to  $E_{\text{GSH}}$ , the reduction potential associated with the glutathione couple in the targeted compartment.

Genetically encoded sensors are based on Green Fluorescent Protein (GFP). GFP is a 238 amino acid, 27 kDa protein that was initially extracted from the bioluminescent *Aequora victoria* jellyfish. The protein was described in a footnote of a paper that was actually focusing on the aequorin protein (Shimomura, Johnson, and Saiga, 1962). Since then, GFP showed attractive features for applications in biology, by being fluorescent and targetable, but chemically inert, stable in a wide range of pH, media and resistant against proteases. The protein was extensively used in biology as a marker for gene expression or protein localization. In 2008, the Nobel Prize in chemistry was awarded to Osamu Shimomura, Roger Tsien, and Martin Chalfie for their respective work on the discovery and development of GFP.

In the case of redox sensors, Østergaard *et al.* initially worked on a GFP variant in which the threonine in position 203 is mutated into a tyrosine. This modification causes a red shift in the fluorescence spectrum with a peak around 528nm, which gave this mutant protein the name Yellow Fluorescent protein (YFP) (R. M. Wachter *et al.*, 1998). The novelty proposed by Østergaard and colleagues was the introduction of a strained disulfide in the vicinity of residues that interact with the chromophore of YFP, which yielded a redox sensitive GFP they named rxYFP. The dithiol and disulfide state of rxYFP can be distinguished by a change in its fluorescence intensity, without any modification of the excitation and emission wavelengths (Østergaard *et al.*, 2001).

Disulfides were also introduced into the structure of GFP to render it redox sensitive. The resulting protein was termed roGFP (Hanson *et al.*, 2004). In this protein, contrary to rxYFP, the equilibrium of the disulfide bond is ratiometric by excitation. This means that the two excitation peaks around 400 and 480nm are strongly dependent on the redox environment of the protein (**Figure 17**).

This ratiometric property means that the redox state of roGFP can be directly determined from the ratios of fluorescence resulting from excitation at 400 and 480nm, while the redox state of rxYFP is often determined by the means of western blot gel, on which the dithiol and disulfide forms can be distinguished and quantified.

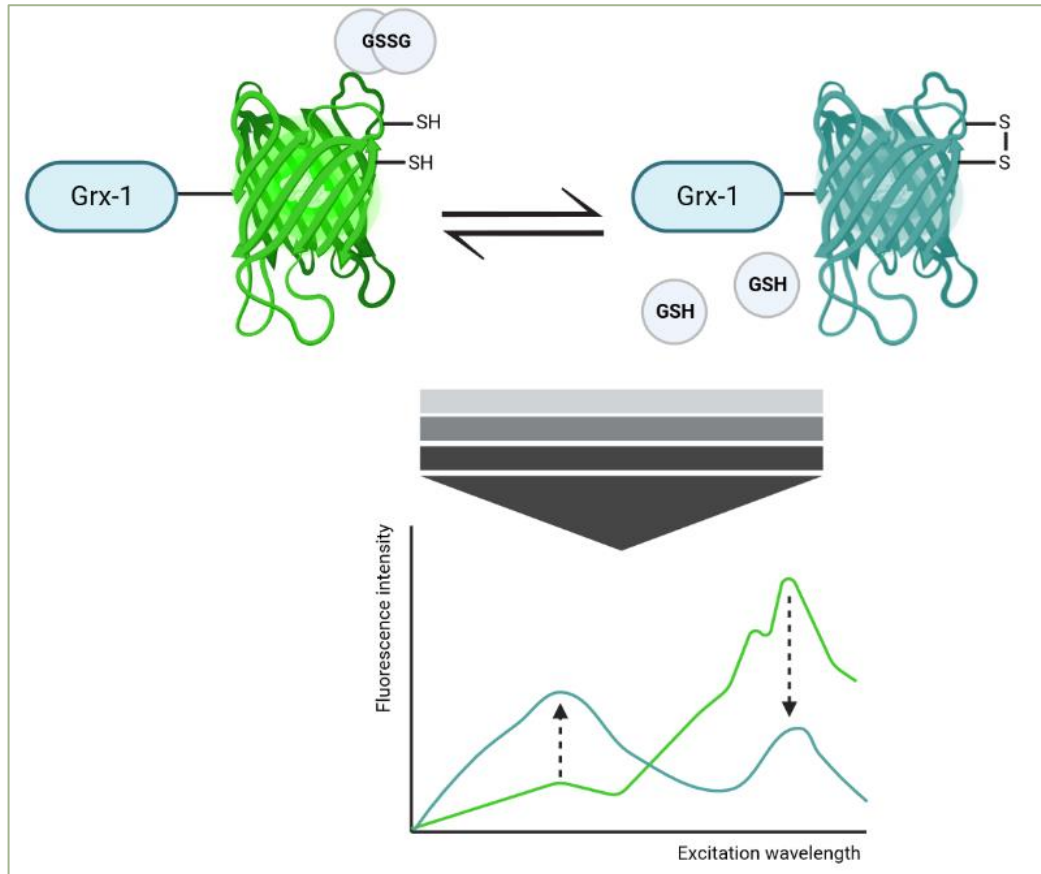


**Figure 17 – Redox sensitive GFP equilibrates with GSH (top) and the ratio of oxidized and reduced forms can be generated from fluorescence spectra (bottom)** Since the GFP and GSH couple are in equilibrium, their Nernst equations can be equalized, and the redox potential of GSH can be calculated from the fluorescence measurements of the sensor.

#### SPECIFICITY TOWARDS GLUTATHIONE

rxYFP and roGFP probes were initially shown to equilibrate *in vivo* with the glutathione redox couple. Dooley *et al.* observed that a BSO pretreatment oxidized roGFPs and sensitized them to H<sub>2</sub>O<sub>2</sub> challenges (Dooley *et al.*, 2004). This specific equilibration is also supported by the observation that the inactivation of GSH synthesis in *Arabidopsis thaliana* cells is accompanied with an oxidation shift of the probe proportional with the severity of the glutathione depletion (Meyer *et al.*, 2007).

Winther *et al.* showed that rxYFP equilibrate with the glutathione couple thanks to the action of glutaredoxins catalysis (Østergaard, Tachibana, and Winther, 2004).

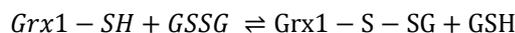
This specificity however, entails the presence of glutaredoxins in the compartment of interest. For that particular reason, fusion proteins were designed. rxYFP was first fused to the yeast Grx1 by Winther and colleagues, which rendered the protein independent of the availability of endogenous glutaredoxins. This fusion also improved significantly both the kinetics and specificity of the probe with the glutathione couple (Björnberg, Østergaard, and Winther, 2006). The same was then done with roGFPs fused to human Grx1 (Gutscher *et al.*, 2008). While the former probe has been less used due to its lack of ratiometric fluorescence, Grx1-roGFPs have been extensively used, and modified to accommodate special needs such as modified midpoint potentials, or enhanced fluorescence (Schwarzländer *et al.*, 2016).

This modification proved its necessity in cells in the determination of the redox potential in the IMS for instance. Hu *et al.* initially determined  $E_{\text{GSH}}$  in the IMS to be -255 mV with the use of an IMS-targeted rxYFP (Hu, Dong, and Outten, 2008). Riemer and colleagues used the same strains and genetic backgrounds, the same targeting sequence, but the dynamic fusion protein grx1-roGFP2 rather than the unfused rxYFP. Their measurements with this probe revealed that the IMS had a much more reducing  $E_{\text{GSH}}$  of -301 mV (Kojer *et al.*, 2012). They suggested that this discrepancy in redox potential might be the result of a limited activity or availability of glutaredoxins in this compartment.

The same phenomenon was observed by Tsunoda *et al.* with ER-targeted probes (Tsunoda *et al.*, 2014). They noticed that the oxidation rate after a DTT pulse of free roGFP2 and its grx1-fused counterpart were significantly different, the rate of the latter being more than halved. They also noticed that the fusion abolished the dependency of roGFP2 on Protein Disulfide Isomerase (PDI), an ER oxidoreductase, in terms of oxidation kinetics.

### Glutaredoxin use as a standalone

Later, the yeast Grx1 protein was used as a standalone to exploit its ability to catalyze its own glutathionylation following the equilibrium (Iversen *et al.*, 2010):



In this context, the thioredoxin fold of Grx1 containing the characteristic CXXC motif was mutated so that the resolving cysteine is absent. As a result, the proportions of reduced and oxidized Grx1 are proportional to that of reduced and oxidized glutathione, proportional to the equilibrium constant defined as:

$$K_{ox} = \frac{[\text{Grx1} - \text{S} - \text{SG}][\text{GSH}]}{[\text{Grx1} - \text{SH}][\text{GSSG}]}$$

This  $K_{ox}$  constant was determined to be  $74 \pm 6$  and subsequently used for determination of the  $[\text{GSH}]/[\text{GSSG}]$  ratio, also called  $R_{\text{GS}}$ , after the protein had been modified to accommodate an N-terminal signal peptide, HA-tag, and an ER retention motif HDEL or KDEL depending on its expression in yeast or in human cells (Ponsero *et al.*, 2017; Montero *et al.*, 2013). Montero *et al.* verified that luminal expression of this mutant did not disturb ER homeostasis in terms PDI-member Erp57 redox state or ER stress onset, which had to be verified, since the ER does not contain Grx enzymes (Montero *et al.*, 2013). The use of this probe as a standalone provided complementary information on the redox state of glutathione, as it gives access to the proportions of reduced and oxidized glutathione, which are not accessible through the use of redox-sensitive GFPs.

## MEASUREMENTS IN VIVO

Because the GFP probes can be genetically targeted to a desired compartment, we can calculate the Nernst equation associated with the probes, noted  $E_{roGFP}$ .  $E_{roGFP}$  is a function of the reduced and oxidized forms of the sensor that can be detected by fluorescence resulting from excitation at around 480 and 400 nm respectively.

$$\Leftrightarrow E_{roGFP} = E'_{roGFP} - \frac{RT}{2F} \ln \frac{[roGFP_{reduced}]^2}{[roGFP_{oxidized}]}$$

Since the probe equilibrates specifically with GSH, we can equate  $E_{GSH} = E_{roGFP}$  and therefore, deduce  $E_{GSH}$  in the compartment where the probe is addressed. Some of the observations conducted with these probes and their corresponding papers were gathered in the following table.

Compartment	Probe	$E_{GSH}$ (mV)	Reference(s)
Cytosol (mammal)	grx1-roGFP2	-290	Gutscher <i>et al.</i> , 2008
Cytosol (yeast)	rxYFP	-289	Østergaard <i>et al.</i> , 2004
Cytosol (yeast)	roGFP2	-320	Morgan <i>et al.</i> , 2013
Cytosol (plant)	grx1-roGFP2	-320	Schwarzlander <i>et al.</i> , 2008
ER (mammal)	grx1-roGFPiE	-208	Birk <i>et al.</i> , 2013
ER (mammal)	roGFPiE	-236	Avezov <i>et al.</i> , 2013
ER (mammal)	roGFPiL	-231	Van Lith <i>et al.</i> , 2011
ER (yeast)	roGFPiE	-230	Delic <i>et al.</i> , 2010
ER (yeast)	rxYFP	-242	Ponsero <i>et al.</i> , 2017
Mitochondria			
Matrix (mammal)	roGFP1	-360	Hanson <i>et al.</i> , 2004
Matrix (plant)	roGFP2	-356	Schwarzlander <i>et al.</i> , 2008
Matrix (yeast)	roGFP2	-340	Ayer <i>et al.</i> , 2013
Matrix (yeast/mammal)	roGFP1/2	-300	Calabrese, 2017
IMS (yeast/mammal)	roGFP1/2	-300	Calabrese, 2017
IMS (yeast)	grx1-roGFP2	-301	Kojer <i>et al.</i> , 2012
Peroxisome (yeast)	roGFP2	-342	Ayer <i>et al.</i> , 2013
Peroxisome (yeast)	grx1-roGFP2	-380	Elbaz <i>et al.</i> , 2014
Nucleus (yeast)	rxYFP	-291	Dardalhon, 2012

**Table 1 – Compartment specificity of  $E_{GSH}$ , in yeast and mammalian cells**

Those sensors revealed a disparity in the redox state of glutathione in organelles. This variability within compartments can be attributed to multiple factors, such as the model of the study. Another factor is the data retrieved from the probe, whether it is by fluorescence or western blotting, might be a source of deviation. Finally, the choice of the sensor's variant is crucial. One key feature of a redox probe is its midpoint potential. The midpoint potential is defined by the middle of the sigmoid curve generated by redox titration of the sensor, it corresponds to the point where the activities of both reduced and oxidized forms of the sensor are equal (Meyer and Dick, 2010). A sensor's midpoint

potential should be adapted to its redox environment, as the reliability of the measurements made with the probe become less reliable as the redox potential of the milieu steers away from that midpoint potential.

The cytosolic glutathione redox potential, or  $E_{\text{GSH}}$ , is fairly reducing, with values ranging from -289 to -349mV depending on the model or the probe that were used. The mitochondrial  $E_{\text{GSH}}$  seems to neighbour values observed in the cytosol with a highly reduced glutathione pool in both subcompartments. Nuclear  $E_{\text{GSH}}$  is also comparable, as was suspected by the fact that nuclear pores might allow free diffusion of glutathione species. Notably, the endoplasmic reticulum displays a much more oxidizing  $E_{\text{GSH}}$  of around -240mV measured in yeast cells, and -208mV in mammalian cells. While no measurements of  $E_{\text{GSH}}$  was done in the vacuole, it can be hypothesized that it would be in the more oxidized range, due to the existence of a dedicated GSSG removal system that redirects cytosolic GSSG in the vacuole (Morgan et al., 2013). However, the disposing of vacuolar GSSG had yet to be elucidated.

The disparity in compartments redox states and their dynamic observations could reflect important disparities in glutathione roles within those compartments, which highlights the necessity of investigation the redox couple locally.

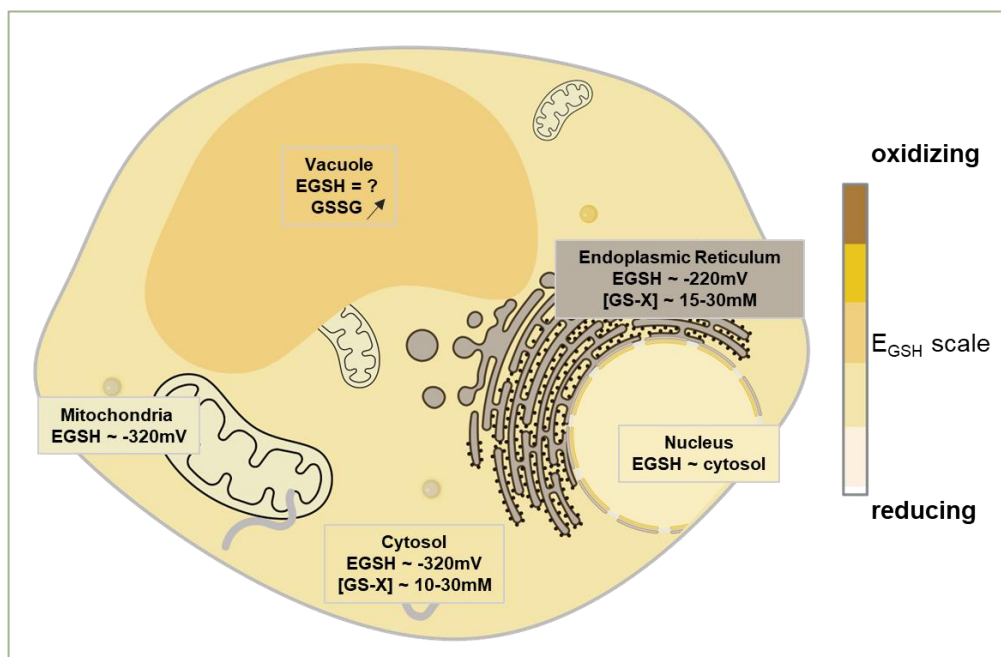


**Figure 18 – Glutathione redox potential in cells** Summary of table 1, adapted from (Oestreicher and Morgan, 2019)

---

### C. CLICKABLE GSH

The previously described techniques have drastically improved the study of free glutathione. We can now quantify reduced and oxidized glutathione in lysates, and reasonably estimate the redox state of the glutathione couple in any compartment of a live cell.

Free glutathione is detected in the millimolar range and as such, is the most prevalent form of glutathione in cells. Nonetheless, as mentioned earlier, glutathione can be found in association with protein thiols in the form of a mixed disulfide, and proteins involved in critical cellular processes such as cell cycle, translation, signalling cascades and mitochondrial proteins were shown to be subjected to some degree of control by glutathionylation (Dalle-Donne et al., 2007). These post-translational modifications have been proved to be involved in protection from hyperoxidation, as in the case of peroxiredoxin 2 in erythrocytes, whose active site cysteine was glutathionylated upon H<sub>2</sub>O<sub>2</sub> treatment; which protected the protein from irreversible oxidation (Peskin et al., 2016). Besides oxidative stress, glutathionylation was also shown to be a protein modification occurring under basal conditions, and is proposed to be involved in redox signaling and protein function modulator. A promising example is the identification of glutathionylation of STAT3, a transcription factor involved in chemoresistance in a variety of cancers. The modification caused apoptosis of chemoresistant, STAT3-expressing cells, suggesting a redox-dependent modulation of the protein function (Butturini et al., 2013).

These features highlight the need for detection of protein glutathionylation, in order to understand and elucidate processes associated with this modification. The detection should be able to discriminate free glutathione from protein bound glutathione, which is not the case with whole lysate glutathione quantifications as we described above.

Methods developed to detect glutathionylations can be based on radiolabelled glutathione by incubation of cells with [<sup>35</sup>S] cysteine. The incubation of radioactivity into proteins is prevented by treatment with a protein synthesis inhibitor, meaning labelling only happens post-translationally. This method led to the first high throughput proteomic approach for glutathionylation identification (Fratelli et al., 2002).

Glutathione can be modified with biotin or even biotin-spermine for subsequent protein pulldown and detection (Chiang et al., 2012), but these tagging functions are rather bulky and might hinder some of the interactions between glutathione and target proteins.

Notably, these techniques imply the addition of modified GSH exogenously, which could have an impact on the redox status of the cell.

Antibody pull-down of glutathionylated proteins can be performed and would avoid the addition of extra GSH, but the specificity of glutathione antibodies is generally not satisfactory enough.

In 2014, the Ahn group developed a technique for the detection of glutathionylated proteins based on click chemistry. Click chemistry encompasses a large array of chemical reactions that share common and convenient features defined by Sharpless and colleagues in 2001. A click reaction should essentially be easy to perform and generate high yields, low byproducts, while working well under a large set of conditions (Kolb, Finn, and Sharpless, 2001).

The Ahn group took advantage of the copper-catalysed azide-alkyne addition, one of the most classic examples of click reaction. This reaction turns an azide and a terminal alkyne into its corresponding triazole using copper catalysis to selectively favour one regioisomer among the two available ones (Hein and Fokin, 2010), see **Figure 19**.

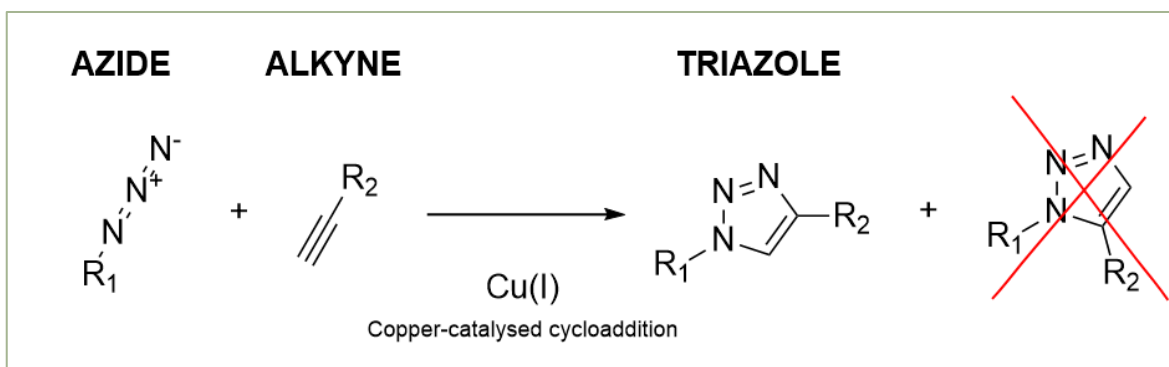


**Figure 19 – Copper-catalysed alkyne-azide cycloaddition**

To detect glutathionylation, the idea was to make cells produce a modified and clickable version of glutathione, bearing the azide handle for cycloaddition (Samarasinghe et al., 2014). To do so, they engineered a mutated glutathione synthetase enzyme that accommodates an azido alanine in place of the usual glycine moiety of GSH (**Figure 20**). Note that in theory, any clickable function could be inserted into glutathione, as long as the modified GS is designed to incorporate the modified amino acid (Kekulandara et al., 2016). By making cells express this modified GS, then feeding them with azido-alanine, 60% of the GSH pool can be turned into an azido-GSH pool in 40 hours.

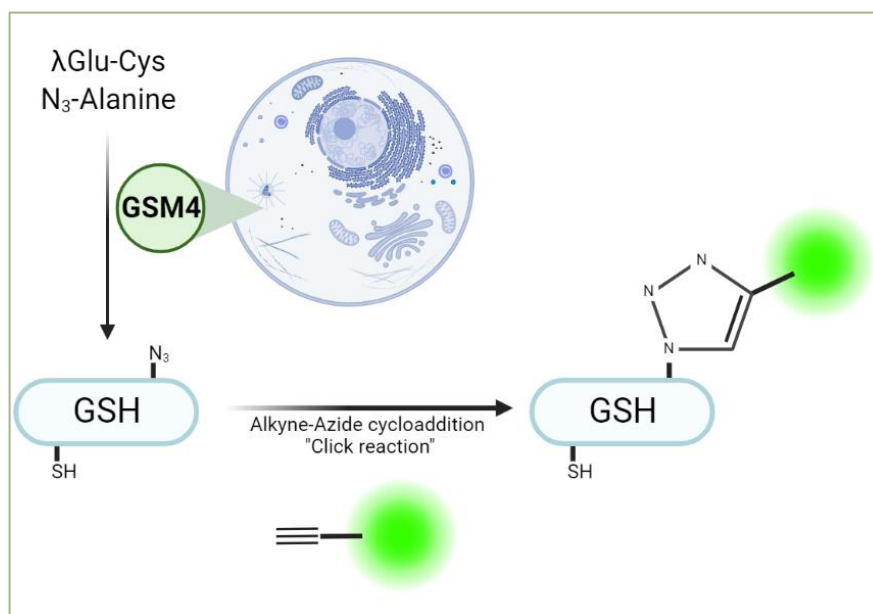


**Figure 20 – Principle of *in situ* click chemistry for glutathionylation detection.** A glutathione mutant (GSM4) is used to incorporate azido-alanine instead of glycine in glutathione, replacing GSH pools with N<sub>3</sub>-GSH pools. N<sub>3</sub>-GSH pools are then free to perform glutathionylation, and the azide handle can be used for detection by subsequent click reaction. (The alkyne-linked molecule can be a fluorophore or a biotin molecule). Adapted from (Samarasinghe et al., 2014)

Azido-GSH is in theory small enough to not be perturbed in its enzymatic interactions, which was confirmed in vitro by assessment of GSH dependant enzyme activity. In cells, it could cross link proteins as expected.

The resulting glutathionylated products can be revealed thanks to the azide handle of azido-GSH by copper-catalysed cycloaddition with biotin-alkyne, either on cell lysates or directly in cell if the alkyne-tag is fluorescent (**Figure 20**).

This clickable glutathione technique was subsequently used for the proteomic glutathionylation analysis in response to glucose starvation and mitochondrial ROS formation (Samarasinghe et al., 2016). This tool was also used for the profiling of glutathionylations in *E. coli* and *Drosophila melanogaster* (Feng et al., 2015).



### I INTRODUCTION TO THE ENDOPLASMIC RETICULUM

The endoplasmic reticulum is the largest organelle in the cell, and consists of a membrane-bound network of tubular sacs and vesicles, in direct communication with the nucleus. It is now widely characterized as a major hub for the biogenesis of lipids and steroids, for calcium storage, and for secreted protein maturation and N-glycosylation.

The ER is a pivotal point for protein synthesis, in particular, oxidative folding. The process of synthesizing proteins was estimated to account for the consumption of up to 45% of the total energy produced by L929 mouse cells (Princiotta et al., 2003). The organelle displays a dedicated oxidative protein folding machinery, shuttling electrons from nascent polypeptides to oxygen. This electron transfer process could be responsible for the production of as high as 25% of total cellular ROS (Tu and Weissman, 2004).

As mentioned previously, glutathione can be found in this compartment, most likely in the millimolar range, which begs the question: what is the role of such a highly reducing compound, inside a compartment this oxidizing?

A big particularity of the redox couple in the ER is the fact that it can be found in a significantly less reducing equilibrium. Indeed, Hwang *et al.* first proposed a GSH:GSSG ratio as low as 3:1 (Hwang, Sinskey, and Lodish, 1992), greatly contrasting the latest estimations of cytosolic GSH:GSSG, that could reach as high as 50 000:1, of course depending on the calculated values of  $E_{\text{GSH}}$  and  $[\text{GSx}]$  (Oestreicher and Morgan, 2019).

This higher GSSG proportion proved compatible with the formation of disulfides in nascent proteins that enter the ER. However, whether the GSH/GSSG couple plays an active part in this process or simply mirrors the reactions happening in the vicinity still remains disputed.

In this chapter, we will cover the multiple redox reactions that the ER encloses and that make it an oxidative hub, as well as the mechanisms that take place when oxidative protein folding fails to accomplish properly. We will then take a look at the role of glutathione in those systems when such a role is described, to understand the possible functions of GSH in the ER.

## A. OXIDATIVE PROTEIN FOLDING IN THE ER: THE ERO1-PDI RELAY

The ability of a protein to accomplish its function is intrinsically linked to its conformation, as it often regulates specific interaction with a substrate. Disulfide bonds are covalent links between two different cysteines that have been brought in close proximity. This covalent link has a locking effect that constrains the protein in a conformation that will be maintained even once the protein is carried outside of the cell. The establishment of native disulfide bonds provide a gain in stability for proteins, in terms of function as well as in terms of thermodynamics. This means that the right conformation is favored compared to the non-folded version of the protein.

The basics of oxidative protein folding were first elucidated by the work of Anfinsen, who studied the refolding of a reduced ribonuclease A *in vitro* (Anfinsen et al., 1961). He showed in this seminal paper that under the right conditions, the protein would spontaneously form disulfide bonds. The set up required molecular oxygen, an optimal pH and peptide concentration, and even with those, the kinetics were much lower than those observed *in vivo*. This study suggested the involvement of a catalyst in the formation of disulfide bonds, and it paved the way for the description of Protein Disulfide Isomerase (PDI) by him and Goldberger 2 years later (Goldberger, Epstein, and Anfinsen, 1963).

They also suggested that protein folding might not be a straightforward process, and that proteins might undergo several rounds of oxidation-reduction or isomerization steps of the non-native or intermediate disulfides to achieve their native confirmation. The formation of non-native disulfide bonds is indeed frequently occurring either as a consequence of defective folding, an extreme example of which being the folding defects induced by mutations (Ushioda et al., 2008; Ronzoni et al., 2016), or as an integral part of the normal folding process of a protein. A processive oxidative folding with initial formation then isomerization of several disulfide bonds along with protein folding was for instance demonstrated for the LDL receptor (Jansens, Van Duijn, and Braakman, 2002). This sequential process is, as we know now, key in the correct folding mechanism of a variety of proteins.

Importantly, PDI is reduced into a dithiol during protein oxidation. However, PDI cannot be efficiently oxidized by oxygen and therefore is not an oxidase *per se*. Its reoxidation thus relies on another protein, ERO1, to cycle back to the disulfide bonded motif that can oxidize proteins (Frand and Kaiser, 1998; Pollard, Travers, and Weissman, 1998; Tu and Weissman, 2002).

## PDI: PROTEIN DISULFIDE ISOMERASE

In mammalian cells, Protein Disulfide Isomerase constitutes a 20-members family of approximately 55 kDa proteins. PDI family members are able to catalyze 3 types of reactions (Hatahet and Ruddock 2009, **Figure 21**):

- Oxidation, in which the dithiol of a protein substrate is converted into a disulfide, by disulfide exchange. These reactions require an oxidized PDI that is reduced in this process.
- Reduction, which is the net opposite of oxidation
- Isomerization, in which pre-existing disulfide bonds in protein substrates are rearranged to produce a novel topology. Isomerization initially requires reduced PDI to perform a nucleophilic attack of the protein disulfide. The mixed disulfide formed between PDI and the protein substrate then has two fates. It can either resolve by releasing an oxidized PDI and leave the reduced substrate available for another run of oxidation: this is the reduction/reoxidation mode. Alternatively, the mixed disulfide undergoes nucleophilic attack by another cysteine of the protein substrate, releasing PDI in a reduced form.

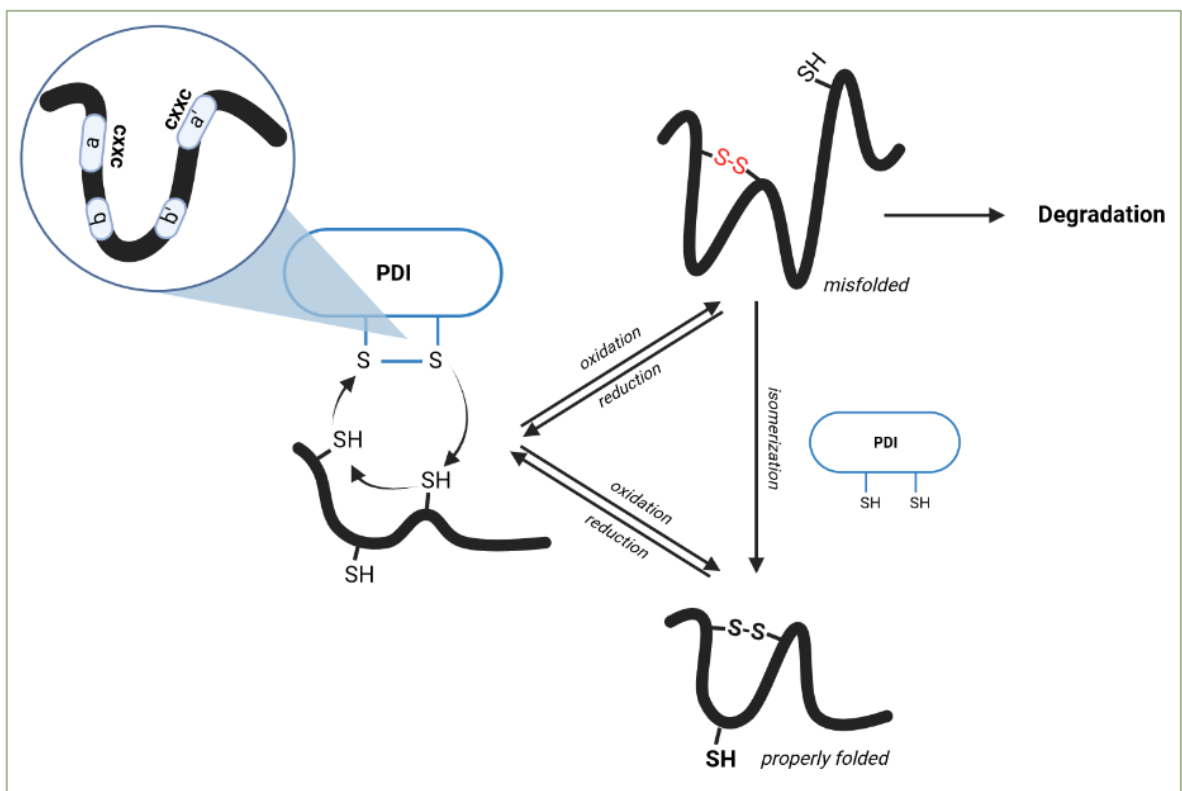


**Figure 21 – PDI catalyzed reactions.** Oxidized PDI performs oxidation reactions, while reduced PDI serves reduction and isomerization. Proteins can go through isomerization as part of their folding pathway, but proteins unable to gain their proper structure are targeted to protein degradation pathways

The canonical member PDIA1 holds a set of four domains: **a**, **b**, **b'**, **a'**, each folded as thioredoxin folds, as well as a C-terminal acidic extension. The **a** and **a'** portions display a characteristic catalytically active CXXC motif that is absent in the **b** and **b'** domains. The cysteines of the **a** and **a'**

motifs hold the ability to be oxidized, and can therefore serve as a relay for oxidation of protein substrates.

PDI is able to perform oxidation and reduction/isomerization reactions. As these reactions respectively require oxidized and reduced PDI, the question arise on how and whether these reactions can occur simultaneously to maintain a proper ER proteostasis.

Interestingly, there appears to be a specialization of the two catalytic sites in PDI.

In yeasts, *in vivo* and *in vitro* data argues for a predominant role of the **a** site for oxidative activities (Vitu et al., 2010). *In vitro*, the **a** domain is preferentially and more rapidly oxidized by recombinant Ero1p than the **a'** domain (L. Zhang et al., 2014). *In vivo*, this translates into a more oxidized **a** domain at steady state, as well as a preferential establishment of mixed disulfides between PDI **a** domain and Ero1p. Functionally, a synthetic lethality is observed between loss-of-function mutant of Ero1p and a Pdi1p strain lacking its **a** domain. Altogether, this argues in favor of a functional difference between the **a** and **a'** sites, with the former ensuring oxidative processes. As a consequence, the preferential oxidation of the **a** over the **a'** domain of yeast PDI provided a mechanism to keep one of the two catalytic domains of PDI preferentially under the reduced state. It was thus proposed in yeast a functional partitioning of PDI catalytic domain, one being involved in oxidation and the other one in reduction and isomerization activities (Niu et al., 2016).

In mammals, the situation is more complex. The **a'** domain is preferentially oxidized by Ero1, but the functional difference is less clear, as alternative oxidation pathways (mentioned in the next section) can preferentially oxidize the **a** domain, which can itself oxidize the **a'** domain through disulfide exchange (Chambers et al., 2010). However *in vivo*, it was observed that Ero1 does drive substrate oxidation through the **a'** domain preferentially (L. Wang et al., 2009).

An additional complexity comes from the fact that different members of the PDI family can handle non-native disulfide bonds. The propensity of PDI family members to catalyze oxidation or reduction/isomerization reactions is primarily thermodynamically determined by the stability of its catalytic disulfide bond. Kinetic factors such as compatibility of the reacting sites, favorable interactions, also play a big part in regulating these reactions as well.

Among the other PDI family members that have been studied, ERdj5 has catalytic sites particularly stable as disulfides (Hagiwara et al., 2011), suggesting it may have a preferential activity as an isomerase/reductase. ERdj5 also contains a J domain allowing its binding to the ER HSP70 chaperone BiP, which could coordinate domain folding with oxidative maturation (Cai et al., 2023). Accordingly, ERdj5 is required for both reduction/isomerization reactions. These include the reduction of terminally unfolded proteins before their elimination by the ER associated degradation (ERAD) and the processive oxidative maturation of the LDL receptor (Ushioda et al., 2008; Hagiwara et al., 2011; Oka et al., 2013).

One important question emerging from these data is how the reduced pools of PDIs are maintained or adapted according to the ER needs. Is it solely due to the differential sensitivity of specific PDI catalytic sites to ERO1-dependant oxidation? Or does this also involve active PDI reduction following the ER import of reduced thiols? The source of reductants capable of supporting PDI activities as

reductase or isomerase could come from the entering thiols themselves, which would be a simple way to adapt PDI redox state to the protein load. An additional reducing power could however be necessary, and its nature is still debated and will be discussed further.

### ERO1: ER OXYDOREDUCTIN 1

The recycling of reduced PDI is performed by a second protein, ER oxydoreductin-1 (Ero1). The enzyme was first identified in yeasts, by two different genetic screens: one screened for mutants defective for the ER export of a model secreted protein, and the other one searched for genes increasing DTT sensitivity when mutated (Frand and Kaiser, 1998; Pollard, Travers, and Weissman, 1998). The use of *ERO1* thermosensitive mutants (termed *ero1-1*) showed that Ero1p activity was essential for disulphide bond formation, and that the invalidation of this essential gene triggered ER stress, when yeast were grown at restrictive temperatures (Pollard, Travers, and Weissman, 1998; Frand and Kaiser, 1998). *In vivo* data showed that Ero1 was directly oxidizing PDI: indeed, myc-tagged Ero1 overexpressed in yeast cells could be coimmunoprecipitated with a PDI trapping mutant. Additionally, the oxidized fraction of PDI was reduced when the *ero1-1* conditional mutant was grown at restrictive temperature (Frand and Kaiser, 1999).

Interestingly, the *ERO1* gene is highly conserved among species, but the essential phenotype of yeast Ero1p is not mirrored in higher eukaryotes. Mice and human cells display two paralogs, Ero1 $\alpha$  and Ero1 $\beta$ . The former is the most ubiquitous whereas the latter was proposed to be restricted to insulin-producing pancreatic cells (Dias-Gunasekara et al., 2005). Knockout experiments of Ero1 $\beta$  led, unsurprisingly, to a misfolded proinsulin phenotype. However, double knockdown of Ero1 $\alpha$  and Ero1 $\beta$  did not affect protein folding to a greater extent (Zito, Chin, et al., 2010).

### ERO1 catalytic cycle

The oxidase activity of Ero1p is supported by its FAD-binding site which can transfer 2 electrons/protons pairs to a molecule of dioxygen as the final electron acceptor (Tu and Weissman, 2002; Sevier and Kaiser, 2006). As a result, for each pair of electrons accepted by oxygen, a disulfide bond is formed in Ero1p and one molecule of H<sub>2</sub>O<sub>2</sub> is created (Figure 22). Importantly, Ero1p preferentially oxidizes PDI thiols over those in the abundant proteins or GSH, which is at the basis of the ERO1-PDI redox relay. This completed the scheme of *de novo* disulfide formation, in which electrons are shuttled from reduced peptides to PDI, then to Ero1 and finally to molecular oxygen (Bulleid and Ellgaard, 2011).

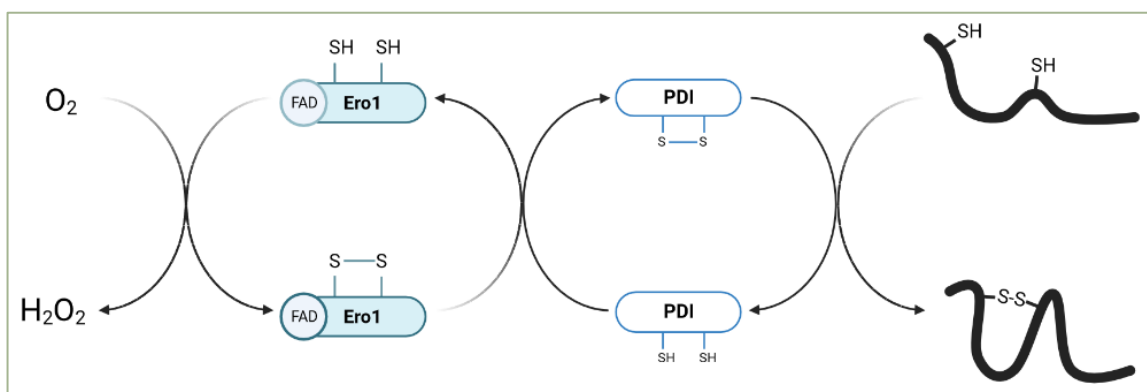


Figure 22 - Ero1-PDI catalyzed disulfide bond formation

Mechanistically, the catalytic activity of Ero1 is dependent on two cysteine pairs that couples PDI oxidation to oxygen reduction. The first pair of cysteines called the shuttle cysteines convey disulfide transfer from oxidized Ero1 to PDI. This shuttle pair is then re-oxidized by a second catalytic cysteine pair present at the rear of the protein that is oxidized by oxygen *via* the FAD cofactor. A flexible loop helps the sequential transfer of disulfides from the catalytic to the shuttling domains. Importantly the catalytic mechanism of proteins from the ERO1 family appears conserved among species. (Delaunay-Moisan, Ponsero, and Toledano, 2017).

### **ERO1 activity is regulated by a PDI dependent mechanism**

Importantly, the activity of ERO1 is regulated. Indeed, excessive Ero1 activity could be detrimental to cell fitness. First, it could promote promiscuous and thus non-native disulfide formation. Second, its constitutive activation would produce high amounts of H<sub>2</sub>O<sub>2</sub> in the presence of unlimited thiol substrates. Both would thus cause ER hyperoxidation leading to ER stress (**Figure 22**).

The first evidence of this regulation was demonstrated using the yeast system: three pairs of cysteines can form long range intramolecular disulfides that constrain the mobility of the flexible loop which normally coordinates the disulfide exchange between Ero1p shuttle and catalytic domains. They thus block the protein in an inactive form (Gross et al., 2006; Sevier et al., 2007; S. Kim et al., 2012). Preventing their formation by mutating the corresponding cysteines led to an hyperactive Ero1p mutant exhibiting ER hyperoxidation and growth arrest phenotypes (Sevier et al., 2007). In mammalian Ero1 $\alpha$  and Ero1 $\beta$ , the regulation occurs according to a different mechanism: two regulatory cysteines are present in the shuttle region, which can form two short range disulfide bridges with each of the shuttle cysteines, thereby covalently locking them in an inactive state. This physically precludes any disulfide exchange with PDI (**Figure 23**). Another regulatory disulfide between cysteines 208 and 241 was identified in Ero1 $\alpha$ , in the vicinity of the FAD cofactor, modulating access to oxygen (Ramming et al., 2015; 2016).

PDI was shown to be a key actor for ERO1 regulation, both in yeast and mammals (S. Kim et al., 2012; L. Zhang et al., 2014) thanks to its ability to perform disulphide bond exchange with ERO1 regulatory disulfides. PDI can act as an activator or an inhibitor of ERO1 activity, depending on its redox state. Reduced PDI is required to reduce ERO1 regulatory disulfides and thus to regenerate the active form of the oxidase. This is best exemplified in yeast where the efficient reduction of ERO1 regulatory disulfides by DTT is significantly delayed in the absence of Pdi1p (S. Kim et al., 2012). On the contrary, a decrease of reduced PDI leads to ERO1 oxidative inactivation. The reformation of ERO1 regulatory disulfides can result from an active reoxidation by oxidized PDI. Alternatively, an autoxidation of ERO1 by its catalytic cysteines may also take place as its reduced PDI substrate becomes scarce.

In summary, PDI directly or indirectly regulates Ero1 activity through reduction and oxidation of its regulatory bonds. This regulation, which is a function of the redox state of PDI, provides a way to couple ERO1 activity to the load of reduced proteins entering the ER. When this load increases, PDI gets more reduced and activate ERO1. On the contrary, when the protein load decreases, oxidized PDI accumulates, promoting ERO1 oxidative inactivation. This would limit Ero1 activation to the strict ER needs.

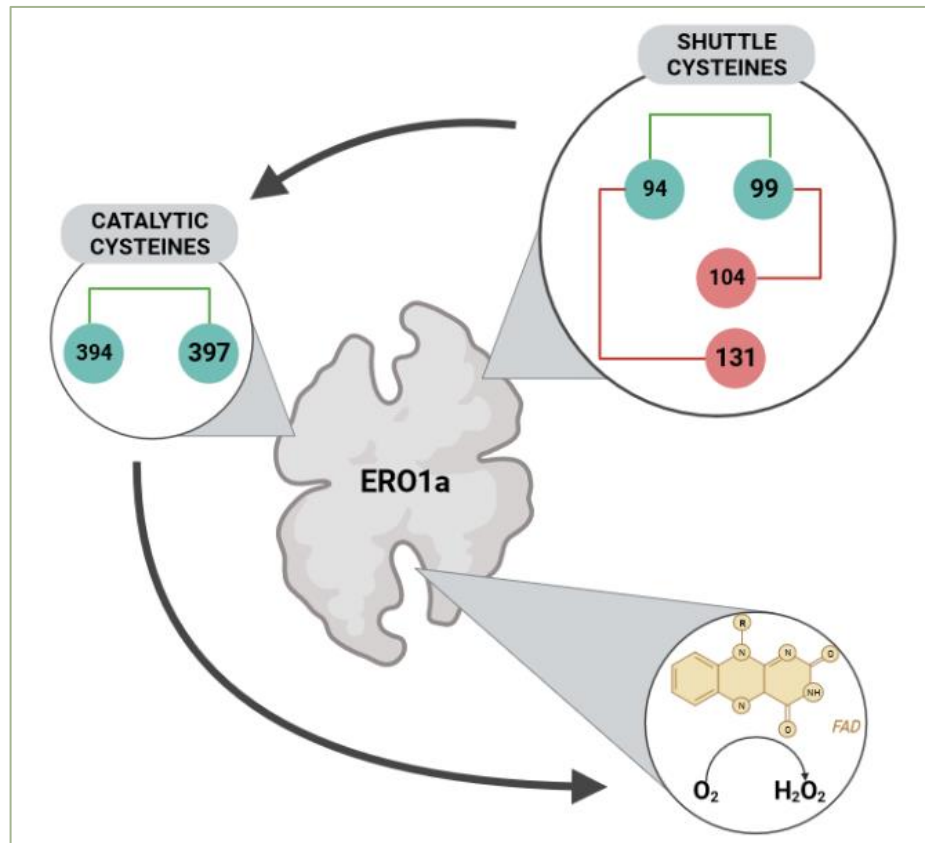


**Figure 23 - Schematic representation of mammalian Ero1a disulfides.** Bold arrows represent electron transfers, green bonds are present in the active form, red bonds in the inactive form. The specific case of regulatory cysteines 208 and 241 is not represented.

## B. ADDITIONAL AND ALTERNATIVE PATHWAYS

Since Ero1 deletion is not lethal in higher eukaryotes, and does not completely abolish protein folding, one could assume that these results hint towards Ero1-alternative pathways for disulfide bond formation.

Inside the ER, 4 sets of residing enzymes have been described as candidates for alternative oxidation in mammalian cells : peroxiredoxin 4 (PRX4, (Zito, Melo, et al., 2010)) and glutathione peroxidases 7 and 8 (GPX7 and GPX8, (Nguyen et al., 2011)) that create disulfide upon scavenging peroxide, and quiescin-sulfhydryl oxidase (QSOX, (Kodali and Thorpe, 2010)), and vitamin K epoxide reductase (VKOR, (Schulman et al., 2010a)) that function in combination with their own electron acceptors.

### PEROXIREDOXIN 4

The absence of lethality of ERO1 knockout in mammals as opposed to yeasts suggested that there might be other compensatory systems for its main function as an oxidase. When looking for ERO1-independent pathways to disulfide bond formation, Zito *et al.* generated a PDI mutant lacking its resolving cysteine (Zito, Melo, et al., 2010). This mutant was used to trap potential PDI oxidants, and ER resident Peroxiredoxin 4 (PRX4) was identified in association with PDI.

The functional importance of PRX4 was demonstrated using mouse and yeast models. In yeast, where a PRX4 homolog is absent, its heterologous expression could rescue the temperature sensitive phenotype of the *ero1-1* mutant. Although the double knockout of Ero1 $\alpha$  and Ero1 $\beta$  provided viable mouse embryo fibroblasts, their phenotype was worsened by the additional PRX4 knockdown, with a decrease in cell survival, impaired collagen secretion, and an overall more reduced ER. The group later confirmed the functional redundancy ERO1 and PRX4 enzymes as they observed that triple knockout of Ero1 $\alpha$ , Ero1 $\beta$ , and PRX4 in mice led to the defective processing of ascorbic acid, and ultimately, in a scurvy phenotype and severe extracellular matrix defects (Zito et al., 2012).

PRX4 was shown to have two functions in the ER: the first one in the disposal of H<sub>2</sub>O<sub>2</sub>, and the second one in the formation of *de novo* disulfides (Tavender, Springate, and Bulleid, 2010). These properties led to a description of the mechanism of disulfide bond generation distinct from that of ERO1: PRX4 is a decamer of five dimers, which individually bear 4 cysteines, 2 peroxidatic, and 2 resolving (Figure 24). The peroxidatic cysteines can react with H<sub>2</sub>O<sub>2</sub>, forming a sulfenic acid. This acid can be attacked by the resolving cysteine, forming an intramolecular disulfide bridge (Bulleid and Ellgaard, 2011). This function can then proceed to disulfide exchange with other dithiol proteins, such as PDI (Tavender, Springate, and Bulleid, 2010). This exchange was shown to be involved in the refolding of reduced RNase *in vitro* (Zito, Melo, et al., 2010). Interestingly, this mechanism could make the process of protein folding all the more efficient, as the H<sub>2</sub>O<sub>2</sub> generated by ERO1 activity upon formation of one disulfide could be used to generate a second. The compensation of ERO1 by PRX4 would involve alternative H<sub>2</sub>O<sub>2</sub> sources, and candidates such as NADPH oxidase 4 (NOX4) (K. Chen et al., 2008) or the mitochondrial transport chain (see next section) have been suggested.

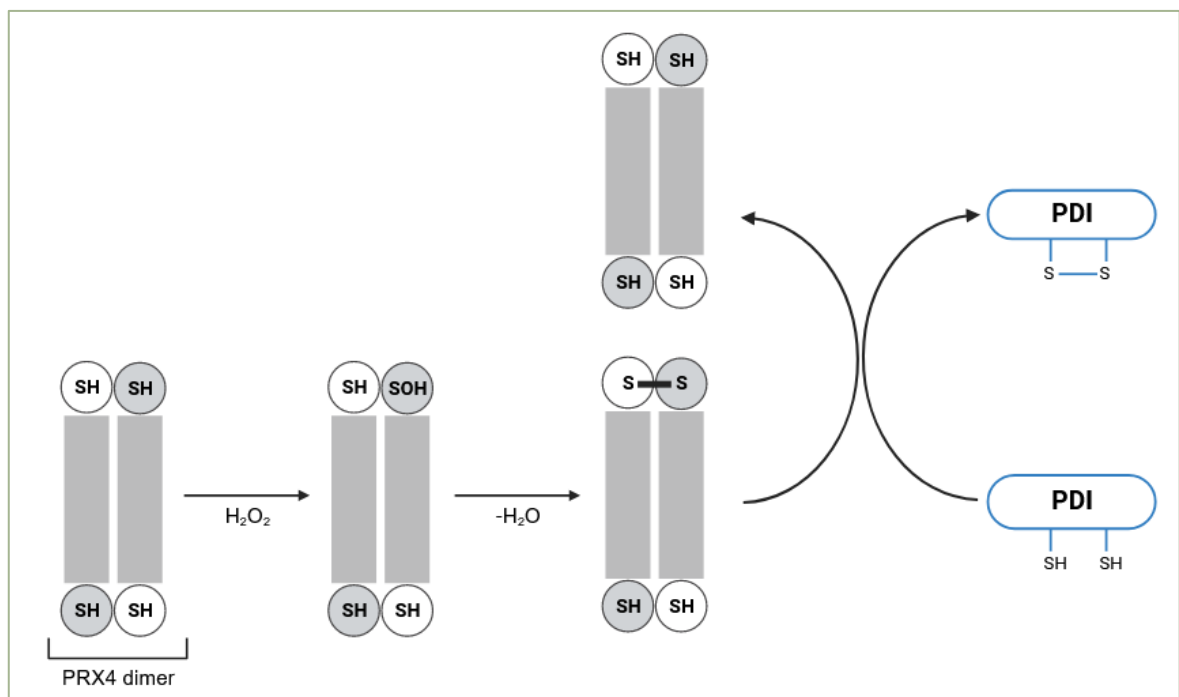


**Figure 24 - PRX4 mechanism of action** The peroxidatic cysteine (grey) of each PRX4 monomer can form a sulfenic acid, which is converted into a disulfide by the resolving cysteine. This disulfide is then transferred to reduced PDI. Adapted from Tavender and Bulleid, 2011

## A MITOCHONDRIAL SOURCE FOR ER OXIDATIVE FOLDING

---

Recently, an alternative mechanism for ER oxidation was proposed by Sitia *et al.* They noted that Ero1 silencing in HeLa cells led to a paradoxical increase in ER H<sub>2</sub>O<sub>2</sub> content, and an increase in ER-mitochondria contact sites. They suggested that, upon Ero1 downregulation, mitochondrial complex III of the electron transport chain was the main source of H<sub>2</sub>O<sub>2</sub> entering the ER (Sorrentino *et al.*, 2022). These results highlighted the existence of more global cooperative mechanisms rather than each compartment functioning as insulated units. Also, they provide a possible source of peroxydes which could fuel PRX4-dependent pathway.

---

## GLUTATHIONE PEROXIDASES 7 AND 8

As described earlier, the ER harbors two glutathione peroxidases (GPX), soluble GPX7 and transmembrane GPX8. GPXs are enzymes that are able to scavenge H<sub>2</sub>O<sub>2</sub>, become oxidized in the process, and are then recycled back to their reduced form by glutathione. *In vitro* experiments showed that GPX7 and GPX8 are also -and better- reduced by PDI (Nguyen *et al.*, 2011), suggesting that they could exploit the oxidative power of H<sub>2</sub>O<sub>2</sub> to fuel the oxidative folding pathway.

Nguyen *et al.* indeed showed in their study that GPX7 and 8 accelerated the *in vitro* refolding of a model protein, when associated with PDI. GPXs also increase the oxygen consumption of Ero1 alone *in vitro*, and was shown to associate with Ero1 *in vivo*. Although they could not co-immunoprecipitate the proteins in the paper, the authors did observe fluorescence upon bimolecular fluorescence complementation. These argues towards a GPX-dependent oxidation of PDI, that could provide a means to use ERO1-generated H<sub>2</sub>O<sub>2</sub>, to optimize the amount of disulfide bonds during by protein folding.

Recent data suggests that GPX7 has a much higher reactivity than GPX8 towards both H<sub>2</sub>O<sub>2</sub> and PDI *in vitro*, and that scavenging of Ero1-generated H<sub>2</sub>O<sub>2</sub> promotes oxidative protein folding through GPX7 (L. Wang *et al.* 2014; Kanemura *et al.* 2020). Although GPX8 was proved to scavenge Ero1-generated H<sub>2</sub>O<sub>2</sub> (Ramming *et al.*, 2014), its involvement in oxidative protein folding *in vivo* is still debated.

---

## QUIESCIN SULFHYDRYL OXIDASE

The search in yeast for proteins that could rescue the lethal phenotype of deleted Ero1p lead to the identification of the flavoprotein Erv2p (Sevier *et al.*, 2001). This protein shares features of the mammalian Quiescin Sulfhydryl Oxidase (QSOX), a flavoprotein that, like Ero1, is able to utilize O<sub>2</sub>, thanks to its Erv domain. The protein can oxidize PDI, and unlike Ero1, can also catalyze *de novo* disulfide bond formation in a broad variety of substrates thanks to a thioredoxin domain containing a CGHC motif. This process was demonstrated *in vitro*, and the presence of PDI greatly enhanced correct disulfide bond formation in a complex model protein (Rancy and Thorpe, 2008).

Recent studies demonstrated that QSOX localizes outside the ER, to the cell wall of plants, the golgi mammalian cells, or secreted from other cell types, hence suggesting a role in post-ER disulfide formation (Limor-Waisberg, Ben-Dor, and Fass, 2013). For instance, knockdown and silencing experiments on QSOX showed that the protein was involved in the incorporation of laminin into the extracellular matrix of fibroblasts, and in lung cancer cell migration (Ilani *et al.*, 2013).

---

## VITAMIN K EPOXYDE REDUCTASE

Vitamin K 2,3 epoxide reductase, or VKOR, is an ER resident, 4-transmembrane domains protein, involved in the reduction of vitamin K 2,3 epoxide into its active form. The latter participates to the post-translational addition of  $\gamma$ -carboxyglutamic acid to proteins, which is crucial for proteins involved in blood clotting (Sinhadri et al., 2017). The reduction of vitamin K<sub>2,3</sub> epoxide is achieved by a thioredoxin-like CXXC motif within VKOR. Vitamin K<sub>2,3</sub> epoxide thus acts as an electron acceptor leaving the luminal CXXC motif of VKORC in its oxidized form. As a result, this relay could provide oxidizing equivalents for the ER, independently of ERO1.

Studies did show that VKOR can oxidize PDI as it was found trapped in complexes or mixed disulfides with PDI family members (Schulman et al., 2010b; Wajih, Hutson, and Wallin, 2007). Moreover, when trying to identify additional oxidative pathways in hepatoma cells, Williams *et al.* observed that inhibiting VKOR activity in ERO1 and PRX4 double knockout was lethal. Using albumin as a model, they showed that the need for ERO1, PRX4 and VKOR correlated with the maintenance of albumin secretion and oxidative folding (Rutkevich and Williams, 2012).

Altogether, these results suggest, in this model, that 3 pathways are necessary to support cell viability and oxidative folding in mammals, and that there is a redundancy in the function of these pathways although the ERO1 pathway is the major one.

### BOX1: Disulfide bond formation in the bacterial periplasm

*The description of the gram-negative bacterial representant Escherichia coli pathway for oxidative protein folding is a handy analogy for protein folding in the eukaryotic ER and should be mentioned.*

In bacteria, disulfide bonds are formed in the periplasm and also require an oxidative machinery. The introduction of disulfide bonds is permitted by the CXXC-containing, non-essential DsbA protein (J. C. A. Bardwell, McGovern, and Beckwith, 1991; Martin, Bardwell, and Kuriyan, 1993). DsbA participates in the oxidative folding through disulfide exchange with client proteins, and is reduced in the process. The maintenance of oxidized DsbA is performed by the transmembrane, non-essential DsbB oxidoreductase (J. C. Bardwell et al., 1993), that shuttles electrons from DsbA to respiratory chain quinones through two set of disulfides (Kobayashi et al., 1997).

This route is strictly oxidative, and does not intervene in the reduction or isomerization of non-native disulfides. These processes are rather ensured by another set of enzymes. DsbC is a soluble homodimer containing two facing CXXC motifs (Metcalf et al., 2000). The enzyme is capable of catalyzing either isomerization of non-native disulfides (Arne Rietsch et al., 1996), or reduction, re-sending the reduced protein to DsbA-assisted oxidation. In this process, DsbC is oxidized, and the maintenance of its reduced form is ensured by DsbD, a membrane-bound protein containing three reactive cysteines that shuttle electrons to DsbC from cytosolic thioredoxin, itself reduced by thioredoxin reductase at the expense of NADPH (A Rietsch et al., 1997).

Despite their close redox potentials, DsbA and DsbC do not react with each other and remain predominantly oxidized and reduced respectively, in the periplasm. These two pathways are kinetically insulated thanks to steric hindrance in the structures of the proteins, precluding interaction.

The decoupling of oxidant and reducing machineries in the bacterial periplasm is all the more interesting when considering the eukaryotic ERO1-PDI relay. Indeed, the latter concentrates both the oxidizing and reducing pathway. The disappearance of a kinetic barrier between oxidation and reduction could suggest the appearance of new evolutive functions.



### III THE UNFOLDED PROTEIN RESPONSE

ER Stress can be defined as an imbalance between the ER folding capacity and its actual folding requirements, resulting in the accumulation of mis- or unfolded proteins, which are then trapped inside the ER. When such a stress happens, a response named Unfolded Protein Response (UPR) is activated thanks to up to 3 classes of receptors inside the ER membrane, depending on the organism: Inositol-Requiring Enzyme 1 (IRE-1), Protein kinase RNA-like ER Kinase (PERK) and Activating Transcription Factor 6 (ATF6). Under physiological conditions, the most abundant ER chaperone Binding Immunoglobulin Protein (BiP, or 78kDa Glucose Regulated Protein GRP78, or Kar2 in yeasts) binds the luminal side of the three transmembrane proteins and is involved in their activation mechanism.

This UPR response has two possible outcomes: the first and primary is to try and restore equilibrium by increasing the folding capacity of the ER and decreasing the protein load on the ER. When such a resolution proves impossible the second outcome precedes ER failure by guiding the cell towards apoptosis. This death sentence for cells unable to resolve a threat to their proteostasis highlights the essentiality of proper protein folding and ER function.

In this sense, the UPR is a critical actor in numerous human diseases. It can be involved in the elimination of cells in protein misfolding diseases such as retinitis pigmentosa, resulting in blindness by retina degradation, or protein overload diseases like type II diabetes that stems from pancreatic beta cells death upon critical UPR. On the other hand, the UPR can be hijacked by malignant cancerous cells to accommodate their hyperactive growth, and by viruses to assist their replication. (Walter and Ron, 2011).

---

#### A. IRE-1

IRE-1 is the most conserved branch of the UPR and sole UPR factor in fungi. Of note, Ire1p activity is dispensable in unstressed basal conditions as  $\Delta IRE1$  yeasts are viable, but *IRE1* knock-out sensitizes cells to ER stress (Cox, Shamu, and Walter, 1993). Ire1p displays two paralogs in mammals; a ubiquitously expressed IRE-1 $\alpha$  and an intestinal as well as pulmonary epithelium specific IRE-1 $\beta$ , hinting towards cell or tissue specificity of the UPR profile (Walter and Ron, 2011; Almanza et al., 2019).

IRE-1 is a type I transmembrane protein with two functions: kinase and endoribonuclease. When activated, IRE-1 can proceed to the spliceosome-independent excision of an intron of the basic leucine zipper (b-ZIP)-containing transcription factor XBP1 (X-box Binding Protein, Hac1 in yeast) (Yoshida et al., 2001; Mori et al., 1996; Cox and Walter, 1996). The exons are then ligated by the tRNA ligase complex in mammals (Jurkin et al., 2014) and constitute the active XBP1s (s for *spliced*) as opposed to XBP1u, (*unspliced*) that can induce genes involved in the ER protein folding and ER Associated Degradation (ERAD) machinery as well as lipid biogenesis.

A second IRE-1 mediated pathway discovered in *Drosophila melanogaster* involves the degradation of ER-localized mRNAs by a process termed Regulated IRE-1 Dependent Decay (RIDD) (Hollien and Weissman, 2006). This process was then shown to be conserved in mammalian cells (Hollien et al., 2009) as well as plants (Mishiba et al., 2013) and fission yeast (Mishiba et al., 2013), whereas

XBP1 splicing seems to be the only downstream effect of IRE-1 RNase ability in the budding yeast *Saccharomyces cerevisiae* (Niwa et al., 2004). RIDD is thus a means for reduction of protein load by degradation of mRNAs.

Upon accumulation of improperly folded proteins, the BiP-bound, IRE-1 inactive monomers dissociate from BiP, oligomerize and the kinase domains become juxtaposed, which leads to *trans*-autophosphorylation, which then activates its endoribonuclease function. The exact mechanism capable of sensing Unfolded Protein and translating it into IRE-1 activating oligomerization is still debated, but involves both BiP binding to IRE-1 and unfolded proteins, either competing for BiP binding or directly stimulating the activation of IRE-1 (Radanović and Ernst, 2021).

---

## B. PERK

Protein Kinase RNA (PKR)-like ER Kinase (PERK) was identified in rat pancreatic islet cells, as a transmembrane, ER-localized kinase (Harding, Zhang, and Ron, 1999; Y. Shi et al., 1998). Like IRE-1, monomeric PERK protein has a luminal domain bound to BiP, and a cytoplasmic kinase domain. Upon ER stress, BiP detaches from the protein, allowing oligomerization, *trans*-autophosphorylation, and activation of PERK.

Active PERK acts in two steps that are timely ordained in response to ER stress: the first step involves a rapid translation block to mitigate pressure on the ER. This is mediated by PERK phosphorylation of eIF2 $\alpha$  on serine 51. EIF2 $\alpha$  is a subunit in the eIF2 heterotrimer involved in protein synthesis initiation by tRNA binding to ribosome subunits. The phosphorylation of the  $\alpha$  subunit results in the inhibition of the trimer, resulting in protein synthesis downregulation and protein load reduction during ER stress (Almanza et al., 2019).

The second step of PERK activation is the stimulation of a complex set of transcription factors, involved in the stimulation of antioxidant response and ER folding or degradation capacity. Although protein load is reduced as a whole as a result of PERK activation, the translation of some proteins is favoured upon PERK activation. Such is the case for the ubiquitously expressed activating transcription factor 4 (ATF4) that is poorly translated in basal conditions (Harding et al., 2000).

While halting translation provides a temporary solution to misfolded protein overload, acting as a pro-survival mechanism, protein synthesis needs to be ultimately restored to sustain cell viability.

Chronic UPR and PERK activation lead to the upregulation of the transcription factor CAAT/enhancer-binding protein (C/EBP) homologous protein, or CHOP/GADD153. ATF4 and CHOP share target proteins in UPR and protein synthesis, and increased CHOP expression has been linked to increased cell death. This occurs not only by enhancing genes encoding pro-apoptotic factors such as BCL-2, but also through the restoration of protein synthesis *via* induction of growth arrest and DNA damage 34 (GADD34). GADD34 interacts with a phosphatase that can dephosphorylate eIF2 $\alpha$ , therefore providing a feedback loop that restores protein synthesis (Novoa et al., 2001). Altogether, protein restoration, ATP depletion and oxidative stress provide a means to either restore protein synthesis or push cell death if the cell does not manage to cope with overload (Han et al., 2013; Urrea et al., 2013).

### C. ATF6

Activating transcription factor (ATF6) is the third UPR transducer in higher eukaryotes. In basal conditions, the protein remains in the ER, associated with BiP. Upon stress, BiP dissociates from the protein and allows ATF6 to relocate to the Golgi, where Site-1 and Site-2 proteases cleave ATF6, generating the active transcription factor (Almanza et al., 2019). Studies suggest that, in HEK 293T and HeLa cells, this translocation is redox regulated. Indeed, Bulleid and colleagues observed that disulfide bonded ATF6 dimers were preferentially translocated to the Golgi apparatus and cleaved by Site-1 proteases. Additionally, they observed that the ER oxidoreductase ERp18 could preferentially reduce disulfide bonded ATF6. Overexpression of the protein reduced the quantity of processed ATF6 and active transcription factor generation while deletion of ERp18 accelerated ATF6 trafficking, suggesting that ERp18 could have a role in maintaining ATF6 in the ER *via* reduction (Oka et al., 2022).

Once in the active form, ATF6 translocates to the nucleus and binds to regulatory elements, activating genes encoding for protein folding, quality control, and ERAD factors (Adachi et al., 2008) as well as XBP1.

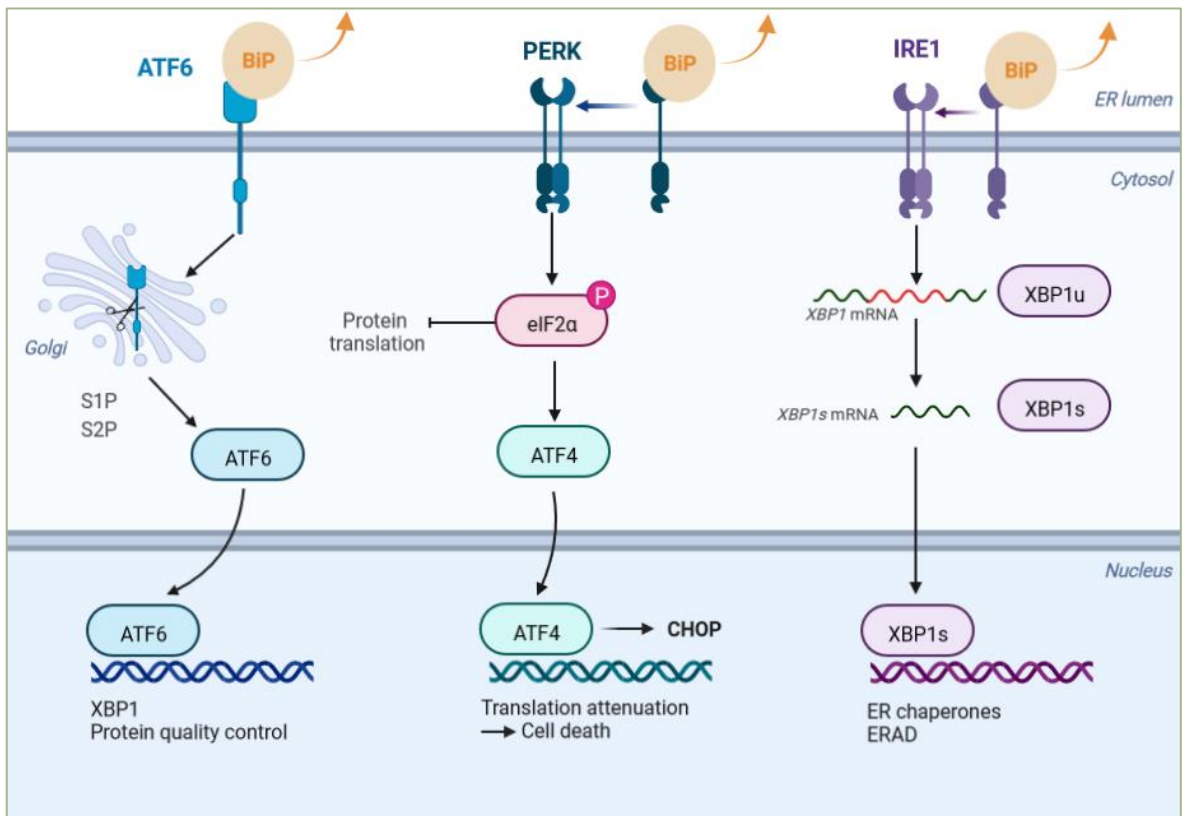


**Figure 25 – UPR transducers.** Adapted from “UPR signaling (ATF6, PERK, IRE1)” by Emma Madden (2023). Retrieved from <https://app.biorender.com/biorender-templates>



## A. HISTORY OF THE SUSPECTED FUNCTION OF GSH IN THE REDOX STATE OF THE ER

Glutathione is present in the endoplasmic reticulum but its reducing nature, substantiated by its numerous roles in versatile reductive reactions, led to question its function(s) in the oxidizing milieu of the ER. As we have seen earlier, the ER is dedicated to the oxidative folding of proteins and disrupting this process through a redox imbalance can trigger UPR with possible consequences on cell life or death. The fact that the GSH/GSSG couple is in equilibrium with PDI, thereby possibly competing with protein substrates for their oxidation, as we will next see, further underlines the peculiarity of a nonetheless evolutionary conserved situation, among eukaryotes and maybe also bacteria (Knoke et al., 2023).

## GSSG AS AN OXIDIZING POWER FOR THE ER?

PDI was known to oxidize proteins *in vitro* and *in vivo* before the discovery of Ero1 (Bulleid and Freedman, 1988; Lambert and Freedman, 1985). Back then, the origin of the oxidizing equivalents provided to PDI to generate disulphides *de novo* was unknown.

In 1991, Lyles and Gilbert evaluated the influence of the redox buffer in protein folding experiments. They observed that a 5:1 GSH:GSSG ratio ([GSH] fixed at 1 mM and [GSSG] at 0.2 mM), had to be used for the folding of RNase A to be optimal. Crucially, they also determined that, while this ratio had to be much more oxidizing than that in the cytosol, it also had to remain reducing enough to maintain PDI in an oxidative folding-competent form, meaning with a reduced fraction (Lyles and Gilbert, 1991a; 1991b). In the absence of Ero1, the glutathione couple was considered as a potential factor controlling the redox state of PDI, to both ensure oxidative folding as well as the necessary maintenance of a reduced fraction of PDI.

A year later, the lab of Harvey F. Lodish provided the first evaluations of glutathione redox state in the ER (further detailed in **Transport of glutathione into the ER**). Strikingly, they determined the ER GSH:GSSG ratio to be between 1:1 and 3:1, which in accordance with the previous *in vitro* data determined for ideal PDI function, enforcing the idea of a role of GSH in PDI regulation. They explained the observation of the more oxidized ER by a preferential ER uptake of GSSG 10 times over GSH, into their microsome models (Hwang, Sinskey, and Lodish, 1992).

These experiments provided a first rationale for the presence of luminal glutathione which led to the widespread assumption that in the ER, GSSG was the provider of oxidizing equivalents for PDI.

## GSH AS A REDUCING POWER FOR THE ER...

The theory was rapidly set aside upon the discovery of Ero1. Ero1 was shown to oxidize GSH into GSSG through PDI which explained the lower GSH/GSSG ratio inside the ER (Cuozzo and Kaiser, 1999). Additionally, the preferential transport of GSSG over GSH was refuted and GSH was proved to be preferentially taken up in microsomal vesicles (Bánhegyi et al., 1999).

With the PDI oxidant discovered, and the focus shifted towards a preferential transport of GSH, the idea emerged that GSH could instead serve as a reducing power. This is also suggested by rescue experiments in yeasts: while the disruption of Ero1 is restored by the addition of the oxidant diamide, the deletion of the GSH synthetic enzyme is rescued by addition of the reductant DTT (Frand and Kaiser, 1998).

### ... FOR THE MAINTENANCE OF REDUCED PDI

---

It ensued that GSH was proposed to be implicated in the maintenance of reduced rather than oxidized PDI. As mentioned above, while oxidation is primordial in protein folding, reduction processes are also crucial, as demonstrated by the fact that isomerization of non-native disulfides is actually rate-limiting in the kinetics of RNaseA folding (Lyles and Gilbert, 1991b).

In human cells, most PDI and PDI-like enzymes residing in the ER are indeed found in a predominantly reduced state (Jessop and Bulleid, 2004; Sato et al., 2013; Hudson, Gannon, and Thorpe, 2015) and a set of experimental elements pointed to GSH as being involved in this process.

From a most theoretical point of view, Thorpe *et al.* underlined that the rapid equilibration of PDI with the glutathione couple, as well as an estimated  $-225$  mV  $E_{\text{GSH}}$  value in the ER were compatible with the maintenance of predominantly reduced PDI family members (Hudson, Gannon, and Thorpe, 2015).

First, Molteni *et al.* observed that glutathione depletion through semi-permeabilization caused PDI to oxidize, which led to the generation of misfolded proteins as well as an acceleration of protein folding. This could be reverted by re-adding millimolar quantities of GSH to semi-permeabilized cells. (Molteni et al., 2004). Chakravarthi and Bulleid observed that overexpression of Ero1 led to the acceleration of protein folding, while depletion of GSH accelerated incorrect disulfide bond formation, arguing that GSH had a role in the reductive pathway of protein folding rather than the oxidative pathway (Chakravarthi and Bulleid, 2004). The same year, Jessop and Bulleid produced microsomal vesicles to show that a low molecular weight component of the cytosol was required to recover the mostly reduced steady state of the PDI family member, Erp57, after it had been artificially oxidized. Out of NAD(P)H, cysteine, cysteamine or GSH, only GSH could restore the PDIs redox state after such an oxidative challenge. Similarly, GSH addition was able to counterbalance the oxidation of Erp57 triggered upon the expression of an hyperactive mutant of Ero1 (Jessop and Bulleid, 2004).

These experiments may however present some caveats. In the previous study, a pre-oxidation of PDI was performed to unmask the impact of GSH on reduction questioning the relevance of these observations in a more physiological setting. The relevance of GSH during isomerization reactions has also been questioned by *in vivo* data suggesting that GSH depletion through deletion of its synthetic enzyme or ER-localized degradation has hardly any effect on PDI function and does not lead to the activation of UPR ((Cuozzo and Kaiser, 1999; Tsunoda et al., 2014)). Additionally, it was demonstrated using semi-permeabilized (SP) cells that the thioredoxin rather than GSH was relevant and sufficient to support the proper oxidative folding of the model substrate, LDL receptor (Poet et al., 2017; X. Cao et al., 2020). It should be noted however that here, the exclusion of GSH was based on inhibition of glutathione reductase rather depletion of glutathione levels. These results still highlighted the need for an NADPH-dependent pathway for proper oxidative protein folding.

## ...OR FOR THE REDUCTIVE ACTIVATION OF ERO1

---

GSH does not directly interact with Ero1, but does so through PDI (Tu and Weissman, 2002). An increased ratio of reduced over oxidized PDI is required for the reductive activation of Ero1, and this could be triggered by GSH, as it was shown that GSH competes with proteins for Ero1 oxidation, which also explains the higher GSSG content (Cuozzo and Kaiser, 1999). However, the needs for reducing equivalents for Ero1 activation may also be met by reduced thiols emanating from the translocation of nascent reduced polypeptide funnelled into the ERO1-PDI relay (Hansen, Roth, and Winther, 2009)

Nonetheless, different experimental evidence shows that ERO1 reductive activation can require or be stimulated by GSH (Kumar et al., 2011; S. Kim et al., 2012). The physiological relevance of this process yet remains to be demonstrated

GSH was shown to be necessary for the reduction of oxidized Ero1 *in vitro* (Niu et al., 2016; L. Zhang et al., 2014; S. Kim et al., 2012).

In both yeast and mammals, GSH was shown to counteract Ero1 activity, as impairment of Ero1 could be rescued by deletion of GSH synthetic enzyme (Cuozzo and Kaiser, 1999) or conversely, addition of glutathione compensates for overexpression of Ero1 (Molteni et al., 2004; Chakravarthi and Bulleid, 2004). This control of the redox state of Ero1 is also by the observation that DTT-treated SP cells re-oxidize much faster in the absence of GSH, which suggests that GSH could buffer Ero1 oxidation (Molteni et al., 2004). Additionally, BSO-elicited glutathione depletion caused a decrease in the toxicity of a hyperactive Ero1 mutant (Sevier et al., 2007). These data suggest that Ero1 activity could be buffered through GSH.

The involvement of GSH in the redox state of Ero1 was also observed in yeast cells subjected to GSH addition and HGT1 overexpression, Ero1 became more reduced in a dose and time-dependent fashion (Kumar et al., 2011). These results also highlighted that, by contributing to Ero1 reduction, GSH could paradoxically contribute to ER oxidation, since regulatory disulfides prevent Ero1-mediated H<sub>2</sub>O<sub>2</sub> formation when the ER becomes too oxidizing. This excessive H<sub>2</sub>O<sub>2</sub> was indeed observed by Kumar *et al.*, resulting in adverse effects on protein folding functions.

A reciprocal control of Ero1 activity and glutathione import into the ER of *Saccharomyces cerevisiae* was suggested by Ponsero *et al.* when they showed that ER GSH import caused Ero1 activation, resulting in H<sub>2</sub>O<sub>2</sub> production. This H<sub>2</sub>O<sub>2</sub> in turn oxidized Kar2, inhibiting GSH import (Ponsero et al., 2017).

## A FUNCTION STILL DEBATED

---

Despite evidence suggesting an interplay between GSH and the Ero1/PDI folding machinery, the demonstration for a physiological role of GSH during oxidative protein folding is less conspicuous. Observations arguing the dispensability of GSH for proper protein folding were made by Chris A. Kaiser in yeast cells. In a  $\Delta gsh1$  mutant devoid of detectable GSH, the maturation of model protein Carboxypeptidase Y (CPY) matured with the same kinetics as wild type cells (Frandsen and Kaiser, 1998). In mammalian cells, Sitia and coworkers studied refolding kinetics of the model protein J chain of Immunoglobulin M (JcM), they did observe that GSH depletion accelerated the process and

caused an increase in non-native forms of the protein (Molteni et al., 2004). This observation was also mirrored in another protein model of human tissue type plasminogen activator (tPA). However, while native tPA formation was faster and associated with more non-native formations under GSH depletion, the maturation of the protein did occur with comparable kinetics as wild-type cells (Chakravarthi and Bulleid, 2004). Ron and colleagues studied another protein model, the LDL receptor (LDL-R). They designed an ER-targeted version of ChaC1, the glutathione specific  $\gamma$ -glutamyl cyclotransferase that degrades glutathione to purge the ER of glutathione. They showed that the maturation of LDL-R was insensitive to the expression of ER-ChaC1.

The essential nature of GSH hinders conclusions as to a role of the molecule in disulfide bond formation. Regarding protein models used in mammals while kinetics seems irrefutable, the isomerization of some proteins is dependent on a possibly GSH-independent pathway, making their study incomplete. Additionally, ChaC1-mediated degradation of GSH still produces redox active metabolites, which further hinders any conclusion. The answer to a physiological role of glutathione is still lacking, and while its role in steady-state oxidative protein folding is questioned by the predominant role of the thioredoxin pathway in that matter, there is a possibility for GSH to be important in situations of ER stress, as proposed by the reciprocal control of Ero1 activity and GSH import in yeasts (Ponsero et al., 2017). While the characterization of a function in that matter is lacking, we could assume that UPR-induced Ero1 needs GSH for reductive activation.

If reduced GSH has been the center of attention lately, Appenzeller-Herzog *et al.* did propose a role for GSSG in Ero1 regulation that would buffer its activation (Appenzeller-Herzog et al., 2010): a dynamic interplay would exist, which utilizes GSSG resulting from Ero1 activation-stimulated disulfide bond formation. Since DTT treatments leads to a swift GSSG production and resorption, that could not be explained by diffusion rates of GSSG (Bánhegyi et al., 1999). Instead, GSSG would in turn oxidize PDI and shut down Ero1 activities, in a process that would also be adaptable to physiological changes.

## TRANSPORT OF GLUTATHIONE INTO THE ER

Given the difficulties underscored above, understanding how glutathione is imported into the ER could be the key to deciphering its role in this compartment. This task has however been a challenge for the past 30 years.

---

### LESSONS FROM MICROSOMES

In 1992, Hwang *et al.* conducted the first assay aiming to understand the redox state and glutathione import into the endoplasmic reticulum (ER). For their study, they designed a small peptide called N-acetyl-Asn-Tyr-Thr-Cys-NH<sub>2</sub> (NYTC). This peptide can freely diffuse across cell membranes, from the extracellular space to the cytosol, and even into the ER or other organelles. The presence of the Asn-Tyr-Thr sequence makes the peptide a target for glycosylation. The rationale behind this design was that the peptide would get glycosylated in the secretory pathway and remain trapped there. Once trapped, the presence of a cysteine residue would allow the peptide to equilibrate with redox species in the compartment, which could be analyzed by HPLC, and their redox state estimated. Their assay had a few limitations in terms of reliability, owing to the localization of the peptide in the secretory pathway rather than the ER, and the specificity of the exchange between the glutathione couple and the peptide. Their observation however led to the first assumption that the ER has a much more oxidizing GSH:GSSG ratio, with values around 3:1 to 1:1. They could also suggest that GSSG was transported preferentially over GSH into the ER, to explain the presence of GSSG in such quantities (Hwang, Sinskey, and Lodish, 1992).

However, subsequent papers provided contrasting observations. Bánhegyi *et al.* used radiolabeled GSH to monitor its traffic through reconstituted rat microsomal vesicles. Doing so, they observed that microsomes preferentially imported reduced GSH over GSSG *via* facilitated transport. This process was bidirectional, time and concentration-dependent, and showed saturability and susceptibility to inhibition to anion transport blockage. This study also highlighted the presence of highly dynamic exchanges of GSH both into and out the microsomes, occurring within minutes and following the direction of the GSH gradient. While GSSG import could proceed into these microsomes, it happened at a much slower rate compared to GSH (Bánhegyi *et al.*, 1999).

Although this supported the presence of a specialized mechanism supporting GSH ER transport, the identity of the transporter responsible remained unknown.

By comparing the modalities of GSH transport in the sarcoplasmic reticulum (SR) rather than ER, using a similar microsome approach, the same authors concluded on a possible role of the SR specific ryanodine receptor RyR1, as a mediator of GSH transport across the SR. Indeed, the SR import of radiolabeled GSH could be inhibited by two different RyR1 inhibitors. While this transport mechanism is likely specific to SR, its relevance in this context is supported by the observation that transfection of mammalian HEK 293 cells with RyR1 lead to the same SR-like GSH transport patterns (Csala *et al.*, 2001; Bánhegyi *et al.*, 2003). These data have however not been further confirmed using whole cell systems.

---

## REDOX SENSORS FOR THE STUDY OF ER GLUTATHIONE

The study of GSH import into the ER greatly benefits from the rise of redox sensors (described in **Glutathione visualization and study tools**). The ability to target probes into the ER allows for *in situ* detection of the glutathione couple, thus integrating cytosolic or other cellular regulations, while also overcoming the limits of *in vitro* investigations such as artifacts from sample preparation or redox state fixation. In conclusion, GSH can be observed, although still indirectly through probes, in real time and in whole cells.

Montero and coworkers took advantage of these probes to evaluate the steady state concentration and redox status of the glutathione couple in the endoplasmic reticulum of HeLa cells (Montero et al., 2013). To do so, they expressed in the ER the yeast Grx1-1cys probe, described earlier in **Glutathione visualization and study tools**), which provided them access to the steady state GSH:GSSG ratio in the ER compartment that they determined to be less or equal to 7. Then, they used the previously determined ER  $E_{\text{GSH}}$  value of  $-208 \pm 4$  mV in HeLa cells (Birk et al., 2013) to calculate the GSH<sup>2</sup>:GSSG ratio from the Nernst equation, which, in conjunction with the determined GSH:GSSG ratio of less than 7, enabled the authors to approximate the concentration of total glutathione in the ER, noted  $[\text{GSx}]_{\text{ER}}$ .

Doing so they concluded that the concentration of total ER glutathione may very well exceed 15 mM in their cell model. Of note,  $[\text{GSx}]_{\text{ER}}$  comprised both GSH and GSSG according to the following formula:  $[\text{GSx}]_{\text{ER}} = [\text{GSH}]_{\text{ER}} + 2 [\text{GSSG}]_{\text{ER}}$ . The authors conducted a comparison between the  $[\text{GSx}]$  value in the ER and that of the cytosol. To do so, they employed the conventional DTNB assay for whole-cell quantification of GSH levels and that was described earlier and concluded that  $[\text{GSx}]$  in the cytosol of HeLa cells was approximately 7 mM.

Based on these results and those from the Banhegyi group, these authors offered a novel hypothesis depicting how the GSH transport into the ER might be controlled. They proposed that the significantly higher  $[\text{GSx}]_{\text{ER}}$  compared to  $[\text{GSx}]_{\text{cyt}}$  could be a universally conserved characteristic of ER physiology, explained by the activity of the ER oxidative machinery together with the differential permeability to the ER membrane of the GSH and GSSG species. Indeed, the free diffusion of cytosolic GSH toward the ER should be powered by the GSH gradient established upon conversion of GSH to GSSG by ERO1-PDI inside the ER. On the contrary, ER-produced GSSG would be trapped inside due to its less effective export thereby leading to higher  $[\text{GSx}]_{\text{ER}}$ . Accordingly, the difference in concentration established between  $[\text{GSx}]_{\text{cyt}}$  and  $[\text{GSx}]_{\text{ER}}$  should be a function of ERO1-PDI activity.

---

## STUDIES IN YEAST COMPLETE THE MODEL

In 2017, Ponsero *et al.* used the same combination of probes to explore GSH transport into the yeast endoplasmic reticulum. This setup first led them to propose an estimation of  $[\text{GSx}]_{\text{ER}}$  at steady state of  $30 \pm 2$  mM (Ponsero et al., 2017). As a first analysis of GSH transport in the yeast ER, Ponsero *et al.* similarly measured  $[\text{GSx}]_{\text{cell}}$  using whole cell extracts and DTNB assay. They also estimated  $[\text{GSx}]_{\text{cyt}}$  by taking advantage of the combination of Grx1 and rYFP probed adapted to the cytosol. By comparing these two measurements, they estimated  $[\text{GSx}]_{\text{cyt}}$  to be 4.5-fold higher compared to the  $[\text{GSx}]_{\text{cell}}$ , a difference which was attributed to the smaller volume of the cytosol. A  $[\text{GSx}]_{\text{cell}}$  value corrected by this 4.5 factor ( $[\text{GSx}]_{\text{cyt.corr}}$ ) was next used as a proxy for  $[\text{GSx}]_{\text{cyt}}$  for further experiments.

At steady state, the cytosolic concentration of glutathione  $[GSx]_{\text{cyt.corr}}$  was estimated at 31.1 mM, which is close to the  $30 \pm 2$  mM measured for  $[GSx]_{\text{ER}}$ , hence, indicating that, contrasting with the results of Montero, the glutathione pools were equally concentrated in the yeast cytosol and ER.

Another important difference pointed by these steady state experiments is a higher GSH:GSSG ratio observed in yeast cells (42:1) compared to HeLa cells (<7:1). This may suggest a lower ERO1 basal activity in yeast compared to HeLa which is also supported by the lower ER  $E_{\text{GSH}}$  in yeast (-242mV) compared to HeLa cells (-208 mV). According to the model proposed by Montero and coworkers decreasing ERO1 activity would accordingly reduce  $[GSx]_{\text{ER}}$  by decreasing the GSSG production and thus glutathione trapping inside the ER. The  $[GSx]_{\text{ER}}$  concentration differences observed between these two studies may also be accounted by technical issues as much as cell model variation. For instance, the radiography that allowed Montero *et al.* to estimate the GSH:GSSG ratio was of poor quality, and their estimation of  $[GSx]_{\text{ER}}$  took this limitation into account. As a result, the authors highlighted that their estimations were conservative, and could very much exceed the value of 15 mM. In any case, both of these studies confirmed the presence of millimolar amounts of glutathione in the endoplasmic reticulum of two eukaryotic species and do not fundamentally contradict each other at this stage.

Ponsero *et al.* took the exploration one step further by taking advantage of HGT1 overexpressing cells to challenge the mechanism of GSH ER transport. Upon exposure to micromolar amounts of GSH, these cells quickly accumulated high levels of cytosolic GSH, which triggered a flux of GSH toward the ER. When GSH intracellular levels were artificially increased, the evolution of  $[GSx]_{\text{ER}}$  as measured by the two biosensors, mirrored that of  $[GSx]_{\text{cyt.corr}}$  in terms of time and concentrations. In agreement with the Banhegyi study using microsomes, these data pointed to a gradient enforced ER transport of GSH through a facilitated diffusion.

As stated above, this GSH ER entrance had severe consequences on ER homeostasis, including UPR induction, Pdi1p and Ero1p reduction, Ero1p activation and a halt in protein secretion altogether driving cell toxicity (Kumar *et al.*, 2011). Ponsero *et al.* took advantage of the toxicity phenotype to look for the GSH transporter. Indeed, if the growth defect was, at least partially, due to GSH import into the ER, impairing GSH import to the ER would mitigate GSH toxicity. This strategy led to the identification of the translocon subunit Sec61 and its homologue Ssh1 as glutathione transporters.

While these data confirmed the relevance of a gradient-dependent transport of GSH toward the ER, the correlative elevation of both  $[GSx]_{\text{cyt.corr}}$  and  $[GSx]_{\text{ER}}$ , even more so in conditions where ERO1 is hyperactive, now poses a challenge to the Montero model and rather suggest that the gradient is more directly imposed by glutathione cytosolic levels.

Ponsero *et al.* next showed that his transport of GSH into the ER is subjected to regulation, which to some extent, mitigates the GSH toxicity observed in HGT1 overexpressing cells. This regulation involves a feedback loop mechanism based on the reciprocal modulation of GSH ER import and Ero1 activation. As GSH enters the ER, it drives a potent ERO1 activation and associated  $H_2O_2$  production, which in turn provokes the oxidation of the HSP70 chaperone Kar2/BiP in a time and dose-dependent manner. Oxidized Kar2 in turn blunted further GSH import into the ER by locking Sec61 in a closed conformation. While mutants mimicking reduced Kar2 further sensitized cells to

GSH toxicity, mutants mimicking the oxidized form of Kar2 rendered them more resistant to GSH toxicity.

Although the experimental conditions using HGT1 are artificial, the observation that an ER stress, stimulated by tunicamycin can similarly lead to a concurrent rise in both  $[GSx]_{Cyt,corr}$  and  $[GSx]_{ER}$  as well as promote Kar2 oxidation, implies that this mechanism may hold physiological relevance.

The relevance of Sec61 in the transport of GSH in mammals has been investigated once. When investigating the cause of previously described calcium-dependent ER reduction (Avezov et al., 2013; 2015; Enyedi, Várnai, and Geiszt, 2010; van Lith et al., 2011), Lizak *et al.* used thapsigargin (Tg), an inhibitor of the Sarco-Endoplasmic Reticulum Calcium ATP-ase (SERCA) that prevents the uptake of calcium into the ER, resulting in a calcium leak from the ER. That calcium leak was accompanied with an ER reduction, that was dependent on the presence of cytosol, and sensitive to BSO, which led them to propose that this reduction was the result of glutathione entry into the ER. However, when investigating the involvement of Sec61 in that import, neither chemical inhibition nor silencing RNA against Sec61 had an impact on calcium-dependent ER reduction, suggesting that in mammalian cells, GSH transport might not be -or at least not totally- similar to what has been described in yeast cells.

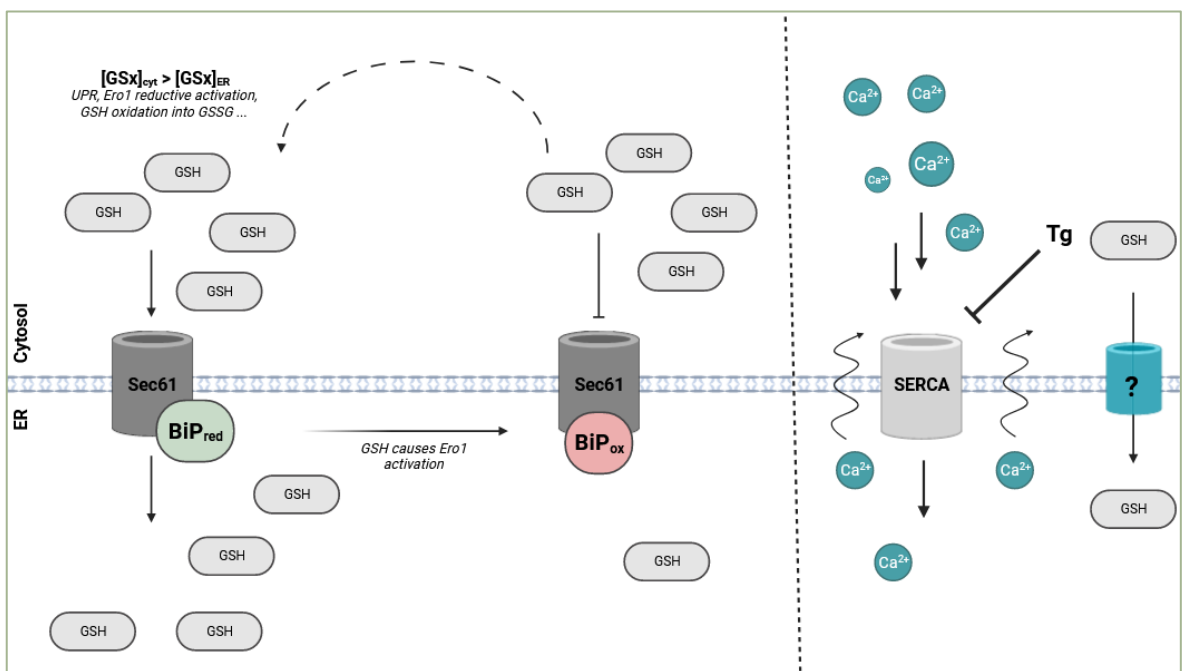


**Figure 26 – Proposed model for ER import of GSH.** Left: adapted from (Ponsero 2017), Glutathione can diffuse passively through Sec61. During ER Stress,  $[GSx]_{cyt}$  and Ero1 synthesis are increased, stimulating GSH diffusion towards the ER. This import provokes Ero1 reductive activation, consuming GSH into GSSG, further stimulating ER import of GSH. Ero1-dependent H<sub>2</sub>O<sub>2</sub> production leads to BiP/Kar2 oxidation, providing a means to inhibit GSH import and Ero1 activation. (Right): Possible calcium-dependent ER GSH import: thapsigargin (Tg) blocks SERCA from pumping calcium, resulting in a calcium leak from the ER, accompanied by GSH-dependent ER reduction, possibly through GSH import via an unknown transporter.

## AIMS OF THE PROJECT

Glutathione was described more than 120 years ago, and has been extensively studied since then. The molecule has long been classified as a major redox buffer, with respect to its function in association with enzymes. Its role in the physiology of the cell however, is yet to be extensively described. We now know that the distribution and redox state of glutathione throughout the cell compartment is highly variable, which raises the question of how and why is this distribution maintained uneven. Additionally, this variability could well reflect disparities in function from one organelle to another.

Among other organelles, the role of glutathione in the endoplasmic reticulum is often questioned and debated. At the moment, the study of its function in this compartment is partially hindered by our limited understanding of the mechanism governing the glutathione ER transport and the lack of tools available to manipulate this transport.

Our objective was to describe and understand the systems involved in trafficking glutathione to the ER with the help of previously described redox sensors. A better comprehension of this transport would yield great advantages: (1) gaining insights into the mechanisms and conditions stimulating glutathione transport could provide valuable indications about the needs and demands of the ER thereby placed on this organelle, and hence, could shed light on the ER functions of this tripeptide. (2) the identification of transport systems would provide us with the necessary tools for precise modulation of ER glutathione pools, thereby enabling us to specifically investigate the consequences of this modulation on ER physiology and functions.

In the long run, managing glutathione transport especially towards the ER could be key to protein folding diseases in which glutathione could be involved.

This project was articulated around two strategies whose goal was to describe thoroughly how glutathione is transported towards the ER.

First, we wanted to challenge the proposed models for GSH ER transport, starting with the gradient hypothesis, using a human whole cell system and taking advantage of the biosensor strategy. Here we first aimed to test the impact on GSH ER transport of conditions triggering either an elevation or a decrease of cytosolic GSH using both pseudo-physiological and artificial conditions. Our goal was to explore how such conditions affected the ER, in terms of redox potential, GSH and GSSG levels as well as proteostasis.

In a second time, we wanted to lead a screening protocol, in order to identify one or several molecules capable of inhibiting transport of glutathione towards the ER, with the hopes that this molecule would lead us, ideally, to a transporter, or at least provide us with a tool to modulate ER GSH levels specifically.



## INTRODUCTION

Glutathione is a small ubiquitous redox active tripeptide ( $\gamma$ -glutamyl-cysteinyl-glycine), found in all eukaryote species and broadly in prokaryotes. Its high cellular abundance (in the millimolar range) has propelled glutathione as a major thiol-reducing redox buffer. Due to its nucleophilic nature, GSH indeed supports electrophiles and heavy metals detoxification and may directly assist oxidant scavenging. However, numerous redox functions of glutathione are rather accomplished through its interaction with dedicated enzymes contributing to the maintenance of cellular redox homeostasis. These include glutathione-peroxidases, which support  $H_2O_2$  reduction and glutaredoxins, which convey disulfide bonds reduction and control the formation of protein-glutathione mixed disulfides, a modification known as glutathionylation. In addition to its thiol-redox dependent functions, glutathione carries an essential but still ill-characterized function in iron metabolism and iron-sulfur biosynthesis. Glutathione exists in two forms, reduced as GSH and disulfide bonded as GSSG. GSSG is formed from GSH oxidation mainly through thiol-disulfide exchange reactions, as GSH delivers reducing power for the catalytic cycle of reductases. In the cytoplasm and mitochondrial matrix, GSSG is regenerated back to GSH, by the action of glutathione reductase, a flavin-containing enzyme relying on the reducing power of nicotinamide adenine dinucleotide phosphate (NADPH). Glutathione is synthesized by a two steps process, both ATP-dependent:  $\gamma$ -glutamyl-cysteine ligase (GCL in mammals) catalyzes the  $\gamma$  bond between L-glutamate and L-cysteine, and the resulting dipeptide is then  $\gamma$ -bonded to a glycine residue by glutathione synthase. In eukaryotes, GSH is widely distributed in the different cellular organelles while these biosynthetic reactions are restricted to the cytosol, which implies the existence of dedicated transport mechanisms. Such process has recently been unraveled for mitochondria GSH import, which confirmed a central role for GSH in iron metabolism. It also illustrated how studying GSH organelle import mechanisms can shed light on its role in physiology.

Glutathione is present in the millimolar range in the Endoplasmic Reticulum (ER). Its function, if any, in this organelle yet remains controversial. ER is a highly redox active compartment where oxidation of nascent proteins entering the secretion pathway takes place. Such disulfide bonds formation is taken in charge by a dedicated system, composed of Protein Disulfide isomerase (PDI) and ER oxidase (ERO1) family members. ERO1 creates *de novo* disulfides, at the expense of  $H_2O_2$  production. Disulfides are then handed over to nascent proteins by PDI. The presence of GSH as a kinetically proficient reducer of PDIs may thus at first seem inappropriate. An ER reducing power is nevertheless believed mandatory to sustain a proper ER proteostasis. First, a fraction of PDI must lie in its reduced form to support optimal oxidative folding, allowing the isomerization/reduction of improperly disulfide-bonded proteins and the maturation of folding intermediates. Second, a prior reduction of terminally misfolded proteins is required for their efficient elimination by the ER Associated Degradation (ERAD) machinery. Both of these functions are likely shared by other members of the PDI family. Among those, ERdj5 emerged as an important player required for both

the oxidative maturation of nascent proteins and the reduction of improperly folded ER proteins. Different models are still being debated to explain how reduced pools of PDI(s) are maintained/fueled and GSH, which directly react with PDIs, was initially described as an important contributor to this process (Molteni et al., 2004; Chakravarthi and Bulleid, 2004; Kumar et al., 2011; Ponsoero et al., 2017). Some doubts have however gradually been cast about its actual relevance. First, GSH depletion in yeast or its ER exhaustion in human cells did not demonstrate any defect in protein folding nor triggered activation of the Unfolded Protein Response (UPR) as would be expected from an ER dysfunction. Similarly, no significant effect of GSH ER depletion on ERAD efficiency could be witnessed. In parallel, alternative pathways for ER reduction have been proposed. These include the transfer of reducing equivalents from the cytosolic thioredoxin pathway, through an unknown membranal intermediate. Restraining ERO1 oxidative activity is another way to maintain a pool of reduced PDI. ERO1 activity is indeed negatively controlled by intramolecular regulatory disulfides which are formed upon accumulation of oxidized PDI. These are either resulting from ERO1 auto-oxidation in the absence of sufficient reduced PDI substrate or from an active PDI dependent oxidation. Increasing the PDI<sub>red</sub>/PDI<sub>ox</sub> ratio will conversely stimulate a PDI-dependent ERO1 reductive activation. This mechanism is thought to adapt ERO1 activity to the load of nascent reduced proteins entering the ER. In this model, the threshold for ERO1 inactivation could autonomously set the PDI redox ratio. Strikingly, ERO1 itself has even recently been involved in the reduction of ERdj5, which there acts as a redox acceptor in place of molecular oxygen (Uegaki et al., 2023). Adding to the fact that PDI family members are themselves organized in redox relays, this overall points to a complex and intertwined control of how PDIs redox states are set. Having that in mind, it is worth noting that stimulating GSH ER transport can nonetheless reduce both PDI and ERO1, questioning a possible contribution of GSH metabolism to ER redox homeostasis in conditions that remain to be defined.

As exemplified for mitochondria, decoding the modalities of GSH organelle transport is a powerful tool to understand GSH local function. Using yeast model, we previously showed that GSH ER transport was responsive to the concentration gradient imposed between cytosol and ER and occurred through a facilitated diffusion mechanism supported by the Sec61 protein translocation channel. Artificially mounting GSH gradient led to potent Pdi1p reduction/Ero1p activation and resulted in secretion block, UPR induction and toxicity. These deleterious effects could be opposed by a negative feed-back loop launched as the Kar2/BiP ER chaperone gets oxidized by Ero1-derived H<sub>2</sub>O<sub>2</sub> thereby blocking further GSH ER transport through Sec61.

Using ER biosensors, we here set out to characterize conditions stimulating GSH ER transport in a human cell line and its consequences on ER homeostasis. It was previously proposed that GSH ER import is triggered by depletion of ER calcium stores (Lizák et al., 2020). Here, we observed that modulating GSH cellular levels also rapidly impacted ER redox state and provided evidence for a gradient dependent transport of GSH. Contrary to yeast, inactivating translocon did not prevent the GSH-induced ER reduction. Imposing a GSH cytosolic gradient led to a limited and sustained ER reduction, which did not significantly trigger UPR nor prevented oxidative folding, yet yielded a moderate reduction of ERO1 and ERdj5. Accordingly, we observed a slight increase in the folding rate of a model substrate. After confirming the existence of calcium-dependent GSH ER transport in

our cell system, we finally proposed that GSH ER transport can follow two paths in mammals: one passive and gradient-dependent and one active and calcium dependent.



---

# RESULTS

---

## MODULATION OF GLUTATHIONE BIOSYNTHESIS IMPACTS GSH-ASSOCIATED ER REDOX POTENTIAL

In yeast, an elevation of GSH intracellular levels is sufficient to trigger the ER transport of GSH with notable physiological effects. To investigate whether modulating GSH cytosolic levels could also impact the reductive properties of mammalian ER, we established different experimental systems enabling the tuning of GSH cytosolic concentrations.

In mammals, the rate of GSH biosynthesis is controlled by the activity of gamma-glutamyl cysteine ligase (GCL), which carries the first and limiting step of GSH biosynthesis in the cytosol. GCL is composed of two subunits, GCLC (catalytic) and GCLM (modifier), the overexpression of each was previously shown to increase total GSH intracellular levels, aka  $[GSx]_{Cell}$ , by 4-times (H. Zhang et al., 2012). We thus transiently overexpressed each GCL subunits, alone or in combination, and monitored their impact on  $[GSx]_{Cell}$  (**Supplemental Figure 1 A-B**). Single overexpression of each GCL subunits significantly elevated  $[GSx]_{Cell}$  but a synergistic effect was observed by jointly overexpressing GCLC and GCLM,  $[GSx]_{Cell}$  then reaching a 4-fold increase in HEK293 cells (**Figure 1A** upper panel and **Supplemental Figure 1B**), rising from  $2.1 \pm 0.7$  to  $8.2 \pm 2.5$  mM. Using these conditions in an engineered cell line stably expressing the ER-localized Grx1-roGFPIe GSH biosensor, we monitored the impact of GCL overexpression on ER GSH reduction potential ( $E_{GSH}$ ). Grx1-roGFPIe quickly equilibrates with glutathione, proportionally to the  $[GSH]^2/[GSSG]$  ratio (Birk et al., 2013), giving access to  $E_{GSH}$  through the Nernst equation. Doing so, we observed that GSH biosynthetic stimulation upon GCLC/M overexpression triggered a significant 13 mV decrease of ER  $E_{GSH}$ , making it drop from  $-217\text{mV} (\pm 4\text{mV})$  to  $-231 \text{ mV} (\pm 4\text{mV})$  (**Figure 1A, lower panel**)

We next sought for conditions to dynamically deplete then replete GSH cytosolic levels. GSH is synthesized from glutamate, cysteine and glycine. We thus surmised that controlling the source of sulfur amino-acids in the medium would dynamically impact glutathione levels. We indeed observed that depriving cells overnight from cystine, the oxidized form of cysteine, led to a strong decrease in  $[GSx]_{Cell}$  (**Figure 1B, upper panel**). Of note, methionine depletion was not required to efficiently deplete GSH pools, indicative of a poorly active transsulfuration pathway in these cells. Conversely, replacing the cystine-starved medium by a complete one led to a quick recovery of glutathione cellular pools (within 2 hours). Mechanistically, cystine starvation directly impacted GSH biosynthesis but also acutely upregulated the GSH-degrading enzyme CHAC1 (**Supplemental Figure 1C**), suggesting that an active GSH degradation contributed to the starvation-induced GSH depletion, possibly as a mean to rebuild cysteine pools. Upon cystine repletion (complete medium), the swift decrease in CHAC1 mRNA levels together with the more persistent up-regulation of the cystine-specific subunit, SLC7A11, of the xCT plasma membrane (PM) cysteine transporter probably accounted for the rapid replenishment of cysteine and thus GSH pools. Of note, no upregulation of GCL subunits was observed in these conditions (not shown).

Having set up this system, we monitored how modulating glutathione levels according to cysteine availability impacted ER glutathione reduction potential. We observed that the  $[GSx]_{Cell}$  decrease induced by cystine starvation translated into a significant increase of ER  $E_{GSH}$  ( $+ 9 \text{ mV}$ ;  $p < 0.0001$ ,

from  $-220.9 \text{ mV} \pm 2.2$  in untreated cells to  $-211.9 \text{ mV} \pm 4.5$  in starved cells ( $n=20$ ) which was fully recovered upon cystine repletion, according to kinetics that followed the rebuild of GSH intracellular pools.

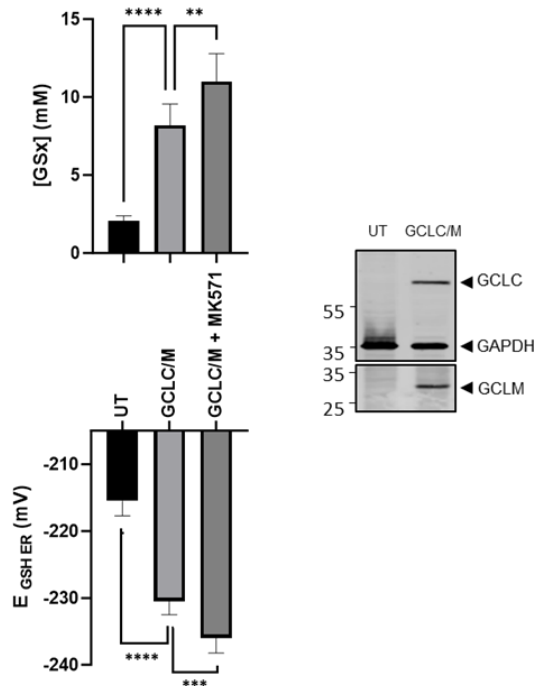
These data thus showed that a modulation of GSH biosynthetic/degradation cytosolic rates directly impacted ER  $E_{\text{GSH}}$ , highlighting that, as in yeast, dynamic GSH exchanges occurs between cytosol and mammalian ER.

**Publication figure 1 – GSH reduction potential in the Endoplasmic Reticulum varies according to GSH intracellular levels.**

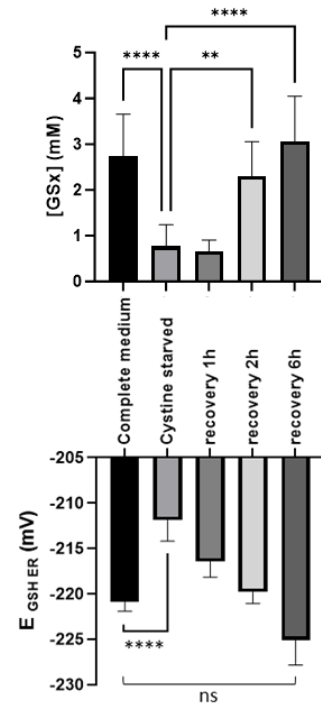
$E_{\text{GSH ER}}$  and  $[\text{GSx}]_{\text{Cell}}$ , respectively referring to GSH ER reduction potential and total intracellular glutathione concentration, were simultaneously assessed in HEK293 cells stably expressing Grx1-roGFPiE. Glutathione intracellular levels were raised either by jointly transfecting the GCLC and GCLM subunits of the glutamate-cysteine ligase (A) in the presence or absence of MK571 ( $300 \mu\text{M}$ , 10 min), or by addition of reduced glutathione (GSH) in the culture medium (C-F). Conversely, glutathione intracellular pools were exhausted by starving cells from cystine overnight, then restored by adding back complete medium during the indicated times (B).  $E_{\text{GSH}}$  values were calculated from Grx1-roGFPiE ratiometric fluorescent measurements using a temperature-controlled microplate reader.  $[\text{GSx}]_{\text{Cell}}$  levels were determined on cell lysates, using a 96-wells plate-optimized GR recycling assay, and expressed in mM after correction by the cell number and cell volume, individually assessed for each experimental condition. (C and E) Kinetic evolution of  $E_{\text{GSH}}$  and  $[\text{GSx}]_{\text{Cell}}$  over a 60 minutes time-course after addition of 2.5 mM GSH in the culture medium. (D and F) Dose response analysis of  $E_{\text{GSH}}$  and  $[\text{GSx}]_{\text{Cell}}$  after addition of 0.25, 0.5, 1, 2.5, 5, 7.5 and 10 mM of GSH in the culture medium during 10 minutes. Data were plotted with 95% CI interval error bars (Kinetic analysis:  $n=4$  to  $n=98$  (average  $n=20$  for GSH treatments) for  $E_{\text{GSH}}$  and  $n=11$  to 105 for  $[\text{GSx}]_{\text{Cell}}$ ; Dose response analysis:  $n=4$  to 92 for  $E_{\text{GSH}}$  and  $n=7$  to 35 for  $[\text{GSx}]_{\text{Cell}}$ ). Comparison GCL (A) or starved conditions (B) with control conditions yielded t-test p-values  $< 0,0001$ . For all assays, one-way ANOVA yielded overall p values  $< 0,0001$  and Tukey's comparison was performed to compare pairs of means. Significance was accordingly plotted on A-F.

**Figure 1**

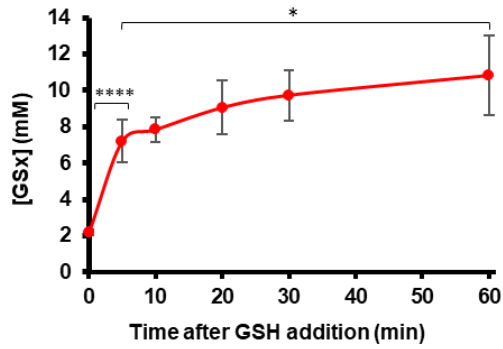
**A**



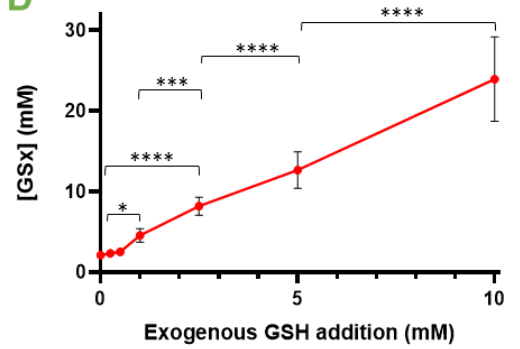
**B**



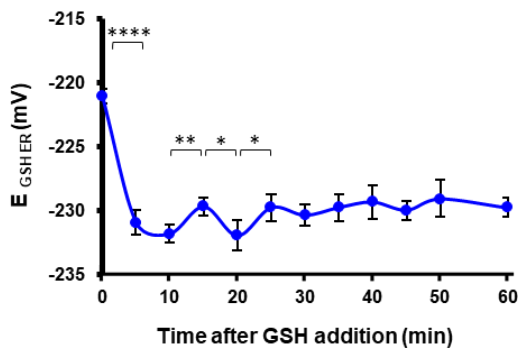
**C**



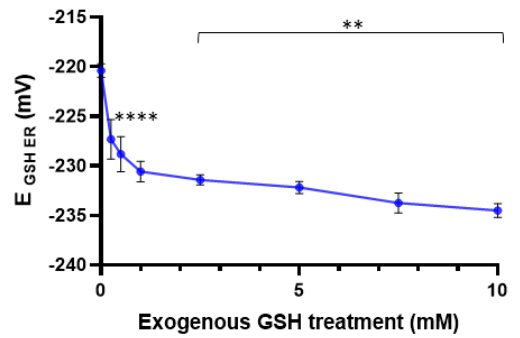
**D**



**E**



**F**



---

## EXTRACELLULAR GSH IS INTRACELLULARLY IMPORTED AND CAUSES A SWIFT AND REVERSIBLE DECREASE OF GSH-ASSOCIATED ER REDOX POTENTIAL

In an effort to achieve a more dynamic modulation of glutathione cytosolic levels and despite the lack of an ascribed high-affinity GSH PM transporter in mammalian cells, we inspected how cells reacted to exogenous GSH exposure. Doing so, we observed that cell treatment with mM doses of exogenous GSH indeed increased intracellular  $[GSx]_{Cell}$  (**Figure 1C and 1D, supplemental Figure 2A**). A basal glutathione concentration of 2.1 mM (+/- 0.6) was measured. When cells were exposed to 2.5 mM of GSH, the increase in  $[GSx]_{Cell}$  occurred as early as 5 minutes after GSH addition and persisted for at least one hour (**Figure 1C**) to reach over 10 mM (10.8 mM  $\pm$  3.4). We then exposed cells to increasing GSH doses and observed a significant elevation of glutathione intracellular levels after 10 minutes of treatment, evident from 1 mM of exogenous GSH treatment.  $[GSx]_{Cell}$  linearly augmented from 2 to 24mM ( $\pm$  5) as we increased treatment doses up to 10 mM GSH (**Figure 1D, supplemental Figure 2A**). To rule out any confounding effect due to unspecific binding of GSH to the PM or to medium contamination, we performed the same GSH dosage procedure, either in the presence of digitonin to create holes in the cell membrane (not shown) or by including a longer wash step of 3 minutes in PBS instead of removing it swiftly (**Supplemental Figure 2C**). In both cases, we lost the  $[GSx]_{Cell}$  increase previously observed upon exogenous GSH treatment, indicating that our dosage reliably reported on GSH intracellular pools. These experiments also suggested that GSH levels could be rapidly restored back to basal concentrations upon removal of exogenous GSH.

We took advantage of these experimental conditions to monitor ER  $E_{GSH}$  upon exogenous GSH addition. We measured an ER  $E_{GSH}$  of -220 mV (+/-3) in untreated cells. Treatment with 2.5 mM exogenous GSH led to a rapid and persistent decrease in ER  $E_{GSH}$  (-11 mV,  $p < 0.0001$ ), matching the kinetics observed for  $[GSx]_{Cell}$  build-up (**Figure 1E**). Interestingly, ER  $E_{GSH}$  slightly but significantly oscillated during the first 30 minutes of treatment, suggesting that a dynamic redox adaptation is at play before a new  $E_{GSH}$  equilibrium value is defined. We similarly monitored how ER  $E_{GSH}$  responded to increasing doses of 10 minutes exogenous GSH treatments (**Figure 1F, supplemental Figure 2B**). Strikingly, doses as low as 0.25-0.5 mM GSH already stimulated a significant decrease of ER  $E_{GSH}$ . When doses were further increased, a comparatively milder but significant ER  $E_{GSH}$  was still observed with a maximum reduction achieved of -14mV ( $p < 0.0001$ ), a value comparable to that observed upon GCL overexpression.

To test the dynamics of this system, we performed washout experiments after GSH treatment (**supplemental Figure 2D**). As previously seen, treating cells with 2.5mM GSH during 10 minutes led to an average  $[GSx]_{Cell}$  increase of 3.5 times. Upon GSH washout, we observed that GSH intracellular levels were rapidly restored back to basal concentrations, as early as 7.5 minutes after GSH withdrawal from the medium. Importantly, removal of exogenous GSH also reversed the  $E_{GSH}$  decrease induced by GSH addition (**supplemental Figure 2E**), further indicating that  $E_{GSH}$  is dynamically set according to  $[GSx]_{Cell}$ . Reestablishment of ER  $E_{GSH}$  yet occurred in a slower and incomplete manner compared to  $[GSx]_{Cell}$ , indicating that ER transported glutathione may be partly trapped in this organelle.

We finally tested whether the rapid elevation of  $[GSx]_{cell}$  observed upon exogenous GSH exposure and the resulting decrease in ER  $E_{GSH}$  were indeed due to a direct import of the metabolite from the medium inside the cell. Alternatively, exogenous GSH is proposed to undergo efficient hydrolysis by extracellular  $\gamma$ -glutamyl transpeptidase and dipeptidases (Orlowski and Meister, 1970), and the resulting amino acids, in particular cystine, could be imported in cells to stimulate GSH cytoplasmic neosynthesis. Xc-, an amino acid transporter composed of xCT (SLC7A11) and 4F2 heavy chain (SLC3A2) subunits, is the major cystine transporter at the PM. It exchanges one extracellular L-cystine for one intracellular L-glutamate (Bannai and Kitamura, 1980; Bannai, 1986), and can be inhibited by erastin (Dixon et al., 2012). GSH neosynthesis can be abolished by inactivating GCL with Buthionine sulfoximine (BSO). While both inhibitors efficiently depleted glutathione pools, neither prevented  $[GSx]_{cell}$  build up upon GSH exposure (**supplemental Figure 3**). Similarly, the swift decrease of ER  $E_{GSH}$  observed upon GSH treatment was not impacted by either BSO or erastin pre-treatment. Altogether, these data showed that cell exposure to GSH led to the rapid and reversible import of this reductive metabolite inside the cell, thus suggesting the existence of a low-affinity GSH transporter in PM of HEK293 cells.

This set of experiments also showed that, similar to the manipulation of GSH metabolism, raising GSH cytosolic levels by promoting the extracellular import of GSH led to a fast and persistent ER reduction.

---

#### THE GSH-INDUCED ER REDUCTION IS IN PART CONDITIONED BY GSH CELLULAR EFFLUX

As we observed that GSH levels can be quickly decreased in washout experiments, we surmised that an active export system is present in our cell system. The multidrug PM transporter MRP1 was previously shown to be an important mediator of GSH cellular export and homeostasis (J. Y. Cao et al., 2019). We thus used MK571 as an inhibitor of MRP1 to monitor how preventing GSH cellular export impacted on both  $[GSx]_{cell}$  and ER  $E_{GSH}$ . MK571 didn't have any significant impact on its own (**Supplemental Figure 2F**). However, when used together with GCLC/M overexpression, MRP1 inhibition led to a further increase in  $[GSx]_{cell}$  which translated into an additional 5mV decrease in ER  $E_{GSH}$  (**Figure 1A**). Similarly, MK571 treatment slightly amplified the ER reduction triggered by exogenous GSH treatment (**Supplemental Figure 2F**).

We thus concluded that in our cell system, a GSH PM export was active to regulate GSH homeostasis, which in part conditioned the extent of GSH-induced ER reduction.

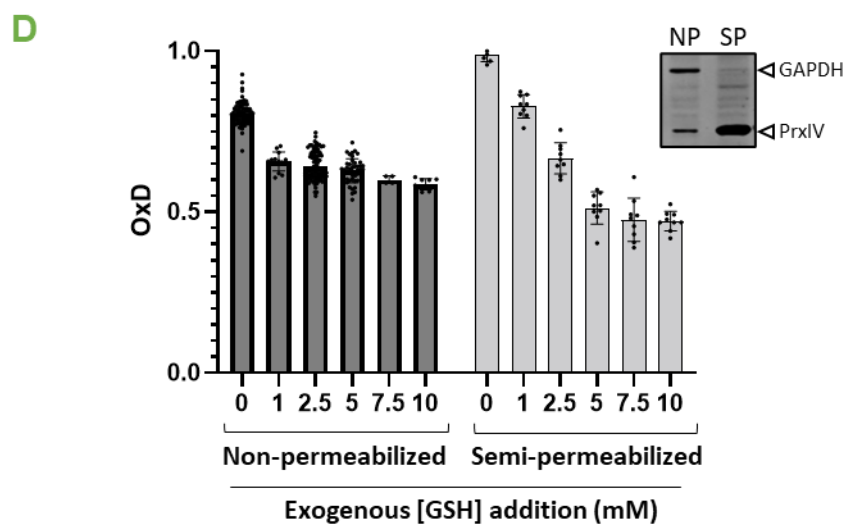
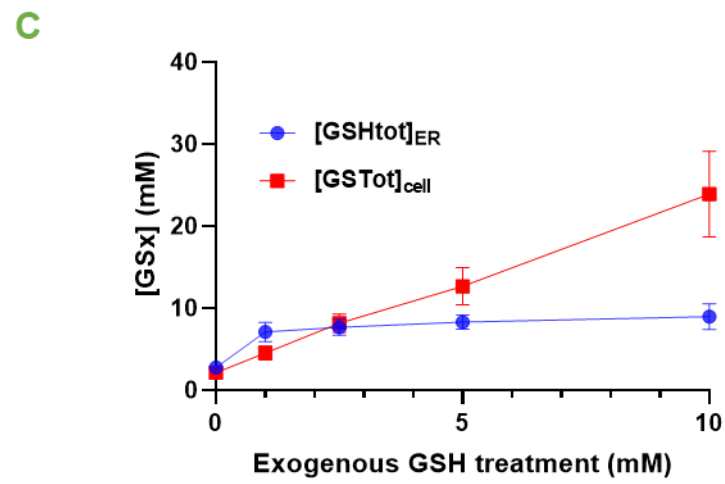
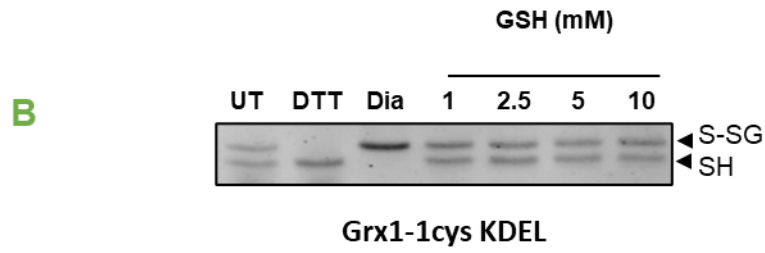
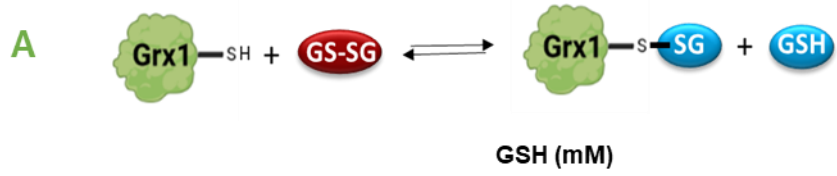
## A CONCENTRATION GRADIENT-DEPENDENT ER TRANSPORT

We so far used  $E_{\text{GSH}}$  as a readout proxy for GSH ER import. We next wished to establish if raising  $[\text{GSx}]_{\text{Cell}}$  could indeed stimulate GSH ER transport and if as in yeast, this transport was a function of the concentration gradient imposed. To do so, we took advantage of a second glutathione biosensor, the Grx1-1cys-KDEL probe. This encodes an ER targeted glutaredoxin lacking its resolving cysteine. Consequently, the glutathionylated state of this monothiol enzyme is set according to the luminal  $[\text{GSH}]/[\text{GSSG}]$  ratio (Iversen et al., 2010; Montero et al., 2013; Ponsero et al., 2017), (**Figure 2A**). This probe was originally derived from yeast glutaredoxin 1 (Grx1) and we codon-optimized its DNA sequence for our human cell system which efficiently improved its expression. We next performed differential alkylation of the reduced and glutathionylated forms of the Grx1-1cys-KDEL protein to separate both redox forms according to their electrophoretic properties (**Figure 2B**). The Grx1-1cys-KDEL probe was approximately 50% oxidized/glutathionylated in untreated conditions (49% +/-5% in SD), which, according to the  $K_{\text{ox}}$  of the enzyme, equated to a mean ratio of reduced to oxidized glutathione ( $[\text{GSH}]/[\text{GSSG}] = R_{\text{GS}}$ ) of 76:1 in the ER (76 +/- 14, after propagating measure uncertainty). By exploiting our previous measurements of ER  $E_{\text{GSH}}$ , we could deduce the ER  $[\text{GSH}]^2/[\text{GSSG}]$  ratio from the Nernst equation, and accordingly calculate the absolute glutathione concentration in the ER (see **Materials and Methods**) ( $[\text{GSx}]_{\text{ER}} = [\text{GSH}]_{\text{ER}} + 2[\text{GSSG}]_{\text{ER}}$ ). In the absence of treatment, this led to a basal ER GSH concentration ( $[\text{GSx}]_{\text{ER}}$ ) of 2.9mM  $\pm$  1,1. This concentration was close to the 2.1 mM ( $\pm$  0.6) measured for  $[\text{GSx}]_{\text{Cell}}$  in untreated cells. We performed the same assay after cell treatment with increasing doses of exogenous GSH during 10 minutes. GSH addition did not cause a significant change in the probe ratio (**Supplemental Figure 4**), which, combined to the corresponding experimental  $E_{\text{GSH}}$  values, yielded calculated  $[\text{GSx}]_{\text{ER}}$ , 2.5 to 3 times higher compared to that in untreated cells (**Figure 2C**), reaching a maximum of 9.2mM  $\pm$  2.  $[\text{GSx}]_{\text{ER}}$  mirrored  $[\text{GSx}]_{\text{Cell}}$  upon exposure to 1 mM and 2.5 mM of GSH. Upon higher doses of GSH exposure,  $[\text{GSx}]_{\text{ER}}$  and  $[\text{GSx}]_{\text{Cell}}$  values uncoupled, with  $[\text{GSx}]_{\text{ER}}$  reaching a plateau while  $[\text{GSx}]_{\text{Cell}}$  still increased. These data thus suggest that, as in yeast, a GSH gradient imposed between the cytosol and the ER could rapidly stimulate an entry of GSH inside the ER. However, this GSH import was more rapidly limited in intensity.

To more directly assess the impact of imposing a GSH gradient on ER, we took advantage of a semi-permeabilized (SP) cell system, using digitonin. Used at low concentrations, this detergent selectively permeabilizes the PM while leaving the ER membrane intact. Non permeabilized (NP) cells, treated with a similar protocol but omitting digitonin were used as controls. To verify our permeabilization conditions, we monitored the expression of GAPDH and PrxIV cells as respective markers for cytosolic and ER proteins (**Figure 2D**, inset). We confirmed that PrxIV signal was maintained in SP cells while GAPDH was lost. We then used NP and SP cells expressing Grx1-roGFPiE to compare their response to GSH-induced ER reduction. Expectedly, the probe was fully oxidized in untreated SP cells. This precluded calculation of  $E_{\text{GSH}}$  and we instead used the percentage of probe oxidation (OxD) as a readout for ER reduction. In SP cells, the probe was rapidly reduced upon exogenous GSH treatment (**Figure 2D**). This reduction occurred in a dose-dependent manner up to 5 mM of exogenous GSH addition, then the probe reactivity decreased. Interestingly, the  $E_{\text{GSH}}$  plateau in whole cells (**Figure 1F**) occurred when  $[\text{GSx}]_{\text{Cell}}$  reached a similar concentration, between 7 and 8 mM  $\pm$  1.5 (**Figure 2C**), suggesting an analogous limiting mechanism may be at play.

Altogether, these data suggested that human cells also possess a GSH ER transport mechanism responding to the GSH gradient-imposed between the cytosol. Our data also indicated that in our cell system, this mode of transport becomes less effective when the cytosolic GSH concentration exceeded 7.5 mM.

**Figure 2**



**Publication figure 2 – Quantitation of GSH ER transport using Grx1-1cys probe and semi-permeabilized cells.**

(A) Scheme of the Grx1-1cys probe and its equilibration with GSH /GSSG couple (B) HEK293 cells, transfected with an ER-localized version of HA-Grx1-1cys, were left untreated or treated with the indicated GSH doses for 10 minutes. The glutathionylated/unglutathionylated ratio of the Grx1-1cys probe (S-SG/-SH) was monitored after immediate blocking of the reduced thiols with iodo-acetamide, followed by an HA immunoprecipitation, then reduction and alkylation of the originally oxidized thiols with 2 kDa PEG-maleimide. Cell treatments with DTT or diamide were used as respective controls for the fully unglutathionylated (-SH) and glutathionylated (-S-SG) forms of the ER Grx1-1cys probe. The -SH/-S-SG ratio of the Grx1-1cys probe, obtained for each experimental conditions, were quantified by densitometry after SDS-PAGE. This ratio is directly proportional to the GSH/GSSG ratio. n=8-15 for each GSH dose tested. One of these dose response experiments is shown. (C) The total concentration of GSH inside the ER ( $[GSTot]_{ER} = [GSH]_{ER} + 2[GSSG]_{ER}$ , blue curve) was deduced for each experimental condition, according to the following equation:  $[GSTot]_{ER} = X_{ER} * (1/Y_{ER} + 2/Y_{ER}^2)$ , where  $X_{ER} = [GSH]^2/[GSSG]$  is calculated based on the ER EGSH measurement (Figure 1F) and  $Y_{ER} = [GSH]/[GSSG]$  is determined from the glutathionylation state of the ER Grx1-1cys probe (Figure 2B), The red curve represents the cellular total GSH concentration ( $[GSTot] = [GSH] + 2[GSSG]$ ), as measured in Figure 1D. (D) HEK293 cells stably expressing ER-located Grx1-roGFPiE were semi-permeabilized (SP), then treated with increasing amounts of GSH (n=9). The percentage of oxidation of the roGFP probe (OxD) was calculated using ratiometric fluorescent measurements and DTT and diamide treatments defined the 0 and the 100% of the probe oxidation. The OxD obtained on SP cells are compared to the OxD obtained upon GSH treatment of non-permeabilized (NP) cells. Both efficient permeabilization and maintenance of ER integrity during the semi-permeabilization procedure were controlled by monitoring the respective loss and preservation of GAPDH and PrxIV proteins detection in SP cells using SDS-PAGE

---

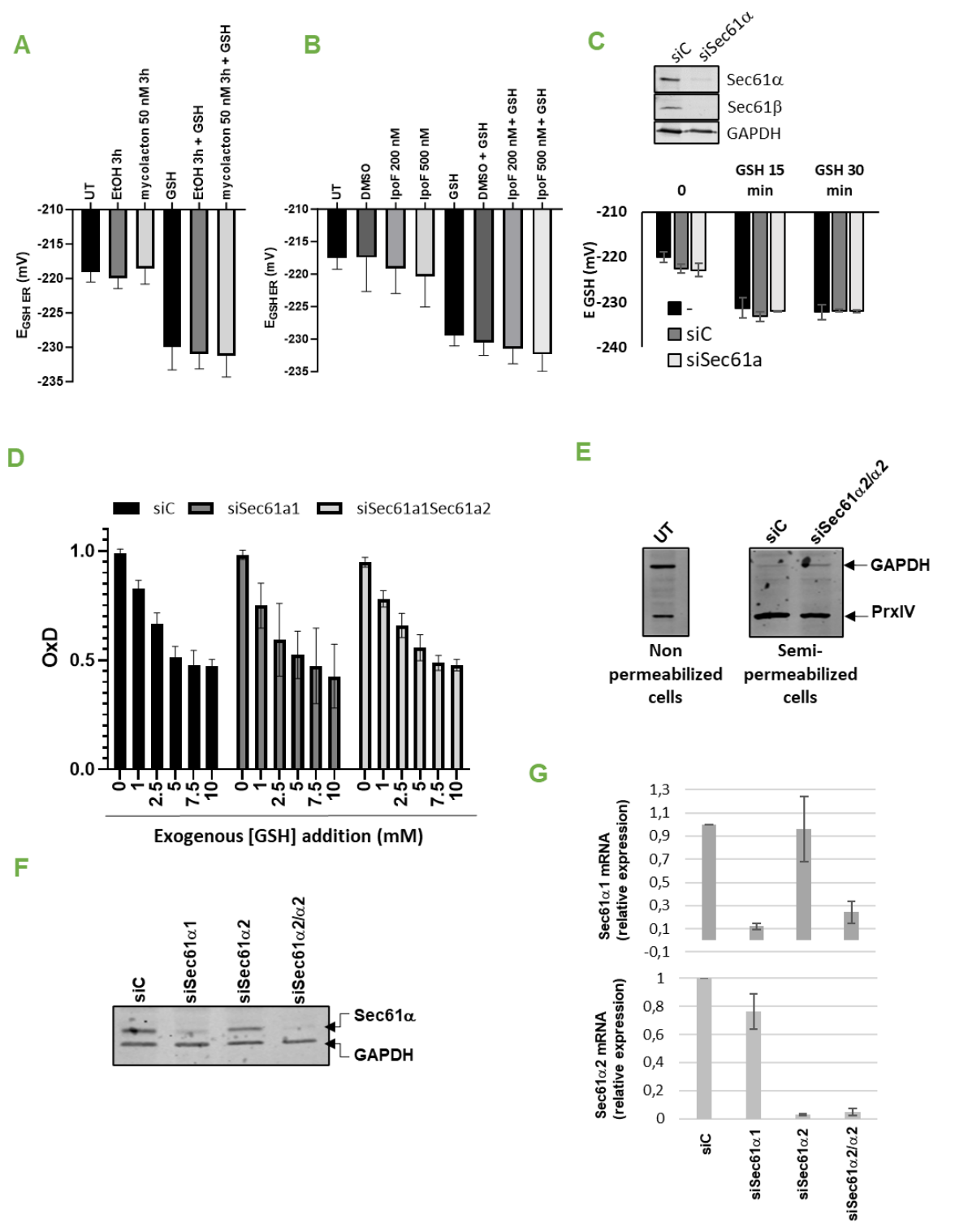
## INHIBITION OF SEC61 DOES NOT PREVENT GSH ER TRANSPORT

In yeast, GSH is transported into the ER by the Sec61-based translocon machinery. The translocon is essential for the ER translocation of both soluble and membrane proteins. It is composed of three subunits, Sec61 $\alpha$ , Sec61 $\beta$  and Sec61 $\gamma$ , where the multipass membrane protein Sec61 $\alpha$  forms the core of a gated-channel across the ER membrane.

To assess the function of the translocon in mammalian GSH ER transport using the previous experimental conditions, we took advantage of the reported development of different Sec61 $\alpha$  inhibitors. Mycolactone is a polyketide-derived macrolide produced by *Mycobacterium ulcerans*. It binds tightly and irreversibly to Sec61 $\alpha$  which alters its conformation. Consequently, mycolactone halts the secretion of co-translationally translocated soluble proteins and that of certain class of transmembrane containing polypeptides according to their hydrophobicity and topology (Hall et al., 2014; Baron et al., 2016; McKenna, Simmonds, and High, 2016; Morel et al., 2018). Mycolactone was proposed to act by “locking” the translocon in a closed conformation, as mycolactone treatment increases the hydrophobic threshold required to trigger channel opening by protein substrates. Mutations conferring resistance to mycolactone localized near the luminal domain which plugs translocon exit, further supporting this model. Ipomoeassin F (ipoF) is a recently characterized Sec61 $\alpha$  inhibitor from the glycoresin family (Zong et al., 2019). Although chemically distinct, ipoF interaction domain overlaps with that of other Sec61 $\alpha$  inhibitors and its functional impact on protein secretion is similar to that observed for mycolactone. While mutational analysis suggests subtle differences in its mode of action (Zong et al., 2019), a recent structure of inhibited human Sec61, using both mycolactone and ipoF confirmed that both of these inhibitors can indeed stabilize the translocon plug domain in a closed conformation (Itskanov et al., 2023). We thus tested the ability of both mycolactone and ipoF to inhibit GSH ER transport. First, we confirmed that each molecule was indeed active by monitoring their ability to block IgM secretion in a reporter cell line (Bakunts et al., 2017) (**Supplemental Figure 5**). As expected, both inhibitors significantly prevented IgM medium excretion compared to control conditions. We then tested the impact of a mycolactone or ipoF pretreatment on GSH-induced ER reduction. In either condition, we could not observe any effect of Sec61 $\alpha$  inhibitors on basal  $E_{\text{GSH}}$  nor on the GSH-induced  $E_{\text{GSH}}$  decrease.

As mycolactone and ipoF inhibitory effects may not be sufficient to affect GSH ER transport, we additionally monitored the impact of knocking down Sec61 $\alpha$ 1 the major Sec61 $\alpha$  subunit of the translocon, by siRNA (**Figure 3C**). Knock-down efficiency was controlled by western blot analysis. As for chemical inhibitors, reducing Sec61 $\alpha$ 1 levels did not impact the ability of exogenous GSH to decrease ER  $E_{\text{GSH}}$ . Finally, we took advantage of the SP cell setting, which offers a clean way to challenge the efficiency of GSH ER transport. We first knocked-down Sec61 $\alpha$ 1 alone but also in combination with the secondary minor isoform Sec61 $\alpha$ 2. As western blot could not discriminate the two isoforms (**Figure 3F**), we used qPCR to control the double knock-down efficiency (**Figure 3G**). As previously, the preservation of ER integrity during the semi-permeabilization procedure was validated using differential GAPDH and PrxIV detection (**Figure 3E**). In all the conditions tested, addition of exogenous GSH provoked a similar dose-dependent reduction of the Grx1-roGFPiE probe (**Figure 3D**), suggesting that, contrary to yeast, Sec61 $\alpha$  inhibition is not sufficient to prevent GSH ER transport.

**Figure 3**



**Publication figure 3 – GSH-triggered ER reduction is not significantly impacted by Sec61 inhibition.**

HEK293 cells stably expressing Grx1-roGFPiE were either treated during 3 hours with two Sec61 inhibitors: Mycolactone (A) or ipoF (B) or transfected for 96h with Sec6  $\alpha$ 1 specific siRNA (C) Treated cells were then challenged with 2.5 mM GSH during 10 minutes and  $E_{GSH}$  was measured as in Figure 1. (D) HEK293 cells stably expressing ER-located Grx1-roGFPiE were transfected with control, Sec61 $\alpha$ 1 specific siRNA or Sec61 $\alpha$ 1 and Sec61 $\alpha$ 2 specific siRNA, then semi-permeabilized (SP)

and OxD monitored as in Figure 2D. (E) The selectivity of the semi-permeabilization procedure after siRNA treatments was controlled using GAPDH and PrxIV as in Figure 2D. The efficiencies of Sec61 $\alpha$ 1 and  $\alpha$ 2 siRNAs were determined using both an antibody directed against Sec61 $\alpha$  (F) and specific qPCR primers selectively detecting either Sec61 $\alpha$ 1 or Sec61 $\alpha$ 2 RNAs (G).

---

#### GSH-DRIVEN ER REDUCTION DOES NOT TRIGGER UPR

As an excessive ER reduction could be detrimental to ER functions, we then asked whether GSH-induced ER reduction triggered ER stress and UPR induction. To do so, we exposed cells to increasing doses or during increasing time of exogenous GSH and monitored the Ire1-dependent processing of the XBP1 transcriptional activator, using semi-quantitative RT-PCR (**Figure 4A**). The SERCA inhibitor Thapsigargin (Tg) was used as a known UPR inducer. Contrary to Tg treatment, none of the GSH treatments, assessed in kinetics or dose response, triggered XBP1 processing, suggesting that the level of ER reduction achieved upon GSH exposure did not impact protein folding negatively. As a control experiment, we treated cells with 0.2 mM DTT for 30 minutes or 1 hour or with 1mM DTT for 1 hour. We chose 0.2 mM of DTT as the ER reduction achieved in this condition was equivalent to that observed upon GSH treatment, while higher DTT doses resulted in much lower ER E<sub>GSH</sub> (**Supplemental Figure 6**). Consistently, 0.2 mM DTT did not promote XBP1 splicing while 1 mM DTT did (**Figure 4A**).

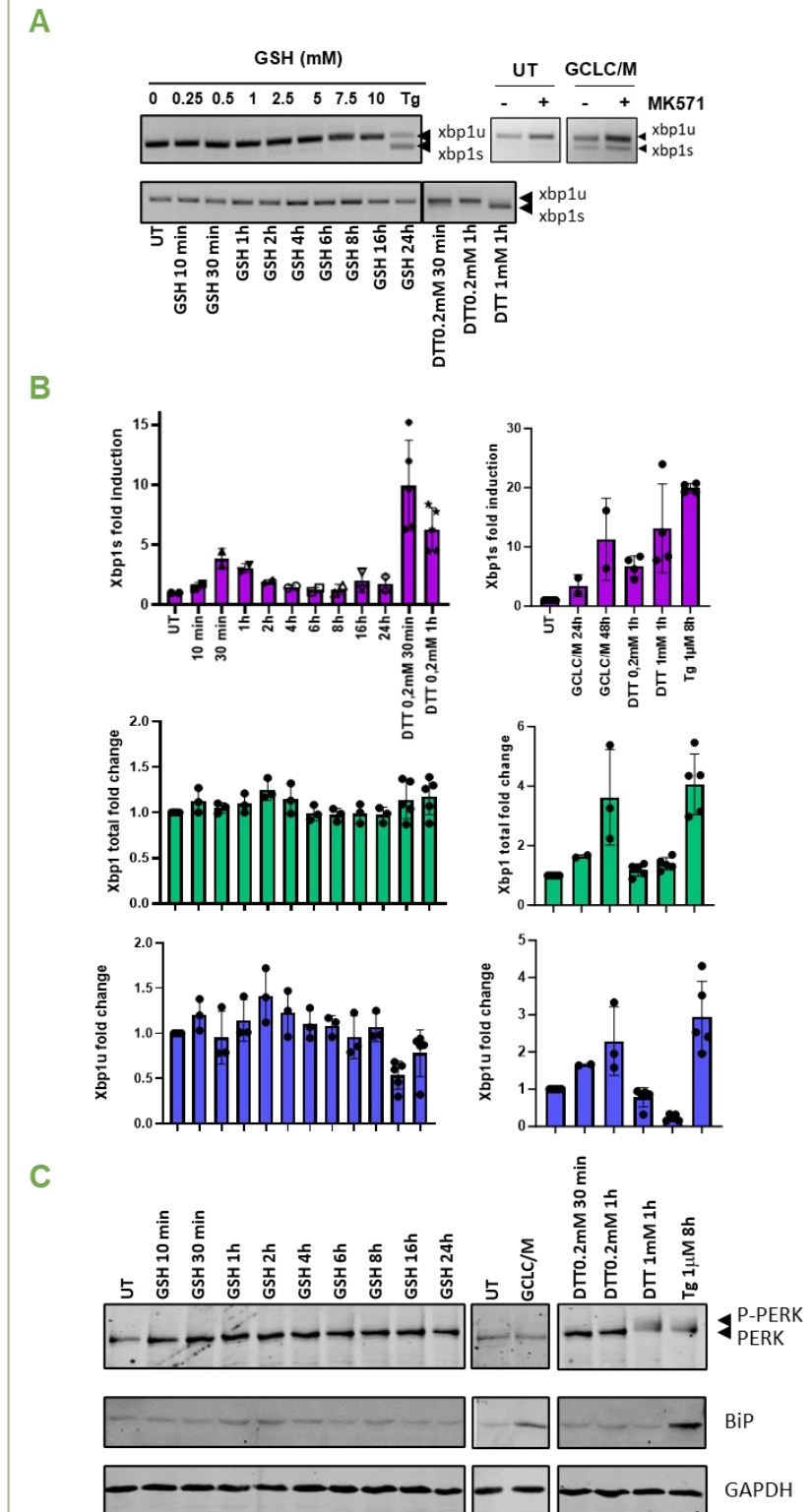
Next, we challenged cells with the continuous ER reduction achieved upon GCLC/M overexpression (**Figure 4A**). This time, RT-PCR analysis of XBP1 processing highlighted a moderate activation of the UPR, suggesting that a more sustained increase in GSH levels and thus ER reduction could impede ER homeostasis. Co-treatment with MK571 did not significantly increase this response.

To have a more detailed picture on how GSH and GCLC/M impacted XBP1 processing, we performed comparative qPCR analyses to detect the full length (XBP1 total), processed (XBP1s) and unprocessed (XBP1u) forms of XBP1 (**Figure 4B**). We confirmed that GCLC/M overexpression increased the levels of XBP1s. This effect was already significant after 24h of expression but more pronounced after 48h. A milder and transient increase of XBP1s could also be unmasked upon exogenous GSH exposure, peaking 30 minutes after treatment. Intriguingly, GCLC/M overexpression led to a significant increase of XBP1 total and XBP1u, which was not seen with GSH treatment. The absolute increase in XBP1s observed in these conditions may this both result from an elevation of XBP1 transcripts levels and a more active Ire1 processing.

To get a more complete picture, we also monitored the levels of PERK phosphorylation and BiP levels (**Figure 4C**). Neither exogenous GSH nor GCLC/M overexpression elicited a clear PERK activation. Sustained GSH production by GCLC/M nevertheless slightly increase BiP levels.

Overall, these experiments showed that a transient and mild ER reduction, as that elicited by exogenous GSH exposure only minimally impacted ER homeostasis, as assessed by UPR induction. On the other hand, the sustained ER reduction triggered by genetic stimulation of GSH biosynthesis, could moderately activate UPR, indicating that ER homeostasis was out of equilibrium in these conditions.

**Figure 4**



**Publication figure 4 – GSH-induced ER reduction does not trigger UPR**

HEK293 cells stably expressing Grx1-roGFPiE were either treated with 2.5mM of exogenous GSH for the indicated times, increasing doses of GSH during 45 minutes or transfected for 48h with GCLC and GCLM expressing plasmids, supplemented or not with MK571 (300μM) for 10 minutes, and the level of XBP1 splicing was monitored using semi-quantitative RT-PCR (A) or qPCR primers respectively monitoring the levels of the spliced (XBP1s), unspliced (XBP1u) and total (XBP1 total)

mRNAs (B) As a comparison, cells were alternatively treated with 0.2 and 1mM of DTT for the indicated times or Thapsigargin (1 $\mu$ M) for 8 hours. (C) PERK phosphorylation and BiP levels were monitored in the same conditions as in A and B, by loading the corresponding protein extracts on SDS-PAGE gels.

---

### GSH-INDUCED ER REDUCTION STIMULATES ERDJ5 AND ERO1 REDUCTION

To better define the consequences of GSH ER transport on ER homeostasis, we assessed how GSH-induced ER reduction modulated the redox state of ER resident enzymes. We first focused on the PDI-like ER Reductase ERdj5. ERdj5 is a J-protein containing six thioredoxin domains, four of which exhibiting disulfide exchange activity (Cunnea et al., 2003; Hosoda et al., 2003). ERdj5 catalyzes the disulfide bond reduction in ERAD substrates (Ushioda et al., 2008) and in the ER calcium importer SERCA2b (Ushioda et al., 2016). It also fuels disulfide isomerization in proteins undergoing processive oxidative folding such as the LDL-Receptor (Oka et al., 2013). As a proficient reductase, ERdj5 is mainly oxidized in basal conditions (Riemer et al., 2009), **Figure 5A**, and its activation requires an initial reduction step, which can be achieved by GSH *in vitro* (Ushioda et al., 2008; Maegawa et al., 2017). To assess whether GSH could stimulate ERdj5 reduction in cells, we first monitored ERdj5 redox state upon GCL overexpression, by alkylating ERdj5 reduced cysteines with a high MW maleimide. In basal conditions, ERdj5 was mostly oxidized (**Figure 5A**). Importantly, expressing GCLC/M subunits enhanced ERdj5 reduction compared to control. We used an ERdj5 mutant lacking cysteines which did not show any slower migrating species in any conditions, confirming the redox nature of the observed electrophoretic shift. To better quantify the impact of increasing cytosolic GSH on ERdj5 reduction, we performed a pulse-treatment with diamide, which led to full ERdj5 oxidation, followed by a washout of the oxidant. The kinetics and amplitude of ERdj5 re-reduction were then monitored in the presence and absence of GCLC/M overexpression. Strikingly, GCL overexpression triggered a stronger and faster re-reduction of ERdj5 upon diamide washout. To better evaluate the ERdj5 responsiveness to GSH, we next exposed ERdj5-expressing cells to exogenous GSH and monitored its redox state overtime. This led to a fast and significant reduction of ERdj5 (**Figure 5B**). These data thus show that increasing the levels of cytosolic GSH impact ERdj5 redox state, potentially providing more reductive power for its reductase activity.

The Ero1 protein family constitutes another ER activity susceptible to ER redox status. Ero1 catalytic rate is subjected to a tight feed-back regulation, involving the formation of intramolecular regulatory disulfide bonds. These maintain Ero1 in an inactive state to prevent ER hyperoxidation while their reduction restores Ero1 activity. In yeast, acutely increasing GSH ER transport, triggers PDI-dependent Ero1p reduction and hyperactivation. We thus tested the impact of GSH ER transport on Ero1 $\alpha$  the ubiquitous mammalian isoform of *ERO1*. Ero1 $\alpha$  regulation involves three intramolecular regulatory disulfides. Two of them, cys99-cys104 and cys94-cys131, engage Ero1 $\alpha$  catalytic cysteines (cys94 and cys99), *de facto* preventing its function as an oxidase. A third one, involving cys208 and cys241, controls a switch regulating the oxygen accessibility to the FAD binding site and the overall FAD redox cycling rate (Ramming et al., 2015). While cys104 and cys131 are dispensable for Ero1 $\alpha$  activity, cys208 and cys241 are part of a still elusive catalytic cycle engaging their heterodimeric association with PDI. This step is required for the full-blown activity of the enzyme in the presence of GSH *in vitro* (Ramming 2016), potentially timely coordinating the O<sub>2</sub>-dependent

oxidation of FAD and the reduction of the catalytic shuttle cysteines according to the availability of reduced PDI (Kanemura et al., 2016).

We thus determined if GSH-dependent ER reduction impeded on Ero1 $\alpha$  redox state which possible effect on its activity. Exogenous myc-tagged Ero1 $\alpha$  was first expressed in HEK293 cells and its redox state analyzed after maleimide blockage of cysteines (**Figure 5B**). We first focused on monomeric Ero1 $\alpha$  (mEro1 $\alpha$ ) and reduction of intramolecular disulfides. m Ero1 $\alpha$  can be resolved in three main redox conformations using a non-reduced SDS-PAGE, one fully oxidized form (Ox1), one partly oxidized form (Ox2) and one reduced form (R). As previously observed, monomeric Ero1 was mainly oxidized in basal conditions, while mM doses of DTT led to the efficient reduction of intramolecular regulatory disulfides, as observed by the decreased electrophoretic mobility of the protein. We next monitored mEro1 $\alpha$  redox state upon treatment with exogenous GSH. We observed in time a slight but significant build-up of the reduced form of mEro1 $\alpha$ . The extent of mEro1 $\alpha$  reduction was comparable to that triggered by 0.2 mM DTT. We then aimed to confirm the GSH-dependent reduction on endogenous Ero1 $\alpha$ . To this end, we used the high affinity 2G4 Ero1 $\alpha$  antibody. Unfortunately, cysteine alkylation, performed as part of the redox trapping procedure, prevented the detection of reduced Ero1 $\alpha$  by 2G4, probably due to epitope masking (**Supplemental Figure 7A**) while other antibodies proved poorly efficient in detecting Ero1 $\alpha$ . Although unsatisfying, we nevertheless monitored endogenous Ero1 $\alpha$  redox state in the absence of cysteine trapping. Surprisingly, DTT and diamide treatment worked as expected, respectively providing fully reduced and oxidized Ero1 $\alpha$  forms. The untreated sample likewise showed a minimally reduced Ero1 $\alpha$  with the expected Ox1 and Ox2 forms. Importantly, we observed that GSH treatment comparatively increased both the Ox1 and Reduced forms of Ero1 $\alpha$ . Altogether, these experiments indicated that GSH-induced ER reduction was able to notably reduce the monomeric form of Ero1 $\alpha$

---

#### GSH-INDUCED ER REDUCTION DOES NOT IMPEDE ER PROTEOSTASIS

Since GSH-induced ER reduction affected the redox state of both Ero1 $\alpha$  and ERdj5, with possible consequences on oxidative folding, we set out to monitor the folding efficiency of the J chain from immunoglobulin M, JcM (Mezghrani, 2001). JcM folding, as heterologously expressed, entails the formation of intramolecular disulfides, but also that of disulfide dimers and oligomers, which can be visualized on a non-reducing protein gel. A DTT pulse was performed on JcM expressing cells, to synchronize disulfide bond formation. The folding efficiency was then determined by timely comparing the rate of disulfide formation upon DTT washout, according to GSH status (**Figure 5F and 5G**). The first and important result from these experiments was that neither GSH exogenous treatment nor GCLC/M overexpression was able to significantly decrease the rate of JcM folding, meaning that the extent of GSH-induced ER reduction was not sufficient to prevent oxidative folding, as seen in yeast. Secondly, when we took a closer look at the gels, examining the kinetics of JcM folding, exposure to exogenous GSH appeared to moderately increase the rate of both JcM monomer and dimer processing compared to untreated cells (**Figure 5G** and **supplemental Figure 8A**). Gel quantification nevertheless proved challenging to perform and could not provide strong statistics to definitely prove this fact.

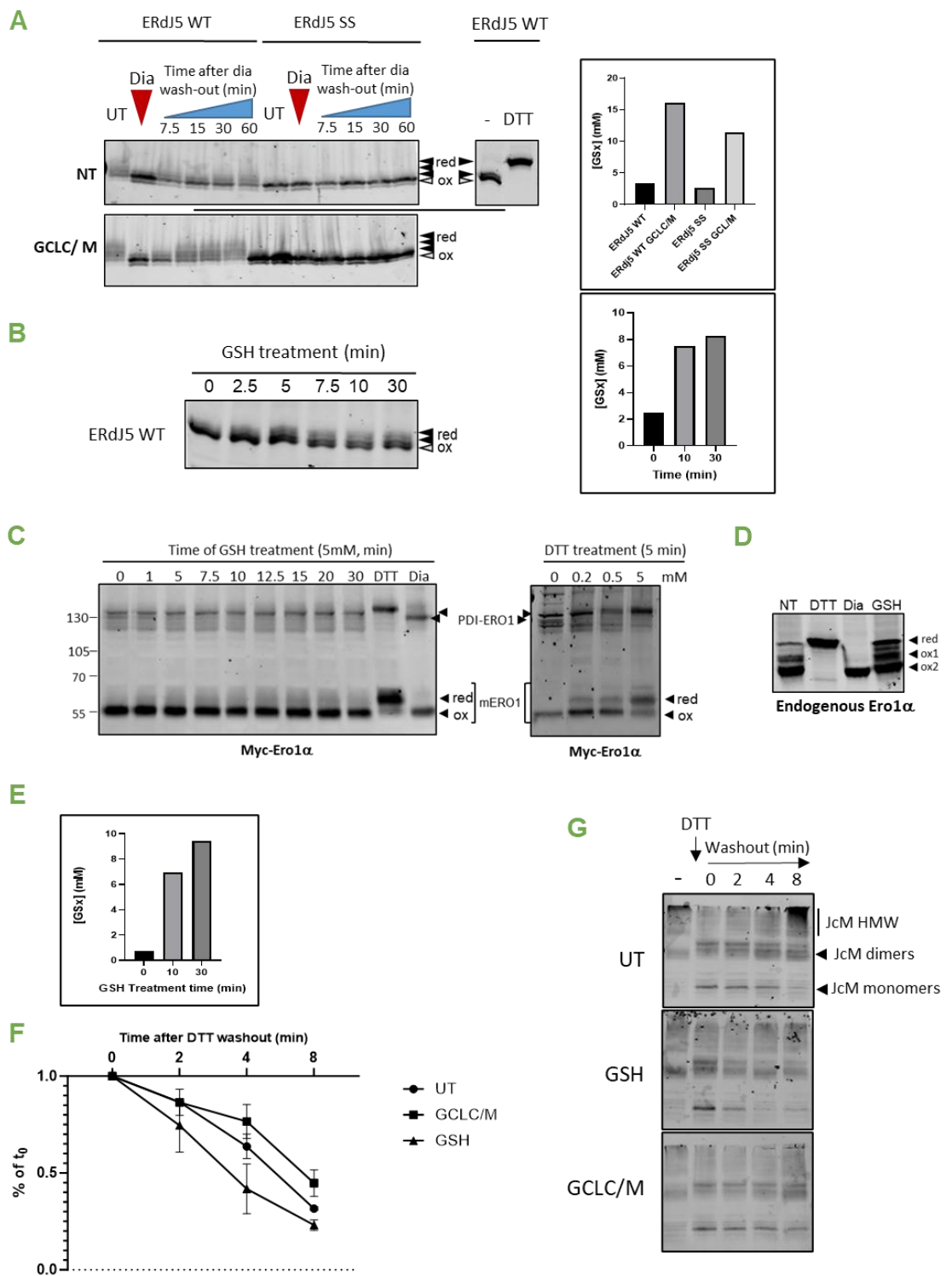
The reductase activity of ERdj5 was shown to be required for the ERAD-dependent degradation of the Null Hong Kong (NHK) misfolded mutant of the alpha1-anti-trypsin ( $\alpha$ 1-AT) protein (Ushioda et

al., 2008). We thus wished to challenge the effect of exogenous GSH treatment and that of GCLC/M overexpression on the degradation rate of this  $\alpha$ 1-AT mutant (**Supplemental Figure 8B**). We could not evidence any decrease in NHK half-life upon GSH-induced ER reduction. As ERdj5 overexpression was previously shown to stimulate NHK degradation (Ushioda et al., 2008), these data suggest that in our experimental conditions, ERdj5 levels rather than that of the ER reductive power was the limiting factor for NHK turnover.

#### **Publication figure 5 – Modulation of ERdj5 and Ero1 redox state and oxidative folding upon GSH-induced ER reduction**

(A) HEK293 cells were transfected with a plasmid expressing a WT or cys-less HA-tagged ERdj5, together with GCLC/GCLM subunits or an empty vector. 24h after transfection, cells were challenged or not during 5 minutes with diamide (5mM), then washed and incubated in complete medium. Cells were collected before and after diamide treatment and at the indicated time after medium refreshment. ErdJ5 redox state was analyzed then by SDS-PAGE after cell lysis using acid trapping method followed by MalPEG alkylation (+2kDa) (B) HEK293 cells transiently expressing WT ERdj5 were challenged with GSH (2.5 mM) and collected at the indicated times. ErdJ5 redox state was analyzed as in (A). For each (A) and (B) conditions, cellular [GSx]Cell was monitored as in Figure 1 to confirm the increase of GSH intracellular levels. (C) HEK293 cells were transfected with myc-Ero1 $\alpha$  WT and were challenged, 24h later, with 5 mM exogenous GSH for the indicated times or with DTT (0.2, 0.5 and 5 mM) or Diamide (5 mM) for 5 minutes. Cells were collected and lyzed in a buffer containing NEM to alkylate free cysteines. Protein extracts were then separated by non-reducing SDS-PAGE and proteins were revealed by anti-myc antibody. mEro1: monomeric Ero1, ERO1-PDI: redox heterodimers linking Ero1 $\alpha$  and PDI (D) HEK293 cells expressing endogenous Ero1 $\alpha$  were treated with DTT (5 mM), Diamide (5mM) or GSH (5mM) for 5 minutes, and lyzed using acid trapping method omitting NEM alkylation to prevent epitope loss. Protein extracts were then separated by non-reducing SDS-PAGE and revealed with anti-Ero1 $\alpha$  antibody 2G4. (F) and (G) HEK293 cells transfected with myc-tagged JcM were treated with DTT and JcM oxidative refolding was followed upon DTT removal by stopping the reaction by NEM trapping at the indicated times. Folding intermediates were then resolved on a non-reducing SDS-PAGE (G) and the disappearance of the reduced monomer quantified (F).

**Figure 5**



---

## THE MECHANISM FOR THE CALCIUM-DEPENDENT ER TRANSPORT OF GSH IS DIFFERENT FROM THAT OF THE GRADIENT-DEPENDENT MECHANISM BUT SYNERGIZES WITH IT

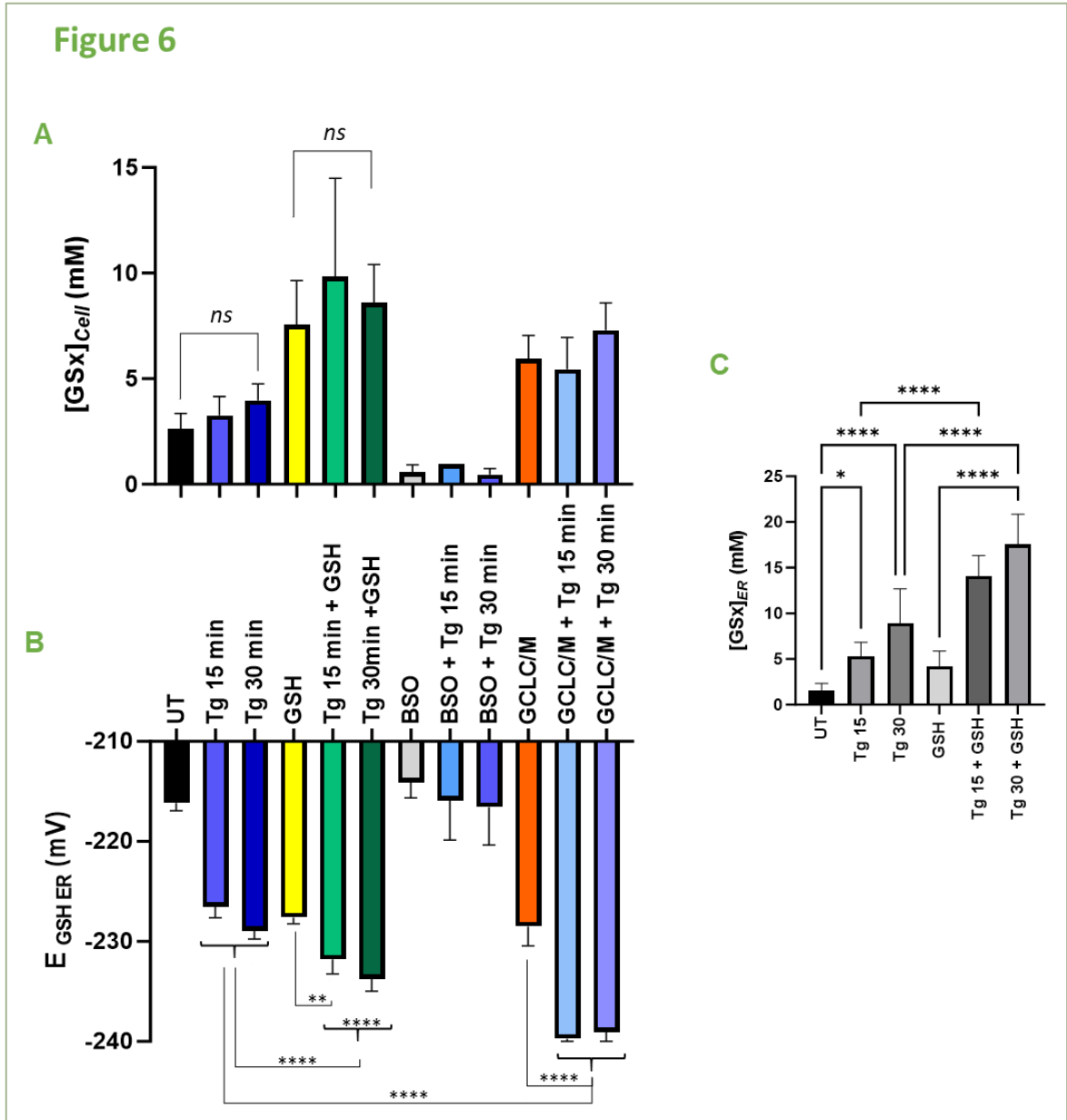
Evidence was previously provided for a calcium-dependent ER reduction (van Lith et al., 2011; Avezov et al., 2013; Lizák et al., 2020), which may differ from the modality of transport described in the current study. These showed that thapsigargin (Tg), which inhibits the ER calcium pump SERCA and thus triggers both depletion of ER calcium stores and UPR, stimulates the reduction of various GSH responsive roGFP probes. Two non-mutually exclusive mechanisms have been proposed to explain this phenomenon. First, ER calcium depletion was suggested to dampen PDI activity (Avezov et al., 2015) by limiting its intra-ER mobility through a calnexin dependent mechanism. The resulting attenuation of PDI-dependent oxidation would explain the  $E_{\text{GSH}}$  decrease observed upon Tg treatment. The second model rather attributes the Tg-induced  $E_{\text{GSH}}$  decrease to a direct transport of reduced GSH inside ER (Lizák et al., 2020). In support of this transport, it is there argued that the Tg-induced ER reduction was lost when cells were previously depleted of GSH by BSO treatment. Of note, this cannot be taken as a definite proof for a GSH ER transport. Indeed, drastically decreasing GSH concentrations will proportionally increase roGFP 'oxidizability', ie its sensitivity to GSSG level (Meyer and Dick, 2010), thereby intrinsically decreasing its ability to sense ER reduction. The authors thus provided additional support for GSH ER transport by evidencing an increase of  $[\text{GSx}]_{\text{ER}}$  upon Tg treatment using Grx1-roGFPiE and Grx1-1cys KDEL probes. These calculations yet relied on conditions where the Grx1-1cys KDEL probe is already almost completely oxidized on the basal level. Moreover, incertitudes from  $E_{\text{GSH}}$  were not propagated to calculate  $[\text{GSx}]_{\text{ER}}$  leading us to question the statistical significance of the obtained values. We thus wished to challenge and extend these findings using our cell and probes systems. We confirmed that BSO induced GSH depletion indeed prevented Tg-induced ER reduction (**Figure 6A and 6B**). We additionally confirmed that Tg treatment induced an elevation of  $[\text{GSx}]_{\text{ER}}$  that became highly significant after 30 minutes of exposure (**Figure 6C**), thereby supporting the occurrence of a Tg-induced GSH ER transport. We next asked if this transport could be the consequence of an increase in GSH cellular levels by measuring  $[\text{GSx}]_{\text{Cell}}$  upon Tg treatment. Importantly, Tg exposure did not significantly modified GSH intracellular levels, indicating that the GSH ER transport observed upon depletion of ER calcium stores, occurred independently of the gradient mechanism. Of note, upon Tg treatment,  $[\text{GSx}]_{\text{ER}}$  became 4 to 5 times higher compared to  $[\text{GSx}]_{\text{Cell}}$ , suggesting a possible active transport.

To further confirm that GSH ER transport occurred by two different modalities, we combined Tg exposure to either GSH treatment or GCLC/M overexpression. In each case, we observed that the ER reduction achieved upon treatment combination was significantly greater compared to that observed when a single stimulus was imposed. Similarly,  $[\text{GSx}]_{\text{ER}}$  calculation evidenced a 10-fold increase in ER GSH levels when cells were exposed to both Tg and GSH, compared to the 2.5 and 4-fold increase observed upon each of the GSH and Tg treatments respectively. Importantly, no additional elevation of  $[\text{GSx}]_{\text{Cell}}$  was observed upon treatment combination.

Altogether, these data provide evidence for the coexistence of two different transport modalities for GSH to enter mammalian ER, which could act in a synergistic manner.

**Publication figure 6 – Cytosolic GSH gradient and Thapsigargin act independently to trigger ER reduction and GSH ER transport.**

(A) HEK293 cells stably expressing Grx1-roGFPiE were treated with 1  $\mu$ M thapsigargin (Tg) during 15 or 30 minutes, alone or in combination with 2.5 mM GSH for 10 minutes, GCLC/M transfection or BSO (200  $\mu$ M 24h). Cellular [GSx]<sub>cell</sub> (A) and E<sub>GSH</sub> (B) values were calculated as in Figure 1B. (C) [GSx]<sub>ER</sub> concentrations were calculated as in Figure 2C, following exposure to 15 and 30 minutes of Tg, alone or in combination with GSH (2.5 mM, 10 min).





---

## DISCUSSION

In this study, we have investigated how manipulations of the GSH metabolism impacted the ER redox homeostasis and functions. To achieve this, we manipulated glutathione intracellular levels either by modifying its biosynthesis or degradation rates, or by promoting the uptake of externally supplied GSH. Both approaches led to the observation that the ER redox state, as defined by ER  $E_{\text{GSH}}$ , promptly reflected the alteration of GSH cytosolic levels. Decreasing GSH pools oxidized the ER while increasing them led to ER reduction. Following cell exposure to extracellular GSH,  $E_{\text{GSH}}$  decreased very rapidly and in a dose-dependent manner. The evaluation of the overall glutathione content within the ER corroborated that  $[\text{GSx}]_{\text{ER}}$  closely paralleled the glutathione levels of the cytosol, as approximated by  $[\text{GSx}]_{\text{Cell}}$ . This evidence led us to conclude that, as previously shown in yeast, GSH could be imported into mammalian ER according to the concentration gradient set by the cytosol. However, unlike in yeast, we observed that this facilitated transport could occur independently of the Sec61 translocon. Also, even though this transport induced a significant reduction of the ER, it only marginally affected ER proteostasis. In particular, GSH ER transport did not hinder oxidative folding and led to a modest and temporary UPR activation unless it was sustained by genetically stimulating GSH synthesis. We finally evidenced that the gradient-dependent and the previously proposed calcium-dependent ER import of GSH act through distinct mechanisms which may ultimately collaborate.

---

### 1) EQUILIBRATION OF GSH LEVELS ALONG THE CONCENTRATION GRADIENT BETWEEN THE CYTOSOL AND THE ER

In steady state conditions, we biochemically estimated intracellular glutathione levels,  $[\text{GSx}]_{\text{Cell}}$ , at approximately 2 mM. Upon cell exposure to GSH,  $[\text{GSx}]_{\text{Cell}}$  increased promptly and linearly, and this elevation was insensitive to the inhibition of GSH synthesis, suggesting that our cells were in fact taking up GSH from the extracellular milieu. This observation was at first surprising and ran counter to the prevailing model outlined by the Meister cycle (Orlowski and Meister, 1970) which posits that extracellular GSH should undergo rapid degradation by  $\gamma$ -glutamyl transpeptidases, producing amino acids that are then available for cellular transport and cytosolic GSH neosynthesis. In addition, when we initially obtained our results, there were no known plasma membrane transporters for GSH. Since then, two transporters from the organic cation/anion transporter family, SLC22A10 and SLC22A15, have been shown to manage extracellular GSH uptake in pancreatic cancer cells (Nayak et al., 2022). Whether the same transporters or another mechanism are at play in our cell system is currently under investigation.

An important characteristic of this uptake was its highly dynamic nature, as highlighted by washout experiments:  $[\text{GSx}]_{\text{Cell}}$  returned to basal levels within minutes after extracellular GSH removal. This feature helped us to confirm the specificity of our dosage experiments and was also instrumental to follow up the dynamics of ER  $E_{\text{GSH}}$  upon washout.

With the use of ER-localized, GSH specific Grx1-roGFPiE, we determined steady state ER  $E_{\text{GSH}}$  to be around -220 mV. This is on par with values in the literature placing ER  $E_{\text{GSH}}$  between -208 mV and -242 mV (Birk et al., 2013; Avezov et al., 2013; van Lith et al., 2011; Delic, Mattanovich, and

Gasser, 2010; Ponsoero et al., 2017). We also verified that GSH treatment did not cause any probe relocation that could account for probe reduction (**Supplementary Figure 9**)

Both the increase of  $[GSx]_{cell}$  imposed after cell exposure to GSH or sustained GSH biosynthesis, elicited by overexpression of  $\gamma$ -glutamyl cysteine ligase (GCL), resulted in a comparable drop of ER  $E_{GSH}$  to a value as low as -235 mV. In particular, genetically boosting GSH biosynthesis raised  $[GSx]_{cell}$  to the same levels as exposing cells to 2.5 mM of exogenous GSH which resulted in a comparable decrease of ER  $E_{GSH}$ . However, while we suggest that an ER reduction always matched an increase in  $[GSx]_{cell}$ , a swift ER reduction was already evident upon cell exposure to 0.25-0.5 mM GSH, while no significant increase in  $[GSx]_{cell}$  could be detected. This is most likely due to the weaker sensitivity of the dosage experiments when approaching the submillimolar range, as suggested by the important dispersion of the values obtained in these assays (Supplementary Figure 2A).

Again, while  $E_{GSH}$  allowed us to say that the ER becomes more reduced or oxidized upon GSH addition or removal respectively, no conclusion could be drawn regarding GSH entering the ER because  $E_{GSH}$  does not hold such quantitative information.

By using two GSH biosensors to access glutathione concentration in the ER lumen, we firstly observed that at steady state, the calculated  $[GSx]_{ER}$  was 2.9 mM  $\pm$ 0.8, which is in the same range as our previous measure of  $[GSx]_{cell}$ . We then confirmed that the decrease in ER  $E_{GSH}$  observed when cells were exposed to GSH, corresponded to a proportional elevation of GSH transport into the ER. This pattern was predominantly observed within a relatively narrow range of GSH concentrations, namely when the cytosolic  $[GSx]_{cell}$  were set between 0 and 8 mM, concentrations above which  $[GSx]_{ER}$  elevation plateaued, despite a still increasing  $[GSx]_{cell}$ . The maximum  $[GSx]_{ER}$  elevation we could get was a 3-fold increase in GSH exposed cells compare to control. The same dose-dependent pattern and limits applied when monitoring ER  $E_{GSH}$  using a semi-permeabilized cell system, suggesting a similar saturability of the transport mechanism in this semi-*in vitro* system. These results are consistent with the 5 mM threshold of saturation observed by Bánhegyi and coworkers (Bánhegyi et al., 1999) for the microsomal import of radioactive GSH.

The passive equilibration of GSH we observed between the cytosol and the ER corroborated the results obtained in *Saccharomyces cerevisiae* by former PhD student Alise Ponsoero. In yeast, however, the estimated  $[GSx]_{cell}/[GSx]_{Cyt.corr}$  and  $[GSx]_{ER}$  reached much higher levels. Contrary to yeast, we did not apply any corrective factor to  $[GSx]_{cell}$  and assumed that it was roughly equivalent to  $[GSx]_{cyt}$ . Although it is possible that a volume correction might have been necessary, the absence of vacuole in human cells and the similar behaviour of our whole versus semi-permeabilized cell systems made us confident that this was a close enough approximation. Significantly, our model could however diverge from the one proposed by Montero et al. in mammalian cells. Using a similar double biosensor method, they had semi-quantified an over twice higher  $[GSx]_{ER}$  compared to  $[GSx]_{cell}$  under steady state conditions and had anticipated from this observation that the accumulation of glutathione inside the ER could be a systemic feature of ER physiology, mechanistically arising from the oxidative activity of this organelle. Indeed, assuming that GSSG has a lesser ER membrane permeability compared to its reduced counterpart (Bánhegyi et al., 1999), they put forward that the ER conversion of GSH into GSSG could act as a driving force for the ER

transport and local buildup of glutathione. In contrast to their findings, we never measured a comparatively elevated  $[GSx]_{ER}$  neither in basal conditions nor after increasing  $[GSx]_{Cell}$ .

This discrepancy could be explained by technical and biological factors. First, their steady state measurements of both  $E_{GSH}$  and GSH:GSSG ratio relied on almost totally oxidized probes, providing respectively a -208 mV ER redox potential and a less than 7:1 GSH:GSSG ratio (Montero et al., 2013). Ours, on the contrary, yielded an average of 80% oxidation or below of the Grx1-roGFPiE probe for a calculated  $E_{GSH}$  of -220mV and a 50% oxidation ratio of the Grx1-1cys KDEL probe for a GSH:GSSG ratio around 75:1. This first suggested that in our cell conditions, the oxidative folding machinery could be less active, resulting in a comparatively less oxidized ER. It is important to note that our values anyway remained considerably more oxidizing than those depicted for the cytosol. Furthermore, variations in the activity of the ERO1-PDI machinery among cells has indeed been documented (Benham et al., 2013). Also, considering Montero's model which links the buildup of glutathione in ER to its conversion into GSSG, a lower activity of the oxidative folding could possibly explain the discrepancy. Another possibility, technical this time, would be that in the Montero study, the more oxidized status of both probes, by placing them out of their linearity range, could intrinsically diminish their ability to accurately report on  $[GSx]_{ER}$ . Of note, the codon-bias optimization probe that we made on the Grx1-1cys KDEL, have not only enhanced our detection capability but has also facilitated a more accurate quantification.

Another important element that we have assessed in our study is the steadiness of the pH upon cell exposure to GSH. Increasing GSH concentration could indeed induce pH variations that should be taken into account for the calculation of  $E_{GSH}$ . We thus measured the pH variations inside the ER using the newly developed ratiometric pHluorin2 probe (Linders et al., 2022). Importantly, we could not evidence any modification in the probe ratio upon cell exposure to GSH (Figure 27), indicating a relative stability of the pH despite the increased  $[GSx]_{ER}$  and further confirming the validity of our calculations.

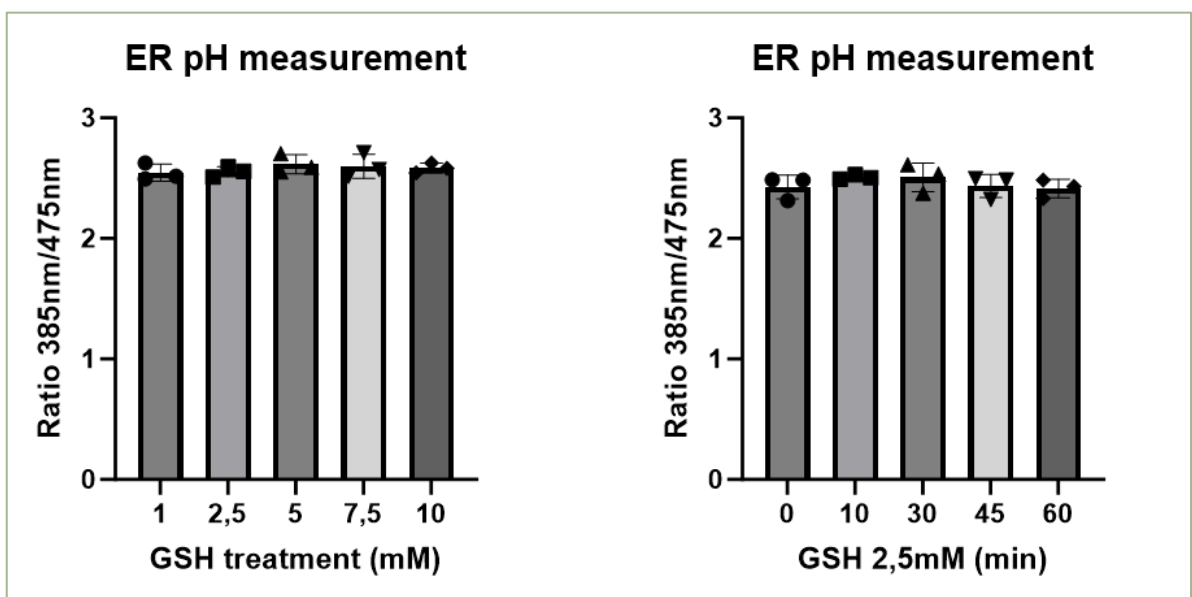


**Figure 27 – Glutathione treatment does not cause variations of the ratio of ER-localized, pH-sensitive pHluorin2.** HEK 293 cells overexpressing ER-localized pHluorin2 were treated with (left)

mounting quantities of GSH for 10 minutes or (right) 2.5 mM GSH for up to 60 minutes. The fluorescence ratio of pHluorin2 at 385 over 475 nm was recorded on a temperature-controlled plate-reader.

A nevertheless intriguing observation was the relatively high GSH:GSSG ratio of 75:1 that we uncovered compared to previous characterizations (Montero et al., 2013; Hwang, Sinskey, and Lodish, 1992; Bánhegyi et al., 1999). The only study where this ratio was measured above 10:1 was the one performed in yeast and using a similar Grx1-1cys KDEL probe, which retrieved a 45:1 ratio in basal conditions (Ponsero et al., 2017). Besides for the Montero study, whose limitations have already been discussed above, it is possible that the lower GSH:GSSG ratio classically assumed from *in vitro* work do not take into account the fact that in cells, GSH oxidation is in competition with thiols from nascent proteins. In agreement with this hypothesis, we observed an oxidation of the ER  $E_{\text{GSH}}$  when cells were treated with the translation inhibitor, cycloheximide. (Figure 28)

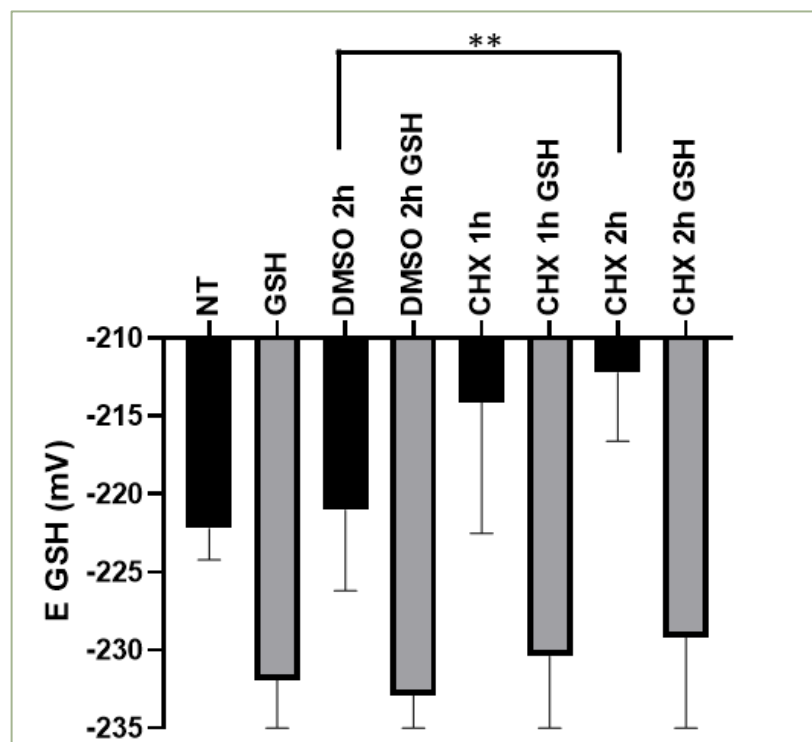


**Figure 28 – Inhibition of protein synthesis causes a more oxidizing  $E_{\text{GSH}}$**   $E_{\text{GSH}}$  was measured in cells stably overexpressing ER-localized Grx1-roGFPiE, treated with 1  $\mu\text{g}/\text{mL}$  cycloheximide (CHX) for up to 2 hours with or without the subsequent addition of 2.5 mM GSH for 10 minutes

---

## 2) REGULATION OF CYTOSOL TO ER GSH INFLUX

As in yeast, we observed that the ER reduction and GSH transport were restrained above a certain threshold value of  $[GSx]_{cell}$ . This threshold was however much higher in yeast compared to our human cell system, which retrieved values in the 7-8mM, even using the simpler semi-permeabilized cell system. We excluded that this was due to a technical limitation of the roGFP biosensor, as all the values measured were sufficiently close to the previously determined -239mV midpoint potential of this probe (Birk et al., 2013). In whole cells, we showed that one limiting factor was an efficient efflux of cytosolic glutathione from the cell, as inhibiting the GSH PM exporter MRP1 slightly increased both  $[GSx]_{cell}$  and the reduction profile of the ER sensor. However, this cannot account for the major restriction that we observed also in the absence of the plasma membrane. Considering the facilitated diffusion mechanism suggested by our data, the easiest explanation to our observation is a saturation of the transporter.

In yeast on the contrary, this transport was shown to be mediated by the Sec61 translocon and a regulatory mechanism involving a feed-back control of GSH ER import was proposed. In this model, the initial rise in luminal GSH resulted in both the UPR-dependent induction and reductive activation of Ero1 subsequently causing an increase in ER-generated  $H_2O_2$ . This increase in  $H_2O_2$  in turn triggered the oxidation of Kar2, which is the yeast counterpart of the ER chaperone BiP. Once Kar2 was oxidized, it blocked the translocon thereby halting further GSH transport.

We consider it unlikely that this mechanism also applies to our cell system. One of the key reasons is that our data have eliminated Sec61 as the primary transporter of GSH in the ER.

---

## 3) SEC61 IS NOT A MAJOR TRANSPORTER OF GSH IN MAMMALIAN CELLS

With our observation that a gradient-driven import of GSH also applied to mammalian ER, Sec61 became a logical candidate to investigate as a potential GSH transporter. Strikingly, using whole cells, we could not evidence any defect in ER reduction upon GSH exposure as we used either drug or genetic approaches to inhibit Sec61 $\alpha$  function. We made sure to investigate the silencing of both Sec61 $\alpha$ 1 and Sec61 $\alpha$ 2, as their yeast counterparts Sec61p and Ssh1p were both contributive to the import of GSH in the yeast ER (Ponsero et al., 2017). Employing semi-permeabilized cells to circumvent possible side effects linked to the inactivation of the translocon brought us to the same conclusion: Sec61 was not the major GSH ER transporter in our cell system.

Finally, we used one last mechanistically distinct drug to try and plug the translocon, cycloheximide (CHX). CHX stalls the translating ribosomes to the translocon, thereby promoting artificial plugging of the channel (von der Malsburg, Shao, and Hegde, 2015). We showed previously that such treatment prevented GSH-dependent ER reduction in yeast. Yet, although CHX treatment led to a more oxidized basal ER  $E_{GSH}$ , it did not impede the ability of exogenous GSH to reduce ER (**Figure 28**).

One could next ask whether any function of Sec61 could still be unveiled, even if it were to serve a secondary mechanism. In that context, the cryo-microscopy 3D structure of the drug inhibited translocon, recently suggested that inhibitors may in fact trap sec61 in an intermediate state, leaving the cytosolic side of the gate open (Gérard et al., 2020) and thus questioning a possible permeability to small molecules. Accordingly, while Sec61 inhibiting drugs, such as mycolactone used in our study

or Eeyarestatins, were shown to hamper the translocation of a broad range of proteins, they were also associated with an enhanced calcium leak in agreement with Sec61 being blocked in a semi-permeable state (Gamayun et al., 2019; Bhadra et al., 2021). Given the relatively small size of GSH, it was conceivable that the drug-inhibited translocon could have also resulted in increased permeability to GSH, had Sec61 been a proficient GSH transporter. However, no basal ER reduction nor any potentiating effect of mycolactone or IpoF on the gradient-dependent ER reduction were observed. As of today, it is yet too premature to definitely rule out the possibility of a secondary Sec61-dependent transport of GSH. Indeed, the very recent publication of new 3D structures which confirm the common binding of IpoF, mycolactone and Eeyarestatin I, to a pocket formed by the partially open lateral gate but fully closed plug domain of Sec61, could not provide a rationale for the observed calcium leakage, let alone the passage of GSH (Itskanov et al., 2023). The negative results obtained from Sec61 inhibitors treatment thus cannot be totally conclusive.

While altogether, these results led us to exclude sec61 as the only transporter for glutathione, it could still be possible that there is a redundancy in the ER transporters of glutathione. In that case, silencing of sec61 would be an additional control to perform to completely rule out the involvement of sec61 in mammalian ER import. An alternative approach to further explore a potential involvement of Sec61 in GSH transport is to introduce specific Sec61 mutations with altered gating capacities that might render them responsive to GSH gradient.

---

#### 4) GSH ENTRY REDUCES THE ER AND ITS RESIDENT PROTEINS WITHOUT NEGATIVELY IMPACTING ITS PHYSIOLOGY

In yeasts overexpressing the GSH PM transporter HGT1, the subsequent import of glutathione to the ER has toxic effects. These are associated with both a reducing stress, compromising oxidative folding and an oxidative stress, resulting from the massive release of H<sub>2</sub>O<sub>2</sub> by the Ero1-PDI system (Kumar et al., 2011). The UPR is activated in response to this GSH transport which likely intensifies the toxic pro-oxidative effect by upregulating ERO1 expression.

In contrast, the gradient-dependent transport of GSH in mammalian ER did not result in any major impairment of ER proteostasis. Only a minimal and brief UPR induction was evidenced by monitoring Xbp1 splicing following exposure to extracellular GSH and the oxidative folding of the model substrate JcM proceeded normally. Sustained GSH biosynthesis, using GCL overexpression, did however cause a stronger UPR induction, yet apparently restricted to the IRE-1 branch. Interestingly, Xbp1 splicing may in this case, not only result from Ire1 activation but also from a quantitatively higher share of Xbp1u. A minor delay of JcM folding could also be suspected in these conditions. These findings, while providing additional support for the notion that GSH transport has a reducing impact on the ER, also indicated that managing a prolonged ER reduction, albeit relatively mild, is less well tolerated by cells. Importantly however, even with a prolonged exposure to the GSH gradient, the induced ER reduction was not able to significantly hinder protein oxidative folding.

The debated function of ER GSH may be to ensure an ample fraction of reduced PDI available for substrate isomerization or reduction. This is a risky deal as a delicate balance between PDI oxidation and reduction should be required to safeguard the proper oxidative folding of protein substrates. In this context, the observation that GSH ER transport could induce a significant yet limited ER

reduction without any obvious deleterious effect, opened up a functional window to enhance the reductive/isomerization capacities of the ER. In agreement with this hypothesis, we could monitor a reduction of the ERdj5 PDI enzyme, in conditions where oxidative folding was still fully functional. In parallel, our monitoring of a very moderate Ero1 reduction, suggested that the GSH-induced ER reduction could in part be compensated by some level of Ero1 activation. The initial oscillations of  $E_{\text{GSH}}$  observed following cell exposure to GSH aligned with this notion, by suggesting that the establishment of a novel ER redox state was a dynamic process that likely entailed rounds of Ero1 activation and deactivation.

Unfortunately, we were unable to conclusively demonstrate that these GSH conditions indeed enhanced the efficiency of protein folding or that of ERAD dependent process. Although transient GSH treatment appeared to slightly accelerate JcM folding and to decrease the appearance of high molecular weight forms, the differences were too subtle to reach significance. In parallel, the degradation of the ERAD and ERdj5 substrate,  $\alpha$ 1-anti trypsin NHK mutant, which requires the prior reduction of its disulfide, was not significantly accelerated following cell exposure to GSH or upon stimulation of GSH biosynthesis.

Our inability to evidence any positive effect of GSH in these conditions could be attributed to the fact that the reducing power may not be a limiting factor in our experimental conditions. Indeed, as noted above and as suggested by the fact that Ero1 is mainly oxidized in all the conditions tested, the ER redox state in our cells is relatively more reduced compared to that measured in HeLa cells for instance. Also, the possibly redundant role of the thioredoxin pathway in supplying the ER with reducing equivalents, may also contribute to mitigate the conditions that could render GSH limiting.

Importantly, the physiological function fulfilled by the gradient-dependent transport of GSH remains elusive, even in yeast. Clues that ER GSH might have a supportive role in preserving ER proteostasis during an ER stress challenge have been brought up by the observation of a simultaneous neosynthesis of GSH and  $[\text{GSx}]_{\text{ER}}$  elevation following yeast treatment with the UPR inducing agent Tunicamycin. The rationale behind this observation could be that an elevated level of reduced PDIs may be necessary to handle an increased load of client proteins in need for disulfide reduction. Alternative GSH-independent mechanisms have however been proposed to facilitate PDI reduction during ER stress. One of these mechanisms involves the binding of misfolded proteins to PDI, which was shown to impede its productive association with Ero1. This not only hinders PDI reoxidation but also accelerates the auto-inactivation rate of the oxidase, which should provide additional time for protein reduction to occur (Moilanen and Ruddock, 2020).

We thus plan to explore alternative substrates and conditions, which will include scenarios such as ER stress inducing conditions, to evaluate and challenge the significance of this GSH-induced ER reduction. An intriguing possibility would be that ER reduction could be a featured consequence of the activation of the NRF2 regulon. The NRF2 transcription factor regulates many enzymes from the anti-oxidant metabolism including GCLC and GCLM enzymes, and has been extensively linked to tumour growth and chemoresistance. It would thus be appealing to challenge how the NRF2-dependent remodelling of GSH levels could affect the ER redox status of the cells and with which consequences.

---

## 5) GSH AND CALCIUM

In various studies, a calcium dependent ER reduction had been observed and among two non-exclusive hypotheses (Avezov et al., 2015; Lizák et al., 2020), one attributed this reduction to an enhanced transport of GSH inside the ER (Lizák et al., 2020). Our results not only confirmed this observation but also provided additional evidence that this calcium dependent mechanism occurred independently of an increase in cytosolic levels of GSH. This suggested that luminal calcium depletion triggered the import of GSH against the concentration gradient, thereby supporting an active transport mechanism rather than the allosteric activation of a calcium responsive channel. Crucially, the levels reached by the GSH ER transport when cells were subjected to both a GSH gradient and a Tg treatment suggested that these two mechanisms may collaborate synergistically. Of note, neither of these two transport modes seemed to require Sec61 nor BiP function, whose inactivation was also proven ineffective to inhibit the calcium-dependent transport of GSH by Lizak and coworkers.

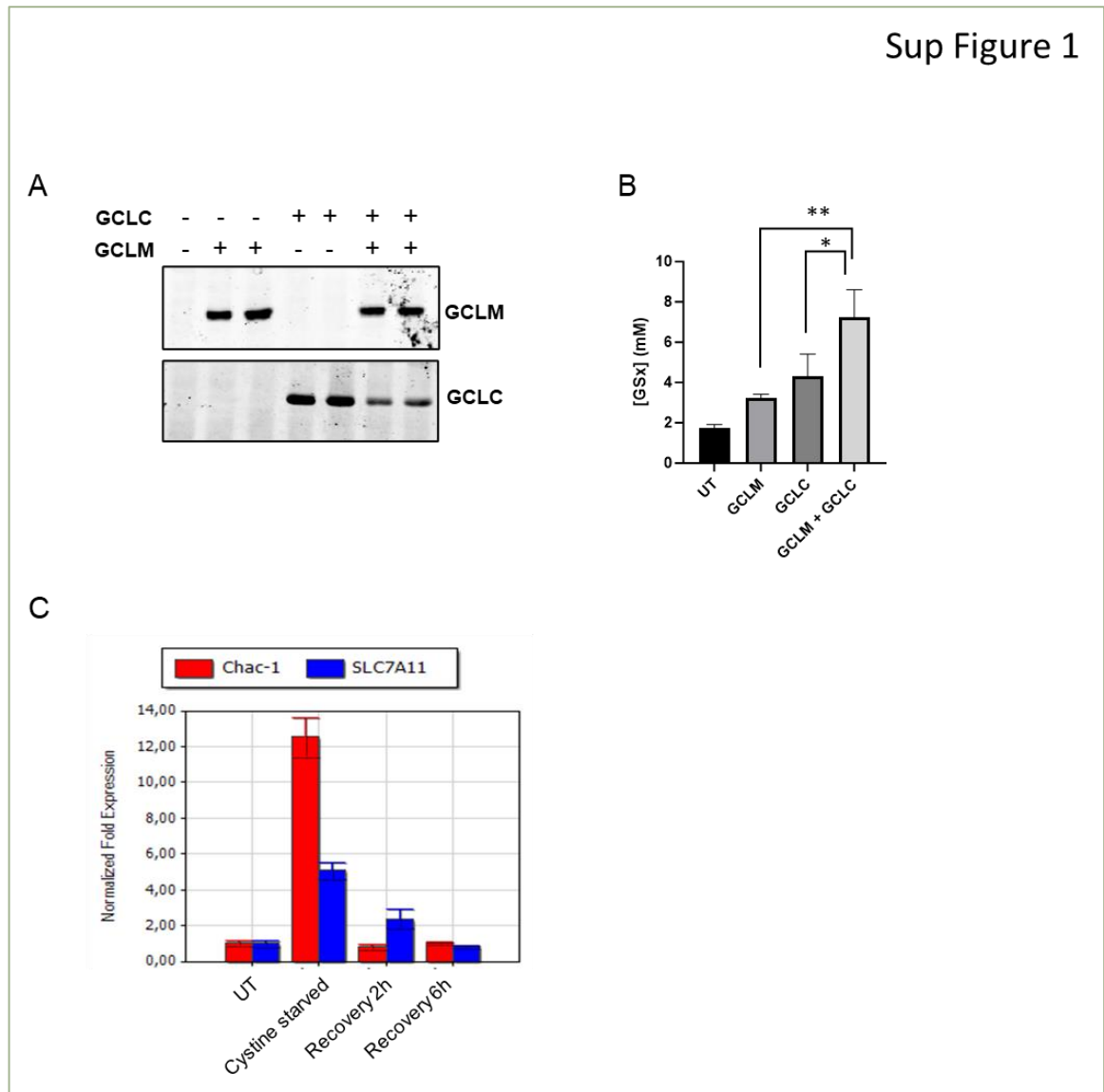
As for the gradient mode, the physiology and transport mechanism behind this calcium-responsive transport of GSH are unknown. An interesting path to explore would be the redox regulation of the different calcium transporters, in and out the ER.

---

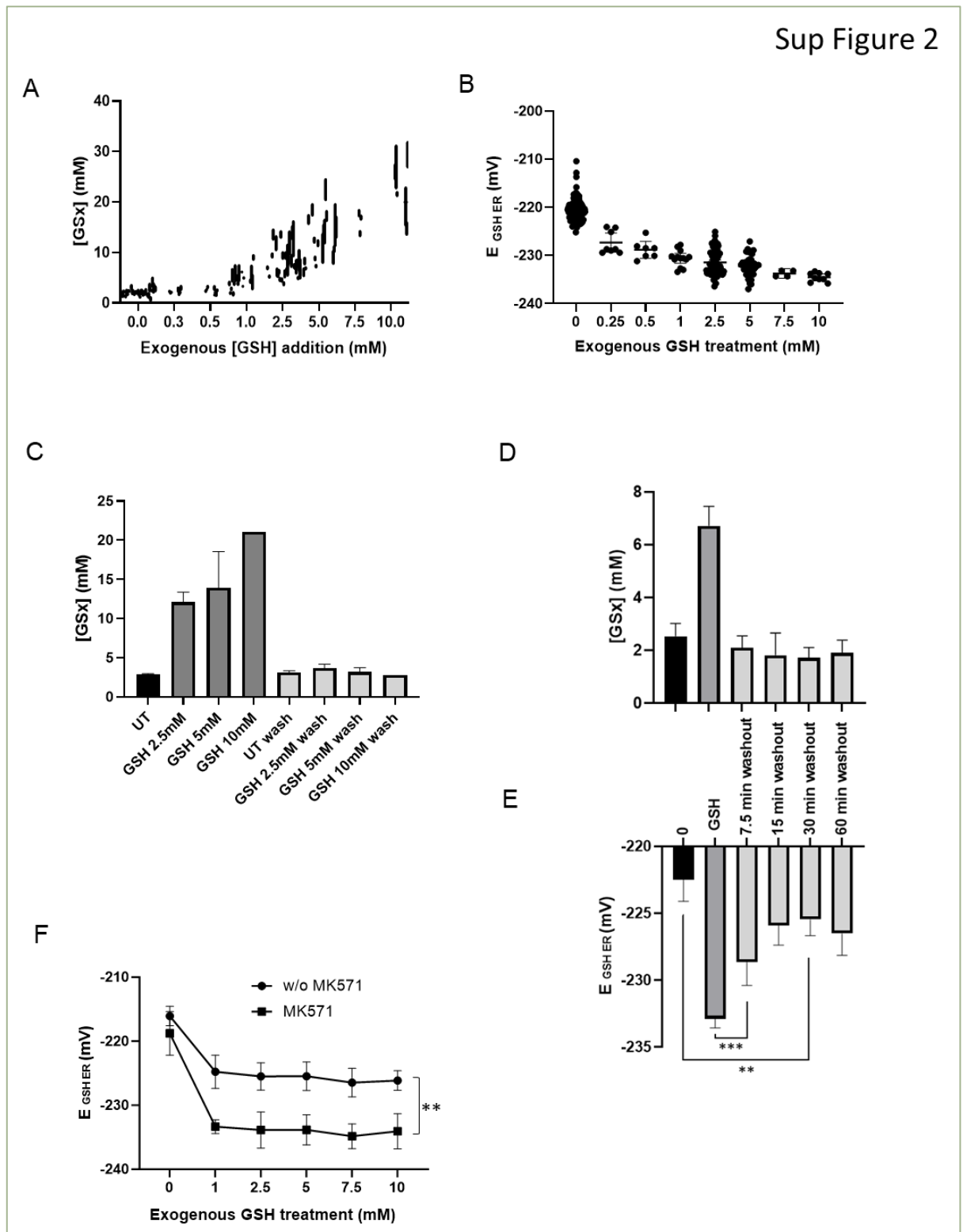
## CONCLUSION

In conclusion, our results have highlighted the existence of two different modes of ER transport for GSH, one resulting from a facilitated diffusion according to the cytosolic gradient and the other one, involving an active and calcium dependent activation of a GSH transporter. Although we could not demonstrate a clear-cut impact of the gradient type transport on ER isomerization/reduction functions of GSH, alternative conditions and substrate may have to be used to unravel the significance of this GSH-induced ER reduction. Physiologically speaking, our data suggest that conditions inducing GSH biosynthesis, such as those elicited by Nrf2 activation could have an impact on ER functions that remain to be explored.





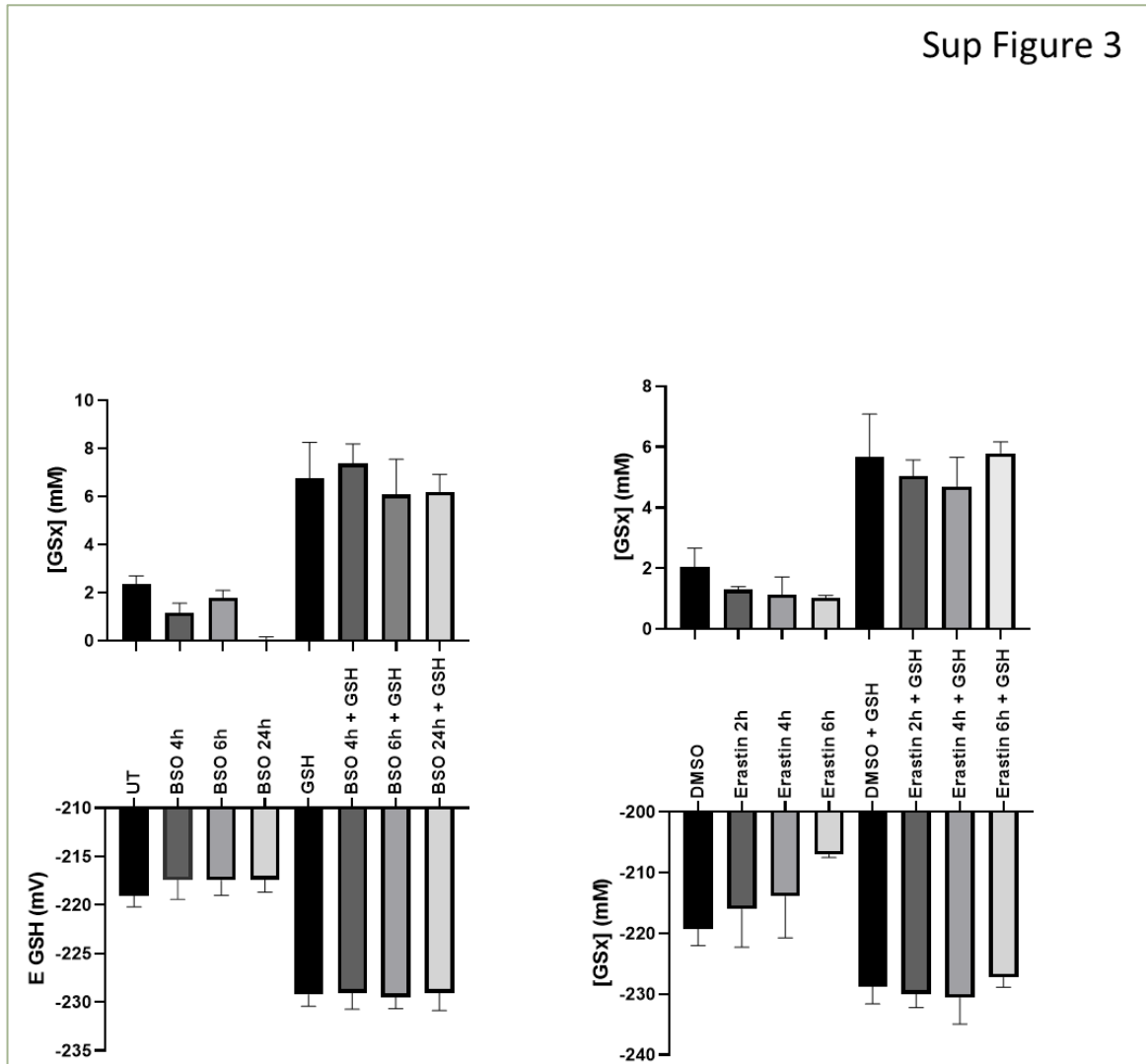
**Supplemental Figure 1.** (A) HEK293 cells stably expressing Grx1-roGFPiE were transfected with GCLC and/or GCLM expressing plasmids. GCL expression was monitored on protein extracts by SDS-PAGE using anti-GCLC and anti-GCLM antibodies. (B)  $[GSx]_{Cell}$  was measured in each of these transfection conditions as described in Figure 1. (C) QPCR analysis of Chac1 and SLC7A11 expression upon overnight cystine starvation and repletion performed on HEK293 cells stably expressing Grx1-roGFPiE.



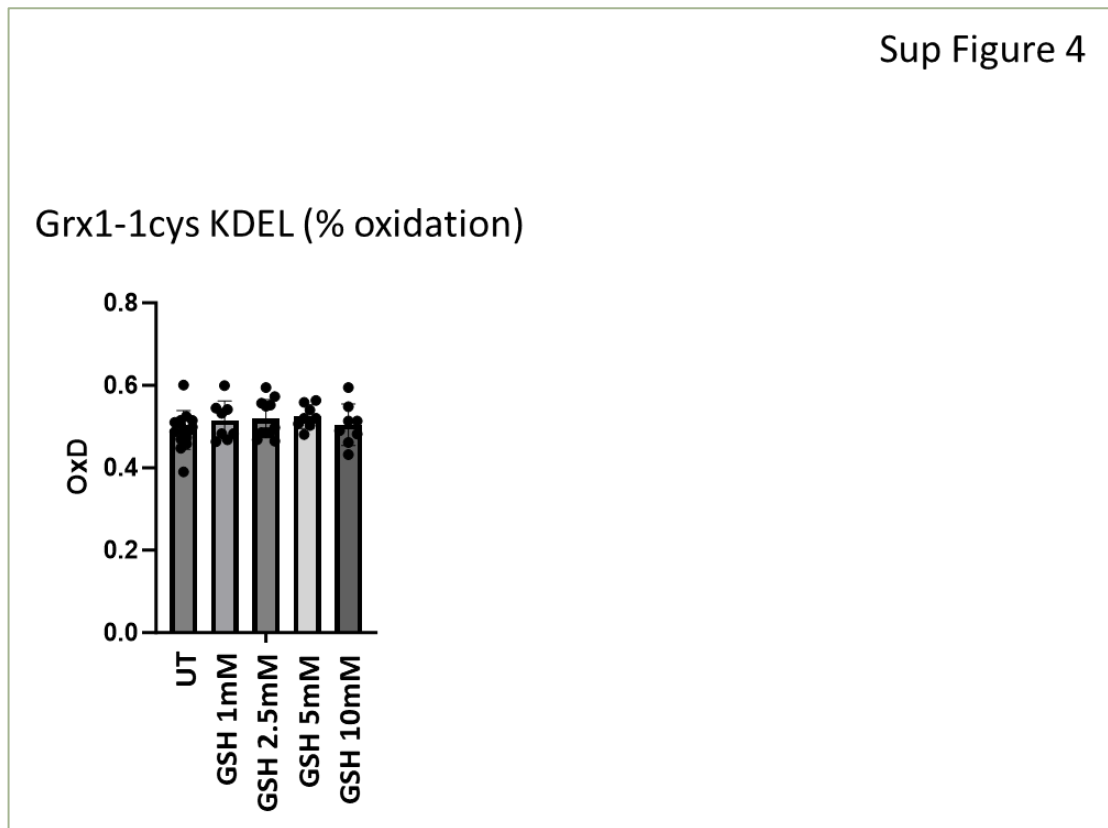
**Supplemental Figure 2. ER  $E_{GSH}$  is sensitive to an increase of GSH cytosolic levels (A)**

Raw values distribution of  $[GSx]_{Cell}$  in response to increasing doses of exogenous GSH treatment, corresponding to Figure 1. (B) Raw values distribution of  $E_{GSH}$  in response to increasing doses of exogenous GSH treatment, corresponding to Figure 1. (C) HEK293 cells stably expressing Grx1-roGFPiE were treated with 2.5 mM, 5 mM or 10 mM of GSH for 10 minutes, washed quickly in PBS and immediately lysed in SSA 5% (dark grey bars). Alternatively, GSH-treated cells were incubated for 3 minutes in the PBS wash (wash

condition) before lysis. Cellular  $[GSx]_{cell}$  values were calculated as in Figure 1B. **(D)** and **(E)** HEK293 cells stably expressing Grx1-roGFPiE were treated for 5 minutes with 2.5 mM GSH and  $[GSx]_{cell}$  **(D)** and ER  $E_{GSH}$  **(E)** were measured as in Figure 1, before and after GSH addition, and after GSH removal, by washing and incubation in GSH-free medium during the indicated times. Data were plotted with 95% CI interval error bars (n=3 to n=17 for  $[GSx]_{cell}$  and n=7 for ER  $E_{GSH}$ , for each condition analyzed). p-values were calculated relative to control or as indicated by the connecting lines on the graph. **(F)** HEK293 cells stably expressing Grx1-roGFPiE were treated for 45 minutes with GSH with or without MK571 (300  $\mu$ M).  $E_{GSH}$  values were collected as in Figure 1.

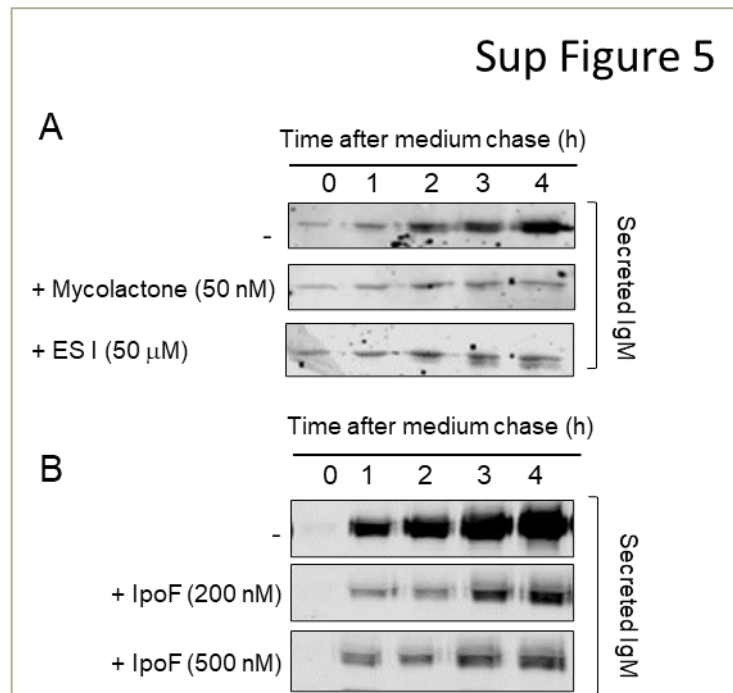


**Supplemental Figure 3. [GSx] and ER  $E_{\text{GSH}}$  are quickly restored upon removal of exogenous GSH.** (A) HEK293 cells stably expressing Grx1-roGFPiE were treated for 4, 6 and 24h with BSO (200  $\mu\text{M}$ ).  $[\text{GSx}]_{\text{cell}}$  and  $E_{\text{GSH}}$  were determined as in Figure 1 before and after treatment with 2.5 mM GSH for 10 minutes. (B) HEK293 cells stably expressing Grx1-roGFPiE were treated for 2, 4 and 6h with erastin (20  $\mu\text{M}$ ).  $[\text{GSx}]_{\text{cell}}$  and  $E_{\text{GSH}}$  were determined as in Figure 1 before and after treatment with 2.5 mM GSH for 10 minutes. Data are represented as means of 3-5 experiments and associated SD.



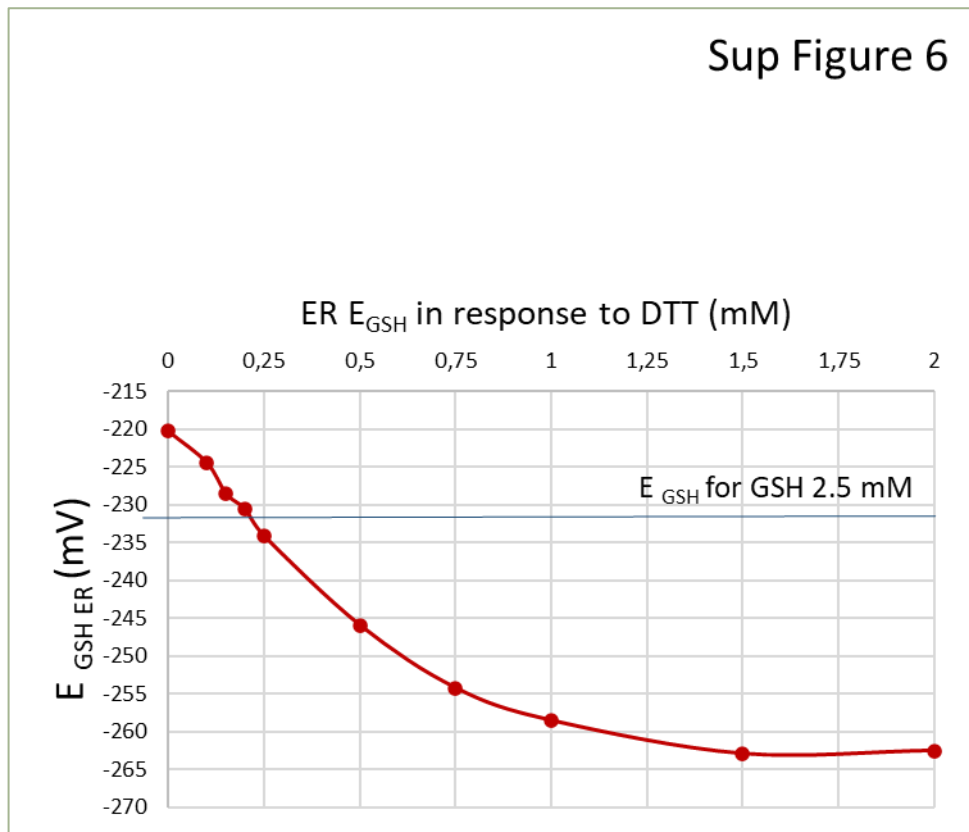
**Supplemental Figure 4. Grx1-1cys KDEL OxD values upon exogenous GSH treatment.** HEK293 cells were transiently transfected with H1-Grx1-1cys KDEL and exposed to 1, 2.5, 5 or 10 mM of exogenous GSH. Cells were processed as in Figure 2B. OxD corresponds to the % of probe oxidation. It is calculated after resolution of the glutathionylated and non-glutathionylated forms of the probe on SDS-PAGE

## Sup Figure 5



**Supplemental Figure 5. Inhibition of protein translocation by the Sec61 inhibitors (A)** Measure of IgM secretion in the culture medium in the presence or absence of mycolactone (A) or IpoF (B). Engineered HeLa cells stably expressing IgM were pre incubated with the inhibitors, then the culture medium was removed, washed twice and fresh medium (Opti-MEM, Gibco) was added. Aliquots of medium were collected at the indicated times after medium refreshment and analyzed by SDS-PAGE to quantify the efficiency of IgM secretion.

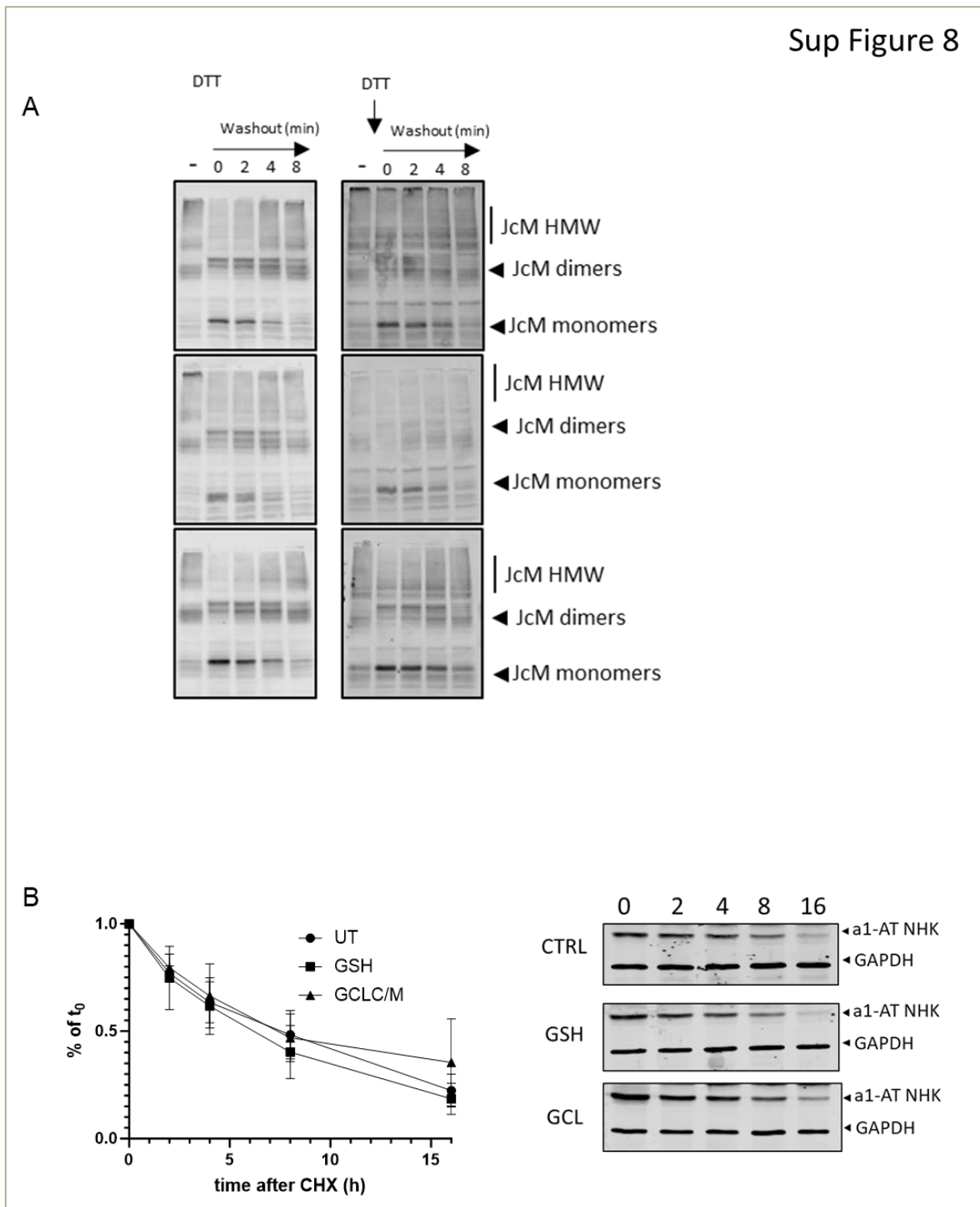
## Sup Figure 6



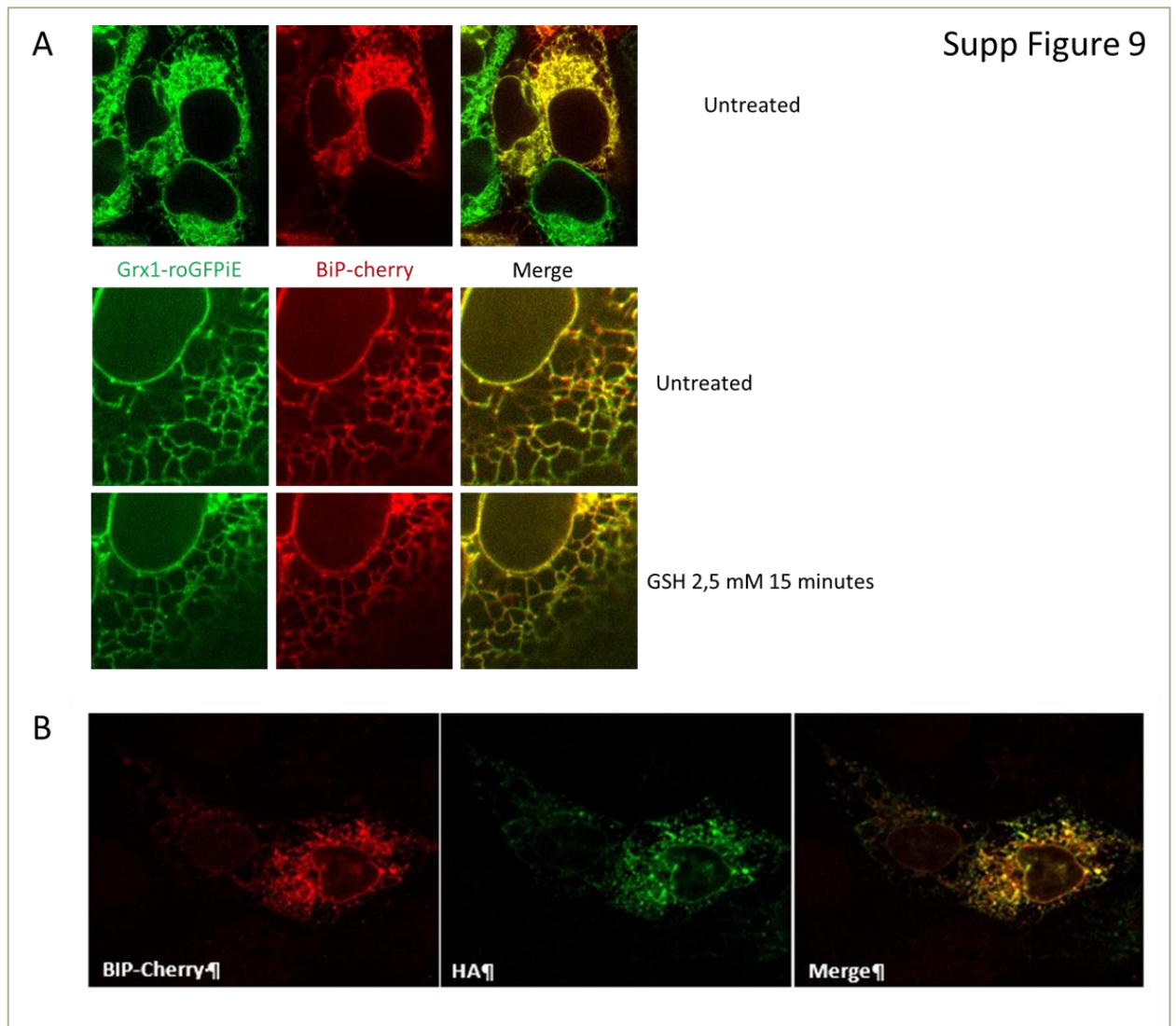
**Supplemental Figure 6. DTT dependant ER reduction.** HEK293 cells stably expressing Grx1-roGFPiE were treated with increasing amount of DTT and  $E_{\text{GSH}}$  was determined as in Figure 1. As a comparison, the extent of ER reduction achieved upon 2.5 mM GSH treatment is plotted as a blue line.







**Supplemental Figure 8. Impact of GSH and GCLC/M treatment on ERAD and protein folding** (A) HEK293 cells were transiently transfected with myc-JcM, were analyzed and processed as in Figure 5G. (B) HEK293 cells were transiently transfected with a plasmid of  $\alpha$ 1-anti trypsin NHK mutant and the half-life of the corresponding protein were determined after adding 1 $\mu$ g/mL CHX in the culture medium.



**Supplemental Figure 9. ER localization of Grx1-roGFPiE and Grx1-1cys KDEL (A)** HEK293 stably overexpressing Grx1-roGFPiE were transiently transfected with a BiP-Cherry plasmid. Red and green fluorescence were recorded and merged. **(B)** HEK293 cells were transiently transfected with a plasmid of Bip-Cherry and HA tagged Grx1-1cys. The latter was detected through immunofluorescence staining (green) and merged to the fluorescence of BiP-Cherry (red)

## CHAPTER 2: PRELIMINARY RESULTS

### I. DISCRIMINATING THE EFFECT OF CYSTEINE FROM THAT OF GLUTATHIONE

#### A. PRESENCE OF EXTRACELLULAR CYSTINE IS NECESSARY FOR ER PROBE REDUCTION

We previously observed in the paper that the modulation of glutathione levels in the cell modulated the  $E_{\text{GSH}}$  readout of our ER redox sensor.

To do so, we used several methods to modulate the levels of glutathione in cells. Among these, we starved cells from cystine overnight, by using a DMEM medium devoid of cystine, the disulfide bonded form of cysteine (DMEM-cys). This starvation led to an increase of the ER  $E_{\text{GSH}}$  value from approximately -215 to -203 mV. When we tried to rescue this starvation-induced oxidation by addition of exogenous GSH, we made an unexpected observation.

While the intracellular GSH levels could indeed be restored by treating the cells with 2.5 mM GSH, reaching 7,5 mM 10 minutes post-exposure, the ER  $E_{\text{GSH}}$  was barely recovered and by no means reached the reducing value expected from the gradient hypothesis (compare the GSH treated conditions with -228mV and -210 mV in non-starved and starved cells respectively. (Figure 29, left panel)

At first, we hypothesized that the 16 hours starvation protocol may have physiological consequences, such as rerouting glutathione fluxes away from the ER, as a way to remobilize cysteine pools. It is also possible that cystine -and therefore glutathione- depletion would cause such an oxidation of the ER that the roGFP probe would be driven out of its range of linearity. This would then make the estimations of  $E_{\text{GSH}}$  less reliable and sensible to redox variations.

To test these hypotheses, we performed starvation kinetics at shorter time points and went down from the initial 16 hours of cystine starvation to as low as 10 minutes of cystine starvation from the medium and subsequently treated cells with exogenous GSH.

Strikingly, we observed that the shortest 10 minutes starvation treatment was already sufficient to prevent the ER probe reduction upon GSH treatment. In these conditions, GSH exogenous treatment could increase  $[\text{GSx}]_{\text{Cell}}$  as expected and independently of starvation, indicating that the mechanism allowing GSH import into the cell was functional. The ER  $E_{\text{GSH}}$  however remained the same around -215 mV as in untreated cells. Importantly, the levels of whole cell glutathione levels were not affected by the 10 minutes cystine starvation, (Figure 29, middle panel), which suggests that these starvation conditions were probably too short for the lack of cystine to have a physiological impact in terms of glutathione metabolism. This experiment therefore ruled out that the lack of response to exogenous GSH was caused by a cell adaptation. Additionally, as the probe was not oxidized by 10 minutes of cystine starvation, this indicated that the lack of ER reduction could not be explained by the probe being out of its linearity range. We also verified that complementing the cystine-free DMEM with the 0.2 mM of cystine usually used in culture media, could restore the GSH-induced ER reduction previously observed using complete DMEM. In these conditions, the treatment with 2.5 mM GSH indeed both increased  $[\text{GSx}]_{\text{Cell}}$  and led to the expected matched reduction of the probe, down to the -228 mV for ER  $E_{\text{GSH}}$ .

We next hypothesized that the GSH-induced ER reduction could be conditioned by the availability of intracellular cystine/cysteine. Interestingly, the previous experiments we made using Erastin (see **Supplemental Figure 3** or **Figure 29**, right panel), an inhibitor of the SLC7A11 cystine transporter at the plasma membrane, showed that preventing cystine import was not sufficient to block the ER reduction elicited by exogenous GSH treatment. This suggested that the lack of extracellular cystine rather than a lack of its cellular import explained the defective ER reduction.

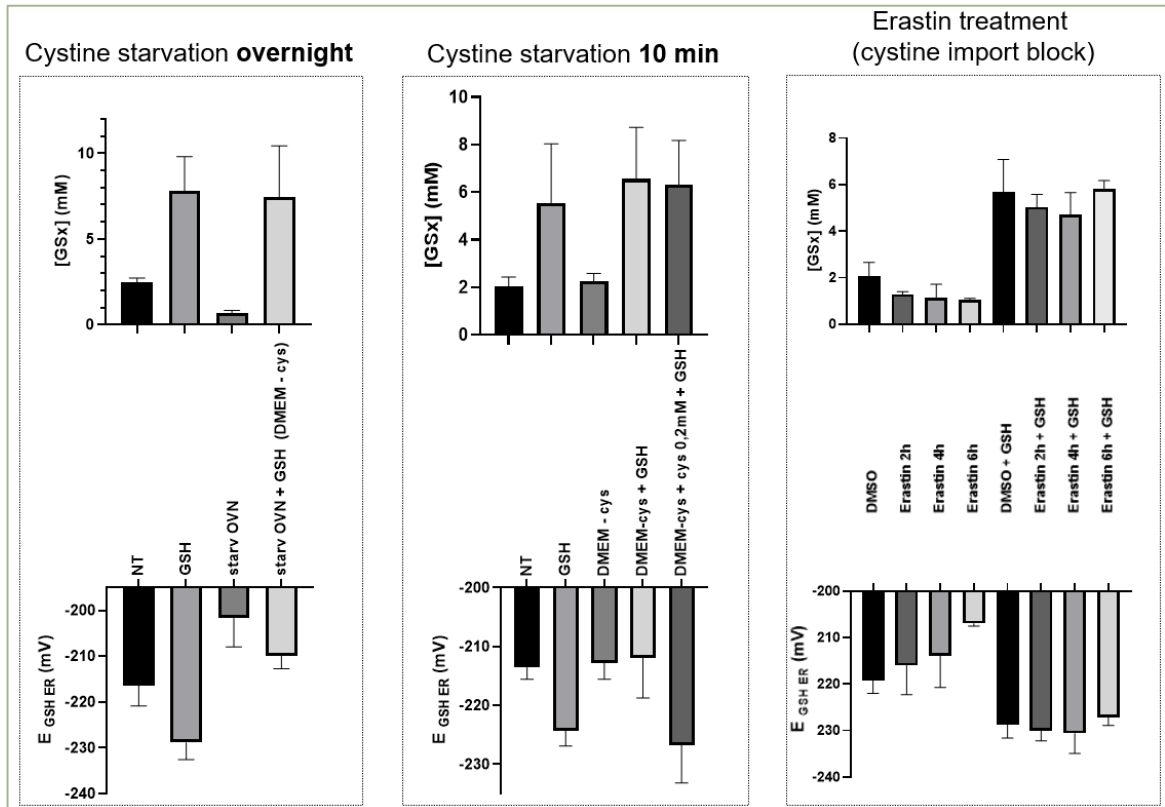


**Figure 29 – Extracellular cystine is necessary for ER probe reduction by GSH**

$E_{GSH ER}$  and [GSx], respectively referring to GSH ER reduction potential and total intracellular glutathione concentration, were simultaneously assessed in HEK293 cells stably expressing Grx1-roGFPiE as described previously. **Left panel:** Cells were either cultured with complete medium or cystine was removed from the culture medium for 16 hours by culturing cells in DMEM devoid of cystine (starv OVN), then cells were left untreated or treated 10 minutes with 2.5 mM GSH. **Middle panel:** Cells were left in complete DMEM or starved for 10 minutes with DMEM devoid of cystine (DMEM-cys). After starvation, cells were left untreated or treated with 2.5 mM GSH for 10 minutes. To assess the necessity for cystine to be present, 0.2 mM cystine were added alongside 2.5 mM GSH. **Right panel:** For cystine import blunting, cells were treated with 20  $\mu$ M erastin for the indicated times, then cells were treated with 2.5 mM GSH for 10 minutes

## B. CYSTEINE CAN CAUSE ER PROBE REDUCTION WITHOUT GSH IN WHOLE CELLS

As cystine import was not required for GSH-induced ER reduction but the presence of extracellular cystine alongside GSH was necessary to decrease ER  $E_{\text{GSH}}$ , we reasoned that GSH and cystine could cross-react to form GSSG and cysteine, and that, one of the two species required for ER reduction. As GSSG could not induce the reduction of ER Grx1-roGFPIE, we shifted our focus on cysteine species.

To challenge a cross-reaction between GSH and cystine, we performed metabolomics to quantify, among other things, intracellular levels of cysteine in **Figure 30**. We made the striking observation that while steady state levels of intracellular cysteine were around 0.05 mM, GSH treatment in complete DMEM, so with cystine, brought intracellular cysteine levels up more than 4 times, at 0.23 mM.

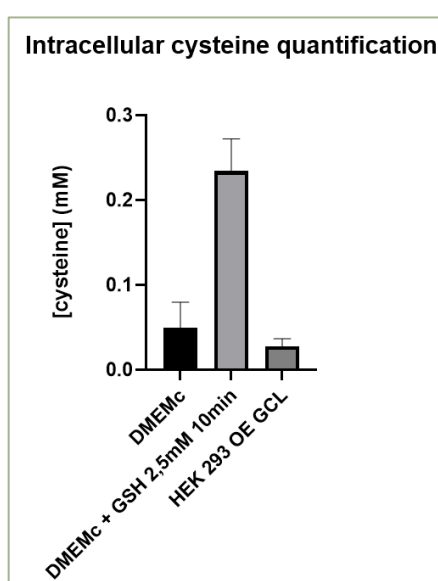


**Figure 30 – Glutathione exogenous treatment, but not GCL overexpression, increases intracellular cysteine levels** Cells either untreated or treated with 2.5 GSH for 10 minutes or transfected with GCLC and GCLM for 48 hours were submitted to HPLC analysis after thiol blocking for cysteine quantification.

To investigate the involvement of GSH and cystine cross-reaction on ER reduction, we added increasing quantities of cystine to a fixed 2.5 mM concentration of GSH, and observed that the probe became increasingly reduced (**Figure 31**). When cells were treated with mounting quantities of cystine alone as a control,  $E_{\text{GSH}}$  stayed stable around the steady-state -215 mV value (**Figure 31**, left panel). This meant that the progression in reduction was not the result of cystine *per se*, nor that of GSH because its quantity was fixed. This rather indicated that the observed reduction indeed required a cross-reaction between GSH and cystine, cystine being the limiting factor for ER reduction.

We then exposed cells to equivalent quantities of cysteine, meaning that for one equivalent of cysteine in the previous assay, we added two of cysteine, since the former is a dimer of the latter. To our surprise, we could when treating cells with increasing quantities of cysteine only, observe the same reduction as the that we saw when adding GSH and cysteine together.

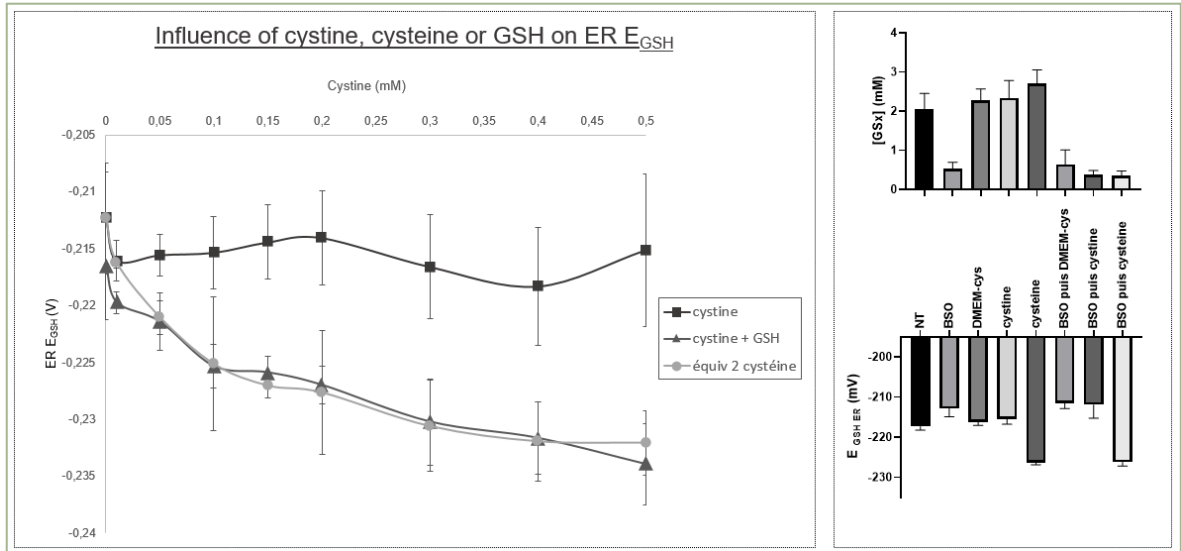


**Figure 31 – Cysteine causes ER probe reduction independently of GSH**  $E_{GSH}^{ER}$  and  $[GSx]$  were simultaneously assessed in HEK293 cells stably expressing Grx1-roGFPiE as described previously. **Left panel:** Cells were either treated with increasing quantities of cysteine, cysteine and 2.5 mM GSH or two cysteine-equivalents of cysteine for 10 minutes. **Right panel:** Cells were either untreated or glutathione pools were exhausted by BSO addition for 24 hours. After, BSO-treated and untreated cells were either cysteine-starved for 10 minutes (DMEM-cys) or treated for 10 minutes with either 0.2 mM of cysteine or two equivalents, 0.4 mM, of cysteine.

This last observation led us to investigate if cysteine could reduce the probe independently of GSH. To do this, we evaluated the ability of cysteine to reduce ER Grx1-roGFPiE in conditions where GSH pools had been previously depleted by BSO treatment (Figure 31, right panel). We renewed the observation that BSO drastically decreased GSH intracellular concentrations and slightly oxidized the probe. Strikingly, cysteine could stimulate a decrease of ER  $E_{GSH}$  even though GSH levels were cut to very low concentrations.

These results indicate that cysteine can reduce the ER when added exogenously, even without any GSH added and even more so, in conditions where intracellular GSH levels are restricted. This suggests that cysteine could have a direct effect of our Grx1-roGFPiE probe.

---

### C. CYSTEINE REDUCTION IS NOT MATCHED IN SEMI-PERMEABILIZED CELLS

The previous observations raised a pivotal question: can cysteine directly and autonomously reduce the probe, or does it act indirectly, by mobilizing residual glutathione pools for instance, to exert probe reduction?

We once again resorted to semi-permeabilization, to discriminate our observations on the ER from any cellular factor, and assess whether cysteine directly caused reduction of the ER. It has to be noted that in whole cells fluorescence measurements, DTT and diamide controls allowed us to define the fully reduced and fully oxidized state of the probe, thereby allowing  $E_{\text{GSH}}$  calculation. When using semi-permeabilization, the steady state value of the probe became so oxidized that it precluded calculation of  $E_{\text{GSH}}$ , so we decided to use the representation of the average ratio of the fluorescence resulting from excitation at 395 over 460 nm. The reasoning and conclusions drawn from this average ratio and  $E_{\text{GSH}}$  calculation remain the same however.

It should be noted that cysteine and GSH were not tested equal in terms of thiol molarity, because we chose conditions that caused a similar reduction of the ER roGFP in non-permeabilized cells. Additionally, the cysteine concentrations used herein are in the same range as those measured for intracellular cysteine by the aforementioned metabolomics experiments (see [Figure 30](#)).

To assess if the reduction of the probe by cysteine occurred similarly on semi-permeabilized and non-permeabilized cells, we measured in each conditions the average ratio upon treatment with 2.5 mM of GSH, 2.5 mM GSH + 0.4 mM of cysteine, or 0.4 mM cysteine alone ([Figure 32](#)).

When treating cells with 0.4 mM cysteine without GSH, we renewed the striking observation that the probe in non-permeabilized (NP) cells became more reduced. However, in semi-permeabilized (SP) cells, although we could observe a decrease in the 395/460 ratio this reduction was clearly not as efficient: the strong cysteine-driven reduction in NP cells was not mirrored in SP cells.

Treatment with 2.5 mM GSH alone reduced the probe, in both NP and SP cells, which verified that semi-permeabilization did not hinder GSH responsivity. GSH led to a similar probe reduction both in NP and SP cells, when added together with 0.4 mM cysteine.

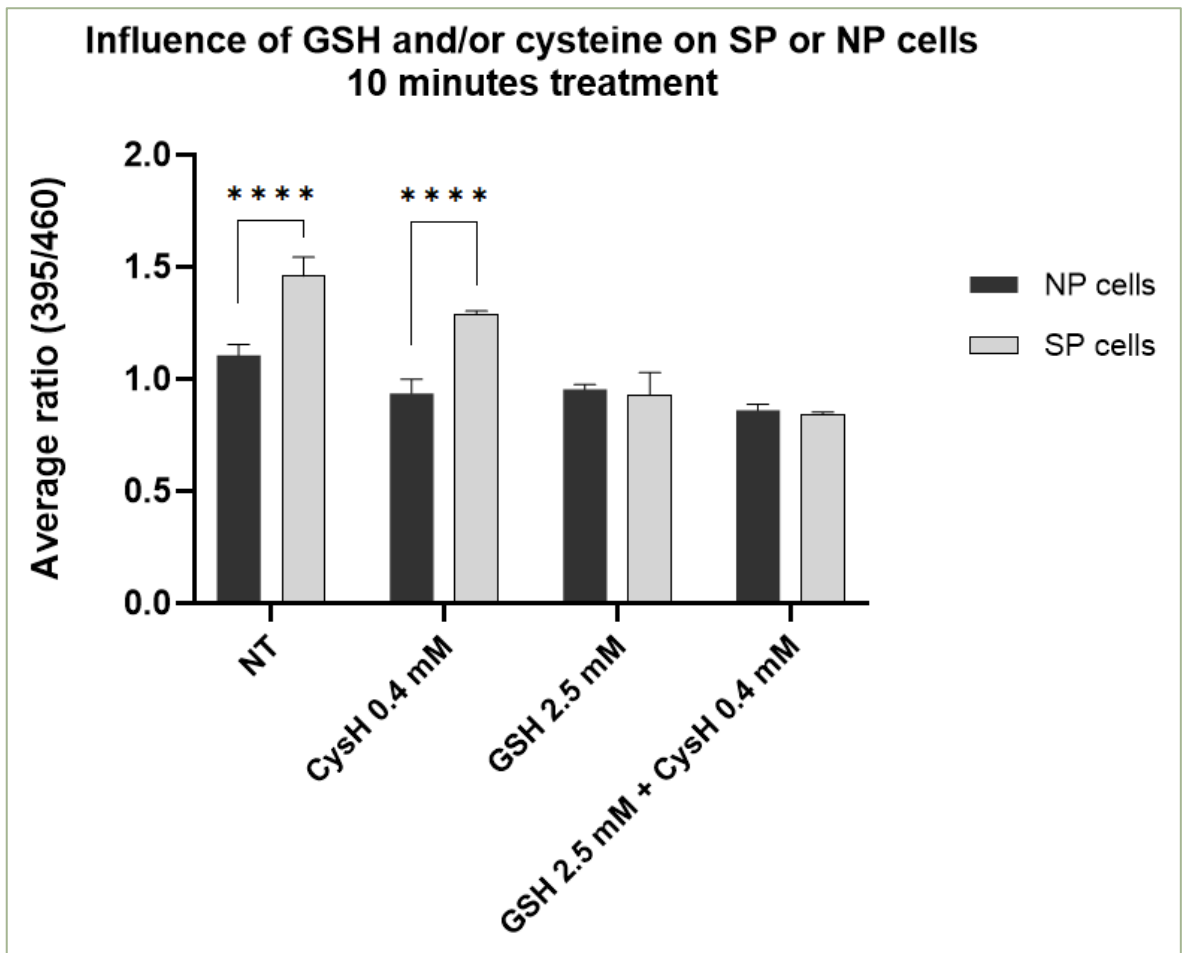


**Figure 32 – Cysteine reduction of the probe in non-permeabilized cells is not mirrored upon semi-permeabilization** Average fluorescence ratio resulting from excitation at 395 over 460 nm was calculated from digitonin-permeabilized HEK 293 cells stably overexpressing Grx1-roGFPiE and compared to that of non-permeabilized cells. Cells were treated with 2.5 mM GSH, 0.4 mM cysteine (CysH) or both, and fluorescence of the probe was recorded after 5; 10 and 15 minutes of treatment. The figure represents n=2 biological replicates as well as a representative 10 minutes time point

We then examined the influence of increasing the cysteine concentrations, ranging from 0.1 to 0.6 mM, on the reduction of the probe in SP cells. This was performed using cysteine alone or in association with a fixed 2.5 mM concentration of GSH (Figure 33)

We could observe that the average ratio of the probe went from 1.5 in untreated cells to 1.24 in cells treated with 0.6 mM of cysteine in a dose-dependent manner. On the other hand, GSH treatment alone caused a swift reduction of the probe, from the 1.5 average ratio to 1.1 after 5 minutes of treatment. This ratio was not significantly changed by the addition of increasing doses of cysteine.

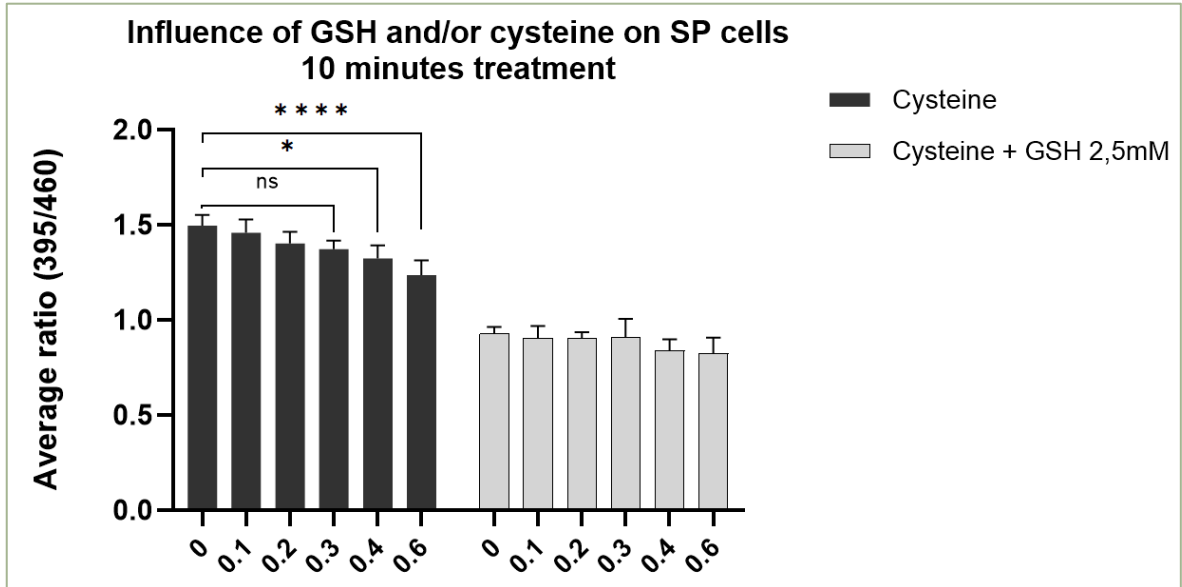


**Figure 33 – Cysteine addition does not cause a GSH-equivalent reduction in semi-permeabilized cells** Average fluorescence ratio resulting from excitation at 395 over 460 nm was calculated from digitonin-permeabilized HEK 293 cells stably overexpressing Grx1-roGFPiE. Cells were treated with a fixed quantity of cysteine only (dark grey), or increasing quantities of cysteine along a fixed 2.5 mM quantity of GSH (light grey). Fluorescence of the probe was recorded after 5; 10 and 15 minutes of treatment. The figure represents n=4 biological replicates as well as a representative 10 minutes timepoint

These experiments show a discrepancy between the extent of the cysteine-dependent reduction of the sensor in whole cells compared to semi-permeabilized cells. While many cellular factors could be involved to explain this difference, we could nonetheless evidence a slight decrease in the probe ratio in SP cells upon cysteine treatment, be it minimal.

#### D. CYSTEINE DOES NOT MARKEDLY REDUCE THE PROBES AT THE CONCENTRATIONS WHERE REDUCTION OCCURRED

The previous results using semi-permeabilized cells suggested that the Grx1-roGFPiE sensor was more responsive to GSH-dependent reduction compared to cysteine. This is in agreement with the Grx1 moiety possessing a high affinity binding site for GSH and not for cysteine (Deponter, 2013), which was behind the rationale for the probe design. However, it is possible that the cysteine levels reached in the ER are higher than we first assumed from the result of our whole cells metabolomics quantifications. In this case, the law of mass action could overcome the lesser reactivity of the probe toward cysteine.

To further investigate if conditions existed where cysteine could directly reduce the probe and also to make up for any issue with thiol equivalency, we semi-purified the HA-tagged grx1-roGFPiE probe by immunoprecipitation. The probe was then treated on beads with 0.8 mM of cysteine, which is twice higher than the exogenous concentration that achieved a significant reduction of the probe when added to whole cells, and a mild reduction of the probe in SP cells (see previous **paragraphs B and C**). On the other hand, we treated the probe with 2.5 mM GSH which is the standard single-point concentration in our assays. To assess for a thiol-equivalent effect, we also treated the purified probe with 2.5 mM of cysteine or 0.8 mM of GSH (**Figure 34**). After 10 minutes of treatment, we proceeded to cysteine alkylation to freeze the probe redox state. The reduced and oxidized forms of the protein were discriminated using redox western blot.

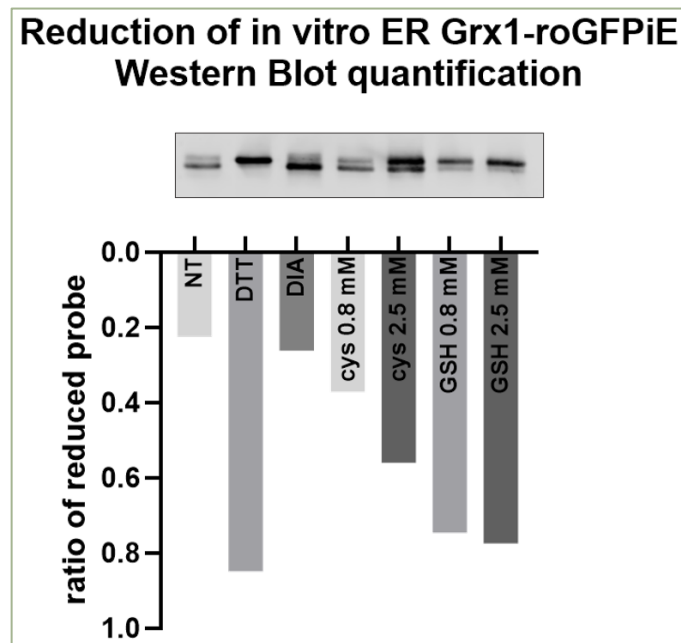


**Figure 34 – Thiol equivalents of cysteine and GSH do not reduce purified Grx1-roGFPiE to the same extent** Redox state of Grx1-roGFPiE probe assessed by HA immunoprecipitation and western-blotting of the probe in the presence of cysteine and GSH. Densitometric quantification of the reduced band was normalized to the sum of reduced and oxidized probe for each sample.

In this experiment, we observed that the semi-purified probe was for the most part in the oxidized form, as expected from the aerobic conditions for extraction. Treatment with DTT and Diamide were included to control the reduced and oxidized forms of the probe respectively.

When we compared the redox state of the purified probe after treatment with thiol equivalent quantities of cysteine or GSH, we could observe that 0.8 mM of GSH caused an almost total reductive shift of the redox state of the protein. Likewise, 2.5 mM of GSH caused a marked reductive shift of the probe, to slightly greater extent than that achieved with 0.8 mM of GSH. Distinctly, 0.8 mM of cysteine only provoked a slight reduction of the probe, and even at a very high molarity of 2.5 mM, cysteine could not achieve the same reduction as that reached with 0.8 mM GSH.

Altogether, our experiments using SP and semi-purified probes subjected to both GSH and cysteine confirmed the higher specificity and reactivity of the probe toward GSH, although a minimal reactivity toward cysteine can be witnessed

We also investigated the ability of both cysteine and GSH to reduce ER-localized Grx1-1cys, in the same effort to verify glutathione specificity of our probes.

An exploratory purification protocol was set-up in which semi-permeabilized cells overexpressing HA-tagged and ER-targeted Grx1-1cys were treated with the increasing quantities of cysteine and GSH that exerted probe reduction in whole cells (**Figure 35**).

We can see in this first experiment that GSH addition causes a dose-dependent and efficient reductive shift of the protein, from 20% to 90% (left panel). On the other hand, cysteine addition had a much milder effect: increasing cysteine concentrations brought the reduction of the probe to a maximum of 55% reduction, still in a seemingly dose-dependent fashion (right panel).

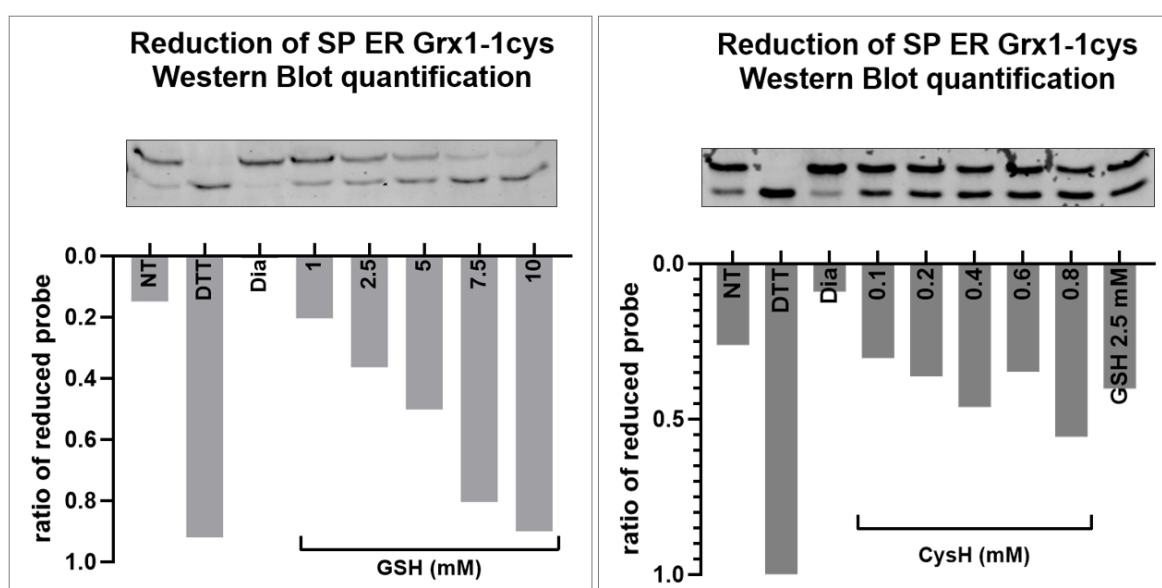


**Figure 35 – Cysteine does not reduce ER localized Grx1-1cys to the same extent as GSH in the concentrations that do in whole cells** Redox state of Grx1-1cys probe assessed by HA Western blotting of SP cell lysates in the presence of cysteine and GSH. Densitometric quantification of the reduced band was normalized to the sum of reduced and oxidized probe for each sample.

This preliminary experiment argues in favor of a greater specificity of our Grx1-1cys system for GSH as well. However, a reducing effect of cysteine, be it limited, was unmasked in all of our experiments, and must be kept in mind.

## E. THAPSIGARGIN-INDUCED REDUCTION OF THE ER IS INDEPENDENT OF CYSTEINE AVAILABILITY

As detailed in the paper, we observed two types of GSH-induced reduction of the ER: one forced by an increase of GSH cytosolic concentrations, and one triggered by treatments stimulating ER calcium leak. The latter appeared to actively mobilize glutathione pools towards the ER.

We have noticed that cystine depletion prevented reduction of the probe in the context of GSH elevation by exogenous addition. We therefore questioned if the necessity of cystine in the medium was also necessary for the second type, Tg-induced, ER reduction.

To do so, we decided to record ER  $E_{\text{GSH}}$  values in whole cells treated with 1  $\mu\text{M}$  of thapsigargin, in complete medium. For comparison, we pre-incubated cells with cystine-devoid medium for 10 minutes before adding thapsigargin (**Figure 36**).

We replicated the observation that the absence of cystine in the medium prevented ER reduction upon GSH treatment. Thapsigargin treatment brought  $E_{\text{GSH}}$  to the same -225 mV as for GSH-treated cells. In contrast to GSH-driven reduction, the ER reduction induced by Tg reduction was effective despite the lack of cystine in the medium. The re-addition of cystine or cysteine in the medium did not significantly modify the redox profile of the probe exposed to thapsigargin.

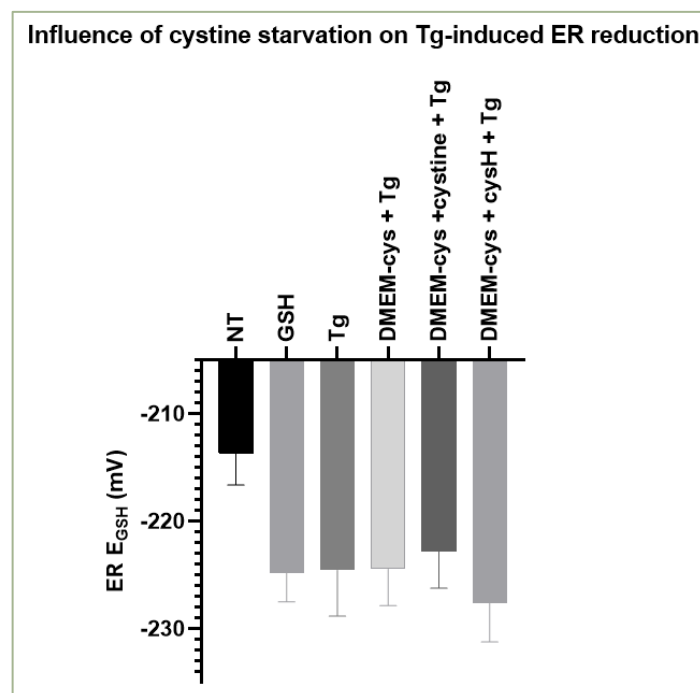


**Figure 36 – Thapsigargin-elicited reduction is independent of the availability of cysteine**

Cells were starved from cystine by culturing them in DMEM-cys for 10 minutes. Then, cells were treated with 1  $\mu\text{M}$  thapsigargin for 30 minutes, either in DMEM-cys, or in DMEM-cys completed with cystine or cysteine. The figure represents  $n=4$  biological replicates

In this experiment, we observed that while ER reduction could be promoted by either GSH addition or Tg treatment, removing cystine from the medium only prevented ER reduction in the former case.

---

## DISCUSSION

Our initial investigations in the context of my PhD project were focused on glutathione trafficking in and out of the ER. Our goal was to address the question of when and how glutathione enters the ER. Based on the results obtained in yeast, a central strategy to answer this question, has been to manipulate GSH intracellular levels in cells and to monitor how ER localized GSH biosensors react to these modulations.

Among these manipulations, we used the fact that cysteine is the limiting amino acid in the synthesis of GSH, and therefore depleted cells from it, in order to lower glutathione levels in cells. One of our strategies to deplete cells from cysteine was to remove cystine from the culture medium and we did so for initially long periods of time, to ensure that cellular pools of GSH would be minimized.

On this occasion, we did observe that the GSH depletion ensuing an overnight starvation of cystine, caused an oxidative shift of the ER localized Grx1-roGFPiE sensor. To control that GSH depletion was the cause of this shift, we tried to replete cells with added exogenous GSH, expecting a reduction of the sensor to the same extent as GSH treated unstarved cells. We however observed that the GSH-driven reduction was far less pronounced in starved cells and could not even bring the  $E_{\text{GSH}}$  value back to that of the steady state, unstarved cells.

Our model for glutathione transport suggests that ER reduction is at least partly a function of the glutathione gradient established between the cytosol and the ER. To explain an absence of reduction, our model would imply that that no gradient was created when we added GSH. This could be the case if extracellular GSH did not enter the cell that is if the cytosolic GSH concentration had not increased.

We however observed the same increase in  $[\text{GSx}]_{\text{Cell}}$ , around 7.5 mM, in cells treated with 2.5mM of exogenous GSH, independently of the cystine starvation status, thereby excluding the possibility that the GSH gradient was defective. Our remaining hypothesis was that, when cellular GSH levels go down to a certain level, its trafficking might be prioritized for essential function such as iron sulfur cluster biogenesis for instance (see **Role in iron metabolism**) by restricting the ER transport of GSH. This hypothesis is limited however: when we treated cells with BSO for as long as 24 hours, we effectively depleted GSH stores, but when GSH was added, reduction of the ER sensor was observed (see **Supplementary Figure 3**)

These results prompted us to investigate shorter starvation time, but to our surprise, even 10 minutes of cystine starvation caused this lack of GSH-driven reduction phenotype. These results excluded the possibility of any major physiological rerouting to happen, as no glutathione depletion occurred after 10 minutes of cystine depletion.

Our next hypothesis was that a sufficient intracellular level of cystine/cysteine was a condition for GSH to enter the ER, which implies that blocking cystine import would have the same effect as the absence of extracellular cystine. However, xCT blockade had no impact on the ability of GSH to reduce the ER. Since it appeared that only the presence of cystine and GSH in the extracellular milieu was a condition for ER reduction, we hypothesized that cross reactions could occur between the two species.

To investigate this hypothesis, we examined ER reduction upon combinations of the cysteine and glutathione redox couple, and it became clear that cysteine played a role in sensor reduction: while cystine and GSH alone could not reduce the probe, the combination of both could. Surprisingly, the same reduction was achieved by cysteine alone, in the absence of extracellular GSH but surprisingly enough, also in BSO-treated cells.

These results suggested that, rather than GSH, the cysteine generated by its cross-reaction with cystine could also be the reason why we first observed reduction of the sensor. This suggestion could be discussed however. Dean P. Jones and colleagues, in an article arguing in favor of a distinct role of the cystine/cysteine couple from that of the glutathione couple, projected the thiol-disulfide exchange rates between the 2 couples. Considering cystine and GSH at physiologically relevant concentrations of 30  $\mu\text{M}$  and 3 mM respectively, the rate of reduction in these conditions would be a relatively slow 2  $\mu\text{M}\cdot\text{min}^{-1}$ , contrasting with our observation of a swift and efficient reduction of our ER-localized sensor (Jones et al., 2004).

Using metabolomics, we anyway observed an increase in cysteine intracellular levels when cells were exposed to extracellular GSH, which supported the hypothesis of a cross-reaction between GSH and cystine in the medium. Different cysteine PM transporters of medium specificity, such as ASCT2 and LAT1, have been identified in the literature which could account for the import of cysteine from the extracellular milieu (Pizzagalli, Bensimon, and Superti-Furga, 2021).

Importantly, these range of evidence questioning a possible role of cysteine in ER reduction prompted us to challenge the specificity of our probe for GSH. We challenged the ability of cysteine to reduce our GSH biosensor by using both semi-permeabilized cells and immune-purification of the probe. Intriguingly, in both experimental conditions, the Grx1-roGFPiE probe did exhibit some dose-dependent reactivity toward cysteine but the reduction achieved by cysteine was inferior to that observed with GSH. In SP cells, the sensor reduction was minimal at the cysteine concentrations which normally trigger a significant ER reduction in whole cells. Making sure to compare equimolar quantities of thiols for both compounds, the reactivity of the immunopurified Grx1-roGFP was also monitored lower toward cysteine compared to GSH.

These results were altogether surprising and raised many questions while highlighting major limitations in our initial experimental setups. First, the most surprising one, is the fact that in the context of the semi-permeabilization protocol, NP cells, which are essentially submitted to the same protocol without the membrane-permeant digitonin, are nevertheless reduced by GSH. This is surprising because this chapter is based on the initial observation that cells grown in a cystine-free medium lack response to GSH-induced ER reduction. NP cells responded to GSH though, despite the fact that no cystine was present in the experimental medium.

A second question concerned the cysteine concentrations that we used to challenge the probe responses using our *in vitro* and *semi-in vitro* assays. Our metabolomics quantifications averaged the intracellular cysteine concentration between 50  $\mu\text{M}$  and 250  $\mu\text{M}$  in untreated or GSH treated conditions respectively, which were both quite ineffective in reducing the roGFP probes *in vitro*. It is however possible that the ER actively pumps cysteine to much higher concentrations, in which case our verifications would be off in terms of cysteine quantity. Additionally, the removal of cytosol entails

removal of ATP, which could also hinder such hypothetical cysteine transport systems towards the ER.

In conclusion, we observed a greater specificity of the probe towards GSH, which was both reassuring and also in accordance with the literature. Other teams did verify the reduction of Grx1-fused roGFP proteins in presence of the cysteine couple or the glutathione couple (Gutscher et al., 2008; Björnberg, Østergaard, and Winther, 2006). Curiously, Gutscher *et al.* pushed the quantities of cysteine up to 10 mM and only noted a very faint reduction of the probe. In our case, 2.5 mM of cysteine did cause a significant reduction, although not to the extent of glutathione, even at 0.8 mM. They were however looking at the fluorescence ratio, while our technique relied on western blot quantification, which could explain some of the discrepancy. Another difference is that we used a Grx1 fusion instead of the plain version of the roGFP probe. Grx1 fusion should however provide a greater specificity toward GSH which contrary to cysteine, has a specific binding site in the glutaredoxin moiety (Deponite\_2013). Another reassuring piece of our data is the fact that, while glutathione treatment causes an increase in intracellular cysteine, overexpression of GCL does not. Additionally, GCL could induce ER reduction even in the absence of cysteine in the medium, indicating that in these cases, it is a rise of intracellular GSH which does cause an ER reduction.

Finally, it is always possible that cysteine still required GSH to achieve ER reduction. Indeed, despite BSO inducing a marked depletion of GSH, our quantification assays become less reliable in the micromolar range. It is thus always possible that a residual pool glutathione could still participate to the ER reduction we observed.

These elements support our belief that the probe reduction in the previous part were indeed attributable to GSH. There is however a reduction of the probe occurring with limited to no amounts of GSH when cysteine is added onto cells. An assay allowing cysteine quantification in the ER would be needed to overcome our imitations in understanding this phenomenon. Both chemical and genetically encoded probes with specificity towards cysteine are starting to emerge. For instance, the team of Weiyang Lin has developed a small molecule functioning as a ratiometric cysteine probe. They used an ER targeting *p*-Toluenesulfonamide moiety linked to a naphthalimide fluorophore, and an acrylate function as a cysteine-sensitive moiety. The probe localized into the ER and showed a satisfactory 4-fold specificity towards cysteine in vitro, when tested with 10 mM of glutathione versus 5  $\mu$ M of cysteine (Dong et al., 2019). Additionally, another article describes the generation of a different small molecular ER targeting probe, capable of distinguishing cysteine, GSH and homocysteine. The principle relied on distinct kinetics of molecular rearrangement following the addition of either GSH, cysteine or homocysteine onto the fluorophore. The probe successfully detected cysteine or homocysteine addition in HeLa cells, but necessitated NEM treatment prior, to block out GSH (Yue et al., 2021).



## II. CHEMICAL SCREENING

With the aim to better understand the traffic of glutathione in and out of the ER, we reasoned that identifying compounds capable of impeding or modulating this transport would be a stepping stone in characterizing the potential transporter GSH. An easy way of identifying candidates would be to set up a high throughput screening, therefore, one of the objectives of the project was to design and conduct this HTS.

To do so, we needed to define two crucial features of the screening protocol: the readout system that we would use to track GSH entrance inside the ER, as well as the conditions in which this transport is stimulated.

---

### A. SETTING UP THE HIGH THROUGHPUT SCREENING

A reliable readout system of GSH transport into the ER needed to be compatible with a screening protocol, with highly reproducible and scalable properties, as well as the generation of a fast readout. The stably expressed GFP probe that gave us access to  $E_{\text{GSH}}$  met these criteria, but presented one limitation: the readout gives us access to  $E_{\text{GSH}}$ , not the quantity of GSH entering the ER. A molecule identified this way would not necessarily be active on GSH traffic, but on the redox state of GSH in the ER. For the purpose of screening, we accepted this limitation and remained careful with conclusions. A secondary screen with potential candidates would then be necessary to confirm if any redox potential signature is relevant in terms of glutathione traffic in or out of the ER.

---

### DESIGN OF A SUITABLE READOUT FOR HTS: THE SUPERFOLDER MUTANT OF GRX1-ROGFPiE

Our lab created a cell line stably expressing the ER-localized redox sensitive GFP: grx1-roGFPiE. As described earlier, this probe is fused to a glutaredoxin to enhance the disulfide exchange rate of the GFP with glutathione, which occurs *via* cysteines 147 and 204. The insertion of a glutamic acid next to the catalytic cysteine 147 (which is what “iE” stands for) displaces the standard redox potential of the probe to make it more oxidized and therefore more suitable to the ER oxidizing environment (Lohman and Remington, 2008).

Although ER localized roGFP constructs have been previously published, the probe proved challenging to detect by fluorescence readouts, and Grx1-roGFPiE was no exception, as our own data shows that the specific fluorescence of the probe is barely twice that of cellular autofluorescence. With the idea of starting a chemical screening using this genetically encoded sensor, the fluorescence intensity of the probe was critical, since we wanted to collect the best signal to noise ratio to extract the maximum of information out of our fluorescence readouts

In 2016, Hoseki and colleagues studied the addition of SuperFolder mutations to an ER roGFPiL (the insertion amino acid in position 147 was in their case, a leucine) (Hoseki et al., 2016). They studied mutants with S30R, T39N, N105T, I171V, Y145F and A206V mutations or a subset of these, and showed improved efficiency of both folding and fluorescence when the first four mutations were added to the roGFPiL backbone.

We thus decided to replicate their mutations to improve the fluorescence of the Grx1-roGFPiE probe. Some major differences should be noted between the probe used by Hoseki, and ours. First, as pointed out, the insertion amino acid. Then, our protein is fused to a Grx1 protein which can modify its folding efficiency, and impact fluorescence. Finally, the roGFPiL probe is derived from the original wild type GFP cDNA, while ours is composed of high usage, humanized codons for expression in mammalian cells. For these reasons, we were curious to investigate the same subsets of mutations including Y145F and A206V, although they were shown to be problematic in their experimental conditions.

We ordered the probe and controlled both its sequence and spectral scans. To be selected, the resulting probe should display increased fluorescence. For a consistent comparison, fluorescence of the probe resulting from excitation at the limiting wavelength 395 nm will be compared to that of probe-devoid cells. Additionally, our enhanced probe should keep its redox responsivity, so we treated cells with DTT and diamide to track that aspect. Additionally, a clear isosbestic point should be determined. An isosbestic point is a wavelength at which the absorbance of two or more species is the same, the presence of this point verifies that the probe is utilizable as a ratiometric probe.

First, we studied a SuperFolder mutant of our Grx1-roGFPiE in which S30R, T39N, N105T, I171V mutations were added, while both A206V and Y145F mutations were absent (the mutant will be called SF1 for clarity in the rest of the experiments). This first set matched the one validated by Hoseki et al. As we can see in **Figure 37**, the probe was responsive to redox changes, as the excitation peak at 385 nm had increased fluorescence in diamide treated cells, while DTT treatment increased the fluorescence resulting from excitation at 455 nm. Additionally, a clear isosbestic point could be observed at 420 nm, ensuring the ratiometric capacity of the probe.

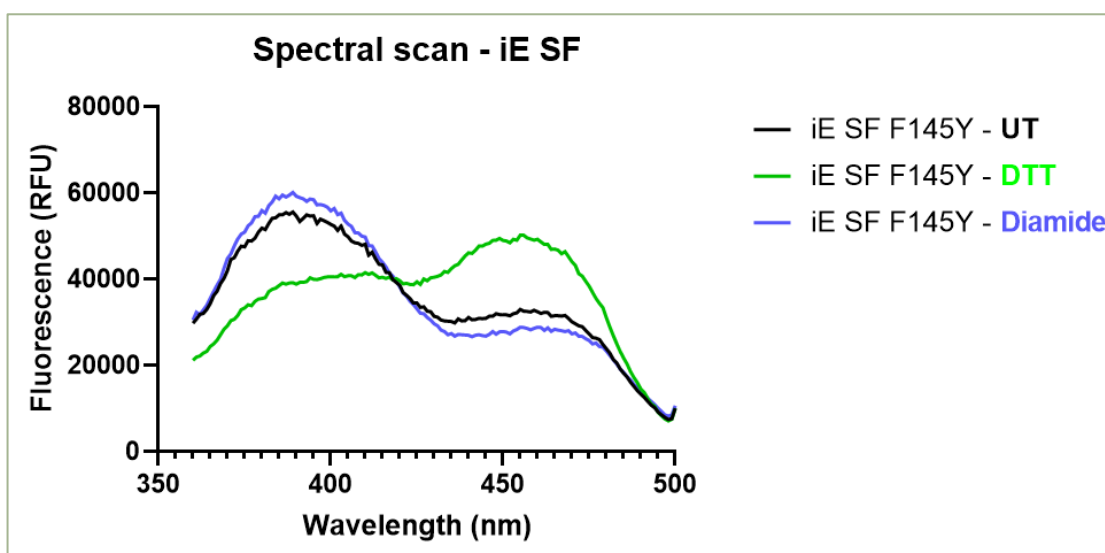


**Figure 37 – iE SF1 mutant probe is responsive to redox treatment** Spectral scan of the probe was recorded in HEPES buffer at excitation wavelengths from 350 to 500 nm. Fluorescence at 530 nm was recorded in wells treated with either HEPES buffer alone, or containing 10 mM DTT or 5 mM diamide for complete reduction and oxidation respectively. Data is representative of three technical replicates

We then compared the fluorescence intensities resulting from excitation at both 395 nm and 460 nm of the starting Grx1-roGFPiE probe and its SuperFolder SF1 counterpart. We observed that fluorescence intensity resulting from excitation at both peak wavelengths almost doubled in the mutant, going from 64 000 and 51 000 to 116 000 and 101 000 respectively (Figure 38).

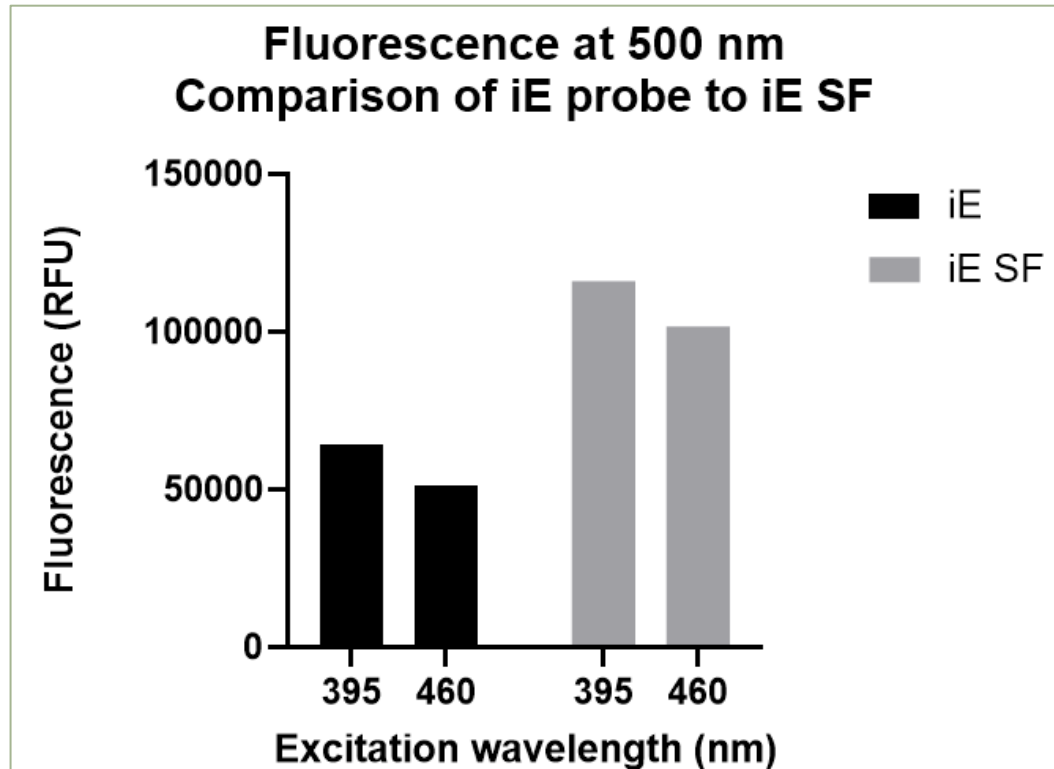


**Figure 38 – The transiently expressed SF Grx1-roGFPiE has a fluorescence intensity increased by more than two times** Fluorescence intensities resulting from excitation at the two peak wavelengths were recorded on fluorescence plate reader. The intensities of steady state Grx1-roGFPiE-expressing cells are compared to their SF counterpart

We wanted to investigate whether introducing two additional SF mutations A206V and Y145F *via* site-directed mutagenesis could further increase the fluorescence quantum yield of the probe. These two residues are however neighboring the two redox active cysteines of roGFP, and the corresponding SF mutations might thus hamper the redox properties of the probe. After addition of the mutations A206V and Y145F mutations in the SF1 construct, we conducted a spectral scan of the transiently overexpressed probe in HEK 293 cells, as depicted in **Figure 39**.

The specific fluorescence reached three times higher than our Grx1-roGFPiE probe which fluorescence reached a maximum of around 50 000 RFU when excited at 395 nm. Strikingly, while the first excitation peak at 395 nm is conserved, the second excitation peak around 480 nm is very faint. Ratiometry is then only partial. Crucially, the probe was totally unresponsive to redox treatment, which makes it unsuitable for use.

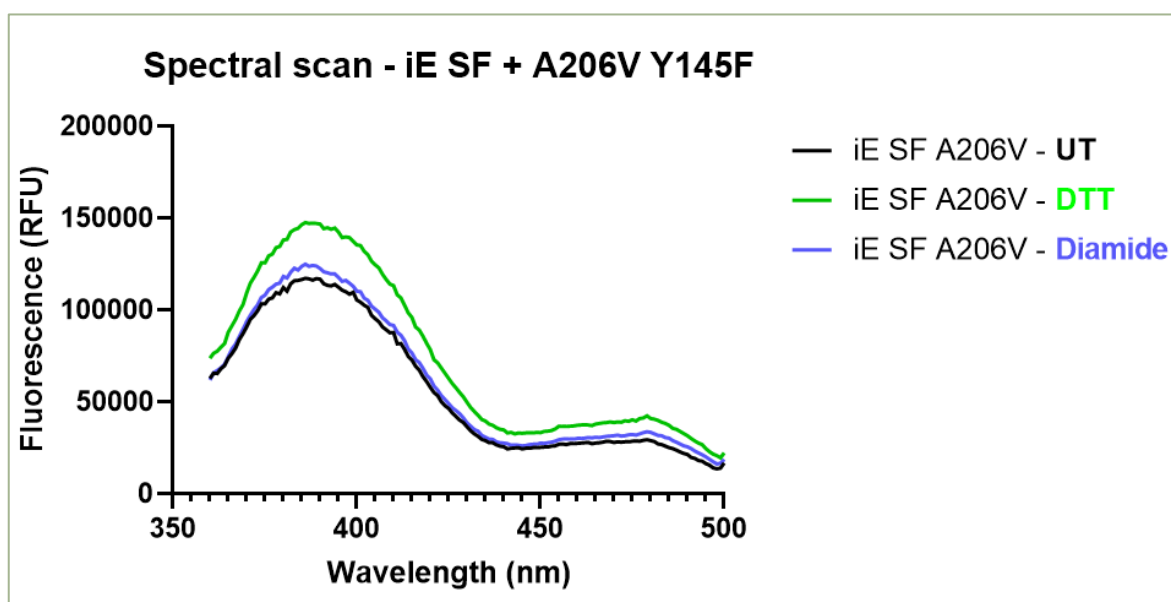


**Figure 39 – iE SF A206V probe is unresponsive to redox treatment** Spectral scan of the probe was recorded in HEPES buffer at excitation wavelengths from 350 to 500 nm. Fluorescence at 530 nm was recorded in wells treated with either HEPES buffer alone, or containing 10 mM DTT or 5 mM diamide for complete reduction and oxidation respectively. Data is representative of three technical replicates

Then, we examined the consequence of adding either the Y145F or the A206V mutation alone on top of the four S30R, T39N, N105T, I171V mutations.

When transiently expressed in HEK 293 cells, the Y145F containing probe was again, totally unresponsive to any redox treatment. As we can see in **Figure 40**, the SuperFolder (SF) probe had an excitation maximum at 385 nm, which was unchanged upon either reductive DTT treatment or oxidative diamide treatment. This time, the presence of only a single excitation peak means that the probe is no longer ratiometric, hence, also unfit for use.

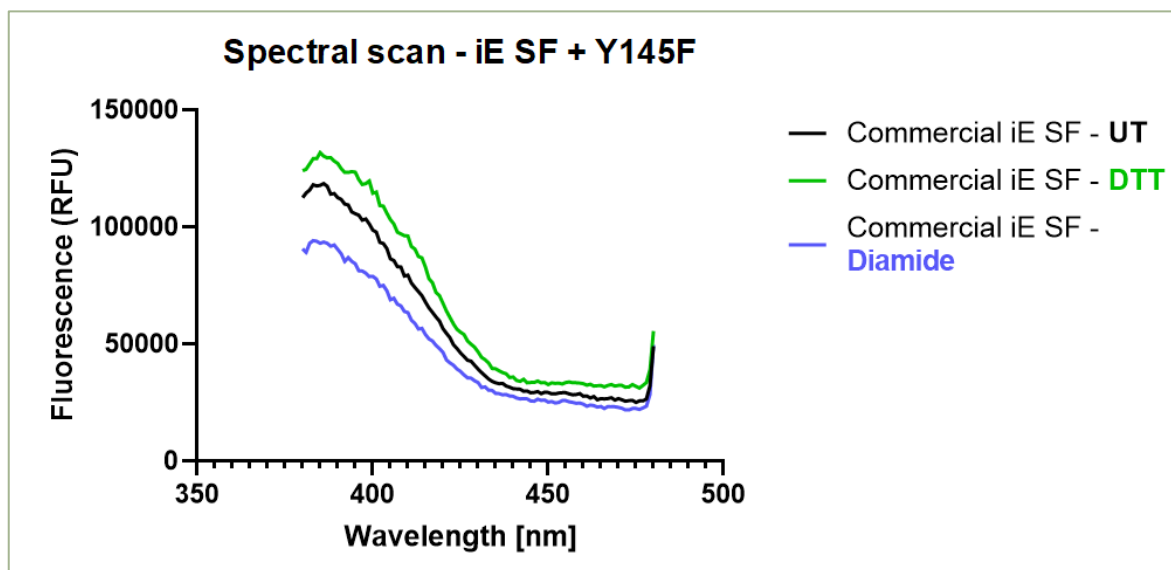


**Figure 40 – Commercial iE SF probe shows no redox responsivity** Spectral scan of the probe was recorded in HEPES buffer at excitation wavelengths from 380 to 480nm. Fluorescence at 530 nm was recorded in wells treated with either HEPES buffer alone, or containing 10 mM DTT or 5 mM diamide for complete reduction and oxidation respectively. Data is representative of three technical replicates

Similar expression of the A206V mutation only, along the four SF mutations of iE SF1 (Figure 41) yielded to a probe bearing the same excitation peaks as those observed for SF1 before, namely one at 385 nm and a second one at 455 nm. We next examined the redox behavior of the probe thanks to treatment with DTT and diamide. We observed the expected increase and decrease of the 455/395nm ratio in reduced and oxidized conditions respectively, the probe was therefore responsive to redox treatment. Critically however, no isosbestic point could be observed, which is a crucial feature of ratiometric sensing.

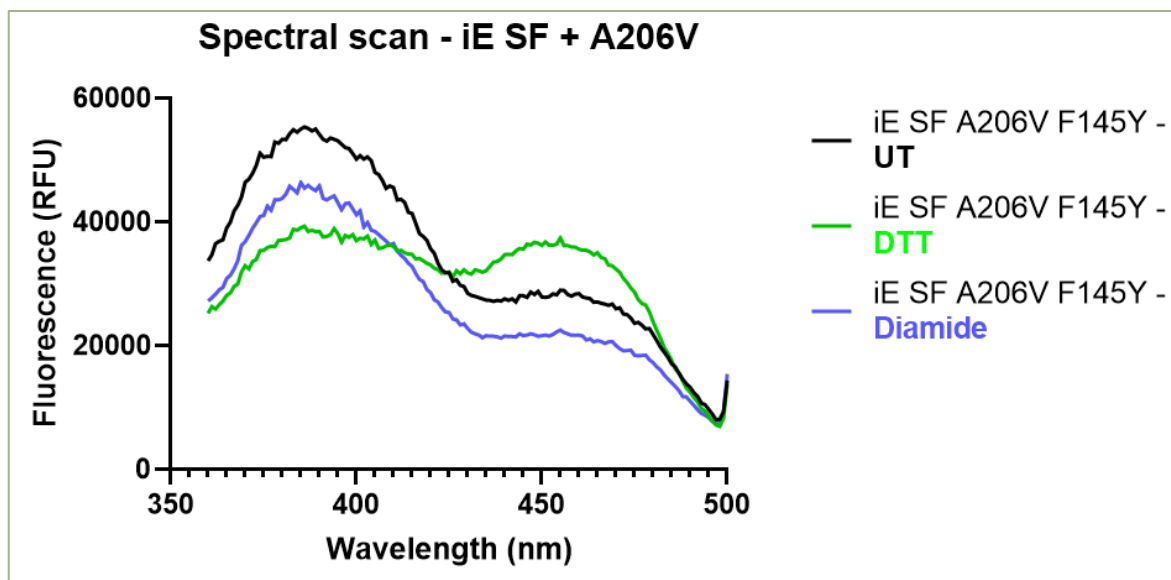


**Figure 41 – iE SF A206V F145Y probe is responsive to redox treatment but loses ratiometric ability** Spectral scan of the probe was recorded in HEPES buffer at excitation wavelengths from 350 to 500 nm. Fluorescence at 530 nm was recorded in wells treated with either HEPES buffer alone, or containing 10 mM DTT or 5 mM diamide for complete reduction and oxidation respectively. Data is representative of three technical replicates

We thus confirmed that the addition of cysteine-neighboring SF mutations was deleterious for either redox responsivity, or ratiometric properties of our probe.

For that reason, we selected the first-described iE SF1 mutant for further experiments (further called SF probe or SF Grx1-roGFPiE), because it displayed the enhanced fluorescence that we were expecting in the beginning along with ratiometric properties and redox responsivity.

Once the probe was validated in sequence, ratiometric usability and fluorescence, we verified that the probe was still responsive to glutathione addition, by performing dose-response experiments on the transiently transfected probe. This characterization was completed by our Master 2 intern Assmaa Ghali as part of her research project. She confirmed that the SF probe responds to GSH with kinetics comparable to that of the non-mutated probe, with a slightly but not significantly lower redox potential as represented in **Figure 42**.

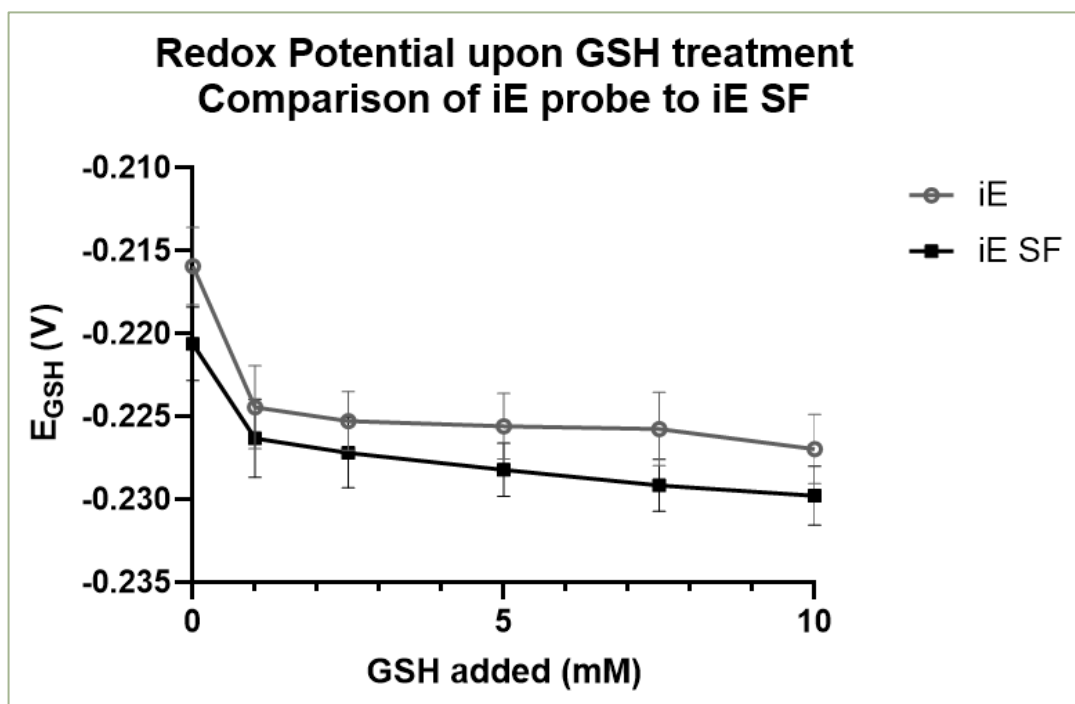


**Figure 42 – Comparison of  $E_{GSH}$  variations according to GSH intracellular levels between Grx1-roGFPiE and SF Grx1-roGFPiE** Glutathione intracellular levels in stable iE and iE SF-expressing cells were raised by 10 minutes addition of reduced glutathione (0.25, 0.5, 1, 2.5, 5, 7.5 and 10 mM) in the culture medium.

We observed cells transiently transfected with the previous SF probe in a CellInsight CX5 plate reader, and compared them to the stable 293 FRTERiE cell line (not shown). We could see that, while the latter had a homogenous fluorescence across all cells, the former displayed patches of fluorescence, with a complete lack thereof in some cells.

Added to the fact that transient transfection is time-consuming, this result highlighted the necessity for us to generate a cell line stably expressing the probe so we subcloned the insert in a pcDNA5 FRT vector to generate a stable cell line with the same protocol as previously described (See Chapter 1 – Paper)

We once again verified the spectral scan of the stably expressed probe (we selected clone 8 of SF Grx1-roGFPIE, called SF C8 for short), this time in stable cell lines, and observed the same properties in the selected stable cell line in terms of absorption peaks, as well as the isosbestic point at 420 nm (Figure 43). We carried the characterization of the probe to ensure its redox responsivity by performing standard analysis of fluorescence during glutathione treatment, both in the context of dose-response and kinetics experiments.

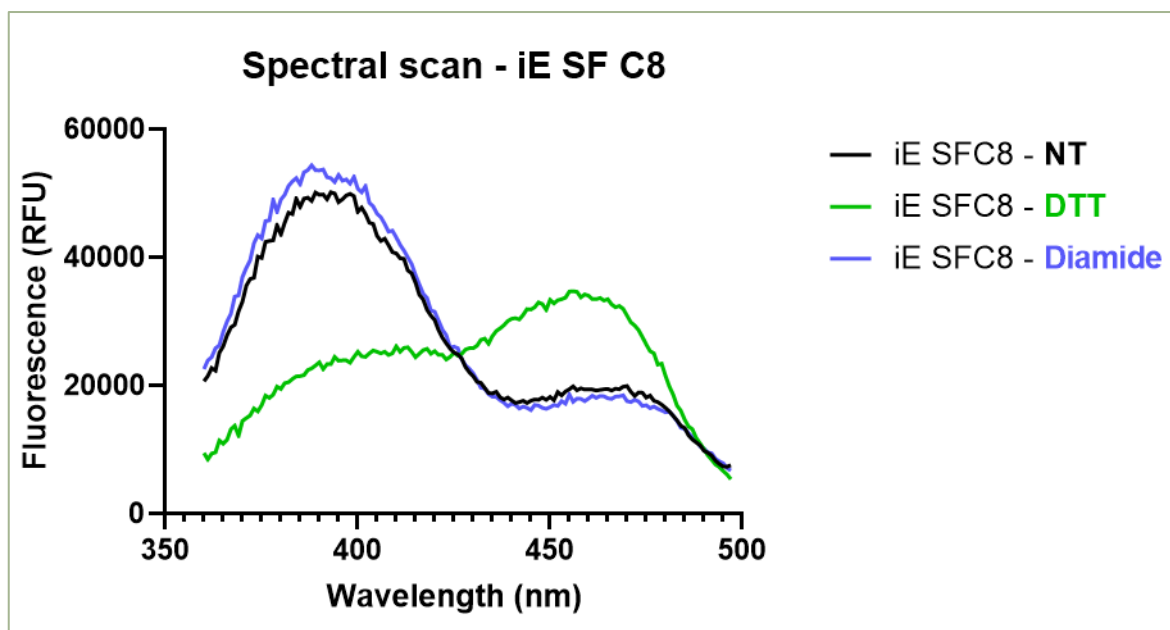


**Figure 43 – Spectral scan of stably expressed SF Grx1-roGFPIE** Spectral scan of the probe was recorded in HEPES buffer at excitation wavelengths from 350 to 500 nm. Fluorescence at 530 nm was recorded in wells treated with either HEPES buffer alone, or containing 10 mM DTT or 5 mM diamide for complete reduction and oxidation respectively. Data is representative of three technical replicates

## DISCUSSION ON THE DESIGN OF THE SUPERFOLDER PROBE

---

The difficulty in studying subcellular glutathione pools is inherent to its nature. As a small, redox sensitive peptide, standard techniques of peptide tagging or extraction become imprecise, if not irrelevant. Proxies that circumvent these limitations, namely redox-sensitive GFPs, have been developed, and the essence of my PhD project was to take advantage of these proxies to study glutathione in the endoplasmic reticulum.

The lab had already acquired and generated a cell line stably expressing ER-localized Grx1-roGFPiE and conducted several studies with it. However, it became clear that the fluorescence of the probe could become limiting in some experiments, since the gap between the autofluorescence of cells and that of the probe, the so-called specific fluorescence, is narrow.

This observation is not surprising as, upon development of the mutants of roGFP1 that rendered the probe more suitable to the ER, Lohman and Remington did observe that fluorescence intensity was negatively impacted by the insertion of an amino acid in position 147 (Lohman and Remington, 2008).

SuperFolder mutations are a set of six mutations that were added into GFPs to improve folding efficiency and therefore fluorescence intensity (Pédélec et al., 2006). In an effort to increase the fluorescence of our own probe, we wanted to construct a SF variant of Grx1-roGFPiE bearing the aforementioned six mutations: S30R, Y39N, N105T, Y145F, I171V, and A206V.

Based on the results of Hoseki *et al.*, we modified our probe to incorporate four of these mutations, and investigated the addition of the 2 remaining ones that are in the vicinity of critical catalytic cysteines (Hoseki et al., 2016). Just like in the work of Hoseki, our generated SF Grx1-roGFPiE sensor was more fluorescent, redox sensitive and ratiometric.

We then tested a variant bearing the full set of SF mutation, including the two cysteine-neighboring mutations A206V and Y145F. The probe showed no difference between reductive or oxidative treatment. Fluorescence intensity over the whole excitation range slightly increased during diamide treatment, and even more during DTT treatment. This elevation of fluorescence upon reduction was also observed by Hoseki and colleagues in the roGFPiL mutant bearing the same mutations, but in their case a clearer excitation peak was observed at 485 nm. We did observe a very faint peak at 485 nm, but nothing like the clear one Hoseki *et al.* observed.

It seemed that modifying the environment of the two catalytic cysteines was deleterious, thus we decided to study mutants bearing only one of the two cysteine-neighboring mutations. First, we studied the response of a sensors bearing only the Y145F mutation. This mutant was totally unresponsive to redox stimuli. This result was not entirely surprising, as Hoseki *et al.* did observe the same lack of redox responsiveness in their roGFPiL bearing the same five mutations. What was unexpected in our case, was the total absence of a second excitation peak at around 465 nm that is expected in roGFPiX probes (Lohman and Remington, 2008). This could be explained by the narrow excitation window we used for this analysis. Indeed, excitation spanned from 380 nm to 480 nm, because at the time, we thought that excitation peaks might be unchanged. However, Hoseki *et al.* did observe a red shift of that second excitation peak, and the setting might not have allowed us to catch it, although the spectrum tendency is not indicative of the apparition of an excitation peak, as it seems to completely flatten between 400 and 450 nm.

We then studied a SF mutant incorporating the A206V mutation only. This time, we could observe the clear apparition of the expected excitation peak at 485 nm. The major peak was at 385 nm in the oxidized form, and at 485 nm in the reduced form. However, the absence of an isosbestic point made the probe unsuitable for ratiometric use. Maybe the fact that they used a roGFPiL probe instead of Grx1-roGFPiE rendered the excitation peak at 485 nm less sensitive to the Y145F mutation than our own. Indeed, the iX amino acid is inserted in its close vicinity, at position 147. Moreover, the fluorescence resulting from excitation at 485 nm is greater in roGFPiL probes than it is in roGFPiE probes (Birk et al., 2013), so a decrease in the fluorescence intensity at this peak would be more marked in roGFPiE probes. Although this result was encouraging, two observations hindered the use of this probe: the oxidation of the probe causes a reduced fluorescence in both wavelengths of excitation, and the changes were not properly ratiometric.

S30R	Y39N	N105T	Y145F	I171F	A206V	Redox responsive	Increased fluorescence	Ratiometric (2 excitation peaks)
●	●	●	●	●	●	✓	✓	✓
●	●	●	●	●	●	✗	✓	~
●	●	●	●	●	●	✗	✓	✗
●	●	●	●	●	●	✓	✓	~

**Figure 44 – Recap of the optical properties of the 4 tested SF mutants**

In conclusion, it appeared evident that tempering the environment of the catalytic cysteines of our probe had adverse effects on the expected features (Figure 44). For that reason, we decided to proceed with the first mutant.

Interestingly, the team Yasuyoshi Sakai reported that they were unable to use the roGFPiL probe to monitor the redox state of the ER in HeLa cells. Since developing the mutated version of roGFPiL bearing four of the six SF mutations they successfully characterized the redox state of HeLa cells upon proteasome inhibition (Oku et al., 2021). Katja Becker and coworkers also used an SF mutation set to optimize a Grx1-roGFP2 probe that they used to monitor the redox state of the cytosol in *Plasmodium falciparum* parasites. In their case, the incorporation of the two SF mutations in position 206 and 145 did not cause adverse effects in excitation spectra. Maybe the absence of an insertion amino acid, the localization of the probe, as well as the use of a roGFP2 instead of a roGFP1, could explain why these mutations were not problematic (Schuh et al., 2018).

While our probe was ratiometric and more fluorescent, there was inconsistency in fluorescence intensities that can be attributed to transient transfection, which produced variable amounts of cells efficiently expressing the probe, as we saw on the images gathered thanks to the CX5 plate reader. Moreover, transient transfection imposes an additional time and resource-consuming step in cell culture. For these reasons, we generated a stable cell line that we now use consistently in the lab.

---

## DEFINING THE CONDITIONS OF ER GSH IMPORT

The second crucial feature was the definition of conditions of GSH import into the ER. This transport would be detected *via* reduction of the ER-localized SF Grx1-roGFPiE, and a deviation from this reduction would lead us to pre-select a molecule as a hit.

In the previously described paper, we recapitulated the observation that ER calcium leakage caused a consequent depletion of ER calcium store which resulted in a reductive shift in the endoplasmic reticulum, which corresponded to a 3-fold increase in  $[GSx]_{ER}$  compared to untreated cells. This confirmed that calcium depletion was accompanied by an elevation of the concentration, likely *via* import of GSH in the ER.

This observation led us to propose a dual system for the import of GSH, one that would equilibrate passively the levels of GSH between the cytosol and the ER, and one that would actively import GSH into the ER as an answer to calcium fluxes.

Importantly, as described in the first section of this chapter, the evaluation of the passive transport of glutathione towards the ER is met with challenges due to its dependency on the availability of cysteine. This dependency on the milieu was not replicated in the second GSH transport system, namely the one we observed upon Tg treatment. The calcium-dependent transport is all the more interesting, as it could be specific to mammalian cells, as calcium stores in lower eukaryotes such as yeasts are mainly vacuolar (Dunn, Gable, and Beeler, 1994).

For these reasons, we decided to conduct the screening in the conditions of GSH transport derived from Tg treatment.

---

## DEFINING THE SCREENING PROTOCOL

We determined previously that we would identify compounds blocking or potentiating the Tg-triggered ER reduction *via* fluorescence readout. Hence, a compound would be selected as a hit if the fluorescence profile upon Tg treatment differed from the fluorescence profile upon Tg treatment alongside the tested compound.

We first had to determine the optimal time and doses used for thapsigargin-elicited ER reduction. To do that, we treated cells with concentrations of thapsigargin ranging from 0.25 to 2  $\mu$ M and calculated the resulting  $E_{GSH}$  in the ER from fluorescence readings, performed every five minutes (300 seconds) for 30 minutes. Starting from a -212 mV, Tg addition resulted in a swift reduction, observed as early as 5 minutes post-treatment. Untreated cells remained at the same  $E_{GSH}$  value. Tg-dependant reduction kept going until reaching values around -225 mV after 1200 seconds, after which the  $E_{GSH}$  stayed stable. (Figure 45).

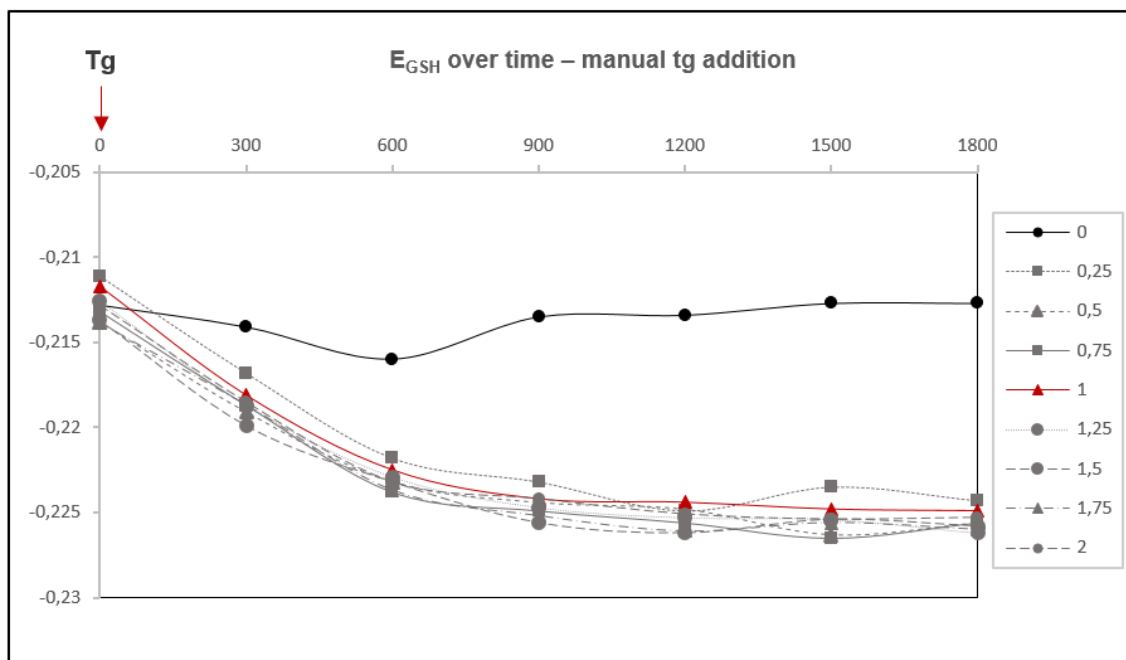


**Figure 45 – Reduction kinetics upon manual Tg treatment** iE SF cells were treated with thapsigargin ranging from 0.25 to 2 μM thapsigargin in HEPES buffer, and E<sub>GSH</sub> was calculated from fluorescence records every 5 minutes for 30 minutes

In parallel, we tested the automated addition feature of the plate reader that would be used for the screening. As we can see in **Figure 46**, the reduction we observed with manual addition is shifted 300 seconds later. The reason for this shift is the incompressible settling time before injection after the plate is introduced in the plate reader. The -225 mV reduction plateau was also observed 1200 seconds after thapsigargin treatment, but distinctly, a greater disparity in E<sub>GSH</sub> was observed. In particular, the redox potential of cells treated with quantities of Tg lower than 1 μM appeared to reach less reduced E<sub>GSH</sub> values.

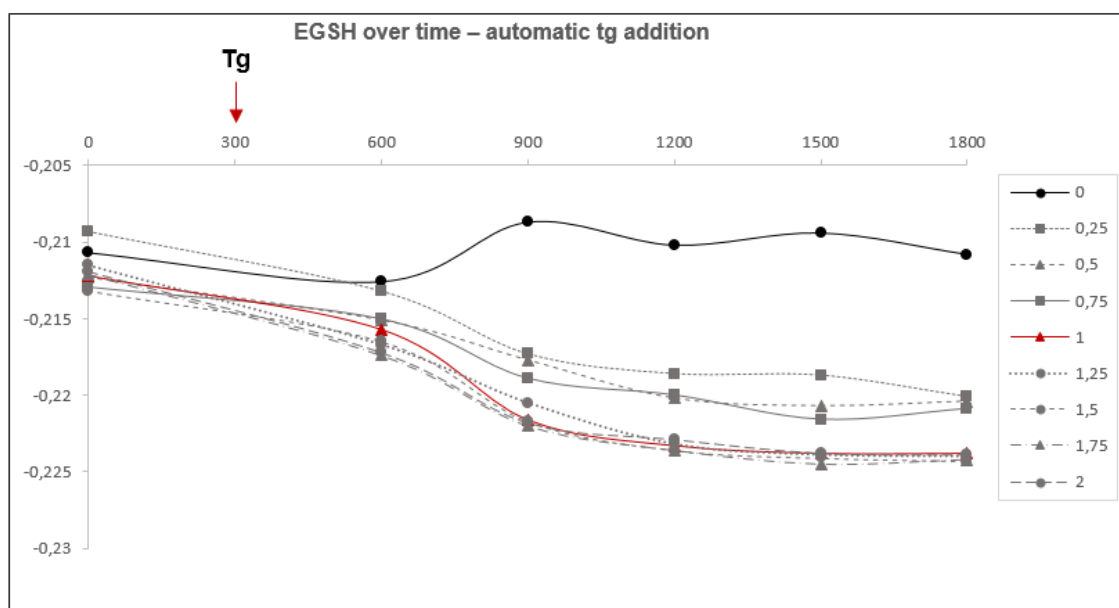


**Figure 46 - Reduction kinetics upon automated Tg treatment** iE SF cells were treated through a pump inside the plate reader with thapsigargin ranging from 0.25 to 2 μM thapsigargin in HEPES buffer, and E<sub>GSH</sub> was calculated from fluorescence records every 5 minutes for 30 minutes

These experiments showed that maximal sensor reduction was reached after 1200 s (20 minutes) of Tg exposure. We decided to treat cells for 30 minutes to ensure full reduction of the sensor. Additionally, we evaluated the possibility to add automation to the protocol by using the plate reader dispenser, but it showed an increase disparity in results as well as an incompressible settling time that could have hindered the possibility for us to scan a maximum of plates in screening rounds.

We then wanted to confirm the minimal dose of thapsigargin that would need to be used to achieve maximal reduction of the sensor after the selected 30 minutes of Tg treatment. We observed tested doses ranging from 0.75 to 2  $\mu\text{M}$  based on the reduction pattern observed during kinetic experiments. The four tested doses reached an  $E_{\text{GSH}}$  value of approximately -227 mV after 30 minutes of treatment.

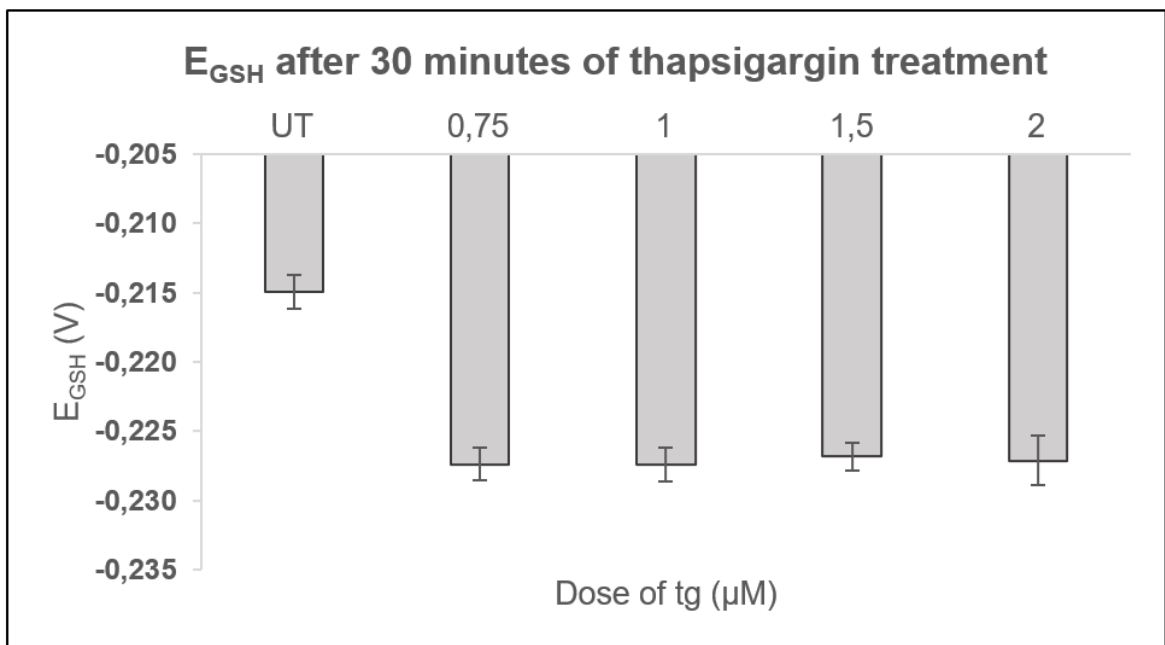


**Figure 47 – Influence on  $E_{\text{GSH}}$  in iE SF cells of a dose response treatment of thapsigargin.** iE SF cells were treated with thapsigargin ranging from 0.75 to 2  $\mu\text{M}$  thapsigargin in HEPES buffer, and  $E_{\text{GSH}}$  was calculated from fluorescence records after 30 minutes of incubation

These experiments allowed us to set up the last part of the screening: after being exposed to the chemicals, cells would be treated with 1  $\mu\text{M}$  of thapsigargin for 30 minutes, in order to detect chemicals capable of modulating the reduction profile of thapsigargin at that time point.

After having defined the two crucial features of the design of our HTS: the readout system, and the conditions that would trigger ER GSH reduction, we next needed to set up the entire timeline of molecule screening.

We took the option to pretreat cells during 30 minutes with the molecules before Tg treatment. This had two advantages. First, it gives time for the molecule to exert its potential effect. Second, we can evaluate the effect the molecule alone has on the fluorescence readouts, that is, whether the molecule has by itself an oxidizing or a reducing effect. A compound fluorescence control was also added onto probe-devoid cells, to deduce any autofluorescence (on top of that of our cells) to our measurement. Cells were then exposed to Tg along with the pre-incubated compound for another 30 minutes, as previously determined, and a second fluorescence record was made (Figure 48) to assess the effect of the molecule on Tg-induced ER reduction.

To simplify the workflow and because fluorescence readings are hampered by the DMEM high autofluorescence levels, all these steps have been performed in HEPES buffer. Cells were thus in HEPES buffer for a total of 1 hour with Tg treatment, which is an acceptable compromise in terms of time spent without physiological medium.

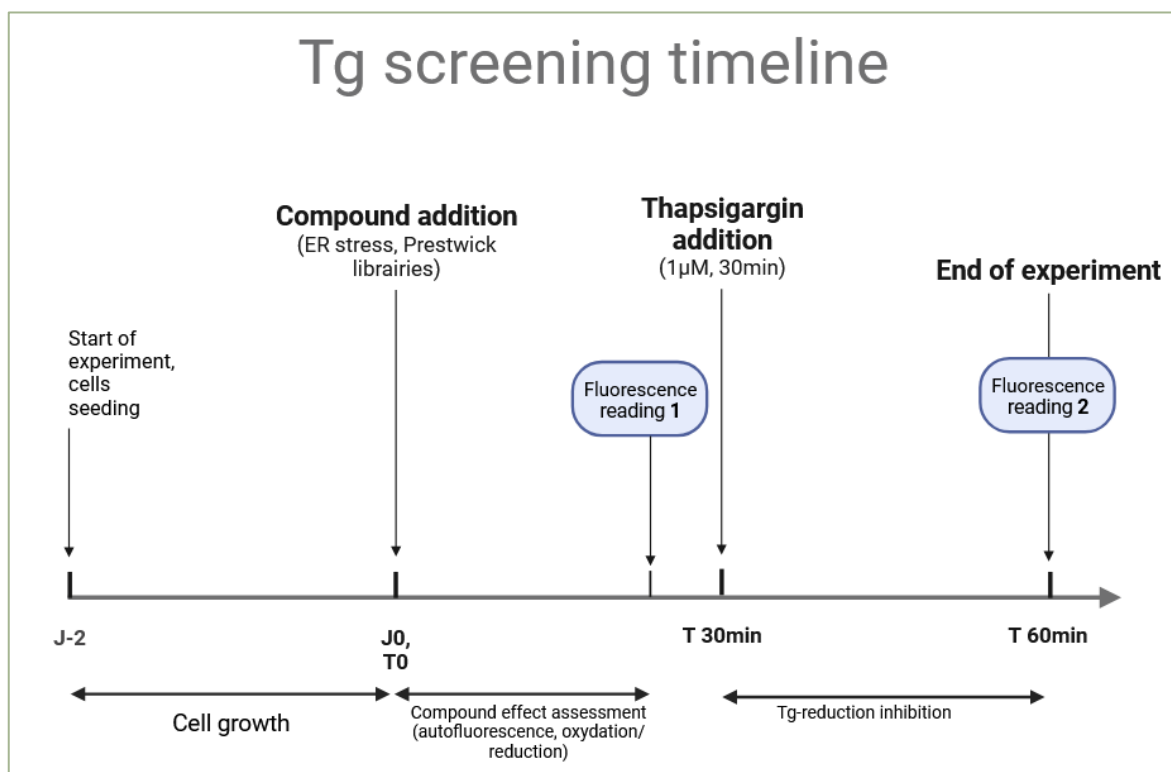


Figure 48 – Screening timeline

We selected two libraries to be tested. The first one was the TargetMol 155-compound library gathering chemicals with ER Stress related activities. This library was used for the first round of screening, and was tested two independent times. The second library we tested was the Prestwick repositioning library, a 1520-compound collection of off-patent drugs, mostly market-approved (FDA or EMA approved) with a set of information regarding activities, targets and mechanisms for each molecule. We arbitrarily fixed the concentrations of tested molecule at 20 µM, which is standard for active compound screening.

Hit selection was performed using the strictly standardized mean difference (SSMD), a statistical method that is considered more robust with high variability data than the usually used Z-score, as it accounts for sample size and standard deviation (see formula):

$$SSMD = \frac{mean_{compound} - mean_{control}}{\sqrt{SD_{compound}^2 - SD_{control}^2}}$$

We used the baseline of 2.5% of false positive rate to define a threshold of  $\pm 1.608$  for hit selection. We calculated two SSMD: SSMD 30 from the data collected after exposition to the compounds alone, then SSMD 60 from the data collected from the compounds with added Tg. A negative SSMD means a reductive shift compared to the control, while a positive SSMD means an oxidizing effect. At 30 minutes, we decided to exclude positive SSMD, as they meant that the molecule would have an oxidizing effect on its own. Negative SSMD at 30 minutes was a criterion to set aside molecules for another study, as they could be deemed thapsigargin-like. To search for candidate inhibitor of GSH ER influx, we thus focused on molecules with a SSMD 30 between the bounds of  $[-1.608; 1.608]$ , as it would guarantee that the molecule had no impact on  $E_{GSH}$  on its own. We next sorted these molecules by their effect on the Tg-elicited ER reduction. In the same way, a negative SSMD meant a potentiation effect of Tg reduction, while a positive SSMD meant an inhibition of Tg-elicited reduction

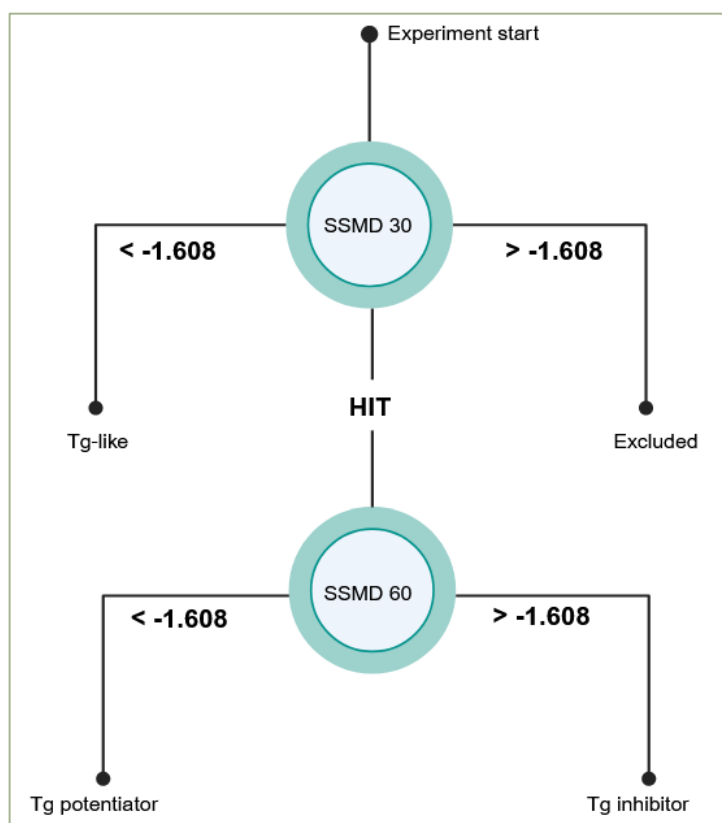


Figure 49 – Decision diagram for sorting chemicals by effect.

---

## B. RESULTS OF THE PRIMARY SCREENS

Our setup allowed the evaluation of 20 compound per plate, the TargetMol (“ER stress” library) could be tested two times, and the Prestwick library one time.

The SSMD at 30 and 60 minutes were gathered and used to filter the molecules based on the criteria defined above.

First, we described the results focusing on hits (hence, molecules with an SSMD at 30 minutes inside the defined boundaries [-1.608; 1.608]), either with an oxidizing effect after Tg (inhibitors), or a reducing effect after Tg (potentiators) (molecules with an SSMD at 60 minutes outside the defined boundaries [-1.608; 1.608]). Tg inhibitors were considered a hit of choice, since a Tg inhibitory compound could suggest the prevention of GSH import into the ER, although again, the use of our E<sub>GSH</sub> probe does not lead directly to an information on glutathione quantity in the ER

Other compounds with a base effect, set aside for other properties or excluded from the study will also be detailed.

---

### HITS WITHOUT BASE EFFECT

For the ER Stress library, out of the 155 molecules tested, and without any additional hit filtering, 51 molecules were extracted as hits, meaning that they had a significant effect on the thapsigargin reduction profile without significantly modifying the redox state in pretreated cells.

These 51 hits were identified when combining the two replicates of screening. Among these 51 compounds, 38 were from the first round, 30 for the second round, and 9 compounds were hits in both screening rounds (**Figure 50**).

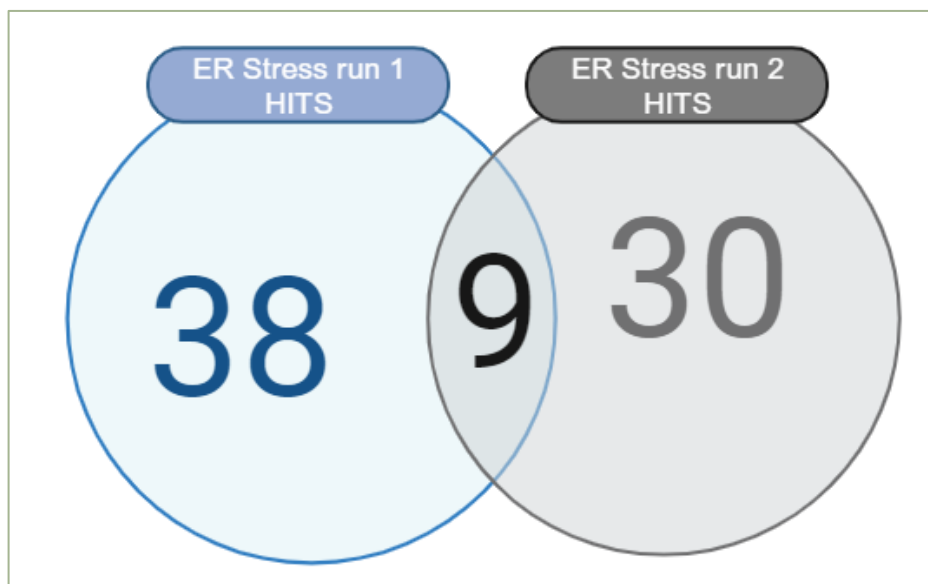


**Figure 50 – Common hits in both screening rounds**

For the 1520-compound Prestwick library, 414, meaning 27.2% of the library, had an SSMD at 60 minutes outside of the defined hit bounds of [-1.608;1.608] and were thus extracted. Among them, 306 chemicals had an SSMD 30 inside the [-1.608;1.608] bounds, and therefore, were extracted as hits. This amount accounted for 20% of the library.

For both libraries, the majority of the hits were Tg-inhibitors (had a positive SSMD at 60 minutes), and a minority were Tg-potentiators (had a negative SSMD at 60 minutes).

In the first round of ER Stress library screening, 3 of the 38 compounds were classified as possible Tg-potentiators, while the 35 remaining were rather Tg inhibitors

In the second round, 6 of the 30 hit compounds were Tg potentiators, and the remaining 24 were Tg inhibitors. Interestingly, in both screen rounds, Polyphyllin I had the second highest scoring SSMD, and the highest conserved score, meaning that this molecule was the most potent Tg inhibitor in the two screening rounds.

Out of the latter 306 hits from the Prestwick library, 34 were Tg potentiators, while 272 were Tg inhibitors.

Since 8 Tg inhibitors were the same molecules between round 1 and 2 of ER Stress screening, the screening resulted in the extraction of a maximum of 323 candidate inhibitors out of 1675 tested compounds. Likewise, 43 Tg potentiators were identified throughout the screenings.

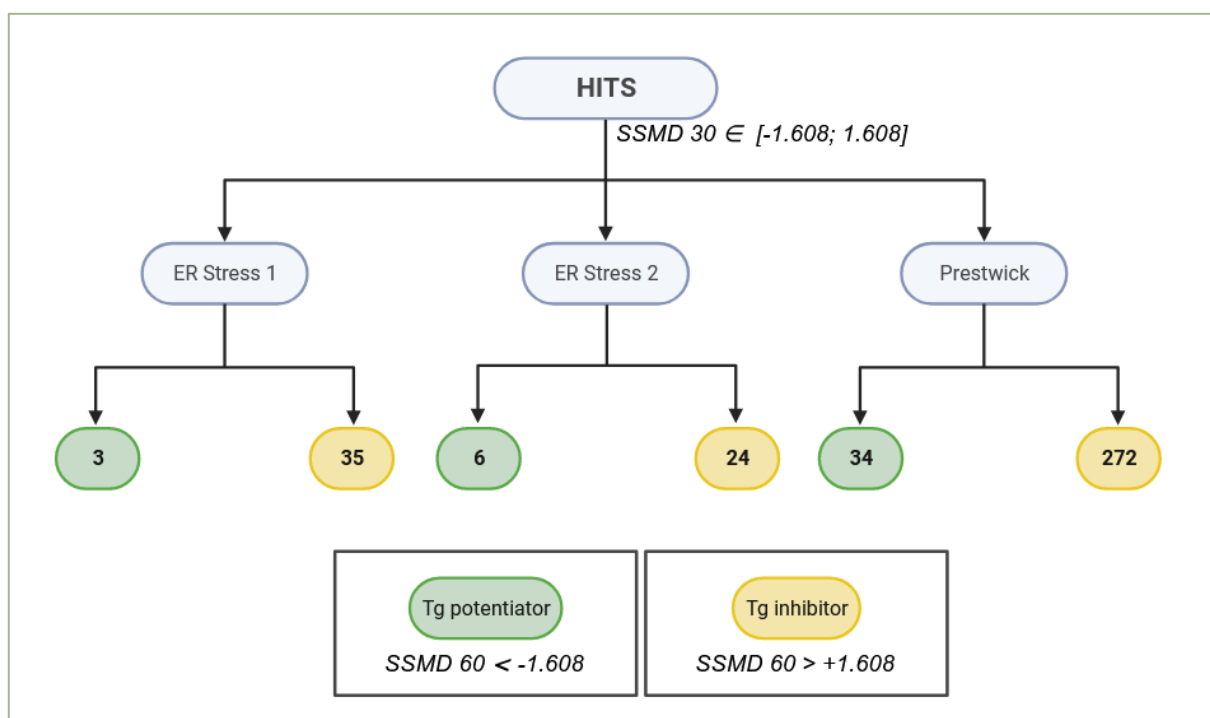
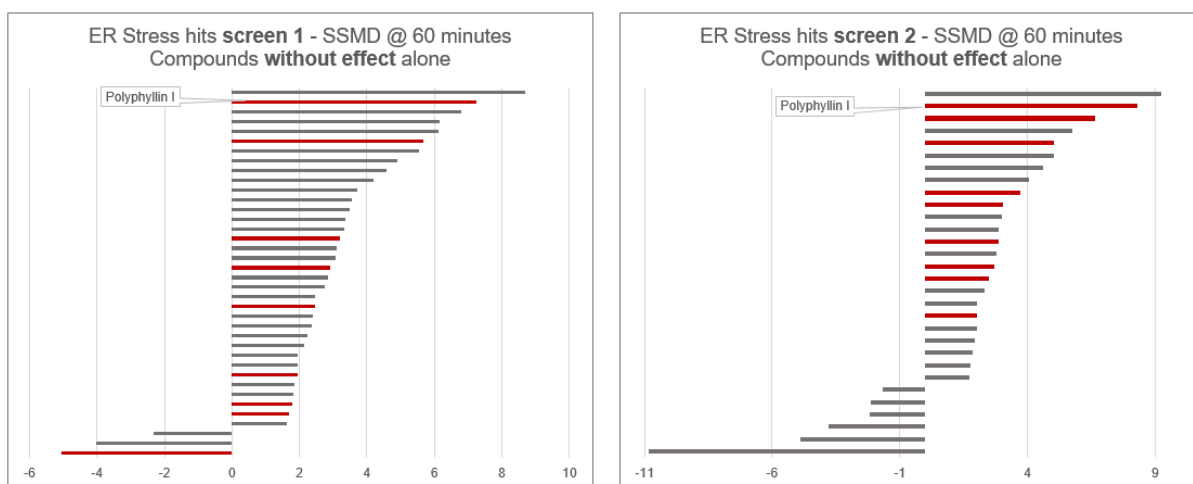
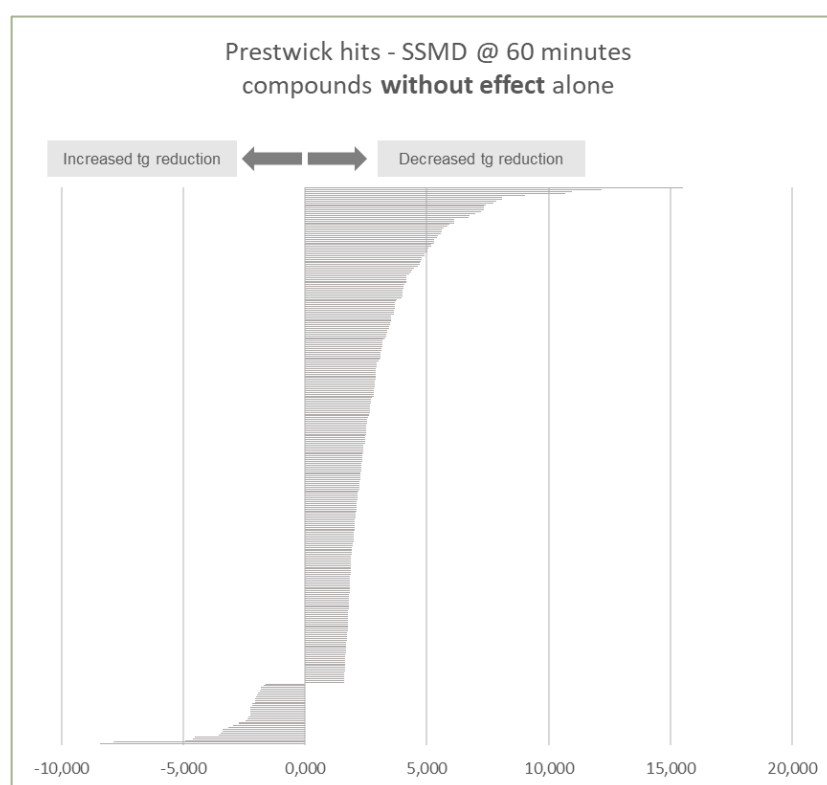


Figure 51 – Recap of the different kinds of hits



**Figure 52 – SSMD of ER Stress hits** Compounds were with no base effect were sorted based on their SSMD at 60 minutes. A positive SSMD signifies a Tg-inhibiting molecule, a negative SSMD represents a Tg potentiator. Red bars symbolize compounds that were hits in both screening replicates



**Figure 53 – SSMD of Prestwick hits** Compounds were with no base effect were sorted based on their SSMD at 60 minutes. A positive SSMD signifies a Tg-inhibiting molecule, a negative SSMD represents a Tg potentiator.

## COMPOUNDS WITH A BASE EFFECT: OXIDIZING MOLECULES

After ER Stress library screening, 21 compounds were excluded from hit selection because they had a positive, greater than 1.608, SSMD at 30 minutes. 15 compounds came from the first round of screening, and 14 from the second, and 8 were found in both of them.

In both screening replicates, all of the pre-oxidizing molecules but one also oxidized the redox potential readout upon Tg treatment (**Figure 54**).

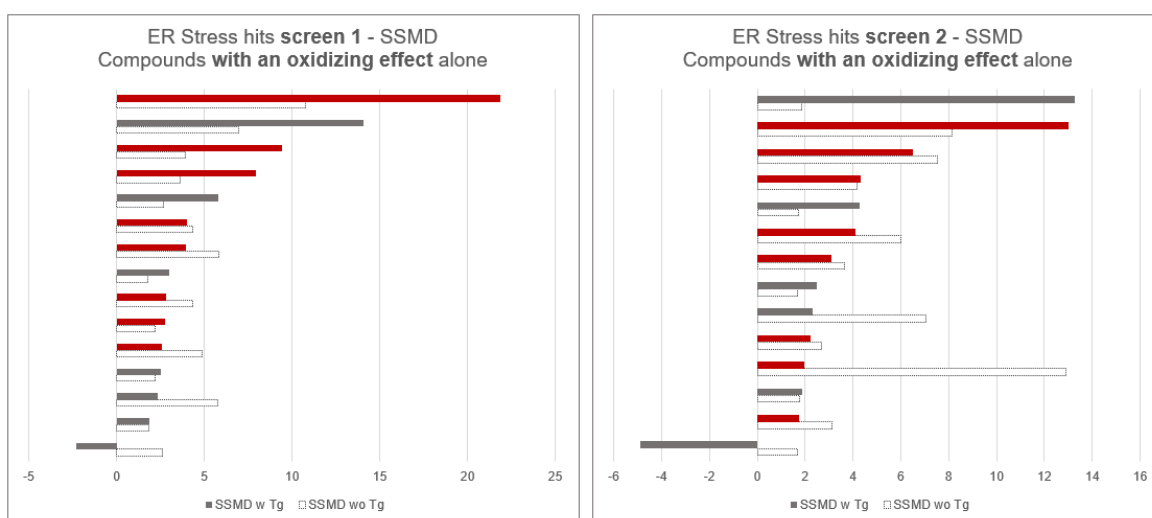


**Figure 54 – Most of ER Stress oxidizing molecules have a Tg inhibitory effect** Molecules with and SSMD at 30 minutes > 1.608 (white bars) were sorted based on their SSMD at 60 minutes (grey bars). Red bars symbolize compounds common in both screening replicates

Likewise, in the Prestwick library, 75 compounds had an oxidizing effect on the probe, and every compound but one was found to oxidize the Tg-induced readout as well, only ofloxacin oxidized the probe alone, while augmenting the Tg-induced reduction of the probe, as pointed out in **Figure 55**

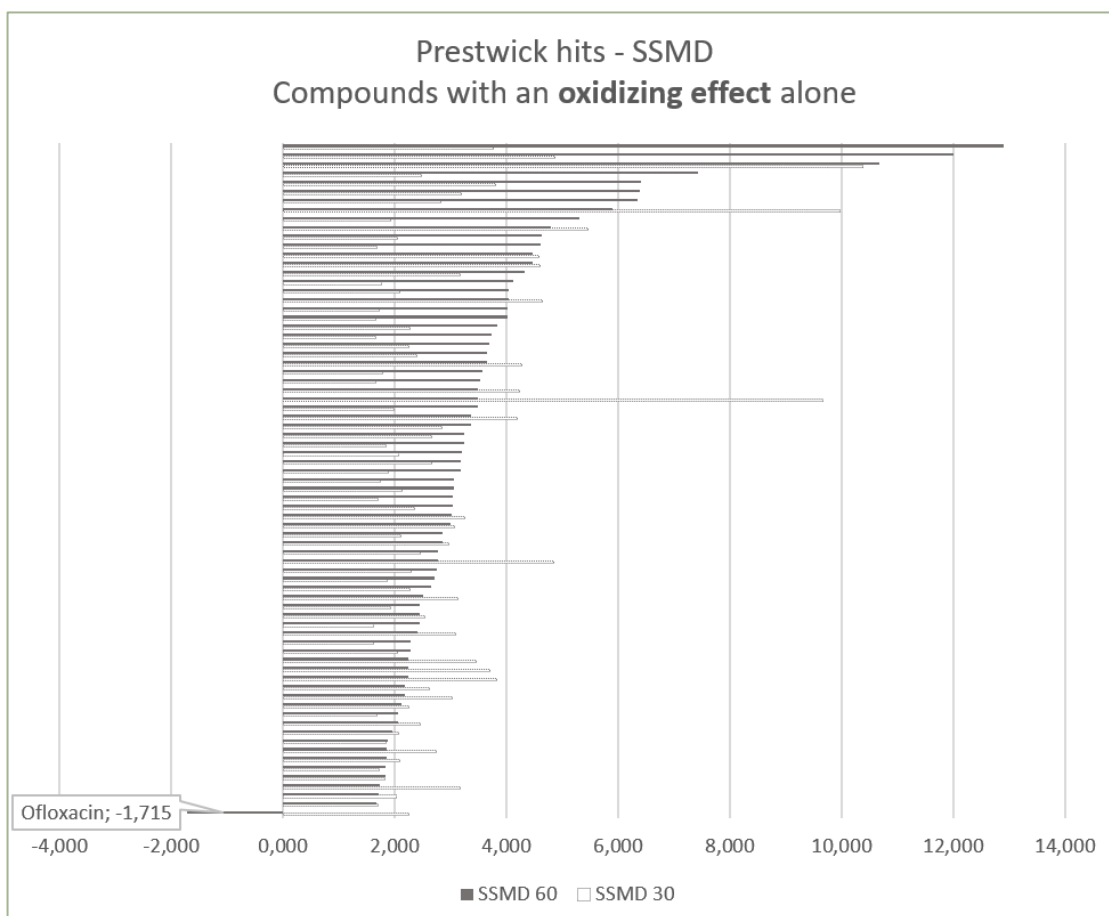


**Figure 55 – Most of Prestwick oxidizing molecules have a Tg inhibitory effect** Molecules with and SSMD at 30 minutes > 1.608 (white bars) were sorted based on their SSMD at 60 minutes (grey bars).

These results confirm the ambiguity for drawing conclusions: is the Tg-inhibitory property that we observe for the majority of molecules a result of pre-oxidation, or the effect we are looking for? For that complicating factor, these molecules were excluded from the analysis

## COMPOUNDS WITH A BASE EFFECT: REDUCING MOLECULES

Finally, 18 compounds throughout the two ER Stress screen rounds had a reducing effect alone, meaning an SSMD at 30 minutes below the -1.608 threshold, as represented by the white bars in **Figure 56**. 5 of those hits were present in both screening rounds (**Figure 56**, red).

These molecules were set aside as potentially “Tg-like” molecules. A reducing compound could either directly reduce the probe, or like thapsigargin, cause an influx of GSH into the ER, which triggers sensor reduction. We could also imagine an influx of cysteine, as we observed that the molecule was capable of reducing the sensor in whole cells.

Notably, most of the molecules that had a reducing effect on the sensor were Tg potentiators. All but 3 molecules in the first round of screening were.

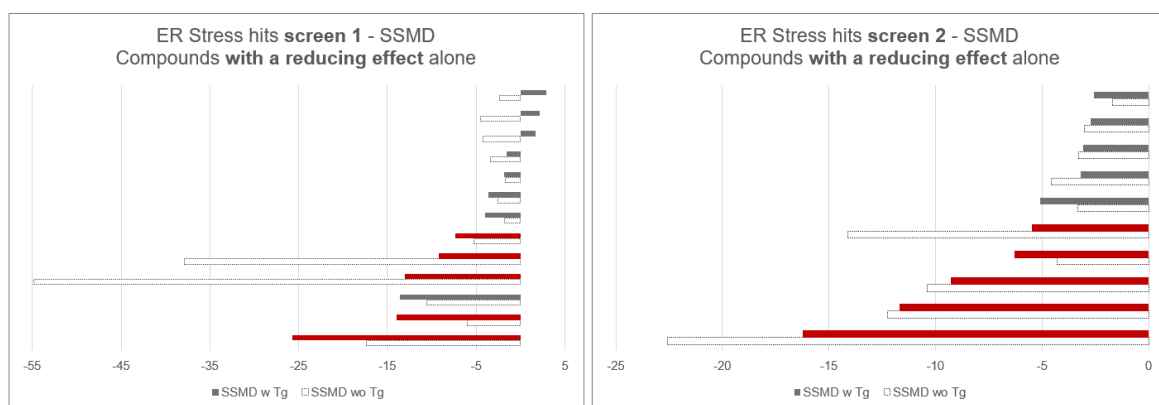


**Figure 56 – Most of ER Stress reducing molecules have a Tg potentiating effect** Molecules with and SSMD at 30 minutes < -1.608 (white bars) were sorted based on their SSMD at 60 minutes (grey bars). Red bars symbolize compounds common in both screening replicates

In the Prestwick library, 32 molecules had this sensor-reducing effect. Of the 32 pre-reducing compounds, 11 were Tg inhibitory, while the 21 were Tg potentiators (**Figure 57**).

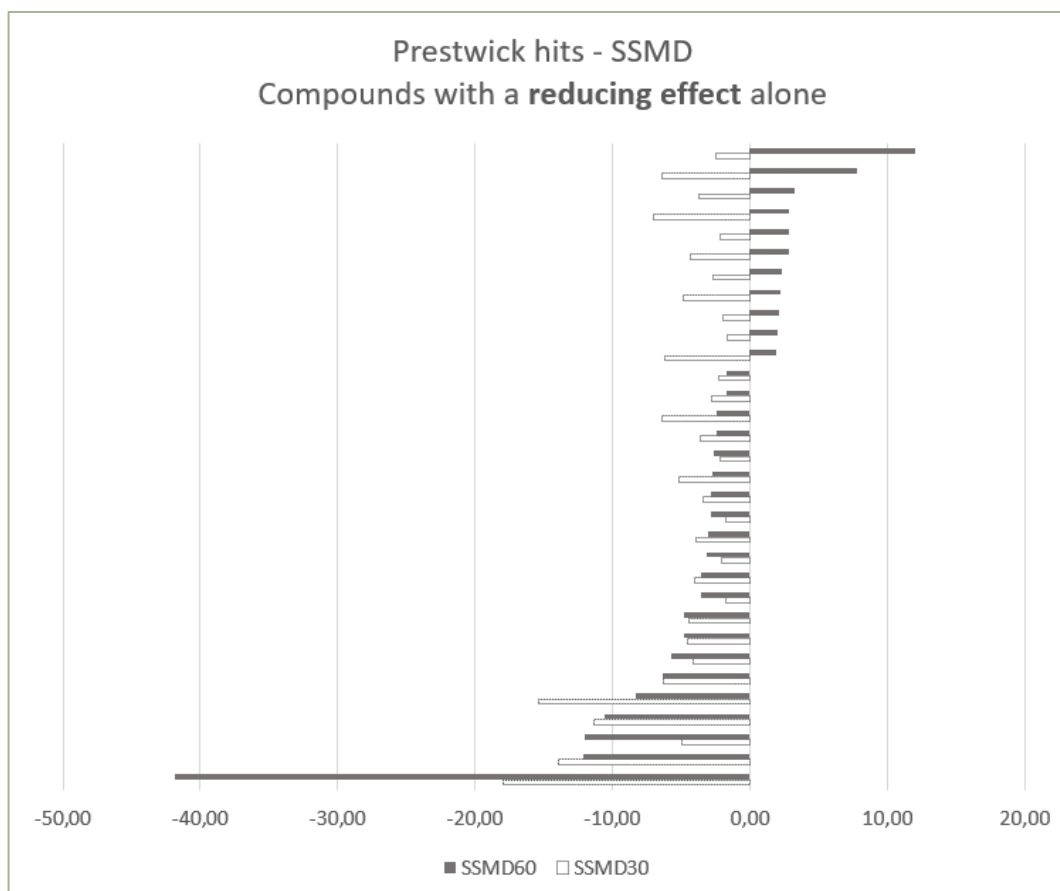


**Figure 57 – Most of Prestwick reducing molecules have a Tg potentiating effect** Molecules with and SSMD at 30 minutes  $< -1.608$  (white bars) were sorted based on their SSMD at 60 minutes (grey bars).

This set of molecules allowed us to extract compounds capable of reducing the ER on their own. This is an interesting feature as a molecule that provokes ER reduction could be due to a stimulation of GSH import. One final set of reducing molecules that could have an interest would be actual Tg-like molecules, meaning compounds that have a reducing effect on their own, but have none when added alongside Tg. This particular filtering does not appear on the aforementioned results, as they had no effect at 60 minutes. When we extracted those, we counted 18 compounds throughout the 3 libraries. Notably, Cyclosporin A was among the top scoring molecules. This molecule was in fact used by Lizak et. al as a Tg-like molecule in their experiments trying to characterize the reduction observed upon calcium depletion from the ER (Lizák et al., 2020).

In conclusion, two sets of distinct function molecules were extracted for further characterization: on the one hand, ideal hits, molecules with no effect alone on the sensor, and a Tg-inhibitory effect. 323 molecules were extracted for a possible further characterization. Additional hit filtering was added to prioritize hits based on their Tg-inhibition strength. Aside from compounds capable of potentially inhibiting GSH import, we reckoned that identifying molecules capable of stimulating its entry might be interesting as well. As a result, 68 compounds with a reducing effect on the probe were identified. Some of these compounds had a Tg-potentiating effect, which could be due to an addition of the effects of both the molecule's stimuli causing ER reduction, and that of Tg. Among the 68 ER-reducing compounds, 18 were categorized as strict Tg-like as they had no impact on Tg-elicited sensor reduction. .

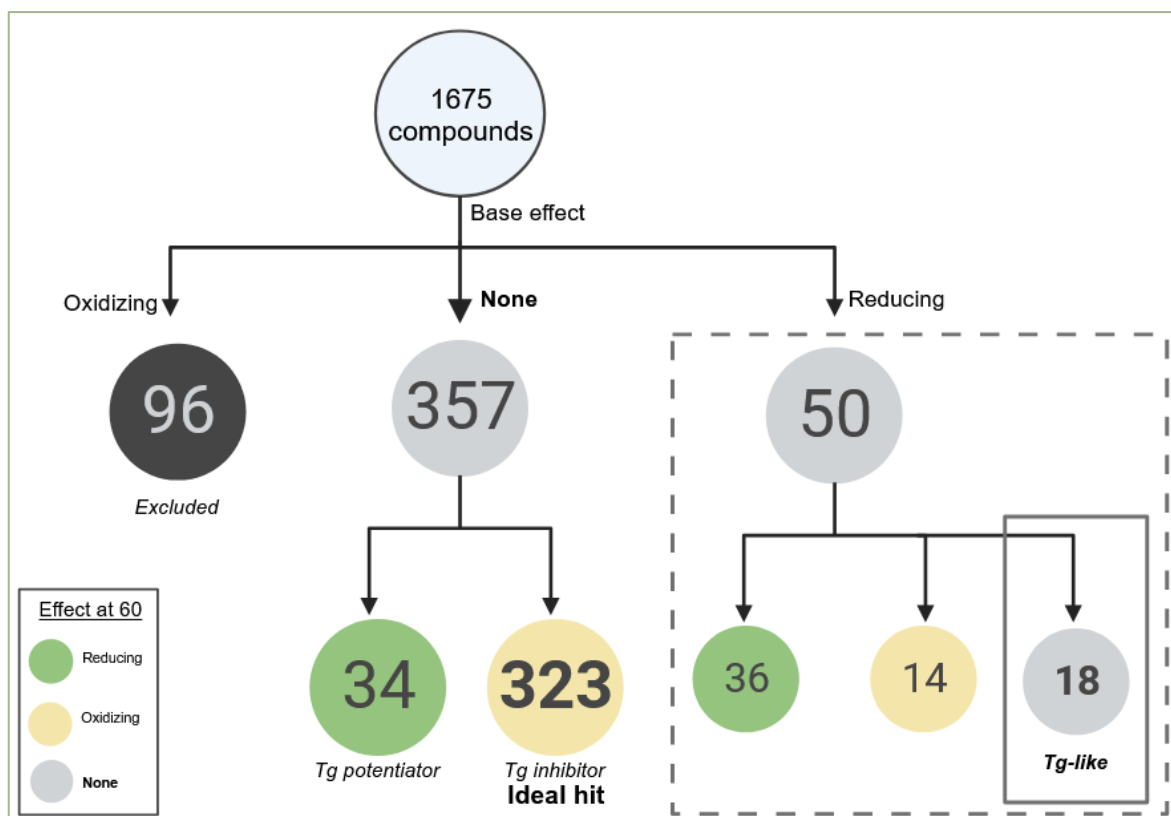


Figure 58 – Recap of all screens hit filtering

---

### C. SECONDARY SCREEN – FUNCTIONAL CHARACTERIZATION

After performing screening experiments and extracting hits, our goal was to characterize further the most promising molecules in multiple aspects. As it was pointed out in the design of the screening protocol, we accepted the approximation of using  $E_{\text{GSH}}$  as a proxy for glutathione influx into the ER, but once again,  $E_{\text{GSH}}$  variation could be the result of ER [GSx] variation, a result of a modification of the [GSH]/[GSSG] ratio, and is also a function of calcium fluxes, all of which must be characterized.

Multiple validations had to be made on molecules extracted from the first screening protocol:

First, the results of the primary screen had to be replicated. We wanted to confirm the effect of the molecule on  $E_{\text{GSH}}$  value with and without thapsigargin. In this step, complementary controls were added, and the screen dose of 20  $\mu\text{M}$  was completed with 3 other ones, to assess a dose effect and determine the quantity that yielded optimal results.

Then, if the effect was confirmed, a time dependency was investigated, by following  $E_{\text{GSH}}$  of cells treated cells with the optimal dose(s) determined prior. These steps are essential as they will provide us with time and doses for the following functional characterization of the effect of the molecule.

After, with the predetermined doses and times of hit molecule, a critical step was to determine if there is a connection between the modification of  $E_{\text{GSH}}$  and the quantity of ER [GSx]. For that, the previously described ER localized Grx1-1cys had to be used to determine the variations of ER [GSx] during treatments with the molecule.

Finally, the last step was to assess the effect of the molecule on calcium fluxes. A potential experimental source of false positives would be if the molecule decreased the efficacy of thapsigargin on calcium leakage. If calcium fluxes are hindered and GSH entry is a function of calcium exit from the ER, then the molecule would indeed stop GSH entry, but not by the means of tempering with a transport system, which was our intention.

These investigations are still underway and were entirely led by Gwenaëlle Le Pavec and Clément Djezvedjian as part of his master's internship, and the characterization of one molecule that was part of his project will be described as an example. The molecule that will be discussed is Polyphyllin I (PLP I), a compound from the ER Stress library, as it had features of what we interpreted as an "ideal" hit. The molecule was detected as a hit in both replicates of the ER stress library screening. It had no significant effect alone on the  $E_{\text{GSH}}$  prior Tg treatment but prevented Tg-induced ER reduction.

## DOSE RESPONSE AND KINETICS CHARACTERIZATIONS OF PLP I

The first objective was to confirm that PLPI indeed inhibited the Tg-dependent ER reduction. To do so, we repeated the experiment in the conditions used for the screen, and performed both dose response and kinetics experiments to determine optimal inhibitory conditions

During the primary screen, molecules were tested at concentrations of 20 $\mu$ M. We decided to study the molecule at higher and lower doses to evaluate the minimal dose required for maximal effect. Clément therefore compared the fluorescence of the SF probe upon treatment with increasing doses of PLPI, ranging from 5 $\mu$ M to 40 $\mu$ M. We replicated the timeline used for the screening, with 30 minutes of compound exposure time, followed by 30 minutes of thapsigargin addition. On this setup, we also added 60 minutes of exposure to the compound alone for a more thorough comparison of PLPI effect.

Just as for the screening, we represented the readout as a ratio of the average fluorescence at 395 over 460nm. As mentioned above, the ratio could be used in conditions where DTT and diamide were harder to control, but are to be interpreted the same way as  $E_{GSH}$ : an increase in average ratio signs a sensor oxidation, while a decrease in average ratio is due to sensor reduction.

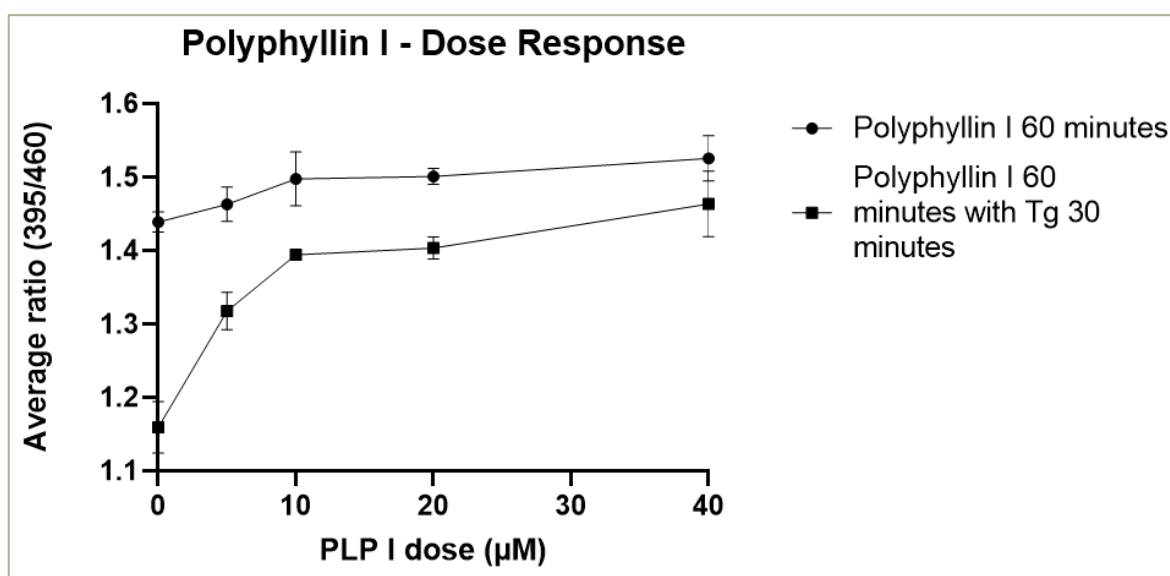


**Figure 59 – Polyphyllin I suppresses Tg-elicited ER reduction in a dose-dependent way.**

Average ratio of fluorescence resulting from excitations at 395/460 nm in iE SF cells was measured upon treatment with thapsigargin for 30 minutes along with 5, 10, 20 or 40  $\mu$ M of PLP I exposure.

N=3 biological replicate, error bars represent standard deviation, and are absent when the bar is smaller than the symbols.

Figure 59 above represents three independent dose-response experiments.

The addition of thapsigargin for 30 minutes caused a substantial reductive shift, from the starting 1.44 average ratio to a lower 1.16 average ratio. Exposure to PLP I for 30 minutes led to the dose-dependent alleviation of that reductive shift. At 5 $\mu$ M PLP I added, the ratio went from 1.16 to 1.31. The maximum was reached at 40 $\mu$ M PLP I added with a ratio of 1.46, although, when taking the standard deviation into account, it seems that a plateau in terms of effect was reached at 10 $\mu$ M of PLP I added, with an average ratio of 1.39.

We can see that untreated cells had a starting average ratio of 1.44. We observed a slight, dose dependent increase of this ratio upon PLP I treatment. An average ratio of 1.50 was reached for cells treated with 20 $\mu$ M PLP I, and the maximum of 1.52 was attained at the maximum dose of 40 $\mu$ M of PLP I added. This suggests that PLP I is capable of oxidizing the sensor on its own, a feature which was not observed during the initial screening procedure, where the compound effect was only monitored for 30 minutes.

After determining the minimal dose of PLP I to be used for maximal effect, Clément evaluated the kinetics of oxidation state of the probe upon PLP I treatment, with the same purpose of finding an ideal incubation time for further characterizations.

The priority doses were 10  $\mu$ M and a comparative 5  $\mu$ M dose based on the dose response experiments. Fluorescence was collected after 5, 15, 30 and 60 minutes of exposure to either PLP I followed by the addition of either 1  $\mu$ M of thapsigargin or medium only, for 30 minutes. (Note that in this set up, PLP I was incubated up until 60 minutes prior to thapsigargin incubation, resulting in a 90 minutes total treatment. For comparison with screening conditions, the condition to be considered should be the 30-minute treatment.)

Two independent experiments were performed to study the kinetics of 5  $\mu$ M PLP I addition on our fluorescence readout. Three were performed for the 10  $\mu$ M dose, and one additional experiment was carried out at the 20  $\mu$ M dose. The results of these experiments are gathered in **Figure 60**.

At 5  $\mu$ M, no significant effect could be determined on the kinetics of PLP I addition on Tg-driven reduction of the sensor. This was surprising, because a significant effect on the reduction profile could be observed in the previous dose-response experiment.

We can also note a slight increase of the average ratio upon treatment with PLP I alone, from 1.42 to 1.50, again speaking for an oxidizing effect of PLPI alone.

At 10  $\mu$ M, we can see that a short pre-incubation time of PLP I for 5 minutes followed by 30 minutes of Tg treatment was sufficient to cause an oxidation of the sensor, hence, inhibits Tg-elicited reduction. Maximal oxidation was attained after 1 hour, where the ratio raised from the starting 1.4 ratio to a more oxidized 1.14 ratio. This effect, does show a time-dependency, but we can see that error bars are quite high.

Notably, the average ratio of cells treated with PLP I increased from 1.42 to 1.56 over the course of the 60-minute experiment. This result verified again that PLP I oxidized the sensor on its own.

Clément performed an additional kinetics experiment with a 20 $\mu$ M dose of PLP I. The same basal oxidation was observed upon PLP I exposure, this time from 1.38 to 1.65. Likewise, the addition of PLP I to 30 minutes of thapsigargin led to an oxidation, from a 1.09 average ratio, to a 1.51 one. These results gathered in **Figure 60 C** are to be interpreted carefully, as they represent a single experiment.

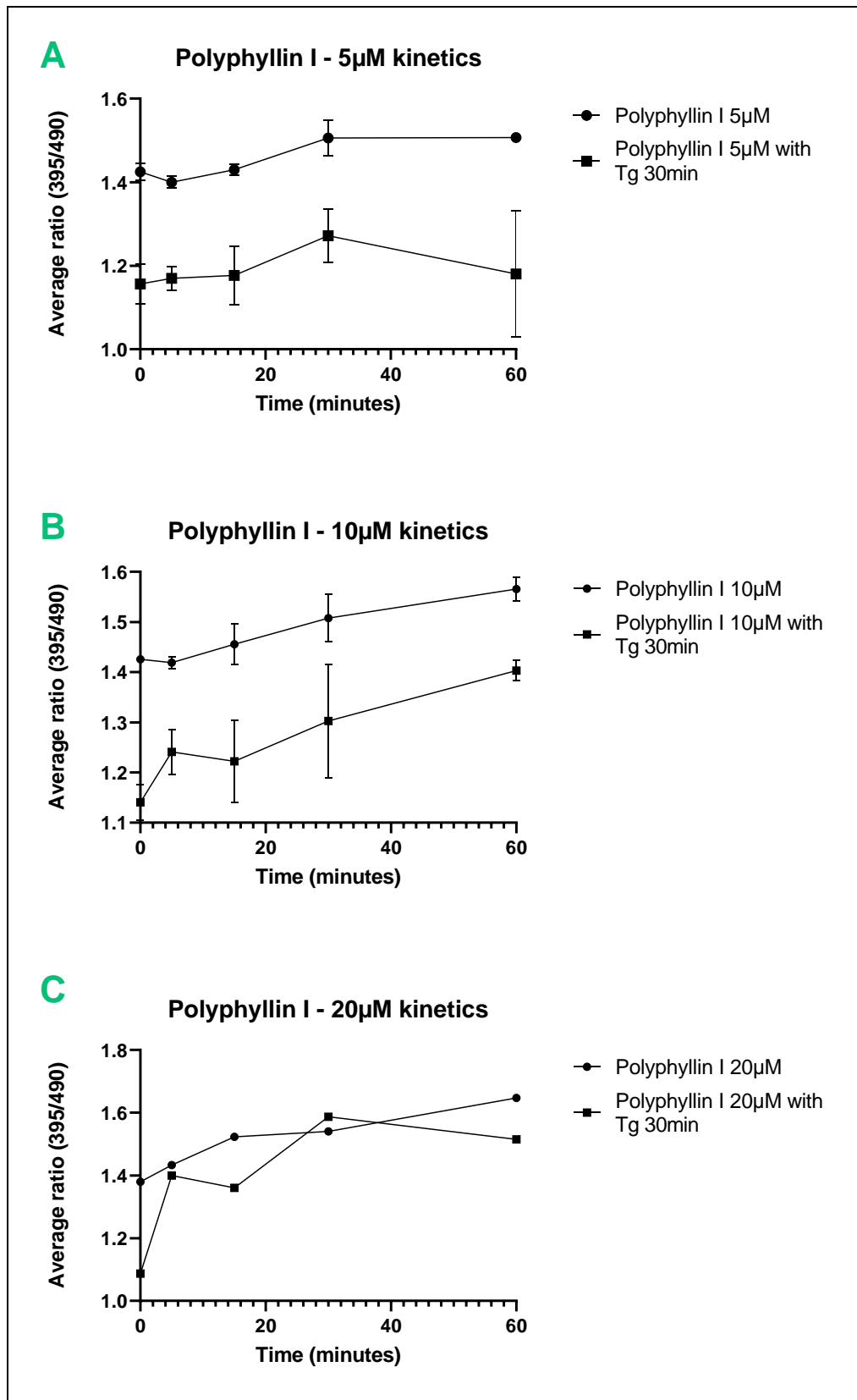


**Figure 60 – Time dependency of Polyphyllin I treatment** Average ratio of fluorescence resulting from excitations at 395/460 nm in iE SF cells was measured upon treatment with thapsigargin for 30 minutes along with 5, 15, 30 or 60 minutes of PLP I **(A)** 5  $\mu$ M, N=2 biological replicates, **(B)** 10  $\mu$ M, N=3 biological replicates, **(C)** 20  $\mu$ M, N=1 biological replicate. Error bars represent standard deviation, and are absent when the bar is smaller than the symbols.

In conclusion, dose response experiments allowed us to define an ideal 10  $\mu\text{M}$  PLP I concentration for further evaluation, as it is the dose from which sensor oxidation seemed to plateau. For kinetics, while results were less significant, we selected the 30-minute time point for further experiments, since it was a good compromise between significance and sensor oxidation by PLP I.

Indeed, we observed an oxidation of the sensor that was dependent on the dose of PLP I added, but that observation was mirrored in Tg-treated cells and also in non-treated cells. This sensor oxidation was observed in kinetics and dose-response experiments, which hinders our interpretations, as the alleviation of sensor reduction upon Tg treatment could be the result of that oxidation by PLP I, and not an inhibition of GSH entry as we expect to see. Alternatively, PLPI could decrease the basal turnover of GSH ER transport, thereby leading to ER oxidation. For that reason, ER [GSx] quantification became important to conduct.

---

### GLUTATHIONE QUANTIFICATIONS

After studying the dose and kinetics responses of the GFP probe, it became clear that while there was a sensor oxidation when PLP I was added to cells alongside thapsigargin, PLP I itself also caused an oxidation. Our question therefore became: does PLP I inhibit the glutathione entry into the ER that is observed after Tg treatment, or does it oxidize the sensor prior, which compensates its reduction upon Tg treatment?

To answer this question, Clément evaluated the intralumenal quantities of glutathione with the use of the Grx1-1cys probe, as described earlier. After transient transfection with ER localized, HA-tagged Grx1-1cys, cells were treated with 5 and 10  $\mu\text{M}$  of PLP I for 30 minutes, then for an additional 30 more minutes with or without thapsigargin (**Figure 61**).

The  $[\text{GSH}]^2 / [\text{GSSG}]$  ratio that could be calculated from the fluorescence measurement of the GFP probe as described in the previous section, was combined with the  $[\text{GSH}] / [\text{GSSG}]$  ratio that can be deduced from western blot quantification of reduced and oxidized ER Grx1-1cys (**Figure 61**)

Two experiments were performed for the quantification of ER [GSX] upon treatment with 5  $\mu\text{M}$  of PLP I, and three experiments were done upon treatment with 10  $\mu\text{M}$  of PLP I.

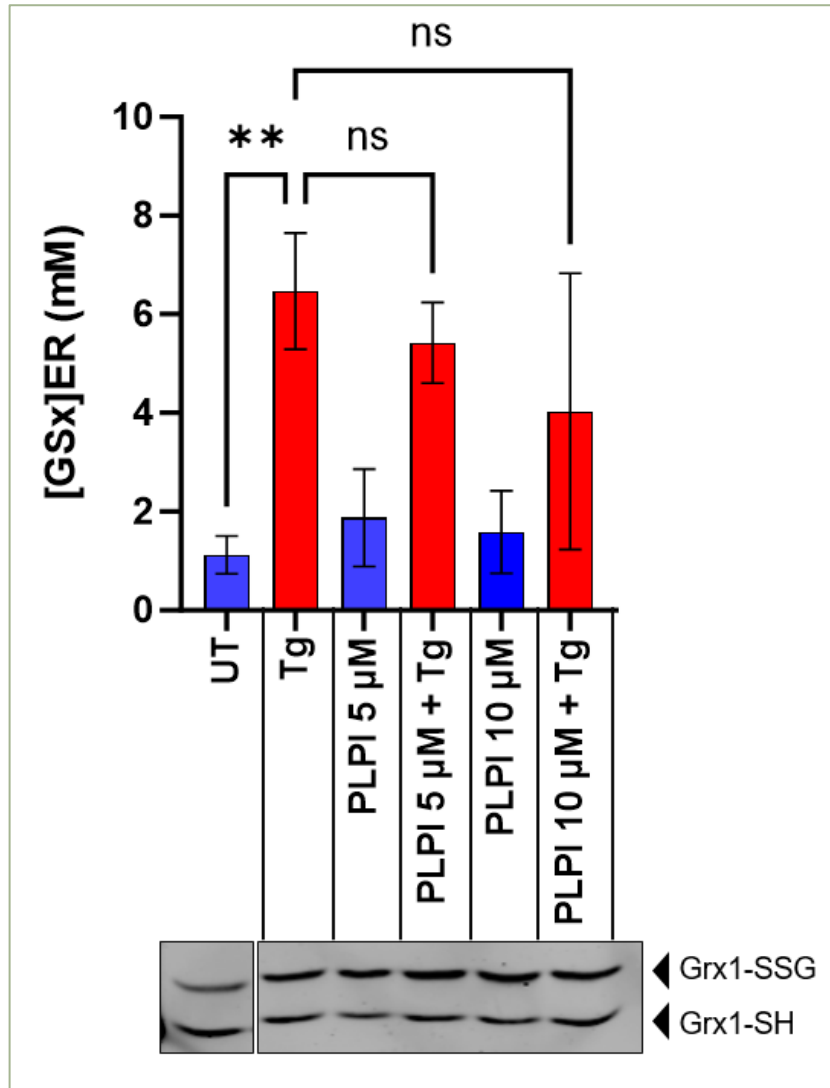


**Figure 61 – Impact of PLP I treatment on Tg-driven ER GSH entry** HEK293 cells, transfected with an ER-localized version of HA-Grx1-1cys, were left untreated (UT) or treated with the indicated and/or polyphyllin I (PLP I) doses for 30 minutes then with or without thapsigargin (Tg) for 30 minutes. The glutathionylated/unglutathionylated ratio of the Grx1-1cys probe (-SSG/-SH) was monitored after immediate blocking of the reduced thiols with iodo-acetamide, followed by an HA immunoprecipitation, then reduction and alkylation of the originally oxidized thiols with 2 kDa PEG-maleimide. Cell treatments with DTT or diamide were used as respective controls for determining the fully unglutathionylated (Grx1-SH) and glutathionylated (Grx1-SSG) forms of the ER Grx1-1cys probe. The -SH/-SSG ratio of the Grx1-1cys probe, obtained for each experimental conditions, were quantified by densitometry after SDS-PAGE. This ratio is directly proportional to the GSH/GSSG ratio. N=2 for 5 μM experiments and N=3 for 10 μM experiments. One of these experiments is shown. The total concentration of GSH inside the ER ( $[GSx]_{ER} = [GSH]_{ER} + 2[GSSG]_{ER}$ ) was deduced for each experimental condition, according to the following equation:  $[GSx]_{ER} = X_{ER} * (1/Y_{ER} + 2/Y_{ER}^2)$ , where  $X_{ER} = [GSH]^2/[GSSG]$  is calculated based on the ER  $E_{GSH}$  measurement determined prior, and  $Y_{ER} = [GSH]/[GSSG]$  is determined from the glutathionylation state of the ER Grx1-1cys probe showed under.

We can observe on Western Blot traces that thapsigargin, but also PLP I, cause a decrease of the [GSH]/[GSSG] ratio. Indeed, in the depicted Western Blot, the untreated conditions show a 33% oxidation of the sensor. This value goes up to around 55% in Tg-treated cells, and around 65% in PLP I treated cells. While this ratio informs us of a more oxidative balance of the redox couple, it does not allow us to conclude on ER [GSx] levels on its own.

To do so, those results were combined to the previously determined  $E_{\text{GSH}}$  values. We renewed the observation that thapsigargin significantly increased glutathione quantity in the ER. PLP I addition on cells did not cause any significant change in ER [GSX] levels. When PLP I was added alongside Tg, those levels seemed to go down at the dose of 5  $\mu\text{M}$ , and that decrease was even more pronounced at 10  $\mu\text{M}$ . However, we can see that the measurement uncertainty is substantial and precludes us to confirm that PLP I addition inhibits glutathione entry in the ER after Tg treatment. Those experiments were still exploratory and several leads for improvement are still available.

---

## CALCIUM FLUXES EXPERIMENTS

The inhibition of Tg-driven reduction of the ER can be explained by several mechanisms. Either the molecule inhibits GSH entering the ER, or the molecule has a role on calcium depletion caused by thapsigargin, which in turn has an incidence on GSH fluxes. The goal of the screening was to identify a molecule with the former mechanism so for this reason, a protocol should be established to verify ER [GSx] levels, but also one to verify ER calcium levels.

Another ratiometric fluorescent probe, ER localized GEM-CEPIA, was used for microscopy quantification of ER calcium levels. The first exploratory experiments were performed by Clément, with the help of PhD student Ilaria Pontisso from the I2BC lab *Calcium Signaling and Microbial Infections*.

In this setup, the probe GEM-CEPIA is a transiently expressed, ER-localized probe, ratiometric in emission, contrary to our redox probe that is ratiometric in excitation. The emission collected at 480 and 535 nm results from a single excitation at 380 nm and the 480nm/535nm ratio varies as a function of ER Ca<sup>2+</sup> levels. The ER calcium levels are expressed in percentage, with the 0% value being determined from the ratio of cells treated with EGTA, a calcium chelator, and the 100% value is determined from the emission ratio in calcium replenished cells thanks to treatment with ionomycin, a calcium ionophore, and Ca<sup>2+</sup>.

To determine the impact of PLPI on ER calcium efflux, cells were first pre-incubated with 5 or 10 µM of PLP I for 30 minutes, then switched to imaging medium where the probe fluorescence was recorded before and after addition of Tg. Two protocols have been used: one where the PLPI is removed while Tg treatment is implemented and another one where PLPI is kept together with Tg in the imaging medium. As seen in the control lanes, Tg treatment is expected to induce a decrease of the probe ratio to reach a plateau. EGTA is then added to cells, to determine if ER calcium stores have effectively been depleted by Tg treatment and to determine the 0% calcium boundary. A calcium treatment is then performed to increase calcium content until an ultimate plateau is reached, defining the 100% values.

Results where PLP I was washed before thapsigargin addition are represented in **Figure 62** (top panel). Upon Tg treatment, luminal calcium dropped rapidly, with a comparable speed in both PLPI treated and untreated cells. Intriguingly, we observed that, while control cells had a calcium content of 55%, PLP I 5  $\mu$ M and 10  $\mu$ M treated cells had 70% and 75% calcium content respectively. Note that calcium repletion kinetics cannot be compared in **Figure 62** because calcium addition is not synchronized on the figure. On the bottom panel representing synchronized repletion kinetics, we see that untreated cells have a 10-minute lag before calcium repletion occurs. In contrast, the PLP I 5  $\mu$ M treated cells show a 5-minute lag before calcium starts re-entering the ER, and the 10  $\mu$ M treated cells show no visible lag.

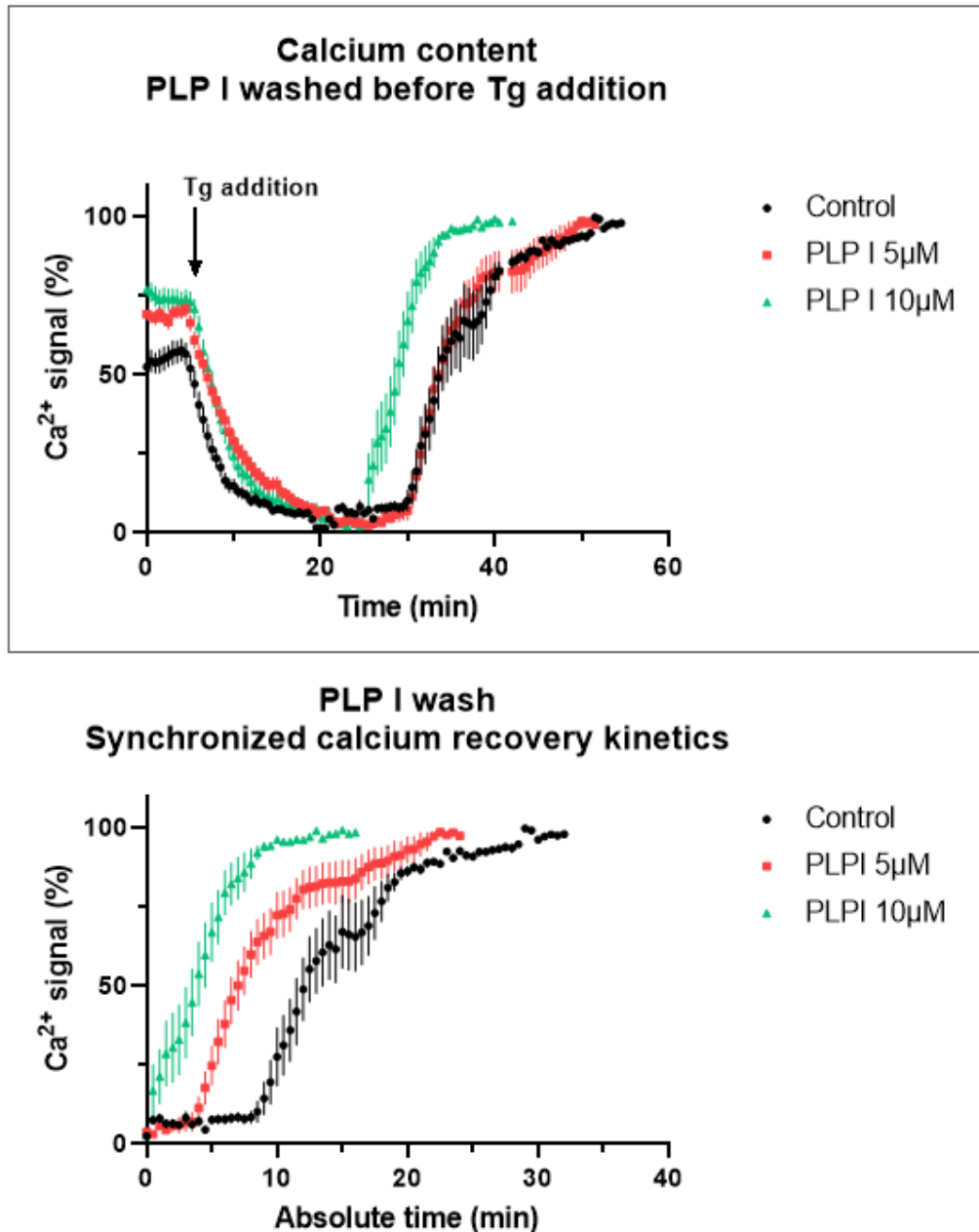


**Figure 62 – PLP I treatment increases ER calcium content and decreases ER repletion kinetics** Cells expressing ER localized GEM-CEPIA were treated with PLP I for 30 minutes prior to recording, then washed. Emissions at 480 nm and 535 nm were recorded, and after recording started, 1  $\mu$ M thapsigargin was added

In the second case, PLP I was not washed before thapsigargin addition, which is the closest condition to that of the screening and our previous experiments with PLP I (Figure 63). We observed that, while control cells had a calcium content of 55%, 5  $\mu$ M PLP I incubation for 30 minutes without wash before starting to record brought calcium levels to 75%. Increasing pretreatment to 10  $\mu$ M PLP I for 30 minutes brought these levels at the maximum value of 100%, which is defined by complete calcium saturation of the probe. Strikingly, when Tg was added on non-washed treated cells, so in the presence of PLP I, calcium depletion occurred at a slower rate. As a result, the calcium content after Tg treatment in 5  $\mu$ M PLP I treated cells was 18%, and that of 10  $\mu$ M treated cells was 27%.

After depleting the remainder of calcium stores with EGTA, calcium was once again replenished. We can see on the bottom panel that the 10-minute lag that occurs before calcium repletion in control cells is completely absent in treated cells.

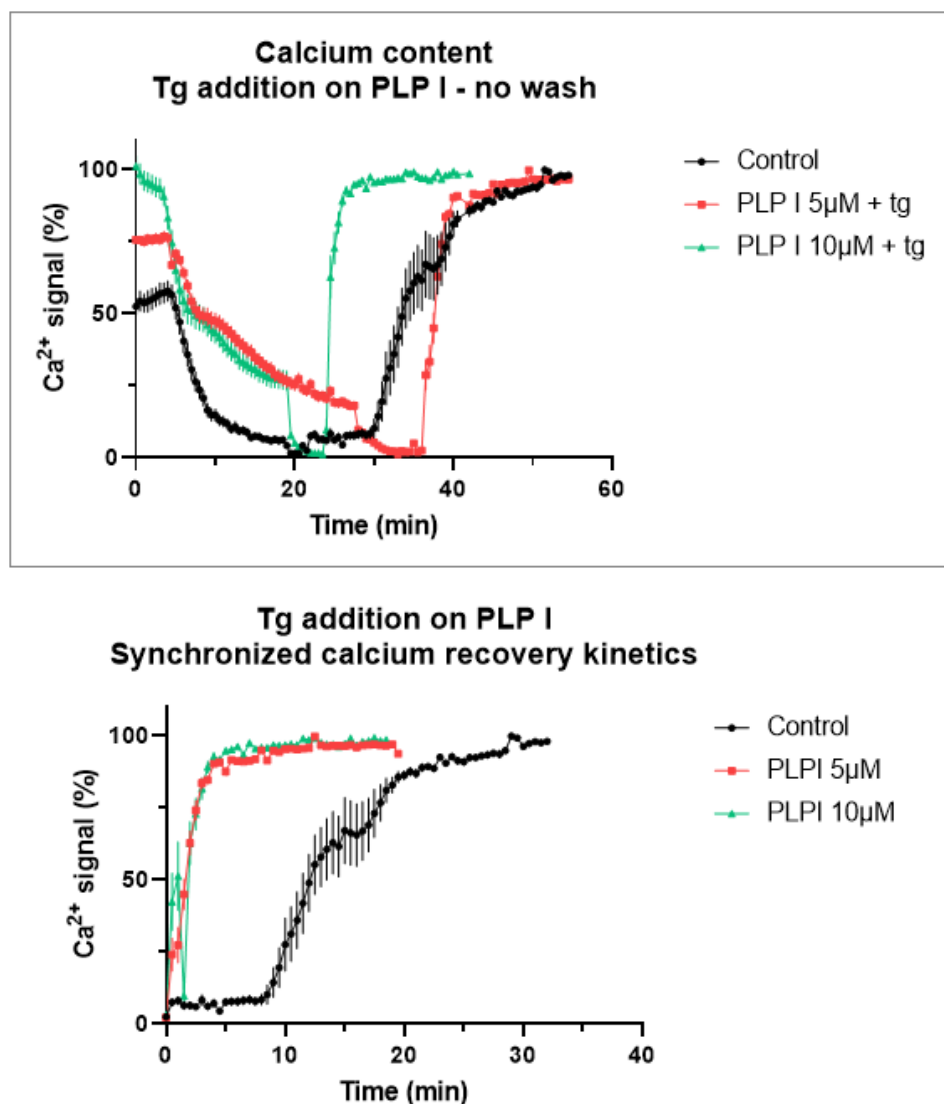


**Figure 63 – PLP I treatment increases ER calcium content and decreases ER repletion kinetics** Cells expressing ER localized GEM-CEPIA were treated with PLP I for 30 minutes prior to recording and kept on cells for the whole recording. Emissions at 480 nm and 535 nm were recorded, and after recording started, 1  $\mu$ M thapsigargin was added alongside PLP I

These experiments allowed us to observe that PLP I had 2 effects on ER calcium content: we saw that ER  $\text{Ca}^{2+}$  quantities increased upon treatments with PLP I prior to Tg treatment. This suggests that PLP I causes an increase of ER calcium stores independently of Tg. The second observation was that calcium stores could not be completely depleted by the action of thapsigargin in the second experimental protocol. This suggests once again that PLP I could either cause an influx of calcium towards the ER, or a retention of calcium inside the ER. Notably, this effect seemed to be reversible, as a washing step alleviated the effects on calcium content increase as well as depletion kinetics.

---

## DISCUSSION

We designed a chemical screening in an effort to gain insights into the traffic of glutathione in and out of the endoplasmic reticulum. To do so, we took advantage of the thapsigargin-driven GSH entry in the ER that can be detected through reduction of our redox sensitive GFP proxy, SF Grx1-roGFPiE. The use of thapsigargin to stimulate the entry of GSH into the ER rather than exogenous GSH addition was motivated by our findings that this later mode of entry is complicatedly intertwined with the metabolism of cysteine, as evidenced in part I of this chapter.

After determining the conditions and timeline of the screening, we defined a method for hit detection. The use of SSMD was recommended to us by Dr Valentin L'Hôte, a PhD student in the lab at the time, who also led a chemical screening on the Prestwick library. The SSMD assuming unequal variances compares the effect of the tested compounds, to that of their controls. A 2.5% false discovery rate is standard in the case of chemical or siRNA screening, and leads to an SSMD threshold of  $\pm 1.608$  defining our first bounds of hit selection (X. D. Zhang et al., 2010; X. D. Zhang, 2007).

We evaluated two effects. The first one was that of a 30-minute exposition to the compound alone, compared to control cells, which led to the calculation of an SSMD at 30 minutes. The second effect we evaluated was the effect of the compound on thapsigargin-treated cells, compared to thapsigargin treated cells as a control, for an additional 30 minutes, which led to the calculation of the second SSMD at 60 minutes.

Initially, our goal was to identify compounds capable of inhibiting thapsigargin-driven ER reduction. Indeed, if a compound is capable of preventing reduction of the ER, there is a chance that it prevents glutathione transport into the ER. Studying such a compound might then help us to identify either the ER GSH transporter itself, or to further characterize the import of GSH into the ER, especially in conditions of calcium depletion.

Since we were interested in compounds that had an effect on Tg-elicited reduction, we therefore based our first hit selection on SSMD values at 60 min. For the Prestwick library, across the two replicates of screening that we did, we found 90 hits out of the 155 tested compounds. While this number seems high, only 22 of these 90 hits were found in both replicates of the screening. Moreover, this number accounts for 3 types of molecules: ones with no effect alone (determined by their SSMD at 30 minutes), ones with a reductive effect, and ones with an oxidizing effect. Additionally, this number is further brought down if we classify their SSMD score. Indeed, X. D. Zhang defined a criterion to classify the size of an effect based on the SSMD. Although this was established for RNAi screenings, the same thresholds can apply to chemical screenings. Accordingly, we defined that  $|\text{SSMD}| \geq 5$  are considered to be extremely strong,  $5 > |\text{SSMD}| \geq 3$  are very strong,  $3 > |\text{SSMD}| \geq 2$  are strong,  $2 > |\text{SSMD}| \geq 1.608$  are fairly strong (X. D. Zhang, 2011).

When classifying hits based on their effect alone (SSMD at 30 min), we realized that the response of molecules with a base effect might be hard to interpret. Indeed, the majority of compounds with an effect alone, displayed the same effect upon thapsigargin addition, and that was observed in both libraries we tested. That is, in the majority of cases, a molecule oxidizing the ER when used alone (SSMD<sub>30</sub>) will also lead to a more oxidized ER upon Tg addition (SSMD<sub>60</sub>). In this case, only

considering the SSMD60 would likely lead to false positive hits. Conversely, a pre-reducing molecule will enhance the reducing effect of thapsigargin on control Tg-treated cells in the majority of cases. The effects of these molecules may thus just be attributable to positive or negative additive effects on the Tg-induced reduction.

For our first trial at in-depth functional analysis, we therefore decided to simplify this question by selecting a molecule that showed no base effect. Meaning that the molecule had an SSMD at 30 minutes below the 1.608 threshold. Additionally, we selected a molecule that had a positive SSMD at 60 minutes; meaning that it prevented the reduction of the ER upon thapsigargin addition, since our initial goal was to identify a molecule capable of inhibiting Tg action. Polyphyllin I was the highest scoring molecule in terms of SSMD in both replicates of the first library we screened, so we decided to proceed with the study of this molecule.

PLP I is a steroidal saponin found in *Paris polyphylla*, a plant that grows in Asia. It is extensively used in traditional herbal medicine to treat a wide range of pain symptoms, from cuts and wounds to skin conditions and cancer treatment (Thapa et al., 2022).

We could confirm that a 30 minutes pretreatment with PLPI indeed inhibited the Tg-induced ER reduction, and that in a dose-dependent manner. However, having included additional controls omitted in the primary screening for the sake of space, we could also observe that a 1-hour exposition to PLPI by itself induced a moderate ER oxidation even at 5  $\mu$ M. While we could clearly monitor a dose response Tg-inhibitory profile of PLPI, optimizing a time of treatment for further analyses was harder, probably due to the lesser number of experiments done leading to higher experimental uncertainties. The pre-oxidizing effect of PLPI was nonetheless obvious from these experiments:  $E_{\text{GSH}}$  (or average ratio value) increased in a time-dependent manner.

This result hindered our interpretations as to whether the seemingly inhibitory effect of PLPI observed on Tg-induced ER reduction was rather resulting from an independent pro-oxidative impact of this compound.

Although no studies have evaluated the redox potential of the ER upon PLP I exposure, the molecule was shown to elevate intracellular ROS in HT-29 and A549 cells, which could explain the elevated  $E_{\text{GSH}}$  (You et al., 2021). Notably, studies on PLP I were usually performed with lower doses, between 0.5 and 2.5  $\mu$ M as well as longer exposure times, between 24 and 72 hours, as the molecule is frequently evaluated in regard to its anticancer activity (Tian et al., 2020). Additional studies report a time dependent increase of intracellular ROS and apoptosis in cells treated with PLP I, but here again, timescales are more in the range of days than hours: when studying the mechanisms of PLP I-induced apoptosis in osteosarcoma cells, Chang *et al.* did observe, physiological effects over the course of 6 hours. They characterized the progressive apparition of ER stress effectors such as BiP, PERK phosphorylation or eIF2 $\alpha$  caused by PLP I treatment, which could suggest a redox imbalance, nonetheless, they did not study redox states upon those changes (Chang et al., 2015).

To possibly distinguish between a direct oxidizing effect of PLPI and an inhibitory effect on Tg-induced ER reduction, we measured  $[\text{GSx}]_{\text{ER}}$  using our second biosensor. PLP I treatment alone showed no significant effect on ER GSH levels but a tendency toward a lesser increase of  $[\text{GSx}]_{\text{ER}}$  could be monitored when cells were concurrently treated PLP I and Tg. These differences were

however not significant, here again, due to the low amount and technical issue lowering the quality of the data. For now, we have to assume that GSH is unchanged upon Tg + PLP I treatment, meaning that the molecule does not prevent GSH from entering the ER upon thapsigargin treatment.

The experiments were led by Clément Djezvedjian as part of his internship project, and the experiment itself proved to be sensitive at two crucial time points (see **Materials and Methods**). A first thiol blocking step with iodoacetamide occurs directly after treatment to fix the redox state of the protein after the experiment (so iodoacetamide essentially blocks reduced thiols). Then later, a TCEP reduction followed by re-alkylation with a high molecular weight PEG allows the alkylation of the released disulphides (so PEGylation occurs on cysteines that were in the disulfide or glutathionylated form).

Out of the four experiments that Clément did, one had to be excluded because a control point was way beyond its usual value: untreated cells showed a 96% reduced Grx1-1cys, opposed to the usual ~50% oxidation we observed. The diamide control was also problematic, as only 71% of the probe was oxidized. These results hint towards an issue upon the reduction-alkylation step that may have been incomplete, since there seems to be a lack of alkylation of the oxidized protein. For the remaining replicates, although the untreated control was slightly more in line with what we expected, the diamide control was never fully oxidized. These experiments require some more investigation into the protocol to make sure that every alkylation step is complete, as it is crucial for the quantification of reduced and oxidized forms of the protein.

Finally, to complete the evaluation of PLP I on thapsigargin effects, we evaluated the effect of PLP I on the calcium profile of thapsigargin fluxes inside the ER. Crucially on this occasion, Clément observed that cells were damaged upon PLP I treatment, especially at the 10  $\mu$ M dose. For this reason, the Fluo-4 indicator to quantify cytosolic calcium could not be used. Fragmentation of the ER was reported, and this could partially explain the inconsistent Grx1-1cys KDEL quantification: if the ER is damaged, the localization of the probe could be altered. This observation warrants further investigation of the subcellular location of the probes.

Regarding calcium fluxes, PLP I led to a slower and thus incomplete decrease of Tg-induced ER calcium store depletion. This effect was also reversible upon PLP I washout. These results further complicated our interpretation of PLP I being an inhibitory molecule for the Tg-induced ER transport of GSH. Indeed, the lesser ER reduction and  $[GSx]_{ER}$  monitored following a combined treatment with PLP I and Tg could be attributed to a flawed depletion of the ER calcium store rather than to an inhibition of GSH influx. In this case, PLPI would affect the signal stimulating GSH flux rather than inhibiting it.

PLP I addition nevertheless had several interesting effects on calcium, that may not directly relate to our current interests. Beside the impaired calcium leak, we observed that PLP I treatment alone increased the ER calcium content. The effect was also partly reversible upon PLPI washout.

These results point toward two possible mechanisms: PLP I could either cause a pumping of calcium into the ER, thus explaining the higher calcium content both in steady state and upon Tg treatment, the slower kinetics would be explained by the counteraction of  $Ca^{2+}$  pumping while Tg causes the exit of  $Ca^{2+}$ . Alternatively, PLP I could act to actively maintain calcium already present inside the ER.

This maintenance would prevent the constitutive calcium leakage, augmenting steady state levels as well as decreasing speed, which could also explain the 2-phase decrease curve. Interestingly, when profiling the proteomic and transcriptomic features of PLP I-induced apoptosis in non-small lung cancer cells, Che *et al.* noticed that calcium-related proteins and gene were upregulated after 1.8  $\mu$ M PLP I treatment for 8 hours. Among them, the annexin 7 protein showed a 2.5-fold upregulation (Siu *et al.*, 2008). Heterozygote mice for this protein were shown to have a reduced capacity for calcium release in their brain, especially through IP3 receptors, while thapsigargin-mediated release was intact (Watson *et al.*, 2004).

To conclude, the aforementioned experiments would need to be replicated. There is a fine line between the effective dose in regard to Tg-elicited reduction inhibition, and PLP I constitutive oxidation. I would fortify the results by replicating treatments under 10  $\mu$ M, since cell degradation seems important above this dose. Lower doses and longer treatment times might mitigate the extreme responses we observed on cell integrity as well. Probe localization would need to be verified at the investigated doses, so that we are sure about the fact that the measures only stem from ER-localized probes, then, GSH quantification would need to be replicated with a protocol that guarantees complete alkylation at critical steps. If then, the compound shows a different calcium release pattern, we could investigate other major channels such as ryanodine receptors or IP3 receptors.

While this chapter was focused on the evaluation of one hit, with a specific hit selection, the screening process provided us with a lot of hit molecules when using only the SSMD criteria. While SSMD can be sorted by strength, we realized that a high SSMD did not necessarily imply an important thapsigargin inhibition. That is because SSMD is calculated by dividing means differences by a sum of standard deviations. The smaller the SD, the higher the score. We therefore added a thapsigargin inhibition filter, where the selected based on SSMD where after sorted by thapsigargin inhibition percentage, and the top scoring molecules are currently under investigation.

## CONCLUSION AND PERSPECTIVES

In this project, we developed a system to explore the dynamics of glutathione fluxes in the endoplasmic reticulum of a mammalian cell model. This model relied on the use of two sensors granting us access to  $E_{\text{GSH}}$  and  $[\text{GSx}]$  inside the ER. Through these experiments, we determined that GSH could be transported toward the endoplasmic reticulum using two potentially synergistic mechanisms.

First, as demonstrated in yeast, GSH can enter the ER following the gradient established between the cytosol and the ER. This transport is saturable, and does not cause major perturbations in terms of ER homeostasis and proteostasis.

On the other hand, as suggested by previous studies, glutathione can be transported towards the ER in response to the depletion of calcium stores. We not only renewed this observation but also completed it by assessing its cooperation with the gradient-dependent ER transport. We showed that Tg-elicited transport functioned independently of the concentration gradient, suggesting an active mechanism, and that the two mechanisms could proceed at least in an additive manner.

The identification of dedicated organellar GSH transporters has greatly improved the assessment of local glutathione function, and recent data has encouraged us to pursue this strategy for defining the role of glutathione in the mammalian ER. In bacteria, GSH is also transported in the periplasm by the CydDC transporter (Pittman, Robinson, and Poole, 2005) and a similar debate regarding its possible function and interaction with the Dsb oxidative folding system has been on-going for many years. Surprisingly it was recently shown that GSSG could compensate for the lack of the DsbA oxidase, which indicated that glutathione could act as an oxidative and not a reducing power for the thiol oxidation model substrates (Knoke et al., 2023). Even more intriguing, GSH but also monothiols such as cysteine could accelerate the oxidative folding of certain protein substrate when DsbA was present. Together with the fact that a *ΔghsA* mutant, impaired in glutathione biosynthesis, exhibited a more reduced periplasm, this might indicate that the periplasmic production of GSSG could directly or indirectly support local disulfide bond formation. These data thus point to a complex function of glutathione in maintaining an optimal operative oxidative folding system. In a funny way, it also calls back to the first hypothesis concerning the role of GSSG in the secretory compartment.

The identification of the mammalian SLC25a39 as a mitochondrial transporter for glutathione proved very valuable to evaluate the consequences of a local GSH depletion, confirming that mitochondrial GSH was crucial for the stability of iron-sulfur cluster-containing proteins (Y. Wang et al., 2021). While Sec61 was involved in yeast GSH transport, our experiments have excluded it, at least partially, from the gradient-dependent transport. Additionally, recent data also excluded Sec61 from being solely responsible for Tg-elicited GSH import. The deletion of Sec61 would anyway prove difficult to assess only GSH function into the ER, as this gene is essential and the Sec61 translocon serves broader functions, such as the critical import of nascent proteins into the ER.

The chemical screening that we performed might provide us with some instrumental tools for the modulation of GSH transport towards the ER, and hence, allow us to lead the same investigations as the ones mentioned above. A complementary approach could be inspired by the investigations that led to the identification of SLC25a39. Quantitative proteomics were performed on purified

mitochondria treated with or without BSO, to assess the most upregulated proteins, among which the transporter stood out. The same could be done in our case: although purifying the ER might be a harder task –but achievable with the use of semi-permeabilization–, a novel system was developed using proximity-biotinylation through a Sec61-TurboID fusion protein, allowing the enrichment of ER proteins through streptavidin purification (K. Kim et al., 2021).

Finally, all of these investigations would have to take into consideration our observation that the metabolism of cysteine might have an impact on that of GSH, which somehow recall the observation recently made in bacteria. While our sensors proved GSH-specific in what we deemed relevant quantities, the evaluation of ER-localized cysteine levels should be tackled to have a better grasp on the involvement of cysteine on artifactual reduction of our sensors but also a possible novel physiological function of this metabolite.





**Materials and methods for chapter 1 - Publication*****Cell Culture, medium and chemicals***

Human Embryonic Kidney (HEK) 293 cells were maintained in DMEM containing Glutamax (Invitrogen #31966047) supplemented with 10 % fetal bovine serum (Eurobio), 100 U/mL penicillin and 100 µg/ml streptomycin and cultivated in 5 % CO<sub>2</sub> at 37 °C. Experiments were performed in the absence of antibiotics. Cystine starvation was achieved by cultivating cells in DMEM, high glucose, no glutamine, no methionine, no cystine medium, from Gibco (#21013-024) supplemented with 0.2mM methionine, 1X glutamax I-CTS, 1mM pyruvate de sodium and FBS 10%.

Culture on 96 wells plate were performed using black glass bottom Corning microplates (#3904 734-1661) pre-coated with poly-L-lysine from sigma aldrich (#P4707).

Cells were transiently transfected using the calcium phosphate technique. HEK293 cells stably expressing the Grx1-roGFPiE probe were generated using the Flip-In system in the dedicated Flip-In HEK293 cell line (ThermoFisher). Stable cell lines were selected using 50 µg/ml of Hygromycin B (Gibco) then maintained in 20 µg/ml for longer time cell culture. Medium was refreshed every 2/3 days.

N-ethylmaleimide (NEM) (#E3876), Nicotinamide adenine dinucleotide 2'-phosphate reduced tetrasodium salt hydrate (NADPH) (#N1630), 5,5'-DITHIOBIS (2-NITROBENZOIC ACID) (DTNB) (#D8130), L-Glutathione reduced (GSH) (#G4251), 5-Sulfosalicylic acid hydrate (SSA) (#390275), Glutathione Reductase from baker's yeast (*S. cerevisiae*) (# G3664-2.5KU), Erastin (#E7781), dithiothréitol (DTT) (#D0632), Diamide (#D3648), DL-Buthionine Sulfoximine (BSO) (#B2640), Mifepristone (#M8046), MK-571 sodium salt hydrate (#M7571) were from Sigma aldrich. Digitonin high purity (#300410-5) and thapsigargin (#586005) were form calbiochem. cOmpete™, Mini, EDTA-free was form Roche (#11836170001). Hygromycin B was from gibco (#10687010). Mycolactone and Ipomoeassin F were kind gifts form Dr CArolien Demangel and Dr Stephen High.

***Plasmids and antibodies***

The Grx1-roGFPiE expressing plasmid was a kind gift from Dr Christian Appenzeller-Herzog (Birk et al). Its sequence was cloned into the pCDNA5/FRT vector between the HindIII and KpnI restriction sites to generate the HEK293 stable cell lines. The HA-Grx1-1cysKDEL sequence was generated by gene synthesis (Genescript) after modification of the original sequence using a human adapted codon bias, then inserted into the pCDNA3.1 vector using NheI and XhoI cloning sites. The pCMV-GCLC and GCLM expression plasmids were kindly sent from Dr Ivor Benjamin's lab (.). The ERdJ5 expression plasmids were generous gifts of Dr Mickael Cheetham (Human Molecular Genetics paper (Athnasiou et al., 2014). JcM and a1-antitrypsine NHK expressing plasmids were kindly provided by Dr Roberto Sitia and Dr Maurizio Molinari. The antibodies used to check GCLC and GCLM expression were from abcam (#ab55436 and #ab55435) then from PTGlabs (#12601-1-AP and #66808-1-Ig). The 16B12 HA antibody used to detect Grx1-1cysKDEL by western blot or immunofluorescence was from Eurogenetec (#MMS-101P-500). The antibody directed against Ero1 was the monoclonal 2G4 antibody from Ozyme (#3264S). The myc9E10 antibody used to detect JcM

was home made. Sec61 $\alpha$  was detected using the monoclonal antibody from Santa Cruz (#sc-393182). The GFP antibody was from Invitrogen (#A6455). Finally, the IgM secretion was monitored using the rabbit anti-mouse IgM (Heavy chain) cross-adsorbed secondary antibody from Bioblock (#61-6800).

### **Total glutathione assay**

Total glutathione was measured using the GR recycling assay based on the GSH-dependent reduction of the Ellman's reagent, DTNB. 10<sup>6</sup> cells were plated in 60mm plates during 48h. Following treatment, the cells were rapidly washed with cold PBS then promptly scraped in 5% SSA before being frozen in liquid nitrogen. Cells were then disrupted by 3 freeze/thaw cycles, alternatively placing them in liquid nitrogen and at 37°C. The supernatant was then recovered after followed centrifugation at 20000g for 10min at 4°C. For each dosage reaction, 5 or 10 $\mu$ L of the cell supernatant was added to 100 $\mu$ L of reaction buffer 1 (0.1M sodium phosphate pH 7.5, 1mM EDTA, 1 unit of glutathione reductase) and placed in 96 wells plates in triplicate. The reaction was initiated well per well by injecting 100 $\mu$ L of the reaction buffer 2 (0.1M sodium phosphate pH 7.5, 1mM EDTA, 0.2mM DTNB, 0.2mM NADPH) pre warmed at 37°C. Glutathione concentrations were determined by monitoring the rate of DTNB reduction, measured by the decrease in absorbance at 412nm over a period of 1min, using a clariostar multimode microplate reader (BMG labtech). The cellular concentrations of total glutathione were next determined by normalizing the sample concentration with both the average cell volume, as determined using a cell sceptor (Merck-Millipore) and the total cell count, that for each experimental condition.

### **Reduction Potential measurements**

HEK293 cells expressing of not Grx1-roGFPiE were seeded into 96-wells black COSTAR96 (#CLS3904 corning costar) poly-L-lysine coated plates at a density of 7,5.10<sup>4</sup> cells per well. 48h after, adherent cells were rapidly switched to Hepes imaging medium (130mM NaCl, 20mM HEPES, 5mM KCl, 1mM CaCl<sub>2</sub>, 1mM MgCl<sub>2</sub>) and ratiometric measurements were performed on blank corrected fluorescence intensities collected at 505nm  $\pm$ 20 from each of the 395 and 460 nm ( $\pm$ 15nm) excitation wavelengths. The experiment was performed in triplicate for each experimental conditions using the plate mode function of the Clariostar microplate reader. Plain HEK293 cells were used to normalize fluorescence intensities in each condition of treatment. Control treatments with DTT or diamide on HEK293 expressing Grx1-roGFPiE served to establish the 0 and 100% of oxidation of the probe in order to deduce the degree of oxidation of the probe (OxD<sub>roGFP</sub>) for each experimental conditions such as  $OxD_{roGFP} = \frac{R-R_{red}}{\frac{I_{460ox}}{I_{395ox}}*(R_{ox}-R)+(R-R_{red})}$  where R<sub>red</sub> and R<sub>ox</sub> and R are the respective fluorescence ratios  $\frac{Em_{395ex}}{Em_{460ex}}$  obtained from the blank corrected emission intensities upon complete reduction or oxidation of the probe or in the studied experimental condition. I460ox and I460red are the fluorescence intensities measured emitted by the fully oxidized or fully reduced probe after a 460 nm excitation. E<sub>GSH</sub> was then calculated according to the following formula:  $E_{roGFP} = E^{\circ}_{roGFP} - \frac{RT}{2F} \ln \left[ \frac{(1-OxD_{roGFP})}{OxD_{roGFP}} \right]$  with E<sup>o</sup><sub>roGFP</sub> = -239mV, R the gas constant (8.315 J K<sup>-1</sup> mol<sup>-1</sup>), T the temperature (298K) and F the Faraday constant (96485 C mol<sup>-1</sup>). Assuming a complete equilibration between the Grx1-roGFPiE probe and the GSH/2GSSG redox pair, E<sub>GSH</sub>=E<sub>Grx1-roGFPiE</sub>.

### **Cell lysis and western blots analysis**

For regular western blot experiments, treated cells were washed in phosphate-buffered saline (PBS), lysed in Lysis Buffer containing 50mM Tris-HCl pH8, 150 mM NaCl, 1% Triton X-100, 1mM EDTA, 0.1% SDS, 1mM PMSF and protease inhibitors. After centrifugation at 20,000 × g, protein concentrations in supernatants were measured using Bradford assay. Samples concentrations were then adjusted to load equivalent protein quantities on SDS-PAGE.

Alternatively, for ERO1 redox analyses, treated cells were quickly washed in PBS containing NEM (25mM), then lysed on ice in IP buffer (50mM Tris pH8, 150 mM NaCl, 1%, Triton-X100, 1mM EDTA, 25 mM NEM, and antiproteases). After 30 minutes incubation, extracts were cleared by centrifugation and directly loaded on a non-reducing 7.5% SDS-PAGE gel (37.5:1). For ERdj5, treated cells were directly lysed in cold TCA, and the extracts were recovered after three acetone washes and resuspension in PBS containing 2% SDS supplemented with 15 mM MALPEG24. After 1h incubation at 25°C, the extracts were loaded on a 7.5% SDS-PAGE.

### **HA-Grx1-1cys pull down assay**

HEK 293 cells were seeded at a  $2 \cdot 10^5$  density in 6-wells plates were transfected or not with the HA-grx1-1cysKDEL plasmid. After 24h, cells were treated and the redox state of the probe was frozen by rapidly washing cells with cold PBS containing 200 mM iodoacetamide, then lysing them in 300  $\mu$ L of Lysis Buffer (as described in the Protein Extractions protocol) complemented with 50 mM iodoacetamide. The obtained supernatants were carefully transferred to new tubes containing 690 $\mu$ L of IP lysis buffer (0.1M sodium phosphate, 1% Triton X-100, pH 8, 0.2 mM PMSF) and 10  $\mu$ L of Pierce anti-HA magnetic beads (Thermo Fished Scientific). Gentle rotary shaking at 4°C was performed for 3 hours minimum. The beads were then washed 3 times with 40 $\mu$ L of IP lysis buffer then one 40- $\mu$ L of PBS. The proteins were then resolubilized by incubating the beads at 95°C for 5 minutes in 40 $\mu$ L of 2% SDS solution. The supernatant from each tube was transferred to a new tube containing TCEP (Sigma), to achieve a final concentration of 10mM TCEP for 10 minutes incubation at room temperature. 40 $\mu$ L of MAL-dPeg from a 15mM in PBS 2% SDS stock then was added. The alkylation process was conducted at 25°C protected from light for 1 hour, after which the samples were frozen at -80°C for subsequent Western blot analysis using 14% SDS-PAGE.

Western blots were quantified by densitometric analysis using the ImageStudio software from LI-COR-Biosciences.

### **Cell semi-permeabilization**

The protocol was adapted from Sitia *et al.*, 2004. Confluent cells were trypsinized and harvested in KHM buffer (110mM potassium acetate, 20mM HEPES pH 7.2, 2 mM magnesium acetate) containing 10mg/mL soybean trypsin inhibitor (Sigma). After resuspension in 600 $\mu$ L per  $10^6$  cells of cold KHM buffer with or without 12mg/mL digitonin, cells were incubated on ice for 5 minutes, and 8 mL of cold KHM were added to dilute digitonin. The samples were next gently centrifuged at 280 × g at 4°C and the pellets resuspended in HEPES acetate buffer (50 mM HEPES, 90 mM potassium acetate) for a 10 minutes incubation on ice. After mild centrifugation at 280 × g/ 4°C, the obtained pellets were resuspended in 100  $\mu$ L KHM for  $2 \cdot 10^6$  cells, next transferred in a 96-wells Costar plate.

Cells were then challenged with different treatments provided in 100  $\mu$ L volumes, and the plate was centrifuged at 200 x g for 2 minutes. The probe response was then assessed as previously described using ClarioStar fluorescence reader.

### **JcM folding assay**

The protocol was adapted from Sitia *et al.*, 2004, a detailed protocol is available on the web page of the Sitia lab. Briefly, HEK 293 cells transfected with JcM were trypsinized the resulting pellets resuspended in 1mL/10<sup>6</sup> cells of DMEM without SVF. Cells were then treated with 10 mM DTT during 5 minutes at 37°C then centrifuged and washed twice with 1mL/10<sup>6</sup> cells of ice-cold PBS. A non DTT treated control was spared. The DTT treated cells were next resuspended in cold complete DMEM and transferred into Eppendorf tubes (10<sup>6</sup> cells per tube, the tubes were pre-chilled on ice and the sample were maintained there as much as possible during handling and treatments). The initiation of the folding reaction occurred upon placing the tubes at 24°C and was terminated every 2 minutes by adding 10 $\mu$ L of a 500 mM NEM resuspended in DMSO at the appropriate times. Cells were then centrifuged and the resulting pellets underwent two rounds of washing with cold PBS each. The pellet was resuspended in 300 $\mu$ L of lysis buffer containing 10 mM NEM and incubated on ice for 20 minutes. Supernatants were transferred to new tubes and mixed with 75 $\mu$ L SB5X without BME. The resulting mixture was then frozen at -80°C and sample were run on a 14% non-reducing gel. Noteworthy, sample boiling or gently sonication could be employed to address viscosity issues, which were common in the samples.

### **pHluorin2 – ER pH measurement**

Plasmid Construction: pHluorin2 plasmids for targeting the endoplasmic reticulum (ER) and glycosylphosphatidylinositol (GPI) membrane can be retrieved from Addgene (plasmid IDs: 171717 and 171721).

Cell Culture and Transfection: Human embryonic kidney (HEK) 293 cells were seeded in 150 mm dishes at 4 million cells per dish in complete Dulbecco's Modified Eagle Medium (DMEM). On Day 2, cells were transfected with 1  $\mu$ g of GPI-pHluorin and 2  $\mu$ g of ER-pHluorin plasmids per 6-well equivalent. On Day 3, cells were seeded into 96-well plates (500,000 cells/mL) for experiments and 6-well plates at the same density for western blot controls.

**Experiment 1: pH Calibration curve for GPI-pHluorin:** Spectral scans were conducted on HEK 293 cells overexpressing GPI-pHluorin at pH levels between 5.5 and 7.5 using 25 mM MES (for pH under 4.5 to 6.5) and 25 mM HEPES (for pH 7 or 7.5 or above) buffer solutions. containing 125 mM KCl and 25 mM NaCl. pH adjustments were made at 37°C using 10  $\mu$ L increments of concentrated NaOH or HCl solutions. After rinsing with the respective pH buffers, cells were equilibrated for 15 minutes at 37°C, followed by spectral scans.

Scan parameters: excitation wavelengths: excitation 1: 385-15nm, excitation 2: 475-10nm;  
Emission wavelength: 510-10nm, untransfected cells were included as blanks for background correction.

**Experiment 2: pH Assessment in the ER:** pH assessment was made after GSH treatment in complete DMEM, either 1, 2.5, 5, 7.5, 10 mM for 10 minutes or 2.5 mM for 10, 30, 45, 60 minutes for HEK 293 cells overexpressing either ER-pHluorin or GPI-pHluorin probes. After treatment, the medium was replaced with HEPES buffer and spectral scans were conducted using the same parameters as in Experiment 1. Untransfected cells were included as blanks for background correction.

### ***Xbp1 splicing using RT-PCR or RT-qPCR***

Total RNA in cells was extracted using RNA plus kit (Machery Nagel). RNA was eluted in ddH<sub>2</sub>O and quantified with a NanoDrop 2000 spectrophotometer (Thermo Fisher Scientific). The RT reaction was performed on 2 µg of RNA per sample, to which were added 4µL FS buffer 5X, 2µL DNTP 5mM, 0,5µL oligo dT and completed to 42.5 µL with ddH<sub>2</sub>O. Thermal cycling was 10 min at 70°C, 2min30s at 62°C and 90min at 42°C. when we arrived at 42°C, 2µL DTT + 0,5µL MMLV are added per sample. At the end of the incubation, 30µL ddH<sub>2</sub>O are added per sample, incubated 10min at 95°C followed by 2min on ice.

5 µL cDNA were used to perform the PCR reaction and amplify both the Xbp1u and Xbp1s forms using the following primer set: 5'-GGAACAGCAAGTGGTAGA /5'-CTGGAGGGGTGACAAC. Thermal cycling was 4 min at 94°C, 35 cycles of 30 s at 94°C and 30 s at 60°C and 50 s at 72°C, followed by 7 min at 72°C. The two Xbp1 forms exhibit a 72nt size difference which was unmasked by migrating the amplified fragments on a 3.5% agarose gel.

Alternatively for RT-qPCR, cDNAs were synthesized by using the cDNA Synthesis Kit (maxima RT kit, Thermo) and hexanucleotides according to the manufacturer. The relative expression of mRNA was calculated by the 2<sup>-ΔΔCt</sup> method by using IQ5 (Biorad). The sequences of the primers for qRT-PCR are presented below. GAPDH served as the reference control gene.

<b>XBP1t forward</b>	5'-TGAAAAACAGAGTAGCAGCTCAGA3'
<b>XBP1t reverse</b>	5'-CCCAAGCGCTGTCTTAACTC-3'
<b>XBP1u forward</b>	5'- CAGACTACGTGCACCTCTGC-3'
<b>XBP1s forward</b>	5'- GCTGAGTCCGCAGCAGGT-3'
<b>XBP1u&amp;s reverse</b>	5'- CTGGGTCCAAGTTGTCCAGAAT-3'

### ***RT-qPCR (TaqMan Sec61)***

RNA in cells was extracted from PBS washed cells using the NucleoSpin RNA Plus kit (Machery Nagel) according to the manufacturer's protocol. RNA was eluted in ddH<sub>2</sub>O and quantified with a NanoDrop 2000 spectrophotometer (Thermo Fisher Scientific). The reaction was performed on 50 ng RNA per sample, to which were mixed 5 µL of TaqPath mix 4X (Thermo Fischer Scientific), 1 µL of primer mix and completed to 20 µL with ddH<sub>2</sub>O. Fluorescence was monitored on a CFX96 Touch Detection System (BioRad). Thermal cycling was 2 min at 25°C, 15 min at 50°C; 2 min at 95°C, 39 cycles of 3 s at 95°C and 30 s at 60°C. All samples were run in technical triplicates. Data were retrieved and analysed in a CFX manager software, GAPDH was used for normalization and the relative expression of mRNA was calculated with the ΔΔCt method. The linearity of the designed

primers' efficiency was verified beforehand on a serial dilution of RNA. TaqMan primers sequences were from Thermo Fisher (Sec61 $\alpha$ 1:[Hs01037690\\_m1](#); Sec61 $\alpha$ 2:[Hs00943749\\_m1](#))

### **Imaging and Immunofluorescence experiments**

Grx1-roGFPiE subcellular localization was performed using live cell microscopy recording on a Yokogawa X1 CSU iLAS 2 Spinning disk confocal microscope. Colocalization was achieved by transfecting HEK293 cells stably expressing the GSH probe with the ER localized mCherry-KDEL. Image acquisition was achieved under temperature and CO<sub>2</sub> control.

Grx1-1cysKDEL localisation was performed by co-transfecting HEK293 cells with both GSH probe and the ER localized mCherry-KDEL. After cell fixation with formaldehyde, and triton permeabilization, cells were incubated successively with an anti-HA primary antibody then an anti-mouse Alexa488 secondary antibody to detect the Grx1-1cys KDEL protein. The mCherry probe was detected through its native fluorescence. Image acquisition was performed using the same spinning disk technology.

### **Calculation of [GSx]<sub>ER</sub> and statistical analysis**

[GSx]<sub>ER</sub> was calculated from the measured E<sub>GSH</sub> and GSH/GSSG ratio, using respectively the Grx1-roGFPiE and the Grx1-1cysKDEL probes as in (Montero et al., 2013)

At equilibrium, E<sub>Grx1-roGFPiE</sub> = E<sub>GSH</sub> =  $E^{o'}_{GSH} - \frac{RT}{ZF} \ln \frac{[GSH]^2}{[GSSG]}$ . Consequently, the GSH<sup>2</sup>/GSSG ratio can be deduced from the E<sub>Grx1-roGFPiE</sub> values and their corresponding standard deviation  $\delta E_{roGFPiE}$ , as  $\frac{[GSH]^2}{[GSSG]} = A = e^{-(E_{roGFPiE} + 0.24) \left(\frac{2F}{RT}\right)}$  with a propagated incertitude of  $\delta A = \frac{2F}{RT} * A * \delta E_{roGFPiE}$

At equilibrium, the Grx1-1cysKDEL probe equilibrates with the GSH/GSSG couple with

$\frac{[GSH]}{[GSSG]} = B = K_{ox} \frac{(1 - OxD_{Grx1})}{OxD_{Grx1}}$  where  $OxD_{Grx1} = \frac{[Grx11cys_{ox}]}{[Grx11cys_{red}] + [Grx11cys_{ox}]}$  with a standard deviation of  $\delta OxD_{Grx1}$  and  $K_{ox} = 74$ . The propagated incertitude on B is  $\delta B = \frac{74}{OxD_{Grx1}} * \delta OxD_{Grx1}$ .

[GSx]<sub>ER</sub> can then be calculated according to  $[GSx]_{ER} = \frac{A}{B} + 2 \frac{A}{B^2}$  with a propagated incertitude  $\sqrt{\left[\left(\frac{1}{B} + \frac{2}{B^2}\right) \delta A\right]^2 + \left[\frac{A}{B^2} * \left(1 + \frac{4}{B}\right) * \delta B\right]^2}$  as the sum of the quadratic errors from the partial differential equations.

## **Chapter 2 – Preliminary results**

### **Transfection**

Ideal plasmid concentration for transfection of SF Grx1-roGFPiE was determined *via* protein expression assay using Western-Blot and fluorescence intensity *via* spectral scan. The transfection procedure for transient expression is described in *Chapter 1 – Publication*.

**Ratiometric fluorescence intensity readings –  $E_{\text{GSH}}$  calculations from Grx1-roGFPIE** Unless otherwise mentioned, the determination of  $E_{\text{GSH}}$  was determined as described in *Chapter 1 – Publication*.

***Cystine starvation experiments (overnight, 10 minutes, erastin, BSO, and thapsigargin)***

Cells stably overexpressing ER localised Grx1-roGFPIE were seeded in 96-wells black COSTAR96 poly-L-lysine coated plates at a  $7.5 \cdot 10^4$  density in complete DMEM for 48 hours.

For cystine starvation from the medium, the culture medium was then replaced with 100  $\mu\text{L}$  per well of DMEM-cys (Gibco) for the indicated times. NB: The commercial DMEM-cys medium does not include cystine, methionine, sodium pyruvate and glutamine, so we added 0.2 mM methionine, 1 mM sodium pyruvate, and 1X glutamax to match the composition of standard DMEM. After the starvation time was reached, 50  $\mu\text{L}$  of DMEM-cys was added, completed with 2.5 mM of final GSH and, when mentioned, 0.2 mM of final cystine for 10 minutes.

For thapsigargin treatments, the culture medium was replaced with 200  $\mu\text{L}$  per well of DMEM-cys with 1  $\mu\text{M}$  thapsigargin for the indicated amount of time. The medium was also complemented with 0.2 mM cystine HCl or 0.4 mM cysteine when mentioned.

For erastin treatments, after 48 hours of growth, the medium was replaced with 100  $\mu\text{L}$  of fresh complete DMEM containing 20  $\mu\text{M}$  of erastin (in DMSO) for the indicated amounts of time. Then, 50  $\mu\text{L}$  of DMEM-cys was added, completed with 2.5 mM of final GSH for 10 minutes.

For BSO treatments, 24 hours after seeding, the medium was replaced with 200  $\mu\text{L}$  of complete DMEM containing 200  $\mu\text{M}$  BSO. After 24 more hours, the medium was replaced with 200  $\mu\text{L}$  DMEM-cys completed with either nothing, 0.2 mM cystine, or 0.4 mM cysteine for 10 or 30 minutes.

For  $E_{\text{GSH}}$  determinations, after the aforementioned treatments, wells were emptied and replaced with HEPES buffer (130 mM NaCl, 20mM HEPES pH7.4, 1mM  $\text{CaCl}_2$ , 1mM  $\text{MgCl}_2$ , KCl 5mM, 5mM glucose) and the ratiometric fluorescence of Grx1-roGFPIE was recorded on a temperature-controlled microplate reader, from which  $E_{\text{GSH}}$  values were calculated.

For [GSx], the aforementioned protocols were optimized for cells seeded in 6-wells plates. At the end of the experiment, [GSx] levels were determined on cell lysates, using a 96-wells plate-optimized GR recycling assay, and expressed in mM after correction by the cell number and cell volume, individually assessed for each experimental condition.

***Intracellular cysteine quantification***

HEK 293 cells were seeded in 60 mm cell culture dishes at a density of  $2.5 \cdot 10^5$  to  $2.5 \cdot 10^6$ . After 48 hours, cells were treated with 2.5 mM GSH in fresh DMEM for 10 minutes. The redox state was stopped by adding to 500  $\mu\text{L}$  of the treatment medium, either 500  $\mu\text{L}$  of a 10% sulfosalicylic acid solution, or 1170  $\mu\text{L}$  of a 100% methanol solution, so that the final concentrations of the samples are 5% SSA or 70% methanol. The solution was conserved for dosage of extracellular milieu. Then, cellular lysates were then gathered in 200  $\mu\text{L}$  of 5% SSA or 70% methanol.

Another group of cells was transiently transfected with GCLC and GCLM plasmids 24 hours after seeding, then 48 hours after transfection, the same protocol was applied.

Once the samples were prepared, cysteine quantifications were performed via HPLC.

First, a calibration curve was established in 50  $\mu\text{L}$  water (0.1% PCA) containing 15N internal standard and quality controls, 50  $\mu\text{L}$  water (0.1% PCA) containing calibration standards, and 100  $\mu\text{L}$  acetonitrile (ACN)

Then, the samples were diluted 1/100 in  $\text{H}_2\text{O}$ , and 50  $\mu\text{L}$  of the solution were precipitated in 200  $\mu\text{L}$  of acetonitrile containing 0.1% formic acid. The mixture was vortexed, centrifuged for 10 minutes at 20 000 x g, and the supernatant was evaporated at 40°C under  $\text{N}_2$  atmosphere. The sample was dissolved in 50 $\mu\text{L}$   $\text{H}_2\text{O}$  (0.1% PCA), then 50 $\mu\text{L}$   $\text{H}_2\text{O}$  (0.1% PCA) 15N internal standard and 100  $\mu\text{L}$  ACN were added. The mixture was centrifuged and 10  $\mu\text{L}$  of the supernatant were pushed through a column + LC-HRMS system.

***Probe purification via HA Immunoprecipitation for cysteine reactivity tests*** described in Chapter 1 - Paper

For purification of Grx1-roGFPiE: the protocol was as previously described for control samples. For cysteine or GSH- treated samples, after the PBS wash step, samples bound to the magnetic beads were incubated with 40  $\mu\text{L}$  of cysteine or GSH in PBS for 15 minutes at room temperature. The reaction was stopped with the addition of 5  $\mu\text{L}$  of iodoacetamide to achieve a 200  $\mu\text{M}$  final concentration. After, the reduction-alkylation steps were replicated as in the previous protocol. Samples were run on a 14% non-reducing SDS-PAGE.

For purification of Grx1-1cys, after the step of 3-hour incubation of the magnetic beads, the IP lysis buffer wash step was complemented with 2 mM DTT in IP lysis buffer. After the PBS wash step, the beads were incubated with 40  $\mu\text{L}$  of cysteine or GSH in PBS for 15 minutes at room temperature. The reaction was stopped with the addition of 5  $\mu\text{L}$  of iodoacetamide to achieve a 200  $\mu\text{M}$  final concentration. After, the reduction-alkylation steps were replicated as in the previous protocol. Samples were run on a 14% non-reducing SDS-PAGE.

### ***Spectral scan***

Cells were seeded in 96-wells black COSTAR96 poly-L-lysine coated plates at a density of  $10 \cdot 10^4$  cells per well on day 0 in complete DMEM. On day 1, wells were rinsed once with HEPES buffer (130 mM NaCl, 20mM HEPES pH7.4, 1mM  $\text{CaCl}_2$ , 1mM  $\text{MgCl}_2$ , KCl 5mM, 5mM glucose), then treated with either HEPES, 10 mM DTT in HEPES or 5 mM diamide in HEPES for 5 min at 37°C. Spectral scans were recorded on a ClarioStar temperature-controlled plate reader. Optic settings were:

Excitation wavelength: from 360 nm to 500 nm, stepwidth 1 nm, bandwidth: 10 nm. Emission wavelength: 530 nm, bandwidth: 20nm. Gain was adjusted based on untreated controls, and usually between 2000-2500.

***Primary screens: Prestwick and ER Stress libraries***

Cells were seeded in 96-wells black COSTAR96 poly-L-lysine coated plates at a density of  $7,5 \cdot 10^4$  cells per well on day 0 in complete DMEM. On day 2, wells were treated with either 144  $\mu$ L HEPES buffer (130 mM NaCl, 20mM HEPES pH7.4, 1mM  $\text{CaCl}_2$ , 1mM  $\text{MgCl}_2$ , KCl 5mM, 5mM glucose) alone to which were added 36  $\mu$ L of molecules from the library (to achieve a final concentration of 20  $\mu$ M). Control wells were treated with 180  $\mu$ L HEPES buffer. Cells were placed for 25 minutes in a 37°C incubator. At 25 minutes, the redox state of the probe was assessed by fluorescence reading on the temperature controlled ClarioStar platereader. At 30 minutes, cells were treated with either 20  $\mu$ L of HEPES buffer for controls or 20  $\mu$ L of thapsigargin 10  $\mu$ M HEPES buffer to achieve a final concentration of 1  $\mu$ M thapsigargin in wells. Cells were then placed in the incubator until 55 minutes, then control wells were treated with 20  $\mu$ L of DTT or Diamide solutions in HEPES to achieve a final concentration of 10mM and 5mM respectively. At 60 minutes, the second fluorescence reading was performed on the platereader.

***Secondary screens: dose response experiments – provided by Clément Djezvedjian***

Cells were seeded in 96-wells black COSTAR96 poly-L-lysine coated plates at a density of  $7,5 \cdot 10^4$  cells per well on day 0 in complete DMEM. On day 2, wells were treated with either 180  $\mu$ L HEPES buffer (130 mM NaCl, 20mM HEPES pH7.4, 1mM  $\text{CaCl}_2$ , 1mM  $\text{MgCl}_2$ , KCl 5mM, 5mM glucose) alone or with 5, 10, 20 or 40  $\mu$ M of PLP I diluted in HEPES buffer and placed for 25 minutes in a 37°C incubator. At 25 minutes, the redox state of the probe was assessed by fluorescence reading on the temperature controlled ClarioStar platereader. At 30 minutes, cells were treated with either 20  $\mu$ L of HEPES buffer or 20  $\mu$ L of thapsigargin 10  $\mu$ M HEPES buffer to achieve a final concentration of 1  $\mu$ M thapsigargin in wells. Cells were then placed in the incubator until 55 minutes, then control wells were treated with 20  $\mu$ L of DTT or Diamide solutions in HEPES to achieve a final concentration of 10mM and 5mM respectively. At 60 minutes, the second fluorescence reading was performed on the platereader.

***Secondary screens: kinetics experiments – provided by Clément Djezvedjian***

The same protocol was applied for dose response and kinetics. Treatment variation: For each dose of PLP I tested (5, 10, 20  $\mu$ M), 180  $\mu$ L of HEPES buffer alone or with PLP I were added and placed in a 37°C incubator for 5, 15, 30 or 60 minutes. Cells were then treated with either 20  $\mu$ L of HEPES buffer or 20  $\mu$ L of thapsigargin 10  $\mu$ M HEPES buffer to achieve a final concentration of 1  $\mu$ M thapsigargin in wells.

***Secondary screens: Live imaging for calcium measurements – Provided by Ilaria Pontisso***

HEK 293 cells were seeded on 25 mm coverslips and transfected with pCIS GEM-CEPIA1er 48 hours after plating. Cells were placed in an observation chamber in imaging medium containing 115 mM NaCl, 5.6 mM KCl, 1.8 mM  $\text{CaCl}_2$ , 1.2 mM  $\text{MgCl}_2$ , 1 mM,  $\text{NaHPO}_4$ , 10 mM  $\text{NaHCO}_3$ , 20 mM HEPES (pH 7.4) and 1 mg/ml glucose. Untreated or pretreated samples were incubated with 1  $\mu$ M thapsigargin followed by 5mM EGTA and 10mM  $\text{CaCl}_2$  in presence of 2  $\mu$ M ionomycin.

Samples were analysed at room temperature on an inverted Nikon eclipse TE200 fluorescence microscope, using a 40x objective. Illuminating sources used were 380 nm for excitation; 480 nm/535 nm for excitation for GEM-CEPIA1er driven by Simple 32 Software from Compix

Incorporated. Images were captured using a CMOS camera (Hamamatsu). Images were analysed with Simple 32 software

### ***Directed mutagenesis via PCR***

For PCR, the guidelines from Thermo Fischer Scientific's Platinum *Pfx* DNA Polymerase were followed and adapted. Thermal cycling was performed in a ProFlex PCR system (Thermo Fischer Scientific) with the following program: 5 min at 94°C, 30 cycles of 30 s at 94°C, 40 s at 52°C, 1 min at 68°C, then 7 min at 68°C, and hold at 4°C.

Reaction mixture for PCR was made of 10µL *Pfx* Amplification Buffer (Thermo Fischer Scientific), 1.5µL dNTP (10 mM), 1 µL MgSO<sub>4</sub> (50 mM), 1.5 µL of each primer (10 µM), 1 µL of template DNA (1 µg/µL), 0.4 µL Platinum *Pfx* DNA Polymerase (Thermo Fischer Scientific). Control of the reaction were performed on 1% agarose gels.

**Primers:** for A206V addition in SFroGFPIE UP:

CACCTGCTCCGTGCTGAGCAAAGACCCCAACGAGAAG

For A206V addition in SFroGFPIE DOWN:

GGTCTTTGCTCAGCACGGAGCAGGTGCTCAGGTAGTGG

To remove Y145F from SFroGFPIE

UPGGACAAGCTGGAGTACAACACTACAACACTGCGAGAGCAACG;

To remove Y145F from SFroGFPIE DOWN:

CGTTGCTCTCGCAGTTGTAGTTGTACTCCAGCTTGTGCC

To clone SFroGFPIE UP (Nhe1):

CCCAAGCTGGCTAGCATGCATCCTGCCGTCTTCC;

To clone SFroGFPIE DOWN (BamHI):

GGACTAGTGGATCCTTACAGTTCGTCCTTGTACAG

## BIBLIOGRAPHY

La mise à jour automatique des citations est désactivée. Pour voir la bibliographie, cliquez sur Actualiser dans l'onglet Zotero.

Le glutathion (ou GSH) est un tripeptide ubiquitaire composé de trois acides aminés : d'un glutamate, lié par une liaison atypique gamma à une cystéine centrale, et d'une glycine terminale. Ce deuxième acide aminé confère au glutathion des propriétés d'oxydoréduction, ou redox, permettant sa détection aussi bien à l'état réduit (GSH) qu'oxydé, soit sous forme de dimère (GSSG), soit sous forme de disulfure mixte avec d'autres cystéines cellulaires (RSSG). Bien que d'autres formes du glutathion soient représentées, les trois susmentionnées sont majoritaires et ont fait l'objet de notre attention au long de ce projet de thèse.

Le glutathion est représenté chez une vaste majorité d'espèces eucaryotes mais aussi procaryotes, et est détecté dans de nombreux sinon tous les compartiments cellulaires, à hauteur de concentration millimolaire. La synthèse du GSH, en revanche, n'a lieu que dans le cytosol ou bien la matrice mitochondriale (ou les chloroplastes chez les plantes), grâce à l'action séquentielle de l'enzyme GCL (gamma-glutamyl-cystéine ligase) puis de l'enzyme GS (glutathion synthetase), chez les mammifères.

Possédant un potentiel redox particulièrement bas, de nombreuses propriétés réductrices sont attribuées au GSH. Ainsi, le GSH sert de cofacteur dans des réactions de réduction –de ponts disulfures, mais aussi de peroxydes ou d'électrophile–, à l'issue de quoi il est converti en GSSG. Pour recycler le GSSG en GSH, l'enzyme glutathion réductase (GLR) consomme une molécule de NADPH. Au-delà de son rôle largement établi de réducteur, le glutathion a été impliqué dans la biogénèse des centres fer-soufre, au sein de la mitochondrie. Dans ce contexte, il est supposé que la nature essentielle du glutathion soit liée à cette fonction plutôt qu'à celle de réducteur. En effet, bien que le glutathion soit présent en larges quantités dans les cellules, une addition de quantités micromolaires suffit à restaurer la viabilité cellulaire lésée en cas de suppression des enzymes de synthèse du GSH. En revanche, de larges quantités de GSH ajouté sont nécessaires pour compenser la perte du système de la thioredoxine. Le système thioredoxine est souvent décrit en parallèle de celui du glutathion, car il sert aussi de réducteur dans le contrôle thiol-redox cytosolique. Comparable au système du glutathion, la thioredoxine est maintenue réduite par la thioredoxine réductase, dépendante du NADPH. Il est proposé que le glutathion serve de système de secours à celui de la thioredoxine. Bien qu'étant un réducteur au sens large, le constat d'un rôle mitochondrial du GSH distinct de son rôle cellulaire plus large, souligne la nécessité d'étudier le glutathion plus localement au sein des organelles.

Le réticulum endoplasmique est l'un des compartiments cellulaires destiné au processus oxydatif du repliement protéique. Ici, les protéines membranaires et sécrétées sont insérées sous forme réduite, dans le but d'obtenir leur conformation finale, cruciale à leurs fonctions biologiques. Ces formes finales peuvent comporter des ponts disulfures, insérés entre autres par le relai PDI-Ero1. ER oxydoreductin 1, ou Ero1, est une protéine capable de créer des ponts disulfures *de novo* grâce au transfert d'électrons de ses cystéines catalytiques à l'oxygène. Dans ce processus, l'oxygène est converti en H<sub>2</sub>O<sub>2</sub>. Les ponts disulfures créés peuvent être transférés à la Protein Disulfide Isomerase (PDI) qui sera elle-même capable de catalyser la formation de ponts disulfures sur les protéines clientes du RE par échange thiol-disulfure. Cet échange est aussi possible entre la PDI et le GSH, présent au sein du RE en quantités millimolaires. Ce constat soulève la question du rôle précis du

GSH dans ce compartiment. En effet, en tant que molécule réductrice, la présence importante du GSH peut paraître contraire aux fonctions dédiées à ce compartiment. Plusieurs rôles ont été suggérés pour le glutathion au sein du RE, du maintien du contrôle redox à l'activité d'Ero1-PDI, en passant par l'alimentation d'une voie de réduction des ponts disulfures non-natifs, intermédiaires au bon repliement protéique ou établis par erreur. Cependant, d'autres études, utilisant des systèmes dont le glutathion a été supprimé, suggèrent que la présence de glutathion n'est pas cruciale aux fonctions du RE. Encore aujourd'hui, la fonction du glutathion au sein du RE fait débat, et nécessite de plus amples recherches.

L'étude localisée du glutathion est rendue difficile par la rareté des techniques disponibles et adaptées. Premièrement, la nature du tripeptide complique les investigations : en effet, en tant que réducteur puissant, le glutathion est sensible à l'oxydation, or, la conservation de son état redox est un point clé dans la définition de ses fonctions. De plus, sa taille et ses cibles protéiques en font une molécule difficile à « tagguer » (équiper d'un marqueur) si l'on souhaite conserver la spécificité de ces interactions. Enfin, étant une molécule essentielle, abondante, et répartie largement au sein des cellules, sa suppression est inenvisageable, et les conséquences sont souvent trop vastes pour en apprécier les effets locaux. Pour ces raisons, l'étude du transport du glutathion et de son rôle physiologique nécessitent des outils d'études spécifiques et dédiés.

Les sondes redox sont un outil de choix : ces protéines ont été dérivées de la Green Fluorescent Protein (GFP) et ont été rendues redox sensibles par l'insertion de cystéines voisines, capables de créer un pont disulfure avoisinant le chromophore de la GFP, modifiant la réponse de fluorescence en fonction de l'état d'oxydation de ces cystéines. Ce pont disulfure s'établit et se défait, et cet équilibre a pu être rendu dépendant du système du glutathion. Ainsi, la fluorescence mesurée permet de déduire l'état redox du glutathion au contact de cette GFP modifiée, aussi appelée roGFP. Cette sonde peut être génétiquement adressée et adaptée à tous les compartiments cellulaires, et permet ainsi l'évaluation de l'état redox du glutathion plus localement que les techniques d'extraction par lyse cellulaire. De plus, ces sondes permettent une étude directement *in vivo*, sans besoin d'extraction.

L'état redox du glutathion est déterminé par le calcul du potentiel redox, ou  $E_{GSH}$ , issu des mesures effectuées par la sonde, injectées dans l'équation de Nernst. Cette mesure ne fournit pas de données quantitatives, mais seulement une idée du ratio  $GSH^2/GSSG$ , et l'évolution de ce dernier en fonction des conditions de traitement appliquées. D'autres techniques permettent la quantification du glutathion. Premièrement, le dosage utilisant l'acide dinitro-2,2'-dithio-5,5'-benzoïque, aussi appelé réactif d'Ellman (ou DTNB) permet la quantification colorimétrique des groupements thiols dans une préparation. Cette technique a été modifiée par ajout de GLR et de NADPH, rendant le test spécifique au glutathion. Cette quantification est réalisée sur des lysats cellulaires, et permet donc la quantification du glutathion cellulaire total, souvent assimilé aux quantités cytosoliques.

Une seconde technique permet la quantification localisée du glutathion. Cette technique repose sur la modification d'une glutaredoxine par le glutathion. Les glutaredoxines possèdent des cystéines capables de créer des ponts disulfures lors de la réduction de leurs substrats, puis ces ponts disulfures peuvent être réduits spécifiquement par le glutathion. Cette spécificité d'interaction a été exploitée pour créer une glutaredoxine comportant une seule cystéine (appelée Grx1-1cys), capable

d'échange avec le couple du glutathion pour former un pont disulfure mixte glutaredoxine-glutathion, aussi appelé glutathionylation. La mesure des proportions de Grx1-1cys libre et glutathionylées est alors proportionnelle au ratio GSH/GSSG. Comme les sondes roGFP, cette Grx1-1cys peut être génétiquement adressée à un compartiment d'intérêt. Utilisée en combinaison avec la roGFP fournissant une quantification du ratio GSH<sup>2</sup>/GSSG, la Grx1-1cys permet l'évaluation quantitative du glutathion dans un compartiment donné.

Ensemble, ces techniques permettent d'accéder à la quantité totale de glutathion, la quantité locale de glutathion, son état redox local, ainsi que les proportions de glutathion oxydé et réduit.

Nous avons utilisé ces techniques d'analyse du glutathion dans le but définir les fonctions du GSH au sein de RE. Pour mon projet de thèse, nous avons adopté la stratégie d'étudier en premier lieu le transport du glutathion. En effet, le glutathion est présent au sein du RE, mais est synthétisé dans le cytosol, ce qui implique des moyens de transport vers le réticulum. Comprendre comment le glutathion est transporté vers le RE permettrait à terme de moduler ce transport, et ainsi, d'étudier localement le rôle du glutathion, sans se soucier des effets de la modulation des niveaux de GSH au niveau des autres organelles. Au-delà de l'étude mécanistique du transport du glutathion, la seconde partie de mon projet de thèse visait à développer un protocole de crible chimique permettant directement l'identification de molécules capables de moduler le transport du glutathion, pour les mêmes raisons. A terme, l'identification d'un transporteur permettrait de comprendre quand et comment est transporté le GSH et les conséquences de ce transport sur la physiologie du RE permettrait de fournir des éléments de réponse quant à une fonction physiologique du GSH dans le réticulum endoplasmique.

La première partie de description des résultats dans ce manuscrit rassemble les éléments de la publication scientifique associée à ce projet de thèse. Dans cette étude, nous avons utilisé une lignée de cellules humaines HEK 293 exprimant constitutivement dans le RE une sonde roGFP sensible au glutathion, appelée Grx1-roGFPiE, nous permettant de calculer le potentiel  $E_{\text{GSH}}$  du glutathion dans le RE. Nous avons recouru à des quantifications totales de glutathion, ou  $[\text{GSx}]_{\text{cell}}$ , ainsi qu'à des quantifications locales  $[\text{GSx}]_{\text{ER}}$ , grâce à l'expression transitoire de Grx1-1cys adressée au réticulum endoplasmique.

Grâce à l'utilisation de ce système, nous avons observé dans un premier temps que la modulation des niveaux cellulaires du glutathion engendrait une réponse rapide de la sonde Grx1-roGFPiE, et qu'en résumé, augmenter les quantités de glutathion cellulaire, tant par l'addition exogène de GSH que par la stimulation de sa synthèse par la surexpression de la GCL causait une réduction de la sonde dans le RE. A l'inverse, la suppression de cystine du milieu (l'acide aminé limitant dans la synthèse du GSH), ou l'inhibition de la GSH par traitement à la buthionine sulfoximine (BSO) causait une oxydation de la sonde, reflétée par une augmentation de la valeur de  $E_{\text{GSH}}$ . Ces effets étaient rapides et réversibles, suggérant des échanges dynamiques entre les pools de glutathion cytosolique et luminal.

Ces échanges sont suggérés par la mesure de la valeur  $E_{\text{GSH}}$  qui, comme mentionné précédemment, n'est pas informative en termes de quantités de glutathion car cette valeur estime le ratio GSH<sup>2</sup>/GSSG. Pour s'assurer de l'établissement de flux, nous avons répété ces expériences en présence de Grx1-1cys surexprimée au sein du RE, nous permettant d'aboutir à l'estimation du ratio

GSH/GSSG dans le RE. Ces expériences nous ont permis d'estimer qu'en l'absence de traitement, le réticulum renfermait environ 2.5 mM de glutathion total, et cette valeur était comparable aux mesures de glutathion total réalisées sur cellule entière. Ensuite, nous avons observé que l'augmentation de GSH au niveau cellulaire causée par l'ajout de GSH exogène était aussi observable au niveau du RE, confirmant l'hypothèse d'une équilibration dynamique, semblant suivre le gradient de concentration établi entre le cytosol et le RE. Cette équilibration semblait limitée lorsque les quantités intracellulaires de GSH avoisinaient les 7.5 mM, suggérant un mécanisme de contrôle de l'entrée du GSH. Nous avons répliqué ces expériences dans des cellules semi-perméabilisées, c'est-à-dire des cellules dans lesquelles la membrane plasmique a été sélectivement solubilisée. Cette expérience permet donc de supprimer les facteurs cytosoliques de nos observations, en n'observant virtuellement que le réticulum « semi-purifié ». Dans ces conditions, nous avons répété l'observation d'une entrée de GSH graduelle, et plus limitée lorsque le GSH atteignait 7.5 mM.

L'hypothèse d'une équilibration des niveaux de GSH selon le gradient établi entre le cytosol et le RE a déjà été vérifiée chez la levure, dont le transporteur responsable a été identifié comme étant Sec61, le canal constituant le translocon par lequel les protéines néosynthétisées pénètrent dans le RE. Par conséquent, nous avons vérifié l'implication de Sec61 dans notre système. L'inhibition chimique de Sec61 ainsi que la réduction de son expression par siRNA ne nous a pas permis d'observer de modifications de la réduction du RE observée lors de l'élévation de des niveaux de GSH par addition exogène, suggérant que, dans notre cas, Sec61 n'est pas –ou pas la seule protéine– impliquée dans le transport du glutathion.

Ensuite, nous avons étudié l'impact physiologique de la réduction du RE causée par l'élévation des niveaux de GSH, en concentrant notre attention sur les fonctions redox du RE. En effet, la réduction médiée par le GSH pourrait entre autres causer une réponse de stress du réticulum, matérialisée par le déclenchement d'une Unfolded Protein Response (UPR) pour permettre au réticulum de s'adapter au challenge réducteur. Nous avons pu observer dans ce contexte que la réduction du RE causée par l'ajout de GSH exogène ne causait pas d'activation de l'UPR, et que l'élévation par surexpression de la GCL pendant plusieurs jours causait une faible activation de l'UPR, suggérant que le maintien chronique d'une réduction pouvait être une source de stress pour le RE.

Nous avons par la suite évalué l'effet de cette réduction par le GSH sur les protéines résidentes du RE, impliquées dans les processus de repliement protéique. Nous avons observé que l'élévation des niveaux de GSH induisait la réduction de ERdj5, une PDI-like majoritairement oxydée à l'état basal, impliquée dans la réduction des ponts disulfures de protéines destinées à être dégradées ainsi que dans les processus d'isomérisation de ponts disulfures. Nous avons aussi pu observer la réduction d'Ero1 lors de l'ajout de GSH exogène. Ces données suggérant que le glutathion était capable de réduire des protéines centrales dans les processus de repliement protéique, nous avons voulu évaluer l'impact de cette réduction sur le repliement d'un modèle protéique, ainsi que sur la cinétique de dégradation d'un second modèle. Dans les deux cas, la réduction du RE provoquée par le GSH n'a pas causé d'impact significatif sur les processus de repliement protéique et de dégradation de modèles protéiques mal repliés, suggérant que la réduction causée par le GSH n'impacte pas négativement l'équilibre protéostatique du RE.

Enfin, nous avons exploré l'existence d'un mode de transport du GSH vers le réticulum dépendant du calcium. De précédentes études ont en effet observé une réduction du RE lors de la déplétion des stocks calciques du RE. Parmi les hypothèses tentant d'expliquer cette réduction, l'une d'elles suggère l'entrée de glutathion. Nous avons étudié cette hypothèse, et constaté qu'en présence de thapsigargine, un inhibiteur de la pompe à calcium vers le réticulum, notre sonde détectait en effet une baisse importante de la valeur  $E_{\text{GSH}}$ . En utilisant la sonde Grx1-1cys, nous avons confirmé que cette réduction signalait bien l'entrée de glutathion dans le RE. De façon importante, cette entrée se faisait sans modification des quantités cellulaires de glutathion, suggérant un mécanisme indépendant du gradient établi entre le cytosol et le RE. Pour étudier le rapport entre ces deux mécanismes, nous avons associé au traitement à la thapsigargine, l'addition de GSH exogène ou bien la surexpression de GCL. Dans ces conditions, nous avons pu observer une additivité entre la réduction due au traitement par la thapsigargine, et celle due au l'établissement d'un gradient de GSH vers le RE. Ces résultats suggèrent donc l'existence de deux voies de transports du glutathion vers le RE, qui pourraient fonctionner de façon concomitante.

Dans la seconde partie de ce manuscrit sont décrits les résultats préliminaires obtenus au-delà du sujet principal de la publication précédemment décrite. Dans un premier temps, nous avons souhaité étudier plus avant l'effet de la déplétion en cystine. En effet, lors d'expériences visant à moduler les niveaux de glutathion intracellulaires, nous avons pu observer que l'absence de cystine dans le milieu de culture prévenait la réduction du RE par le GSH. Nous avons pu confirmer que la présence de cystine dans le milieu, mais pas la possibilité de son import par son transporteur principal xCT, était la condition *sine qua non* pour la réduction du RE par le GSH. Nous avons alors supposé que la réaction croisée entre GSH et cystine pouvait générer de la cystéine, qui alors aurait un effet réducteur. Nous avons conduit des expériences pour délimiter le rôle de chacun des métabolites, et il est alors apparu que même en l'absence de GSH intracellulaire, le traitement par la cystéine semblait capable de produire une réduction du RE. Ces résultats étaient à la fois surprenants et inquiétants, car ils remettaient en cause la spécificité de nos outils de détection du glutathion. Pour cette raison, nous avons de nouveau recouru à la technique de semi-perméabilisation pour s'affranchir de facteurs cellulaires et étudier l'impact du traitement par la cystéine sur un réticulum « semi-purifié ». Dans ces conditions, les quantités de cystéine provoquant une forte réduction du RE en cellule entière n'avaient pas le même effet, bien qu'une légère réduction persistât. De plus, l'immunoprécipitation des sondes Grx1-roGFPIE et Grx1-1cys au moyen de leur tag HA nous a permis de mettre directement ces sondes au contact des quantités de GSH ou de cystéine provoquant une réduction de la sonde. L'étude des formes réduites et oxydées de ces sondes au contact du GSH et de la cystéine nous a permis de vérifier que le GSH réduisait en effet ces sondes de façon bien plus efficace que la cystéine. Ces résultats nous ont ainsi permis de confirmer la spécificité de nos sondes, et bien que nous n'ayons pu élucider le mécanisme en jeu, il semblerait qu'en cellule entière, la réduction du RE par le GSH soit dépendante en partie du métabolisme de la cystéine.

En parallèle, nous avons développé et conduit un protocole de crible chimique dans le but de découvrir des molécules capables de moduler le transport du glutathion vers le réticulum. Un crible nécessite des conditions de génération et d'extraction de données compatibles avec le haut débit, pour cette raison, nous avons choisi d'utiliser une version que nous avons au préalable amélioré de

notre sonde fluorescente Grx1-roGFPiE comme proxy de l'entrée du glutathion dans le RE. En utilisant ce proxy, nous avons gardé à l'esprit que les molécules sélectionnées sur la base de ce critère nécessiteraient de plus amples confirmations pour vérifier leur impact réel sur les flux de glutathion. Nous avons choisi d'utiliser la réduction du RE provoquée par la fuite calcium hors du RE comme condition stimulant d'entrée de GSH, plutôt que l'addition de GSH exogène, pour éviter un maximum de biais. En effet, le constat que la cystéine conditionnait la réduction du RE a pu être réalisé dans des conditions d'addition de GSH exogène, en revanche, cette observation n'était pas conservée lors de la réduction du RE observée après traitement à la thapsigargine. Nous avons testé deux banques de composés chimiques, la première comportant 155 composés ayant des activités ayant un rapport avec le stress du réticulum, et une seconde de 1520 composés hors brevet, avec diverses activités thérapeutiques décrites. Ce protocole de crible nous a permis d'étudier les molécules et de les classer selon leur effet seul (la molécule est-elle oxydante, réductrice, ou neutre au niveau du RE après 30 minutes d'exposition ?), puis de leur effet par rapport à celui de la thapsigargine (la molécule inhibe-t-elle l'effet de la thapsigargine, l'amplifie-t-elle, ou est-elle neutre ?). Différents effets peuvent porter un intérêt dans la modulation des flux du glutathion, mais notre attention pour définir les différentes étapes de ce protocole de crible s'est initialement portée sur un hit « idéal », qui serait une molécule à l'effet neutre seule, et qui serait capable d'inhiber la réduction du RE causée par la thapsigargine. La polyphyllin I (PLP I) correspondant à ces critères, nous l'avons sélectionnée pour définir les caractérisations secondaires requises à l'issue du crible primaire. Dans un premier temps, nous avons confirmé les données obtenues lors du crible secondaire en élargissant les doses et temps de traitement initialement utilisés. Dans ces conditions, nous avons pu observer que la PLP I avait finalement un effet lorsqu'appliquée seule, celle-ci oxydant la sonde roGFP. Nous avons poursuivi les caractérisations en complétant les mesures de potentiel  $E_{GSH}$  avec l'utilisation de Grx1-1cys afin d'aboutir à une quantification des niveaux de GSH pour vérifier si l'inhibition du signal de la thapsigargine était due à l'inhibition d'une entrée de GSH dans le RE. A ce stade, bien qu'une diminution des quantités de GSH luminal lors du traitement de PLP I associée à la thapsigargine peut être envisagée, la qualité des résultats ne nous permet pas de conclure sur un effet statistiquement significatif, et demandera davantage d'optimisation. Nous avons toutefois complété l'étude avec un ultime test. La modulation du signal de la thapsigargine pouvant provenir de l'inhibition des flux de GSH, mais aussi des flux calciques, nous avons caractérisés ces derniers au moyen d'une sonde GEM-CEPIA. Ici aussi, les résultats présentés constituent les premières expériences exploratoires et demanderont à être affinées. Toutefois, nous avons pu établir une élévation des quantités lumineuses de calcium lors du traitement de nos cellules par la PLP I, suggérant que cette molécule pourrait agir sur le métabolisme calcique, et alors indirectement, sur le trafic du glutathion. Ces observations ont toutefois été rendues ardues par la dégradation cellulaire observées lors du traitement par la PLP I. Si la PLP I n'a finalement pas présenté les caractéristiques d'un hit idéal, notamment dû à ses effets oxydants, ses effets sur le métabolisme calcique, ainsi qu'à ses effets sur la morphologie cellulaire, cette molécule nous aura permis de développer les lignes de procédé qui seront nécessaires à l'évaluation d'autres composés prometteurs révélés par les cribles chimiques.



